

CARBOHYDRATE APPROACHES TO DELIVERING THERAPEUTIC AGENTS ACROSS THE BLOOD BRAIN BARRIER

Corrine Kluvers

BMedChem (Hons), GradCertCommRes

A thesis submitted for the degree of Doctor of Philosophy

School of Chemistry, Monash University

July 2013

General Declaration

I hereby declare that this thesis contains no material that has been accepted for the award of any other degree or diploma at any university or equivalent institution and that, to the best of my knowledge, this thesis contains no material previously published or written by another person, except where due reference is made in the text of this thesis.

Signed: _____ Date: _____

Corrine Kluvers

Under the Copyright Act 1968, this thesis must be used only under the normal conditions of scholarly fair dealing. In particular no results or conclusions should be extracted from it, nor should it be copied or closely paraphrased in whole or in part without the written consent of the author. Proper written acknowledgment should be made for any assistance obtained from this thesis.

I certify that I have made all reasonable efforts to secure copyright permissions for third-party content included in this thesis and have not knowingly added copyright content to my work without the owner's permission.

Table of Contents

General Declaration.....	ii
Table of Contents	iii
Abstract.....	vi
Acknowledgements.....	viii
Abbreviations and Acronyms.....	x
Chapter 1. Introduction.....	3
1.1. Motor Neurone Disease	3
1.1.1. Disease Symptoms, Statistics and Outcomes.....	3
1.1.2. Disease Pathology/Causes	4
1.1.3. Treatment Options	8
1.2. Peptide Nucleic Acids	15
1.2.1. Structure, Properties and Applications.....	15
1.2.2. Previous Work with PNAs for the Treatment of MND.....	17
1.3. PNA and Small Molecule Transport to the CNS	25
1.3.1. The Blood Brain Barrier	25
1.3.2. Example Transport Mechanisms.....	27
1.3.3. Sugar Conjugates.....	28
1.4. Project Aims.....	30
1.5. References.....	30
Chapter 2. Glycosyl Esters and Vitamin E Derivatives	43
2.1. Introduction.....	43
2.1.1. Vitamin E as a Treatment for MND.....	43
2.1.2. Vitamin E Derivatives.....	45
2.1.3. Aims and Synthetic Plan.....	48
2.2. Results and Discussion	48
2.2.1. Glucosyl and Galactosyl Ester Library.....	48
2.2.2. Synthesis of Novel Vitamin E Glycosyl Esters	51
2.2.3. Alternate Synthetic Pathways to Novel Vitamin E Glycosyl Esters	54
2.2.4. Benzyl Protected Glycosyl Esters	62
2.3. Conclusions and Future Directions	65

2.4. Experimental Details	67
2.4.1. General Experimental Methods.....	67
2.4.2. Synthesis of Glucosyl and Galactosyl Ester Library	68
2.4.3. Synthesis of Vitamin E Derivatives	82
2.5. References.....	96
Chapter 3. Functional PNA Monomers	103
3.1. Introduction.....	103
3.1.1. Modified Peptide Nucleic Acids.....	103
3.1.2. PNA Modifications for Increased Solubility and Cell Penetration.....	106
3.1.3. Aims and Synthetic Plan	108
3.2. Results and Discussion.....	109
3.2.1. Design and Synthesis of Glycosylated Building Blocks for <i>N</i> -Terminal Conjugation	109
3.2.2. Design and Synthesis of Glycosylated PNA Monomers – Replacing the Nucleobase	113
3.2.3. Conclusions and Future Directions	138
3.3. Experimental	140
3.3.1. Synthesis of Chiral Glycosylated Building Blocks	140
3.3.2. Synthesis of Achiral Glycosylated Building Blocks	142
3.3.3. Synthesis of the PNA Monomer Backbone.....	146
3.3.4. Synthesis of Rigid-Linked Glycosylated Monomers.....	147
3.3.5. Synthesis of Succinic Anhydride-Linked Glycosylated Monomers	163
3.3.6. Synthesis of Alkyl-Linked Glycosylated Monomers	166
3.4. References.....	174
Chapter 4. Conjugated Peptide Nucleic Acids and their Physical Measurements.....	179
4.1. Introduction.....	179
4.2. Peptide Nucleic Acid Preparation	180
4.2.1. Peptide Nucleic Acid Synthesis.....	180
4.2.2. Peptide Nucleic Acid Purification	189
4.2.3. Peptide Nucleic Acid Characterisation	189
4.3. Quartz Crystal Microbalance: Analysis of PNA – Membrane Interaction....	190
4.3.1. Overview	190
4.3.2. Procedure	193
4.3.3. Results and Discussion.....	200

4.4. Thermodynamic Investigation of PNA Conjugates	209
4.4.1. PNA/DNA Binding	209
4.4.2. Thermodynamic Analysis to Determine Binding Ability	210
4.4.3. UV-vis Thermal Melt Method	214
4.4.4. Isothermal Titration Calorimetry (ITC) Method	220
4.5. Conclusions and Future Directions	225
4.6. References	227
Appendix.....	233

Abstract

This thesis describes synthetic approaches for improving the efficiency of transport of small molecules and DNA analogues past the blood brain barrier towards the development of a treatment for motor neurone disease.

Chapter one introduces motor neurone disease (MND) and describes potential causes of the disease. A mutation to the antioxidant enzyme, copper zinc superoxide dismutase (SOD1), is known to be associated with familial cases of motor neurone disease, potentially through an oxidative stress and/or a toxic gain of function mechanism. The susceptibility of selective motor neurones to MND could be due to altered AMPA receptor subunit expression. Treatment options include small molecule antioxidants, and antisense agents to block unwanted gene production. Previous work in our laboratory has seen the design, synthesis and evaluation of PNAs aimed to down-regulate an AMPA receptor subunit and the mutated SOD1 enzyme. While promising, the results indicate that the therapeutic potency of PNAs would be enhanced by improved delivery through the blood brain barrier.

Chapter two focuses on analogues of vitamin E, a known antioxidant. Natural vitamin E is very lipid soluble and does not cross the BBB, therefore more hydrophilic analogues are required for the treatment of motor neurone disease. The use of silver carbonate as a promoter to form β -orientated glycosyl esters was explored for the production of 6 glycosylated vitamin E derivatives. Various syntheses of glycosyl ester vitamin E derivatives were explored. One method involved the synthesis of and application to the vitamin E carboxylic acid derivative **24**. For example, glucosyl ester vitamin E derivative **25** was produced from the silver carbonate glycosylation of **24** in high yield. An alternative, and more appropriate synthetic strategy involved the use of benzyl protecting groups. This required the preparation of the benzyl bromide sugar **34** *in situ* from the benzyl 4-pentenyl sugar **33**. Glucosyl ester vitamin E derivative **35** was produced from the silver carbonate glycosylation of **24**.

Chapter three examines the synthesis of PNA monomers linked to glucose and galactose as a means to improve the bioavailability of PNA oligomers. Two sites on

the PNA structure were explored for modification – the so-called site X and Y. Examples of site X include glycosylation of L-serine with glucose and galactose to produce the glycosylated building blocks **39** and **40**. For site Y, three strategies were explored. First, aromatic linking groups were used to produce “rigid-linked” glycosylated monomers, **71** and **72**. Incorporation of a flexible linker was achieved using succinic anhydride, producing **75** and **76**. However, this pathway was low yielding and complications in removing the *C*-terminus protecting group were experienced. The third strategy involved the installation of an alkyl-linking group, leading to **85** in good yield.

Chapter four consists of three smaller sections, connected by a common theme of peptide nucleic acids (PNA). The first section details the synthesis, purification and characterisation of a library of PNA oligomers that incorporate glycosylated building blocks **39**, **40**, **71** and **72**. The second section describes the use of the quartz crystal microbalance to investigate the interaction of a selection of PNA conjugates with a synthetic lipid bilayer. It was found that all glycosylated PNAs display transmembrane insertion. The third section focuses on the thermodynamic properties of the glycosylated PNA oligomers when binding complementary DNA. Two techniques were used: i) a UV-visible spectroscopic method investigating a thermal melt process between a PNA strand and its complementary DNA sequence; and ii) isothermal titration calorimetry to measure conjugation of the PNAs to complementary DNA. All thermodynamic parameters calculated indicate that binding is not hindered, and in some cases improved, by the attached glycosylated building blocks.

Acknowledgements

I would like to start by thanking Prof. Steven Langford for the support, time, dedication and patience he has given me throughout my time in his research group. He has always supported my interests, both in and outside of chemistry, and given me the time to explore other worlds before helping me to complete this thesis. I have learnt so much from him and will always be grateful for the experiences I have gained by working with him.

A huge thank you goes to all past and present Langford Group members with whom I have had the pleasure of working. It really makes life better when you have a great group of people to complain to and joke with. I'd especially like to thank Kat and Brad for our lab time discussions and Laura, Amy, Manny, Jess, Kris, Brenton, Heather, Tina, Kat, Brad and Elisse for our ongoing friendship.

I would also like to thank A/Prof. Lisa Martin for introducing me to the world of QCM and for her ongoing support and dedication to my work. Thanks also to Joyee, Slavica and Stefania for answering all of my questions.

I am indebted to the staff of the School of Chemistry for their help throughout my candidature. I'd especially like to thank Peter Nichols for his NMR help, Sally Duck for her mass spec work, Victor de Guzman for his help with HPLC and Kristina Konstas and Craig Forsyth for their last minute X-ray crystallography work.

A huge thanks also goes to Irv for teaching me all about PNA synthesis, Elisse for teaching me how to run UV thermal melts and ITC experiments and to Heather for running the computational modelling experiments.

I gratefully acknowledge the Australian Government for financial support in the form of an Australian Postgraduate Award, and Monash University for generously providing me with a travel grant to allow me to present my work overseas.

I would like to express my gratitude to Daryl, Laura, Jeromy, Mum and Dad for taking the time to read drafts and provide invaluable feedback.

Of course none of my achievements would have been possible without the ongoing love and support of Mum, Dad and Elise. While the details of my work

were sometimes too technical to understand, and it may have seemed like I would never finish, they were always positive, encouraging and believed in me.

Finally, to the love of my life, my deepest thanks. I met Jeromy the week I started my PhD, and throughout, he has been my rock. For listening to presentations over the phone, fixing computer problems, sitting with me on the weekend at HPLC, learning about chemistry and my molecules, listening to my rants, supporting me to go back to the thesis full-time and encouraging me to finish; I must say "Jeromy is great".

Abbreviations and Acronyms

9mer	9 Unit oligomer
12mer	12 Unit oligomer
A	Adenosine
Ac	Acetate
ACN	Acetonitrile
AcOH	Acetic acid
ALS	Amyotrophic Lateral Sclerosis
AMPA	α -Amino-3-hydroxy-5-methyl-4-isoxazolepropionic acid
Ar	Aromatic
AS-PNA	Antisense peptide nucleic acid
ATP	Adenosine triphosphate
ax	Axial
BBB	Blood brain barrier
Bhoc	Benzhydryloxycarbonyl
Bn	Benzyl
BnBr	Benzyl bromide
C	Cytosine
CNS	Central nervous system
COSY	Correlation spectroscopy
CPP	Cell penetrating peptides
CSF	Cerebralspinal fluid
DAST	(diethylamino)sulphur trifluoride
DCC	<i>N,N'</i> -Dicyclohexylcarbodiimide
DCM	Dichloromethane
DIEA	<i>N,N'</i> -Diisopropylethylamine
DMF	<i>N,N'</i> -Dimethylformamide
DNA	Deoxyribonucleic acid
DSC	Differential scanning calorimetry
EAAT	Excitatory amino acid transporter

EDC	1-Ethyl-3-(3-dimethylaminopropyl)carbodiimide
ESI	Electrospray ionisation
EtOAc	Ethyl acetate
EtOH	Ethanol
eq	Equatorial
FALS	Familial ALS
Fmoc	Fluorenylmethoxycarbonyl
G	Guanine
GluR3	AMPA subunit
GLUT-1	Glucose transporter
HATU	(Dimethylamino)- <i>N,N</i> -dimethyl(3 <i>H</i> -[1,2,3]triazolo[4,5- <i>b</i>]pyridin-3-yloxy)methaniminium hexafluorophosphate
HBTU	<i>N,N,N',N'</i> -Tetramethyl- <i>O</i> -(1 <i>H</i> -benzotriazol-1-yl)uronium hexafluorophosphate
HMQC	Heteronuclear multiple quantum correlation
HOBt	1-Hydroxybenzotriazole
HPLC	High performance liquid chromatography
HRMS	High resolution mass spectrometry
IP	Intraperitoneal
ITC	Isothermal titration calorimetry
JMOD	<i>J</i> -modulation
MeOH	Methanol
<i>m/z</i>	Mass-to-charge ratio
MND	Motor neurone disease
MP	Melting point
MPA	3-Mercaptopropionic acid
mRNA	Messenger RNA
MS	Mass spectrometry
MVK	Methyl vinyl ketone
NMDA	<i>N</i> -methyl-D-aspartate
NMP	1-Methyl-2-pyrrolidone
NMR	Nuclear magnetic resonance
NS-PNA	Nonsense peptide nucleic acid

NSC	Neuroblastoma × spinal cord
PBS	Phosphate buffered saline
PC	1 2-Dimyristoyl-sn-glycero-3- phosphocholine
Pd/C	Palladium on carbon
PEG-PS	poly(ethyleneglycol)/polystyrene
PKC	Protein Kinase C
PNA	Peptide Nucleic Acid
ppm	Parts per million
Py	Pyridine
QCM	Quartz Crystal Microbalance
R _f	Retention factor
RISC	RNA-induced silencing complex
RNA	Ribonucleic acid
ROS	Reactive oxygen species
RP-HPLC	Reverse phase HPLC
SALS	Sporadic ALS
SAR	Structure-activity relationship
siRNA	Small/short interfering RNA
SLB	Supported lipid bilayers
SOD1	Copper zinc superoxide dismutase
SPS	Solid-phase synthesis
T	Thymine
TFA	Trifluoroacetic acid
TLC	Thin layer chromatography
T _m	Melting temperature
TMG	2-(α -D-Glucopyranosyl)methyl-2,5,7,8-tetramethylchroman-6-ol
TPPA	Trimethyl phosphonoacetate
ΔG	Change in Gibbs free energy
ΔH	Change in enthalpy
ΔS	Change in entropy

CHAPTER 1

INTRODUCTION

Chapter 1. Introduction

1.1. Motor Neurone Disease

1.1.1. Disease Symptoms, Statistics and Outcomes

Motor neurone disease (MND), or Amyotrophic Lateral Sclerosis (ALS) is an aggressive neurodegenerative disease.^{1,2} MND has a worldwide new case incidence rate of 0.3-2.5 people per 100,000 per year,³ with Caucasian populations displaying the higher incidence rates.¹ As MND is a terminal disease, this also equates to the death rate associated with the disease. Prevalence, i.e. the proportion of people living with the disease at any one time, is estimated to be 1 in 15,000 people in Australia.⁴

Disease development usually occurs between the ages of 55 and 65 years.⁵ The incidence of MND appears to be higher in males than in females,^{6,7} as it is in smokers,^{5,8-10} war veterans¹¹ and football players.^{3,12} Diagnosis usually occurs 14 months after symptoms¹³ begin due to the lack of a diagnostic test or biomarker for the disease and the similarity of symptoms with other neurodegenerative diseases.^{3,7,14}

MND involves the selective death of both upper and lower motor neurones in the brain and spinal cord,^{1,2,7} which controls various muscles resulting in muscle weakness, leading to muscle atrophy and eventual paralysis of the patient.¹⁵ As neurones do not regenerate, MND is a terminal disease. Symptoms associated with MND include weakening of the mouth and throat muscles⁵ leading to difficulties with swallowing, breathing and speech,^{3,7} muscle weakness in the hands, arms and legs,^{3,5,15} muscle twitching and cramping^{3,5} and cognitive impairment and/or dementia in some cases.^{5,15,16} Secondary symptoms of MND include fatigue, pain, excess and thickened saliva, drooling, emotional lability, depression, anxiety, sleep disturbance, constipation, urinary urgency or incontinence, malnutrition, dehydration, hypermetabolism, slurred speech, pain, head drop and curving of the spine.^{3,5,7,17,18} Patient death typically occurs within 3 years of symptom onset^{2,3} due to respiratory failure⁵ from loss of function of the neurones controlling the diaphragm.²

1.1.2. Disease Pathology/Causes

Motor neurone disease is not very well understood.^{3,5,7} Associated defects in particular genes and molecular processes are known, however why these defects cause ALS is unknown. The majority of cases of ALS are sporadic (SALS) with 5-10% of all cases being inherited, or familial (FALS)^{2,5,7} usually in an autosomal dominant manner.⁵ ALS is now considered to be a result of defects in multiple genes and pathways and rather than being considered a single disease, it is now regarded as a syndrome.² A case of ALS is considered to be familial when one or more first or second degree relatives also have ALS.² The clinical appearances of familial and sporadic ALS cases are similar except that familial ALS usually has a younger age of onset.² The similarities of the clinical presentations of SALS and FALS suggests a common disease pathology.¹⁴

There are currently 13 genes, that when mutated, are implicated in both SALS and FALS.^{2,3,7,19,20} These genes and/or their protein products are connected to RNA metabolism,^{2,7,19} protein aggregation,^{2,3,19} axonal transport,² nucleotide repeat expansions,^{3,21,22} and free radical generation/destructive oxidation reactions.^{7,23-25} Superoxide dismutase (SOD1) was the first gene to be implicated in ALS²⁶ – both SALS and FALS forms. There are over 150 known mutations of the SOD1 gene that are implicated in ALS (Figure 1.1).³

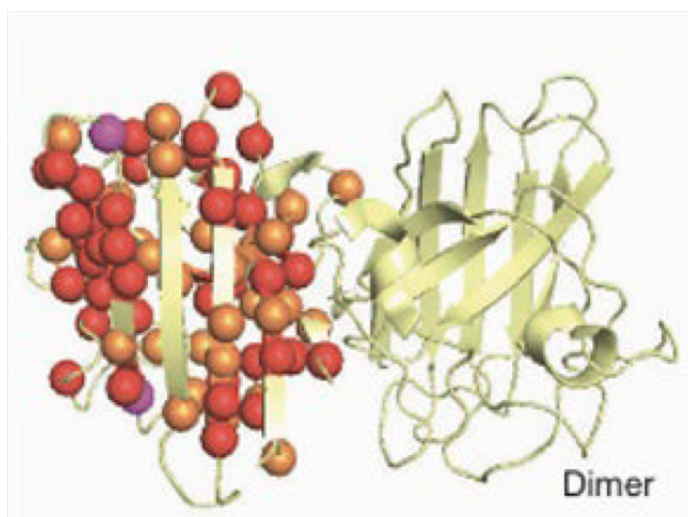


Figure 1.1: Structure of Cu, Zn-superoxide dismutase enzyme (SOD1), showing positions of mutations known to lead to FALS and SALS. Purple ball = site of more the 3 mutations; red ball = site of more than 1 mutation; orange ball = site of single mutation, insertion, deletion.³

CHAPTER 1 - INTRODUCTION

The SOD1 gene codes for the copper zinc superoxide dismutase enzyme (SOD1), which is found in the cytoplasm of all mammalian cells. This enzyme acts as a free radical scavenger and as such, converts superoxide radicals^{7,27} ($\text{O}_2^{\bullet-}$), which are toxic by-products of cellular respiration, to hydrogen peroxide and molecular oxygen.²⁸ The copper ion in the active site is responsible for the catalytic conversion¹⁴ by being alternatively oxidised, and reduced by superoxide radicals (Figure 1.2).²⁹ The copper ion is oxidised from Cu^+ to Cu^{2+} when it catalyses the conversion of a superoxide radical to hydrogen peroxide and conversely, the copper ion is reduced from Cu^{2+} to Cu^+ when it catalyses the conversion of superoxide radical to molecular oxygen. Superoxide radicals are generated through cellular respiration, and if not removed/converted, can cause oxidative stress to the cell. Neurones are susceptible to oxidative stress as they require significant energy. The large size of these cells, i.e. a cell body that is 50-60 μm and an axon that can be 1 meter long, means they have a high metabolic demand and hence, through cellular respiration, a high level of superoxide radicals are produced to meet this demand, relative to other cell types.^{30,31}

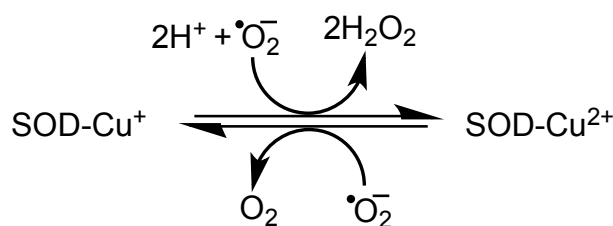


Figure 1.2: How SOD1 works. SOD1 converts superoxide radicals to hydrogen peroxide and molecular oxygen. The copper ion in the active site of SOD1 is alternatively oxidized and reduced and thus alternates between oxidation states of +1 and +2.²⁹

The various mutations known to exist in the SOD1 gene are thought to result in a misfolded, destabilised protein³² that exposes the catalytic copper ion.^{23,29} This results in a toxic gain of function of the enzyme,^{14,24} oxidative stress and cell death. A mutated SOD1 enzyme has enhanced activity with abnormal substrates,¹⁴ and may, for example, facilitate the increased production of peroxynitrite (ONOO^-) as well as increased nitration of proteins by peroxynitrite.²³ Furthermore, a mutated SOD1 enzyme has been thought to lose the ability to bind the necessary zinc ion, resulting in oxidative stress to the cell.³³ Without zinc, SOD1 is less efficient at scavenging superoxide radicals.¹⁴ There appears to also be a

concomitant increase in tyrosine nitration¹⁴ due to the increased efficiency of zinc deficient SOD1 to catalyse the peroxynitrite-mediated process.³³ *In vitro* studies have shown that zinc-deficient SOD1 enzymes induce apoptosis in motor neurones.³⁴

Another potential cause of motor neurone death in ALS is glutamate-induced excitotoxicity.^{29,35} Glutamate is the main excitatory neurotransmitter in the central nervous system (CNS). It is released from presynaptic neuronal terminals by calcium-induced exocytosis and binds to receptors such as NMDA, AMPA, kainate and metabotropic on post-synaptic neurones. Upon binding to the receptors, glutamate causes the associated channels to open to allow the influx of cations including Ca^{2+} , Na^{+} , K^{+} and Mg^{2+} . Usually, the glutamate is removed from the synapse by glutamate transporters to avoid over-stimulation of the neurone. There are five subtypes of glutamate transporters known, however the EAAT2 transporter (also referred to as the GLT-1 transporter) is responsible for the majority of glutamate removal for motor neurones.^{29,35}

High levels of glutamate in the CNS of some ALS sufferers have been found^{36,37} and altered glutamate metabolism due to diminished levels of glutamate transporters has been shown to be the cause.³⁸ It has been shown that decreased levels of the EAAT2 glutamate transporter results in elevated extracellular calcium ion levels and neurodegeneration.^{35,39} Significantly, reduced levels of EAAT2 have specifically been found in ALS patients.^{38,40} Interestingly, the levels of mRNA corresponding to the glutamate transporters have been found to be normal in ALS patients, suggesting translation or post-translation problems are the cause of diminished glutamate transporter levels.^{40,41}

Excess glutamate in the synapse of neurones, as shown in Figure 1.3, can cause the activation of the various postsynaptic receptors for longer periods, resulting in an excessive influx of Ca^{2+} into the neurone. Increased intracellular calcium levels then leads to cellular damage and neuronal death by the generation of reactive oxygen species (ROS), free radical production, activation of lipases, nucleases and proteases that cleave and inactivate cellular enzymes and structural proteins, damage lipid membranes and fragment nucleic acids.^{42,43}

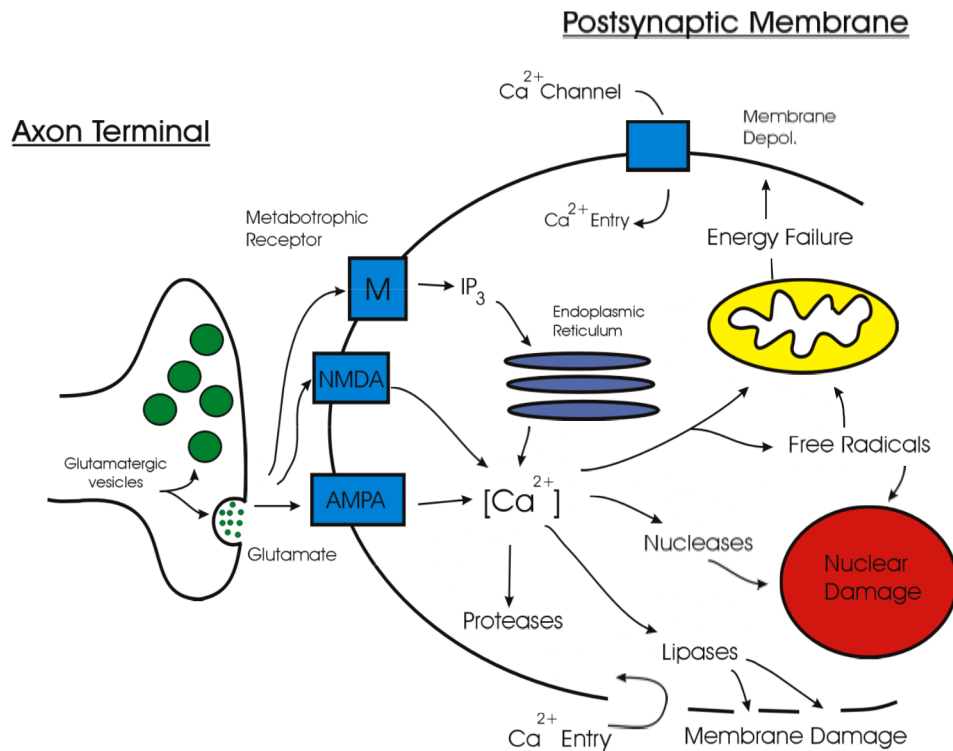


Figure 1.3: Cellular effects of glutamate excitotoxicity.

The susceptibility of selective motor neurones to excitotoxicity-induced death could be due to altered AMPA receptor subunit expression. The AMPA (α -amino-3-hydroxy-5-methyl-4-isoxazolepropionate) receptor is heterogenic and composed of the subunits GluR1-4 in varying combinations and mediates fast neurotransmission. Subunits GluR1-4 are each composed of approximately 900 amino acids, share 68-73% homology, and arise from separate genes.^{44,45} AMPA receptors are located on postsynaptic neurones and are ligand-gated, or ionotropic receptors.⁴⁵ Glutamate binding to the AMPA receptor causes the channel to open and allow mainly monovalent cations, Na^+ and K^+ , to move into the cell and propagate the action potential. The presence of the GluR2 subunit renders the channel impermeable to Ca^{2+} ions (Figure 1.4).^{44,46} The reason for this is that the GluR2 subunit contains a positively charged arginine residue, rather than a neutral glutamine residue that is found in subunits GluR1, 3 and 4 at the corresponding position,⁴⁴ hence repelling Ca^{2+} ions. The change in residue is due to editing of GluR2 RNA^{44,47} because the corresponding codon in the DNA of all four subunits is for glutamine.⁴⁷

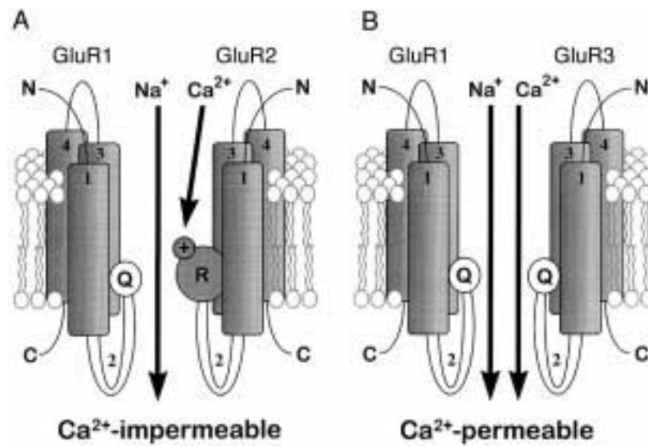


Figure 1.4: A: The presence of the GluR2 subunit with the positively charged arginine residue renders the receptor channel impermeable; B: The presence of the GluR3 subunit with the glutamate residue results in a permeable receptor channel for Ca^{2+} .⁴⁸

An unbalanced or altered AMPA subunit expression has been noted in some cases of ALS. One explanation is insufficient GluR2 RNA editing resulting in Ca^{2+} permeable channels.^{49,50} Other studies have shown that there is a decrease in the levels of GluR2 mRNA in the spinal cord of ALS patients, leading to more Ca^{2+} permeable AMPA receptors.⁵¹ A decrease in the GluR2 protein has been observed in SOD1 transgenic mice, suggesting the mutant SOD1 enzyme creates a cellular environment that leads to post-transcription events that result in reduced translation or stability of the GluR2 protein.⁵² Furthermore, proteomic studies have found increased levels of the GluR3 subunit protein in the lumbar spinal cord of SOD1 transgenic mice.⁵³ Tortarolo *et al.* also observed an increase in the amounts of GluR3 mRNA and subunit protein in the motor neurones of SOD1 transgenic mice.⁵²

1.1.3. Treatment Options

The various contributing factors implicated in progressing ALS present a number of potential therapeutic targets. To date, there is only one drug that has been approved for ALS treatment. Riluzole, or 6-(trifluoromethoxy)benzothiazol-2-amine, a product of Aventis, is a small-molecule inhibitor of glutamate release (Figure 1.5).^{7,54} Riluzole is thought to work by interfering with presynaptic sodium channels.⁵⁵ While Riluzole has been shown to slow the progression of ALS, and in particular, slow the deterioration of muscle strength and extend life by around 2-3 months,^{56,57} this therapy seems specific for those patients with bulbar-

onset ALS, i.e. for patients in which the ALS first affected the muscles of the mouth and throat; there was no significant extension of life observed in patients with limb-onset ALS.⁵⁷ Adverse side-effects such as increased lack of strength, increased spasticity, stiffness, nausea, altered liver function and increased blood-pressure have been observed, however these side-effects generally do not continue once treatment has ceased.^{56,57} Riluzole is expensive with one year's treatment costing over \$7200⁵⁸ and its beneficial effects are moderate⁵⁶ and so a better therapeutic approach is needed.

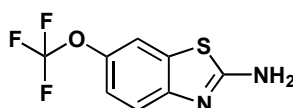


Figure 1.5: Structure of Riluzole.

Conceptually, there are two broad classes of potential therapeutic agents that could address the various pathological causes of ALS: small molecules, such as Riluzole, and antisense agents.

1.1.3.1. Small Molecule Treatment Approaches to MND

The complicated nature of the pathology of ALS means there are potentially many drug targets for small molecule therapeutics. For example, the increased levels of ROS could be targeted with antioxidants, the increased levels of intracellular Ca^{2+} could be targeted with calcium chelators, excess glutamate levels could be reduced with glutamate-release inhibitors (Riluzole) or an up-regulation of the glutamate transporter, EAAT2 and the effects of excess glutamate could be reduced with glutamate receptor antagonists/blockers.

There are several small molecules currently in clinical trials for the treatment of ALS (Figure 1.6). Ceftriaxone, a β -lactam antibiotic, is in phase III clinical trials for ALS.³ Ceftriaxone has been found to increase transcription levels of EAAT2 as well as increase the transporter's activity and hence it displays neuroprotective properties.⁵⁹ The use of Ceftriaxone in ALS animal models has resulted in a delay in motor neurone loss and an increase in survival.⁶⁰

Arimoclomol is a hydroxylamine small molecule that has been shown to cause a reduction in the levels of ubiquitin-positive protein aggregation in the spinal cords of transgenic SOD1 mice.⁶¹ Furthermore, Arimoclomol is a co-inducer of the

heat-shock response and acts to prolong the action of heat shock proteins.⁶¹ These proteins function to ensure the correct folding of the cell's proteins as they are being formed as well as to refold damaged proteins.⁶¹ In the motor neurones of MND sufferers, the presence of the mutated SOD-1 enzyme means the availability of heat shock proteins is diminished, resulting in a diminishing of their normal protective functions and hence treatments aimed at increasing the levels of heat shock proteins is a promising strategy for MND treatment.⁶² Arimoclomol has been shown to increase the survival of transgenic SOD1 mice and delay disease progression.⁶² Arimoclomol is currently in phase II/III clinical trials.³

Edaravone is a free radical scavenger and acts as an antioxidant against lipid peroxidation⁶³ that has shown to improve ALS symptoms and reduce SOD1 aggregation. It recently completed phase III clinical trials and results are pending publication.³ Structure-activity analysis revealed that the electronic properties of substituents of the 2-pyrazolin-5-one core did not affect the activity but lipophilic substituents (phenyl group) were required for lipid peroxidation inhibitory activity.⁶³

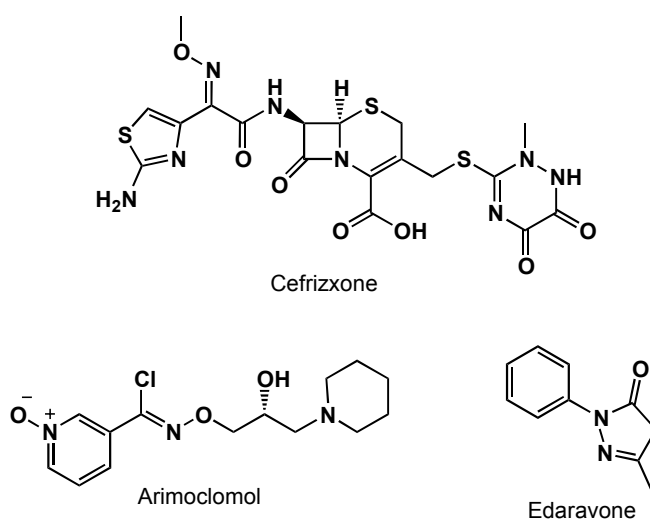


Figure 1.6: Drug compounds currently in clinical trials for the treatment of ALS.

1.1.3.2. Antisense Agents as a Treatment Approach to MND

An alternative treatment approach is to target the genetic material responsible for the disease. Antisense therapies include DNA, RNA or their analogues, that are designed to bind, in a complementary manner, to a nucleic acid target, an mRNA sequence, which leads to a protein product that has been implicated in a disease.

Figure 1.7 shows that the first DNA strand (sense strand) and the second DNA strand (antisense strand) are complementary to each other. It is the latter that is copied into complementary mRNA, which is therefore referred to as a sense strand. Any sequence that binds mRNA is called antisense. A sequence that binds a DNA sense strand (coding strand) is called antigene.

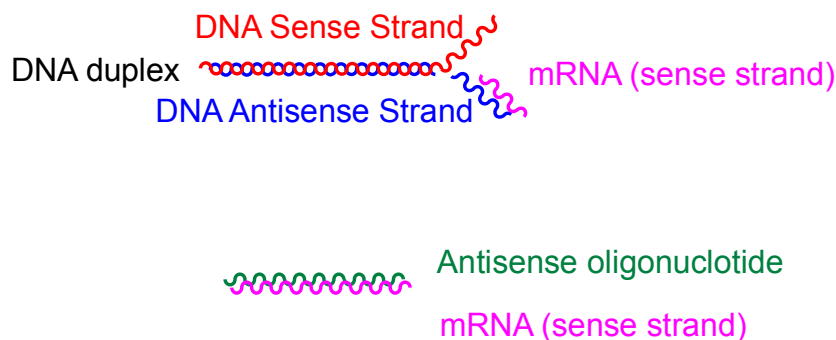


Figure 1.7: Antisense oligonucleotides are complementary to a mRNA strand, which is complementary to the DNA antisense strand.

Genetic information starts in the form of a gene in DNA, which is then transcribed into pre-mRNA before it is edited and spliced, known as RNA intermediary metabolism, to produce the mature mRNA strand, which is transported to the cytoplasm and finally translated into the polypeptide product. Involved in this process of information transfer are both coding RNAs, that lead to a translated protein product, and noncoding RNAs, that modulate the transfer of information. Each of these steps of protein production from DNA can potentially be interrupted by oligonucleotide therapeutics.

There are a number of different modes of action that are displayed by oligonucleotide antisense drugs. Essentially they all function to down-regulate, or otherwise modulate, the production of specific protein products. Crooke *et al.* have reviewed the various methods by which antisense drugs have been shown to act to effectively down-regulate the production of the unwanted protein.⁶⁴ In summary, occupancy-only mechanisms involve the hybridisation of the antisense oligonucleotide to its complementary RNA sequence to physically or sterically block the binding of factors or proteins required for normal protein synthesis.⁶⁵ This mechanism can be applied to modulate splicing or prevent translation.⁶⁶⁻⁶⁹

Another mode of action of antisense oligonucleotides is occupancy-activated destabilisation in which steps required to stabilise the pre-RNA strand, such as 5'

capping⁷⁰ and 3'-polyadenylation,⁷¹ are prevented. Another example of occupancy-activated destabilisation is the RNase H mechanism, which is the most common antisense mechanism. RNase H is an endogenous enzyme that non-specifically cleaves RNA that is only in RNA-DNA duplexes.^{72,73} The hybridisation of the therapeutic antisense oligonucleotide to its target RNA strand may induce the RNase H enzyme to cleave the RNA strand and render it unable to be translated into a protein product.⁷⁴ An antisense drug must be single stranded and DNA-like to activate this pathway. A similar mechanism is that of double-strand RNases, which are enzymes that degrade RNA-RNA-like duplexes.⁷³ A double stranded siRNA (short/small interfering RNA), comprising a sense and an antisense strand, is taken to RISC (RNA-induced silencing complex that contains an RNase). The sense strand is removed before the antisense strand is used by RISC to cleave the target RNA.⁷⁵ Therefore double stranded oligonucleotide drugs can exploit this pathway to down-regulate target RNA sequences and their protein products.

Another potential mode of action of antisense therapeutics is *via* the control of micro-RNAs. Micro-RNAs are RNA sequences 19-23 nucleotides in length and when they form a duplex with a complementary RNA sequence, cleavage of the target sequence is induced.⁷⁶ Antisense drugs designed to bind to micro-RNAs can influence the levels of various mRNAs, which can lead to a change in levels of various protein products.

The advantage of the antisense therapeutic approach is that it is specific in its target.⁷⁷ For example, specific protein isoforms can be targeted, without affecting related proteins, as has been done for specific isoforms of Protein Kinase C (PKC).⁷⁸ Furthermore, the generality of the approach means that developments and improvements made in design and pharmacokinetic properties for one antisense drug can be applied to others, with the specificity of each drug due to the sequence of nitrogenous bases.

The first reported use of an oligonucleotide as an antisense agent showed the promise of this therapeutic approach, however the problems with the use of natural DNA and RNA (Figure 1.8) have driven a large amount of medicinal chemistry work to develop modified oligonucleotides.^{64,79} These problems include: (1) insufficient stability in biological systems due to their recognition by endogenous nucleases; (2) insufficient pharmacokinetics due to poor plasma half-

lives; (3) insufficient target affinity since DNA has a lower affinity for RNA than RNA has for itself.

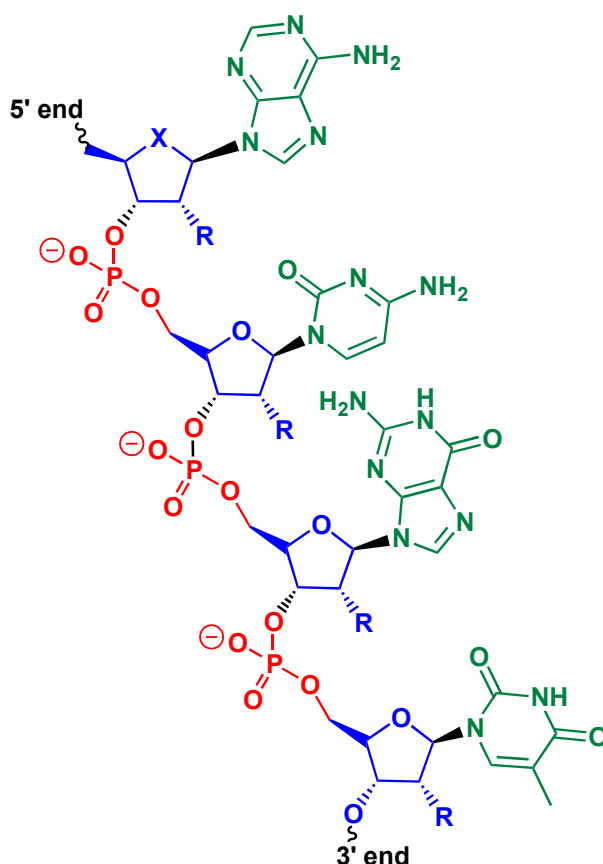


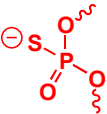
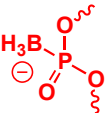
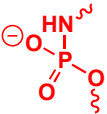
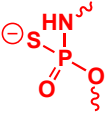
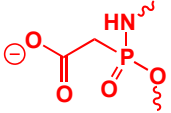
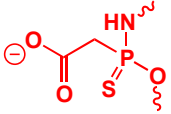
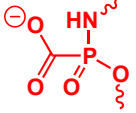
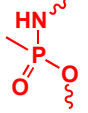
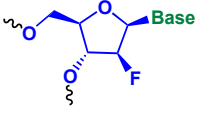
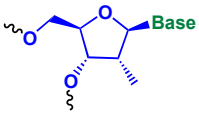
Figure 1.8: Structure of a natural oligonucleotide showing sections that can be modified to increase stability. Red – Phosphate linkage; Blue – Ribose sugar; Green – pyrimidine or purine base.

There have been many modified oligonucleotides developed in the years since the advent of antisense therapy. Table 1.1 shows some of the more common modifications that have been made, with the colours of the modified structure corresponding to those in Figure 1.8. Further details of each type of modified oligonucleotide, their benefits and disadvantages, as well as details of less common modifications, can be found in the references cited in Table 1.1. Generally, the 1st generation oligonucleotides, in which the phosphate link is modified, exhibit good resistance to nucleases and good pharmacokinetics however they show poor affinity (lower melting temperature) to their RNA target and can cause sequence-independent toxicity. The 2nd generation oligonucleotides involve modifications at the 2' position of the ribose sugar. Benefits obtained by these modifications include increased hybrid stability, increased nuclease resistance and decreased

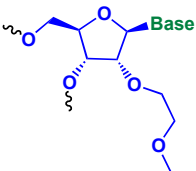
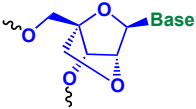
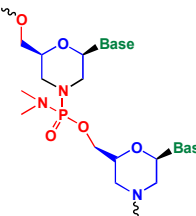
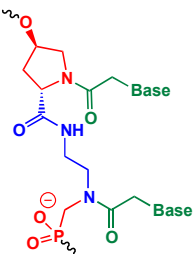
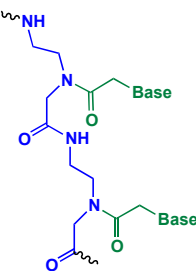
CHAPTER 1 - INTRODUCTION

toxicity, however they are generally unable to activate RNA cleavage by RNase H. The 3rd generation of modified oligonucleotides generally involve an entire different backbone structure and hence the sugar phosphate backbone of natural oligonucleotides has been replaced. With the 3rd generation modifications come resistance to degradation in biological systems and strong mRNA affinity, however they are unable to activate RNase H.^{64,80}

Table 1.1: Modifications of oligonucleotides to increase their drug-like nature

Modified section	Modification ⁶⁴	Modified Structure ⁶⁴	Mechanism of action ^{64,80}	Example Reference	Development stage ^{68,81}
Linkage	Phosphorothioate		RNase H	82	1 st generation
	Boranophosphate		RNase H	83	
	N3'-P5' phosphoramidate		Steric blocking	84	
	N3'-P5' thiophosphoroamidate		Steric blocking	85	
	Phosphonoacetate		RNase H	86	
	Thiophosphonoacetate		RNase H	86	
	Phosphonoformate		RNase H	87	
	Methylphosphonate		Steric blocking	88	
Sugar	2'-Fluor		RNase H	89	2 nd Generation
	2'-O-Methyl		Steric blocking	90	

CHAPTER 1 - INTRODUCTION

	2'-O-Methoxymethyl		Steric blocking	91	
Backbone	Locked Nucleic Acid		Steric blocking	92	3 rd Generation
	Morpholino Phosphorodiamidate		Steric blocking	93	
	Hydroxyproline Backbone		Steric blocking	94	
	Peptide Nucleic Acid		Steric blocking	95	

The implication of various genetic mutations, particularly in the SOD1 gene and the down-regulation of the GluR2 AMPA receptor subunit leading to increased intracellular Ca^{2+} levels and excitotoxicity make ALS a disease suitable for antisense therapy. Antisense drugs that are currently being developed for the treatment of MND include a small interfering RNA to silence mutant SOD1 mRNA⁹⁶⁻⁹⁸ and a phosphorothioate and a 2'-O-(2-methoxy)ethyl-modified antisense oligonucleotide against mutated SOD1 mRNA.⁹⁹

1.2. Peptide Nucleic Acids

1.2.1. Structure, Properties and Applications

Peptide nucleic acids (PNAs) are mimics of DNA in which the phosphodiester backbone is replaced with an achiral *N*-(2-aminoethyl)glycine (pseudopeptide) backbone^{100,101} (Figure 1.9).

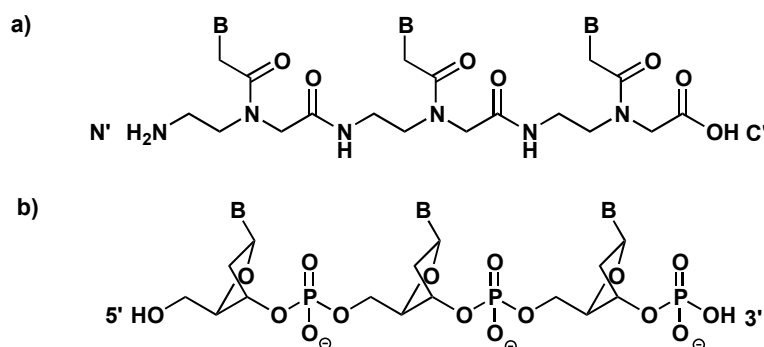


Figure 1.9: a) General structure of PNA; b) General structure of DNA showing terminal nomenclature.

Although they contain an altered backbone, PNAs still contain the same pyrimidine (C and T) and purine (A and G) bases as DNA, attached to the backbone with methylene carbonyl linkers.¹⁰² For this reason, PNA is able to hybridise with complementary DNA or RNA sequences, obeying Watson-Crick base pairing.^{103,104} PNA is able to bind in both parallel and anti-parallel orientations, however the anti-parallel is preferred.¹⁰⁵

As a result of the altered backbone, PNA is considered neutral, not possessing the extensive negatively charged backbones of DNA and RNA. This feature results in minimal electrostatic repulsion between PNA/DNA and PNA/RNA complexes and hence PNA display higher binding affinities and stabilities than DNA in chimeras.¹⁰⁵ This stability is illustrated by an increase in melting temperature, T_m , of approximately 16 °C and 22 °C respectively for PNA/DNA and PNA/RNA complexes compared to the corresponding DNA complexes for a particular sequence.¹⁰³ Melting temperatures are often used as a quantitative measure of strength of binding.

The specificity of PNA has also been found to be superior to that of DNA which is a very important feature in terms of drug development.¹⁰⁵ This is evidenced by a greater discrimination of single base mismatches in the target RNA or DNA by PNA, relative to DNA.^{103,106,107}

A further advantage of PNA is its resistance to endogenous nucleases, proteases and peptidases, which allow PNA to be stable in serum and cellular extracts and therefore have long *in vivo* half lives.^{108,109} The achiral, “unnatural” backbone means PNA are not typical substrates for nucleases. The sequence of amide bonds found in PNA are unlike peptide bonds found in natural polypeptide

chains and are therefore not recognised as substrates for proteases and peptidases.¹⁰⁸

Owing to their high affinity, high specificity and high *in vivo* stability, PNAs have been used for a variety of applications. These include use as a tool in molecular biology and biotechnology,¹¹⁰⁻¹¹⁴ use in diagnostics,^{115,116} use as biosensors^{106,117} and use as therapeutics in an antigenic (binding to DNA) or antisense manner.¹¹⁸⁻¹²¹

1.2.2. Previous Work with PNAs for the Treatment of MND

Work in our laboratory for the treatment of ALS has seen the design, synthesis and biological testing of PNA sequences aimed to down-regulate the GluR3 AMPA receptor subunit and the mutated SOD1 enzyme. The salient aspects of this research will now be summarised.

1.2.2.1. *GluR3 AMPA Subunit Target*

Early work in our laboratory involved the design of a 12mer PNA sequence based on an identified target region from the GluR3 protein that was not conserved in the other AMPA receptor subunits, in other words, a region unique to the GluR3 subunit. The mRNA sequence that produced the amino acids of the target region was deduced. The resultant antisense PNA sequence designed to bind in an anti-parallel fashion to the target region of the GluR3 AMPA receptor subunit mRNA is shown in Figure 1.10.^{53,122}



Figure 1.10: 12mer AS-PNA sequence designed against GluR3.

The ability of the GluR3 12mer AS-PNA to down-regulate GluR3 subunit expression was initially tested *in vitro*.^{53,122} *Neuroblastoma × spinal cord* (NSC-34) cells (from an immortalised cell line) are commonly used as a model system for motor neurone studies as they mimic motor neurones *in vivo*. NSC-34 cells express many morphological and physiological properties of primary motor neurones such as establishing contacts with cultured myotubes, producing and storing acetylcholine, maintaining action potentials, expressing neurofilament proteins and inducing myotube twitching.¹²³ Of greater relevance, these cells were found to express low levels of GluR2 relative to GluR1, 3 and 4 also.¹²² The GluR3 12mer

AS-PNA, and a 12mer nonsense control PNA sequence (NS-PNA) were used to treat NSC-34 cells for 72 hours. The NS-PNA constitutes a scrambled, unrelated sequence and was used to check that PNAs do not exhibit non-specific targeting or toxicity. The cells were then lysed and Western blot analysis with an anti-GluR3 primary antibody was used to analyse the cells' proteins. The GluR3 12mer AS-PNA was repeatedly shown to down-regulate GluR3 expression in a dose-dependent manner, while the nonsense control 12mer sequence showed no change in GluR3 expression (Figure 1.11). This promising result illustrated the therapeutic potential of the GluR3 12mer AS-PNA sequence.

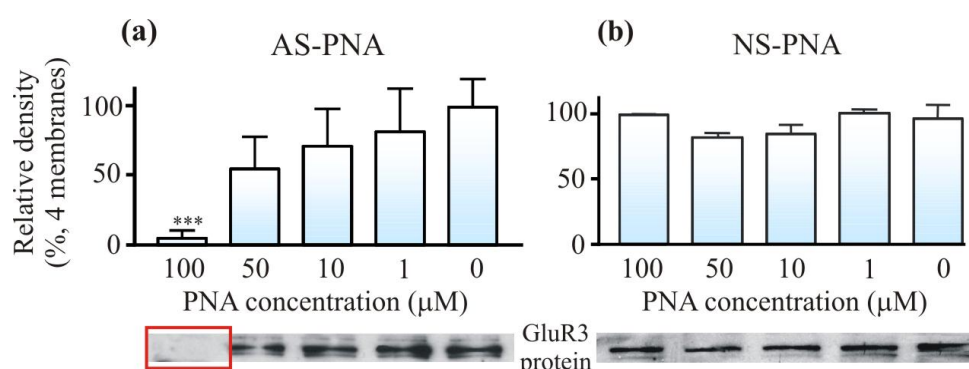


Figure 1.11: Western Blot analysis reveals (a) a dose dependent decrease in GluR3 expression in the presence of AS-PNA; (b) GluR3 expression remains constant in the presence of NS-PNA.¹²²

The effectiveness of the GluR3 12mer AS-PNA was then assessed in SOD1^{G93A} transgenic mice.^{53,122} Twelve mice received AS-PNA treatment (1 mg/kg) while six mice received NS-PNA treatment *via* intraperitoneal (IP) injection three times a week. The progression of the disease was monitored in the mice on a regular basis. It was found that on average, the mice receiving the AS-PNA survived 15 days longer than those mice receiving the NS-PNA, as shown in Figure 1.12 in the Kaplan-Meier survival curve. This is a significant result as it demonstrates that the 12mer AS-PNA effectively minimises the susceptibility of motor neurones to excitotoxicity *in vivo* and hence has the ability to delay disease progression. When considering the human to mouse lifespan ratio, an increased survival of 15 days in AS-PNA treated mice translates to potentially 1.5 years increased survival for humans. This is a considerable result as the increase in survival expected with Riluzole administration is only 2-3 months and it highlights the potential of this 12mer AS-PNA as a viable therapeutic option for MND.

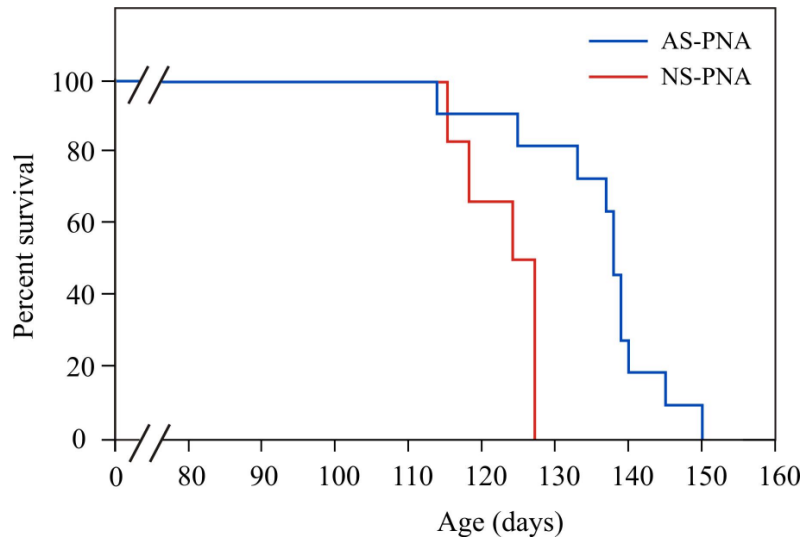


Figure 1.12: Kaplan-Meier survival curve of mice treated with AS-PNA and NS-PNA.¹²²

Furthermore, the onset of hind-limb paralysis was delayed in AS-PNA treated mice, with a difference of 15 days between the two groups (Figure 1.13). Measuring the time it took for the mouse to fall off a rotarod assessed the development of hind limb paralysis. Correlated with hind-limb paralysis is weight loss. It was found that mice treated with the NS-PNA lost more weight than those treated with AS-PNA (Figure 1.14). This is an indication of greater motor neurone and muscle degeneration in NS-PNA treated mice.

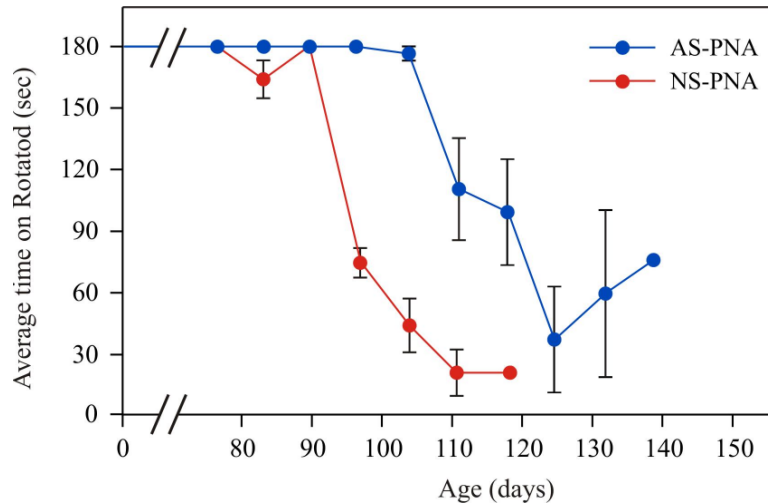


Figure 1.13: Results of Rotarod test that measure hind limb strength. As hind limb strength decreases, the time the mice are able to stay on the Rotarod decreases. The hind limb strength of the AS-PNA treated mice was preserved for longer than that of the NS-PNA treated mice.¹²²

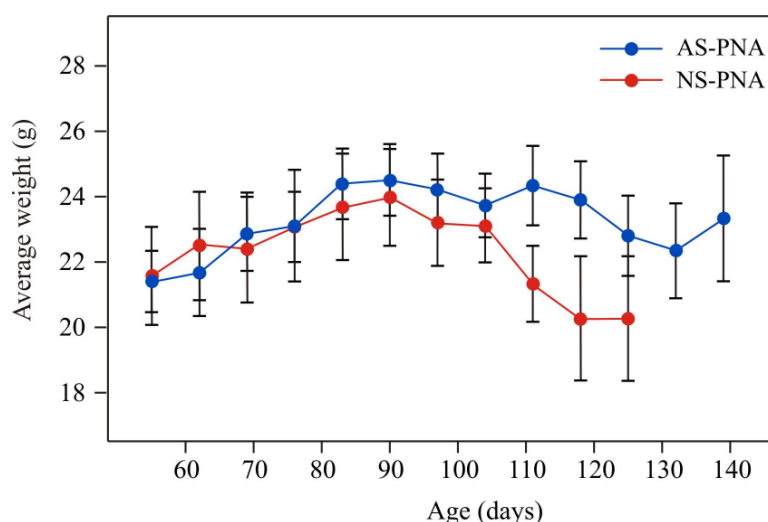


Figure 1.14: Weight loss of mice over time. AS-PNA treated mice displayed less weight loss than NS-PNA treated mice.¹²²

Tissue analysis of the lumbar spinal cord and kidney of the AS-PNA treated mice revealed that there was a slight decrease in GluR3 expression in the kidneys, however there was no change in GluR3 expression in the lumbar spinal cord.^{53,122} Conjugation of fluorescein to the AS-PNA allowed visualisation of its uptake into NSC-34 cells. After one hour of incubation with flu-AS-PNA, a strong fluorescence was seen in the cytoplasm of the NSC-34 cells, however a nuclear stain revealed no flu-AS-PNA in the nuclei of the cells indicating antisense rather than antigene behaviour.^{53,122}

1.2.2.2. *Mutated SOD1 Enzyme Target*

Our research group has also considered the mutated SOD1 enzyme a valuable therapeutic target for the treatment of ALS.¹²² Three 9mer PNA sequences were designed from adjacent regions of the 5' terminus of the human SOD1 mRNA. These regions were the initiation codon, the middle of the 5' region and a region concerned with upstream control. Only one of these sequences, from the middle of the 5' region, displayed any ability to down-regulate the mutated SOD1 enzyme. This sequence (Figure 1.15) was designed to bind in an anti-parallel fashion to the mRNA of mutated SOD1.



Figure 1.15: 9mer AS-PNA sequence designed against SOD1.

In vitro tests using the SOD1 9mer AS-PNA involved NSC-34 cells that had previously been transiently transfected with a plasmid expressing the mutated SOD1 protein.¹²² Initially, Western blot analysis indicated that the SOD1 9mer AS-PNA completely eliminated protein expression, however these results could not be reproduced. It was assumed that poor uptake of the AS-PNA into the cells was responsible for the lack of reproducibility. Therefore, liposomes were used to deliver the PNA into the cell and the subsequent Western blot analysis revealed that the SOD1 9mer AS-PNA, with liposomal delivery, could reproducibly completely inhibit mutated SOD1 expression at the microgram level.

The effectiveness of the SOD1 9mer AS-PNA was then assessed in SOD1^{G93A} transgenic mice.¹²² Seven mice received AS-PNA treatment and seven mice received NS-PNA treatment *via* intraperitoneal (IP) injection three times a week. Treatment started at 60 days of age because this corresponded to the typical age of ALS onset in humans. The progression of the disease was monitored in the mice on a regular basis. It was found that on average, the mice receiving the AS-PNA survived for an average of 5.5 days longer than those mice receiving the NS-PNA, as shown in Figure 1.16 in the Kaplan-Meier survival curve.

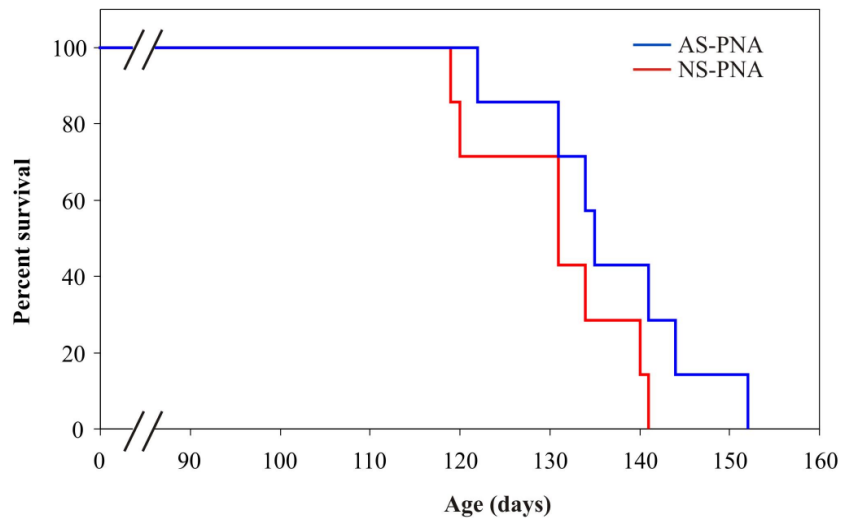


Figure 1.16: Kaplan-Meier survival curve of mice treated with AS-PNA and NS-PNA.¹²²

The onset of hind-limb paralysis (motor impairment) was delayed in AS-PNA treated mice and they were found to be more active in general. However some AS-PNA treated mice exhibited rapid hind-limb deterioration in the later stages of disease progression and so similar end results were observed for the AS and NS

treated mice. It was found that there was no difference in weight change between AS and NS treated mice.

Tissue analysis for the SOD1 protein of the lumbar spinal cord, brain and kidney revealed no difference in protein expression between the AS and NS treated mice. Visualisation of fluorescein-conjugated PNAs revealed that without liposomes to enhance cellular uptake, the PNAs were only located surrounding the cells.

The results described above suggested that the *in vivo* delivery of the SOD1 9mer AS-PNA needed to be improved.¹²² The PNA was conjugated to the cell penetrating peptide (CPP), Tat (Figure 1.17), at the N-terminus of the PNA sequence with two spacer molecules included in-between the peptide and PNA to ensure the PNA was unhindered and the peptide is allowed flexibility.¹²² The Tat peptide belongs to a family of peptides known as “Trojan peptides” that have a general cell-penetrating ability and are therefore often conjugated to other molecules for the purpose of transporting them into cells.¹²⁴

The Tat protein is an 86 amino acid factor involved in activating transcription of HIV and hence essential for gene expression of the virus.¹²⁵ It has been found that cells readily take up this protein.¹²⁵ There are more than 10 peptide fragments of the Tat protein that are known to translocate into the interior of different cell types.¹²⁶ The particular Tat-derived peptide sequence conjugated to the AS and NS PNA sequences by our group was a short peptide from the N-terminal region of the Tat protein¹²² that has been shown to deliver 120 kDa proteins to mice brains by IP injection.¹²⁷

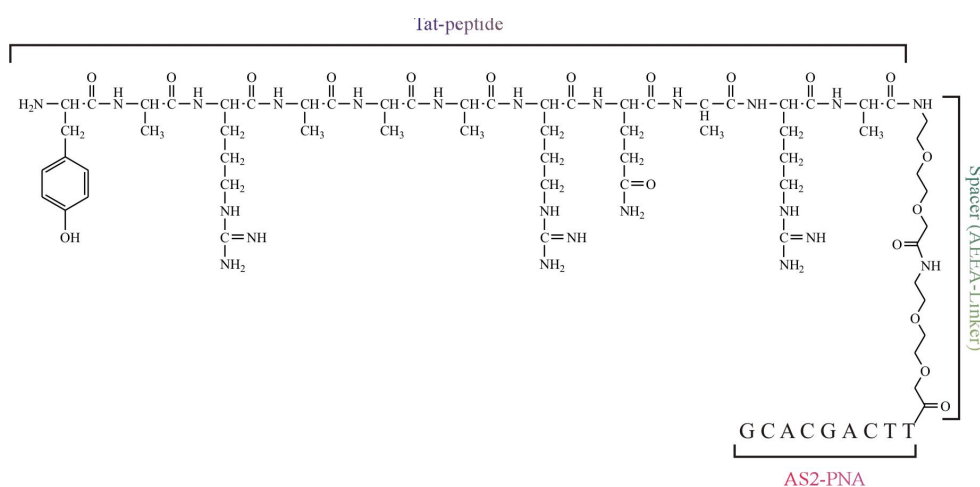


Figure 1.17: Structure of the Tat peptide conjugated to the AS-PNA.¹²²

In vitro studies in which the Tat-PNA was incubated with NSC-34 cells for 72 hours revealed that the Tat-PNA conjugate was able to down-regulate SOD1 expression without the use of liposomes; however delivery of the conjugate with liposomes produced greater inhibition of the mutated SOD1 enzyme.¹²² This indicates that while the conjugated Tat peptide significantly improved the delivery of the PNA, there remained a proportion of PNA unable to enter cells. Figure 1.18 shows that AS-PNA inhibits the human mutant SOD1 enzyme in a dose-dependent manner with as little as 10 μ M PNA showing some inhibition, 100 μ M PNA inhibiting most mutant enzyme, and 200 μ M PNA showing 100% inhibition.

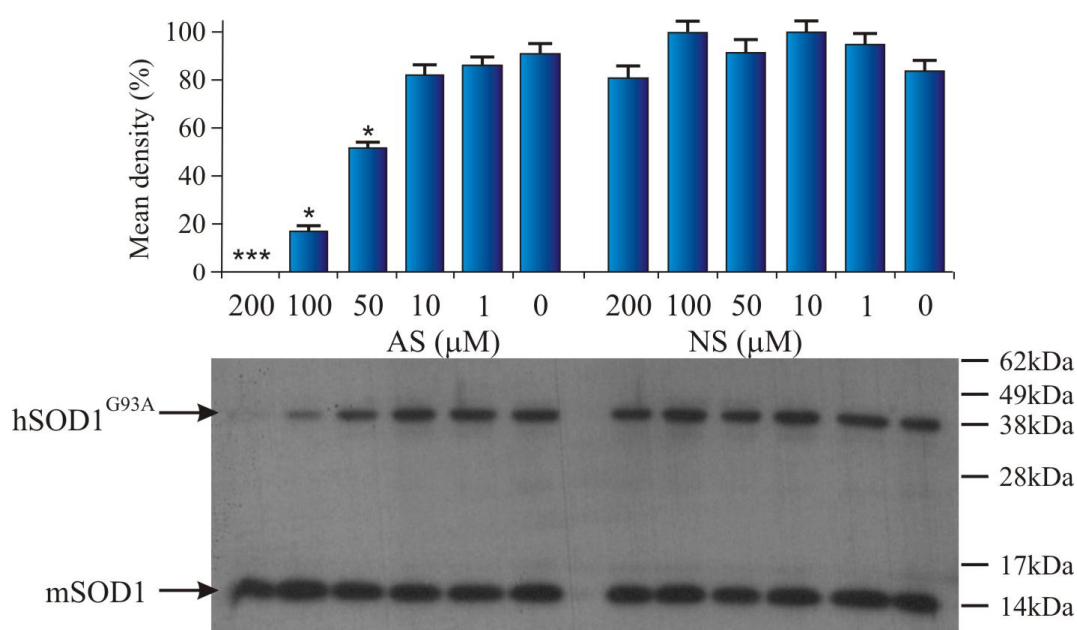


Figure 1.18: Western Blot analysis indicates that AS-PNA shows a dose-dependent inhibition of the human mutant SOD1 enzyme (top band at 38kDa) while this is not observed for the NS-PNA. The lower band at 14kDa represents the mouse SOD1, acting as a protein loading control. *In vitro* results obtained after 72 hours incubation.¹²²

In vivo studies in which mice were injected thrice weekly with 5 mg/kg of either Tat-AS-PNA or Tat-NS-PNA, revealed that Tat-AS-PNA treated mice survived on average for 3.2 days longer than Tat-NS-PNA treated mice (Figure 1.19). Hind-limb strength, average weight and tissue analysis trends appeared similar to those of the non-Tat conjugated PNAs. These results emphasize the great leap that is made from *in vitro* to *in vivo* testing due to the greater number of variables involved with *in vivo* testing.

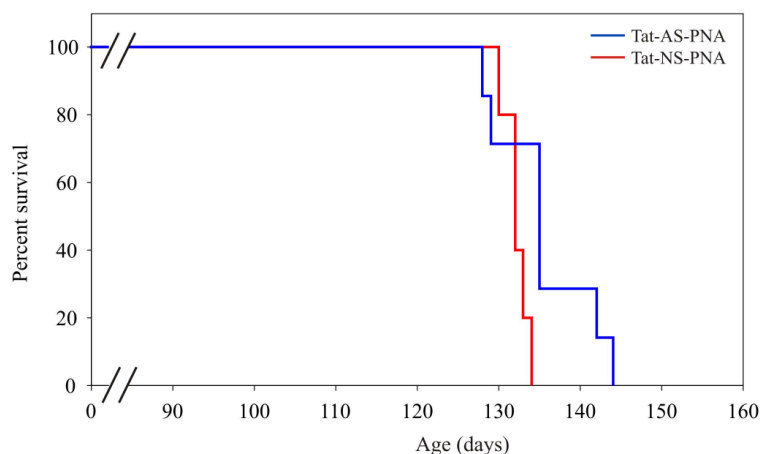


Figure 1.19: Kaplan-Meier survival curve of mice treated with Tat-AS-PNA and Tat-NS-PNA.¹²²

1.2.2.3. Conclusions from Previous Work and Basis for Present Work

The results of the GluR3 12mer PNA indicated the potential of this antisense sequence to be used as an effective therapeutic. The unmodified PNA sequence was able to cross cellular membranes without the use of liposomes or CPPs to suppress the expression of the GluR3 protein and, in a transgenic mouse model, was able to minimise the susceptibility of motor neurones to excitotoxicity and therefore delay disease progression. However, with no evidence of a decrease in GluR3 protein expression in the lumbar spinal cord but a small decrease in GluR3 protein expression in the kidneys, the tissue analysis suggests that the GluR3 12mer PNA is rapidly cleared after systemic administration. Therefore, it can be concluded that the therapeutic effectiveness of the GluR3 12mer PNA could be enhanced if it were directed to neuronal tissue to increase its potency and reduce its rapid clearance from the system.

The results from the SOD1 9mer PNA showed promise in that when cellular uptake was aided, the PNA was able to down-regulate mutated SOD1 expression. The *in vivo* results indicated that the SOD1 9mer PNA was less effective in the mouse model than would have been expected from the *in vitro* results. The attempt to improve the cellular uptake of the PNA and its effectiveness, with the conjugation of Tat, resulted in similar results as those of the unmodified PNA. A reason for this is that while Tat increases cellular uptake, it is non-specific and so the PNA most likely did not sufficiently reach its motor neurone target in the CNS. Furthermore, the PNA could have experienced rapid kidney clearance or the Tat peptide may have been cleaved from the PNA before it was delivered to its target.

Therefore, we concluded that the therapeutic effectiveness of the SOD1 9mer PNA could be enhanced if it were directed to neuronal tissue to increase its potency and reduce its rapid clearance from the system.

The motivation for the present work was to explore options to improve the delivery of the therapeutic PNA sequences to their intended site of action. There are contradicting reports regarding the ability of PNA sequences to cross cellular membranes, suggesting that cellular uptake of PNA could be sequence specific.^{53,128-130} It is widely accepted, however, that unmodified PNAs are unable to cross the blood brain barrier (BBB),¹³¹ or at least only a negligible proportion of the administered dose is able to cross through to the CNS. The inability of the GluR3 12mer PNA and the SOD1 9mer PNA to efficiently cross the BBB and reach their intended site of action is the motivation for the present work.

Another motivation for the present work was to explore small molecule MND treatment options and an alternative or complementary treatment to PNA therapies. Vitamin E is a known antioxidant and naturally occurs to stop free radical propagation in the body. Its natural function is therefore suited to treat MND and the synthesis of many vitamin E derivatives has been the focus of study in our group previously.¹³²⁻¹³⁴ The focus of the present work in terms of vitamin E small molecule treatment of MND is the synthesis of vitamin E derivatives that are able to reach their site of action, motor neurones, in the CNS. Vitamin E, its derivatives and its potential as a small molecule therapeutic for MND treatment are further discussed in Chapter 2.

1.3. PNA and Small Molecule Transport to the CNS

1.3.1. The Blood Brain Barrier

The blood brain barrier (BBB), as its name suggests, is a physical barrier between the brain and the blood. It was first discovered over 100 years ago when it was found that coloured dyes injected into the vascular system entered all organs except for the brain and conversely, dyes injected into the cerebrospinal fluid entered all neuronal tissue but were unable to enter the blood supply of the brain.¹³⁵ It is now known that the BBB (Figure 1.20) is formed by tight junctions between endothelial cells of brain capillaries.^{136,137} The tight junctions thus create an impermeable barrier that does not allow paracellular movement. Effectively,

the permeability of the BBB is inversely proportional to the tightness of the intercellular junctions between endothelial cells. Furthermore, endothelial cells of the brain possess very few endocytotic vesicles and so transcellular movement is limited.¹³⁶ The endothelial cells of brain capillaries also contain oxidative enzymes and peptidases that act as metabolic barriers to many substances attempting to enter the brain.¹³⁸

Tight junction: ●

Adherens junction: ■

P-glycoprotein: ▲

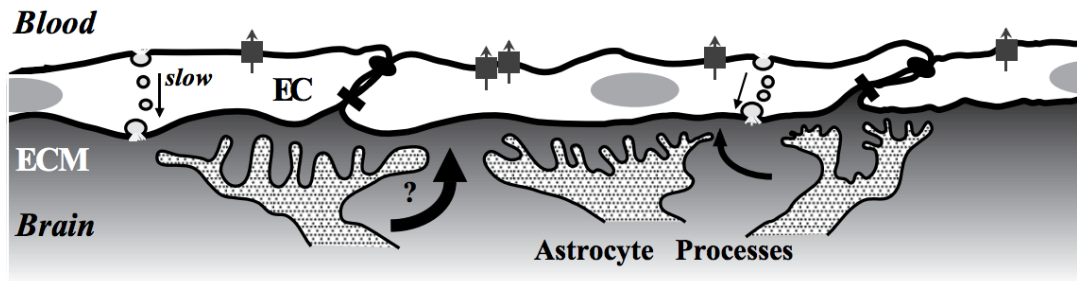


Figure 1.20: Structure of the BBB.¹³⁶

The BBB prevents the passage of most molecules, except those that are small and lipophilic as they can pass through the lipid bilayer of the endothelial cells.^{135,136} However, the P-glycoprotein transporter works to export lipophilic molecules back into the blood stream from endothelial cells.^{135,136} Peptide nucleic acids are unable to cross the BBB because they are too large and hydrophilic.^{131,139}

The purpose of the BBB is to protect the brain from neurotoxins and other unnecessary substances in the blood and only allows vital nutrients and hormones to enter the brain. The passage of desired substances into the brain is made possible by a range of transport systems that are designed to carry specific substances into the brain such as glucose, amino acids and monocarboxylic acids.¹⁴⁰⁻¹⁴⁶ These include facilitated diffusion, carrier mediated, endocytosis and active transport (ATP dependent) mechanisms. Furthermore, it is thought that another purpose of the BBB is to prevent neurotransmitters, that are hydrophilic, from leaving the brain.¹⁴⁰ The brain has a high metabolic rate and so has a large blood supply. It would not be economical if, once secreted, neurotransmitters were swept away in the blood stream and left the brain. With the BBB preventing

the neurotransmitters from leaving the brain, re-uptake mechanisms allow them to be recycled.

1.3.2. Example Transport Mechanisms

There is a number of potential mechanisms by which drugs can be modified to increase their ability to cross the BBB.¹⁴⁷ Table 1.2 lists a summary of some example mechanisms that have been explored to increase BBB transport.

Table 1.2: Mechanisms to transport therapeutic agents across the BBB¹⁴⁸

Transport Mechanism	Type/Explanation	Example	Example reference
Invasive	Neurosurgical implants	Intracerebroventricular infusion, Intranasal drug administration, Intracerebral implants, Convection-enhanced diffusion	149
	BBB disruption: Opening tight junctions or Enhancement of endothelial pinocytosis	Osmotic, Vasoactive (Bradykinin, Histamine, Serotonin), Cytokine-mediated	150
Lipid-mediated	Conjugation of Lipid		
	Carriers to encourage passage through lipid membrane	Dihydropyridine, docosahexanoic acid, adamantane	151
	Incorporation of drug into Liposomes	Small unilamellar vesicles, multivesicular liposomes, immunoliposomes	152
	Incorporation of drug into Nanoparticles	Biodegradable polymers	153
Carrier-mediated transport	Conjugation of or mimic a naturally transported small substrates to utilise endogenous transporter	Hexose, monocarboxylic acid, large neutral amino acid, choline, adenosine, Thyroid hormone	154
Receptor-mediated Transcytosis of peptides	Conjugation <i>via</i> a linker of endogenous peptide or protein to utilise receptor mediated transcytosis	Peptidomimetic monoclonal antibodies, modified plasma proteins, transferrin, insulin-like growth factor, leptin	155

1.3.3. Sugar Conjugates

The sugar transporter of the BBB is GLUT-1, located in the endothelial cell membranes of the brain's blood vessels.¹⁵⁶⁻¹⁵⁹ First cloned in 1985,¹⁶⁰ the glycoprotein contains 492 amino acids and has a molecular weight of 54.2 kDa.¹⁶¹ The GLUT-1 transporter protein is composed of twelve transmembrane, amphipathic α -helices (Figure 1.21).

GLUT-1 is part of the GLUT family of facilitative glucose transporters¹⁶² and functions to transport glucose down its concentration gradient. The transport process is saturable and stereoselective,¹⁶³ and it has been found that GLUT-1 is specific for β -*O*-linked glycosides.¹⁶⁴ GLUT-1 has a 5 mM affinity for D-glucose and a 17 mM affinity for D-galactose,¹⁶³ however, galactosides have been reported to be 1700 times more potent in the brain than glucosides.¹⁶⁵ One explanation for this is that the binding site for GLUT-1 alternates between facing the extracellular side and the cytoplasmic side of the membrane, via a conformational change,¹⁶³ which allows GLUT-1 to act as a bi-directional transporter. GLUT-1 facilitates the movement of glucose out of the brain, but not galactose, thereby keeping the galactoside in the brain.¹⁶⁴

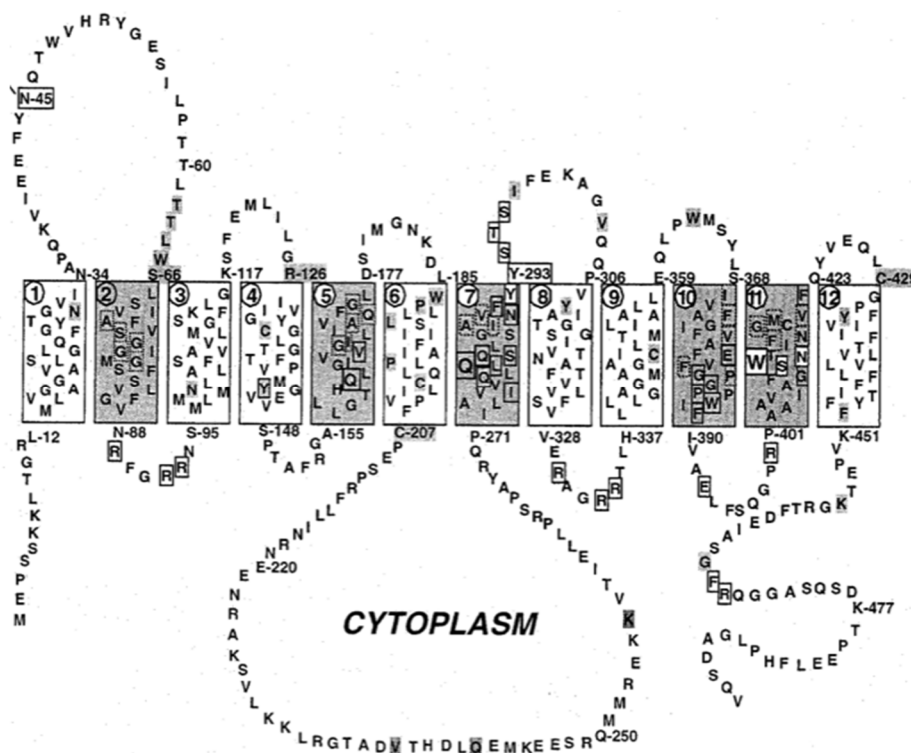


Figure 1.21: Structure of the GLUT-1 transporter protein.¹⁶¹

There have been many reports in the literature of improved drug activity in the brain when glyco- or galacto-conjugates of small molecules¹⁶⁶⁻¹⁶⁹ and peptides^{164,170-172} have been utilised (Figure 1.22).

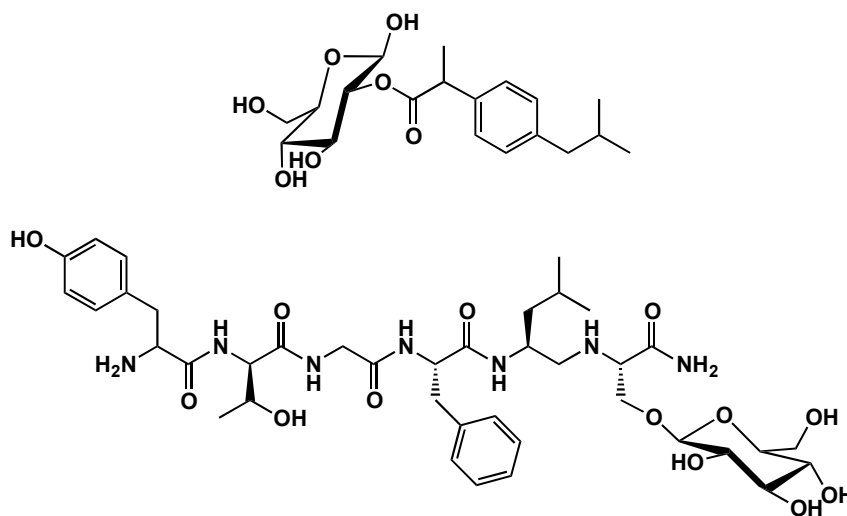


Figure 1.22: Examples of (top) small molecule, Ibuprofen, glycol-derivative¹⁶⁷ and (bottom) peptide, enkephalin, glycol-derivative.¹⁷⁰

It is assumed in these studies that the glycosylated conjugates are taking advantage of the endogenous carrier mediated system of the BBB and that the GLUT-1 transporter protein is responsible for the increased BBB penetration of the drug conjugates. However, subsequent literature suggests that the transport of the glycopeptides *via* GLUT-1 has not been proven.¹⁴⁸ Nevertheless, Gynther *et al.* reported that glyco-ketoprofen and glyco-indomethacin conjugates were able to inhibit brain uptake of radio labelled [¹⁴C]D-glucose in an *in situ* rat brain perfusion model, signalling that these conjugates bind the GLUT-1 transporter and that these conjugates were able to cross the BBB.¹⁶⁶ Furthermore, Dhanasekaran and Polt have shown that glycosylated enkephalin peptides are able to penetrate the BBB and have suggested that their transport is *via* transcytosis.¹³⁸

While the exact mechanism of transport may not always be known or understood, there are many reports of increased BBB penetration leading to increased activity in the CNS of glycosylated derivatives. Possibly contributing to this outcome are the various pharmacokinetic advantages of glycosylated derivatives such as increased hydrophilicity (for formulation and dissolution purposes) and significant plasma half-lives of the conjugates (approximately 80 minutes in serum and more than 7 hours in the brain¹⁶⁴). Therefore, regardless of

the resultant transport mechanism, the conjugation of monosaccharaides is expected to improve the delivery of compounds, both PNA and vitamin E, to the CNS.

1.4. Project Aims

The aims of this project are as follows:

- Explore synthetic methodology and design options to create glycosylated building blocks that can be incorporated into automated solid phase PNA synthesis.
- Synthesise and characterise various glycosylated PNA conjugates.
- Conduct thermodynamic tests to investigate the ability of the glycosylated PNA conjugates to bind their complementary DNA sequences.
- Conduct biomimetic membrane interaction studies to investigate the influence of the conjugated glycosylated building blocks on the ability of the PNA sequence to interact with a biomimetic membrane.
- Explore synthetic methodology and design options to create glycosylated Vitamin E analogues. Antioxidants are considered a small molecule treatment alternative for ALS that could benefit from enhanced delivery to the CNS. This complements other work being undertaken within the group.

1.5. References

1. Sathasivam, S., *Singapore Med. J.*, **2010**, 51, 367-373.
2. Al-Chalabi, A. and Hardiman, O., *Neurodegen. Dis. Manage.*, **2012**, 2, 355-360.
3. Pratt, A., Getzoff, E. D. and Perry, J. J. P., *Degener. Neurol. Neuromuscul. Dis.*, **2012**, 2, 1-14.
4. *Motor Neurone Disease Research Institute of Australia Inc.*, **2012**, <http://www.mndresearch.asn.au/>.
5. Gordon, P. H., *CNS Drugs*, **2011**, 25, 1-15.
6. Johnston, C. A., Stanton, B. R., Turner, M. R., Gray, R., Blunt, A. H., Butt, D., Ampong, M., Shaw, C. E., Leigh, P. N. and Al-Chalabi, A., *J. Neurol.*, **2006**, 253, 1642-1643.
7. Kiernan, M. C., Vucic, S., Cheah, B. C., Turner, M. R., Eisen, A., Hardiman, O., Burrell, J. R. and Zoing, M. C., *Lancet*, **2011**, 377, 942-955.

CHAPTER 1 - INTRODUCTION

8. Nelson, L. M., McGuire, V., Longstreth, W. T. and Matkin, C., *Am. J. Epidemiol.*, **2000**, *151*, 156-163.
9. Gallo, V., Bueno-de-Mesquita, H. B., Vermeulen, R., Andersen, P. M., Kyrozi, A., Linseisen, J., Kaaks, R., Allen, N. E., Roddam, A. W., Boshuizen, H. C., Peeters, P. H., Palli, D., Mattiello, A., Sieri, S., Tumino, R., Jimenez-Martin, J., Diaz, M. J. T., Suarez, L. R., Trichopoulou, A., Agudo, A., Arriola, L., Barricante-Gurrea, A., Bingham, S., Khaw, K., Manjer, J., Lindkvist, B., Overvad, K., Bach, F. W., Tjonneland, A., Olsen, A., Bergmann, M. M., Boeing, H., Clavel-Chapelon, F., Lund, E., Hallmans, G., Middleton, L., Vineis, P. and Riboli, E., *Ann. Neurol.*, **2009**, *65*, 378-385.
10. Weisskopf, M. G. and Ascherio, A., *Ann. Neurol.*, **2009**, *65*, 361-362.
11. Horner, R. D., Kamins, K. G., Feussner, J. R., Grambow, S. C., Hoff-Lindquist, J., Harati, Y., Mitsumoto, H., Pascuzzi, R., Spencer, P. S., Tim, R., Howard, D., Smith, T. C., Ryan, M. A. K., Coffman, C. J. and Kasarskis, E. J., *Neurology*, **2003**, *61*, 742-749.
12. Chio, A., Calvo, A., Dossena, M., Ghiglione, P., Mutani, R. and Mora, G., *Amyotroph. Lateral Sc.*, **2009**, *10*, 205-209.
13. Chio, A., *J. Neurol.*, **1999**, *246*, III/1-III/5.
14. Rowland, L. P. and Shneider, N. A., *N. Engl. J. Med.*, **2001**, *344*, 1688-1700.
15. Phukan, J., Elamin, M., Bede, P., Jordan, N., Gallagher, L., Byrne, S., Lynch, C., Pender, N. and Hardiman, O., *J. Neurol. Neurosurg. Psychiatry*, **2012**, *83*, 102-108.
16. Lomen-Hoerth, C., Murphy, J., Langmore, S., Kramer, J. H., Olney, R. K. and Miller, B., *Neurology*, **2003**, *60*, 1094-1097.
17. Miller, R. G., Jackson, C. E., Kasarskis, E. J., England, J. D., Forshe, D., Johnston, W., Kalra, S., Mitsumoto, H., Rosenfeld, J., Shoesmith, C., Strong, M. J. and Woolley, S. C., *Neurology*, **2009**, *73*, 1227-1233.
18. Arnulf, I., Similowski, T., Salachas, F., Garma, L., Mehiri, S., Attali, V., Behin-Bellhesen, V., Meininger, V. and Derenne, J., *Am. J. Respir. Crit. Care Med.*, **2000**, *161*, 849-856.
19. Strong, M. J., *J. Neurol. Sci.*, **2010**, *288*, 1-12.
20. Millicamps, S., Salachas, F., Cazeneuve, C., Gordon, P., Bricka, B., Camuzat, A., Guillot-Noel, L., Russaouen, O., Bruneteau, G., Pradat, P., Le Forestier, N., Vandenberghe, N., Danel-Brunaud, V., Guy, N., Thauvin-Robinet, C., Lacomblez, L., Couratier, P., Hannequin, D., Seilhean, D., Le Ber, I., Corcia, P., Camu, W., Brice, A., Rouleau, G., LeGuern, E. and Meininger, V., *J. Med. Genet.*, **2010**, *47*, 554-560.

CHAPTER 1 - INTRODUCTION

21. DeJesus-Hernandez, M., Mackenzie, I. R., Boeve, B. F., Boxer, A. L., Baker, M., Rutherford, N. J., Nicholson, A. M., Finch, N. A., Flynn, H., Adamson, J., Kouri, N., Wojtas, A., Sengdy, P., Hsiung, G. R., Karydas, A., Seeley, W. W., Josephs, K. A., Coppola, G., Geschwind, D. H., Wszolek, Z. K., Feldman, H., Knopman, D. S., Petersen, R. C., Miller, B. L., Dickson, D. W., Boylan, K. B. and Graff-Radford, N. R., *Neuron*, **2011**, 72, 245-256.
22. Lee, T., Li, Y. R., Ingre, C., Weber, M., Grehl, T., Gredal, O., de Carvalho, M., Meyer, T., Tysnes, O., Auburger, G., Gispert, S., Bonini, N. M., Andersen, P. M. and Glitler, A. D., *Hum. Mol. Genet.*, **2011**, 20, 1697-1700.
23. Beckman, J. S., Carson, M., Smith, C. D. and Koppenol, W. H., *Nature*, **1993**, 364, 584.
24. Wiedau-Pazos, M., Goto, J. J., Rabizadeh, S., Gralla, E. B., Roe, J. A., Lee, M. K., Valentine, J. S. and Bredesen, D. E., *Science*, **1996**, 271, 515-518.
25. Bruiln, L. I., Beal, M. F., Becher, M. W., Schulz, J. B., Wong, P. C., Price, D. L. and Cleveland, D. W., *Proc. Natl. Acad. Sci. U.S.A.*, **1997**, 94, 7606-7611.
26. Rosen, D. R., Siddique, T., Patterson, D., Figlewicz, D. A., Sapp, P., Hentati, A., Donaldson, D., Goto, J., O'Regan, J. P., Deng, H., Rahmani, Z., Krizus, A., McKenna-Yasek, D., Cayabyab, A., Gaston, S. M., Berger, R., Tanzi, R. E., Halperin, J. J., Herzfeldt, B., Van den Bergh, R., Hung, W., Bird, T., Deng, G., Mulder, D. W., Smyth, C., Laing, N. G., Soriano, E., Pericak-Vance, M. A., Haines, J., Rouleau, G. A., Gusella, J. S., Horvitz, H. R., & Brown, R. H., *Nature*, **1993**, 362, 59-62.
27. Maruyama, H., Morino, H., Ito, H., Izumi, Y., Kato, H., Watanabe, Y., Kinoshita, Y., Kamada, M., Nodera, H., Suzuki, H., Komure, O., Matsuura, S., Kobatake, K., Morimoto, N., Abe, K., Suzuki, N., Aoki, M., Kawata, A., Hirai, T., Kato, T., Ogasawara, K., Hirano, A., Takumi, T., Kusaka, H., Hagiwara, K., Kaji, R. and Kawakami, H., *Nature*, **2010**, 465, 223-227.
28. McCord, J. M. and Fridovich, I., *J. Biol. Chem.*, **1969**, 244, 6049-6055.
29. Cleveland, D. and Rothstein, J., *Nat. Rev. Neurosci.*, **2001**, 2, 806-819.
30. Barber, S. C. and Shaw, P. J., *Free Radical Biol. Med.*, **2010**, 48, 629-641.
31. Shaw, P. J. and Eggett, C. J., *J. Neurol.*, **2000**, 247, I/17-I/27.
32. Deng, H., Hentati, A., Tainer, J. A., Iqbal, Z., Cayabyab, A., Hung, W., Getzoff, E. D., Hu, P., Herzfeldt, B., Roos, R. P., Warner, C., Deng, G., Soriano, E., Smyth, C., Parge, H. E., Ahmed, A., Roses, A. D., Hallewell, R. A., Pericak-Vance, M. A. and Siddique, T., *Science*, **1993**, 261, 1047-1051.
33. Crow, J. P., Sampson, J. B., Zhuang, Y., Thompson, J. A. and Beckman, J. S., *J. Neurochem.*, **1997**, 69, 1936-1944.

CHAPTER 1 - INTRODUCTION

34. Estevez, A. G., Crow, J. P., Sampson, J. B., Reiter, C., Zhuang, Y., Richardson, G. J., Tarpey, M. M., Barbeito, L. and Beckman, J. S., *Science*, **1999**, 286, 2498-2500.
35. Maragakis, N. J. and Rothstein, J. D., *Arch. Neurol.*, **2001**, 58, 365-370.
36. Rothstein, J. D., Tsai, G., Kuncl, R. W., Clawson, L., Cornblath, D. R., Drachman, D. B., Pestronk, A., Stauch, B. L. and Coyle, J. T., *Ann. Neurol.*, **1990**, 228, 18-25.
37. Shaw, P. J., Forrest, V., Ince, P. G., Richardson, J. P. and Wastell, H. J., *Neurodegeneration*, **1995**, 4, 209-216.
38. Rothstein, J. D., Martin, L. J. and Kuncl, R. W., *N. Engl. J. Med.*, **1992**, 326, 1464-1468.
39. Rothstein, J. D., Dykes-Hoberg, M., Pardo, C. A., Bristol, L. A., Jin, L., Kuncl, R. W., Kanai, Y., Hedlger, M. A., Wang, Y., Schielke, J. P. and Welty, D. F., *Neuron*, **1996**, 16, 675-686.
40. Rothstein, J. D., Van Kammen, M., Levey, A. I., Martin, L. J. and Kuncl, R. W., *Ann. Neurol.*, **1995**, 38, 73-84.
41. Bristol, L. A. and Rothstein, J. D., *Ann. Neurol.*, **1996**, 39, 676-679.
42. Choi, D. W., *Trends Neurosci.*, **1988**, 11, 465-469.
43. Mark, L. P., Prost, R. W., Ulmer, J. L., Smith, M. M., Daniels, D. L., Strottmann, J. M., Brown, W. D. and Hacein-Bey, L., *Am. J. Neuroradiol.*, **2001**, 22, 1813-1824.
44. Hollmann, M. and Heinemann, S., *Annu. Rev. Neurosci.*, **1994**, 17, 31-108.
45. Shaw, P. J., *J. Neurol. Sci.*, **1994**, 124 (Suppl.), 6-13.
46. Hollmann, M., Hartley, M. and Heinemann, S., *Science*, **1991**, 252, 851-853.
47. Sommer, B., Kohler, M., Sprengel, R. and Seeburg, P. H., *Cell*, **1991**, 67, 11-19.
48. Pellegrini-Giampietro, D. E., Gorter, J. A., Bennett, M. V. L. and Zukin, R. S., *Trends Neurosci.*, **1997**, 20, 464-470.
49. Kawahara, Y., Kwak, S., Sun, H., Ito, K., Hashida, H., Aizawa, H., Jeong, S. and Kanazawa, I., *J. Neurochem.*, **2003**, 85, 680-689.
50. Takuma, H., Kwak, S., Yoshizawa, T. and Kanazawa, I., *Ann. Neurol.*, **1999**, 46, 806-815.
51. Virgo, L., Samarasinghe, S. and de Belleruche, J., *Neuroreport*, **1996**, 7, 2507-2511.

CHAPTER 1 - INTRODUCTION

52. Tortarolo, M., Grignaschi, G., Calvaresi, N., Zennaro, E., Spaltro, G., Colovic, M., Fracasso, C., Guiso, G., Elger, B., Schneider, H., Seilheimer, B., Caccia, S. and Bendotti, C., *J. Neurosci. Res.*, **2006**, *83*, 134-146.
53. Rembach, A., Turner, B. J., Bruce, S., Cheah, I. K., Scott, R. L., Lopes, E. C., Zagami, C. J., Beart, P. M., Cheung, N. S., Langford, S. J. and Cheema, S. S., *J. Neurosci. Res.*, **2004**, *77*, 573-582.
54. Doble, A., *Neurology*, **1996**, *47*, S233-S241.
55. Barnham, K. J., Masters, C. L. and Bush, A. I., *Nat. Rev. Drug Discovery*, **2004**, *3*, 205-214.
56. Miller, R. G., Mitchell, J. D., Lyon, M. and Moore, D. H., *Cochrane Database Syst. Rev.*, **2007**, *CD001447*, 1-28.
57. Bensimon, G., Lacomblez, L. and Meininger, V., *N. Engl. J. Med.*, **1994**, *330*, 585-591.
58. *Australian Government, Department of Health and Ageing*, **2013**, <http://www.pbs.gov.au/medicine/item/8664B>.
59. Lee, S., Su, Z., Emdad, L., Gupta, P., Sarkar, D., Borjabad, A., Volsky, D. and Fisher, P. B., *J. Biol. Chem.*, **2008**, *283*, 13116-13123.
60. Rothstein, J. D., Patel, S., Regan, M. R., Haenggell, C., Huang, Y. H., Bergles, D. E., Jin, L., Hoberg, M. D., Vldensky, S., Chung, D. S., Toan, S. V., Bruljn, L. I., Su, Z., Gupta, P. and Fisher, P. B., *Nature*, **2005**, *433*, 73-77.
61. Kalmar, B., Novoselov, S., Gray, A., Cheetham, M. E., Margulis, B. and Greensmith, L., *J. Neurochem.*, **2008**, *107*, 339-350.
62. Kieran, D., Kalmar, B., Dick, J. R. T., Riddoch-Contreras, J., Burnstock, G. and Greensmith, L., *Nat. Med.*, **2004**, *10*, 402-405.
63. Watanabe, K., Morinaka, Y., Iseki, K., Wantanabe, T., Yuki, S. and Nishi, H., *Redox Rep.*, **2003**, *8*, 151-155.
64. Crooke, S. T., Vickers, T., Lima, W. and Wu, H. In *Antisense Drug Technology: Principles, Strategies and applications*; Crooke, S. T., Ed.; CRC Press: Boca Raton, 2008; Vol. 2nd Edition, p 5-46.
65. Kole, R., Krainer, A. R. and Altman, S., *Nat. Rev. Drug Discovery*, **2012**, *11*, 125-140.
66. Sazani, P. and Kole, R., *J. Clin. Invest.*, **2003**, *112*, 481-486.
67. Baker, B. F., Lot, S. S., Condon, T. P., Cheng-Flournoy, S., Lesmik, E. A., Sasmor, H. M. and Bennett, C. F., *J. Biol. Chem.*, **1997**, *272*, 11994-12000.
68. Mansoor, M. and Melendez, A. J., *Gene Regul. Syst. Bio.*, **2008**, *2*, 275-295.

CHAPTER 1 - INTRODUCTION

69. Brown-Driver, V., Eto, T., Lesnik, E., Anderson, K. P. and Hanecak, R. C., *Antisense Nucleic Acid Drug Dev.*, **1999**, 9, 145-154.
70. Baker, B. F., *J. Am. Chem. Soc.*, **1993**, 115, 3378-3379.
71. Vickers, T. A., Wyatt, J. R., Burckin, T., Bennett, C. F. and Freier, S. M., *Nucleic Acids Res.*, **2001**, 29, 1293-1299.
72. Hausen, P. and Stein, H., *Eur. J. Biochem.*, **1970**, 14, 278-283.
73. Crooke, S. T., *Curr. Mol. Med.*, **2004**, 4, 465-487.
74. Agrawal, S., Jiang, Z., Zhao, Q., Shaw, D., Cai, Q., Roskey, A., Channavajjala, L., Saxinger, C. and Zhang, R., *Proc. Natl. Acad. Sci. U.S.A.*, **1997**, 94, 2620-2625.
75. Holen, T., Amarzguioui, M., Babaie, E. and Prydz, H., *Nucleic Acids Res.*, **2003**, 31, 2401-2407.
76. Kim, V. N. and Nam, J., *Trends Genet.*, **2006**, 22, 165-173.
77. Freier, S. M. and Watt, A. T. In *Antisense Drug Technology: Principles, Strategies and Applications*; Crooke, S. T., Ed.; CRC Press: Boca Raton, 2008; Vol. 2nd.
78. Way, K. J., Chou, E. and King, G. L., *Trends Pharmacol. Sci.*, **2000**, 21, 181-187.
79. Stephenson, M. L. and Zamecnik, P. C., *Proc. Natl. Acad. Sci. U.S.A.*, **1978**, 75, 285-288.
80. Malik, R. and Roy, I., *Expert Opin. Drug Discov.*, **2011**, 6, 507-526.
81. Chen, X., Dudgeon, N., Shen, L. and Wang, J., *Drug Discov. Today*, **2005**, 10, 587-593.
82. Eckstein, F., *Antisense Nucleic Acid Drug Dev.*, **2000**, 10, 117-121.
83. Summers, J. S. and Shaw, B. R., *Curr. Med. Chem.*, **2001**, 8, 1147-1155.
84. Faria, M., Spiller, D. G., Dubertret, C., Nelson, J. S., White, M. R. H., Scherman, D., Helene, C. and Giovannangeli, C., *Nat. Biotechnol.*, **2001**, 19, 40-44.
85. Pongracz, K. and Gryaznov, S., *Tetrahedron Lett.*, **1999**, 40, 7661-7664.
86. Sheehan, D., Lunstad, B., Yamada, C. M., Stell, B. G., Caruthers, M. H. and Dellinger, D. J., *Nucleic Acids Res.*, **2003**, 31, 4109-4188.
87. Yamada, C. M., Dellinger, D. J. and Caruthers, M. H., *J. Am. Chem. Soc.*, **2006**, 128, 5251-5261.
88. Hamma, T. and Miller, P. S., *Antisense Nucleic Acid Drug Dev.*, **2003**, 13, 19-30.

CHAPTER 1 - INTRODUCTION

89. Li, F., Sarkhel, S., Wilds, C. J., Wawrzak, Z., Prakash, T. P., Manoharan, M. and Eglo, M., *Biochemistry*, **2006**, *45*, 4141-4152.
90. Prakash, T. P., Allerson, C. R., Dande, P., Vickers, T. A., Sioufi, N., Jarres, R., Baker, B. F., Swayze, E. E., Griffey, R. H. and Bhat, B., *J. Med. Chem.*, **2005**, *48*, 4247-4253.
91. Teplova, M., Minasov, G., Tereshko, V., Inamati, G. B., Cook, P. D., Manoharan, M. and Egli, M., *Nat. Struct. Biol.*, **1999**, *6*, 535-539.
92. Jepsen, J. S., Sorensen, M. D. and Wengel, J., *Oligonucleotides*, **2004**, *14*, 130-146.
93. Summerton, J., *Biochim. Biophys. Acta*, **1999**, *1489*, 141-158.
94. Efimov, V., Birikh, K. R., Staroverov, D. B., Lukyanov, S. A., Tereshina, M. B., Zarsky, A. G. and Chakhmakhcheva, O. G., *Nucleic Acids Res.*, **2006**, *34*, 2247-2257.
95. Doyle, D. F., Braasch, D. A., Simmons, C. G., Janowski, B. A. and Corey, D. R., *Biochemistry*, **2001**, *40*, 53-64.
96. Miller, T. M., Kaspar, B. K., Kops, G. J., Yamanaka, K., Christian, L. J., Gage, F. H. and Cleveland, D. W., *Ann. Neurol.*, **2005**, *57*, 773-776.
97. Ralph, G. S., Radcliffe, P. A., Day, D. M., Carthy, J. M., Leroux, M. A., Lee, D. C. P., Wong, L., Bilsland, L. G., Greensmith, L., Kingsman, S. M., Mitrophanous, K. A., MAzarakis, N. D. and Azzouz, M., *Nat. Med.*, **2005**, *11*, 429-433.
98. Raoul, C., Abbas-Terki, T., Bensadoun, J., Guillot, S., Haase, G., Szulc, J., Henderson, C. E. and Aebischer, P., *Nat. Med.*, **2005**, *11*, 423-428.
99. Smith, R. A., Miller, T. M., Yamanaka, K., Monia, B. P., Condon, T. P., Hung, G., Lobsiger, C. S., Ward, C. M., McAlonis-Downes, M., Wei, H., Wancewicz, E. V., Bennett, F. and Cleveland, D. W., *J. Clin. Invest.*, **2006**, *116*, 2290-2296.
100. Nielsen, P. E., Egholm, M., Berg, R. H. and Buchardt, O., *Science*, **1991**, *254*, 1497-1500.
101. Egholm, M., Buchardt, O., Nielsen, P. E. and Berg, R. H., *J. Am. Chem. Soc.*, **1992**, *114*, 1895-1897.
102. Dueholm, K. L., Egholm, M., Behrens, C., Christensen, L., Hansen, H. F., Vulpius, T., Petersen, K. H., Berg, R. H., Nielsen, P. E. and Buchardt, O., *J. Org. Chem.*, **1994**, *59*, 5767-5773.
103. Egholm, M., Buchardt, O., Christensen, L., Behrens, C., Freier, S. M., Driver, D. A., Berg, R. H., Kim, S. K., Norden, B. and Nielsen, P. E., *Nature*, **1993**, *365*, 566-568.

CHAPTER 1 - INTRODUCTION

104. Egholm, M., Nielsen, P. E., Buchardt, O. and Berg, R. H., *J. Am. Chem. Soc.*, **1992**, *114*, 9677-9678.
105. Nielsen, P. E. and Egholm, M. In *Peptide Nucleic Acids Protocols and Application*; Nielsen, P. E., Ed.; Horizon Bioscience: Trowbeidge, 2004; Vol. 2nd Edition, p 1-36.
106. Wang, J., Palecek, E., Nielsen, P. E., Rivas, G., Cai, X., Shiraishi, H., Dontha, N., Luo, D. and Farias, P. A. M., *J. Am. Chem. Soc.*, **1996**, *118*, 7667-7670.
107. Jensen, K. K., Orum, H., Nielsen, P. E. and Norden, B., *Biochemistry*, **1997**, *36*, 5072-5077.
108. Demidov, V., Potaman, V., Frank-Kamenetski, M., Egholm, M., Buchard, O., Sonnichsen, S. and Nielsen, P., *Biochem. Pharmacol.*, **1994**, *48*, 1310-1313.
109. Dean, D. A., *Adv. Drug Delivery Rev.*, **2000**, *44*, 81-95.
110. Demidov, V., Frank-Kamenetskii, M. D., Egholm, M., Buchardt, O. and Nielsen, P. E., *Nucleic Acids Res.*, **1993**, *21*, 2103-2107.
111. Demers, D. B., Curry, E. T., Egholm, M. and Sozer, A. C., *Nucleic Acids Res.*, **1995**, *23*, 3050-3055.
112. Orum, H., Nielsen, P. E., Jorgensen, M., Larsson, C., Stanley, C. and Koch, T., *BioTechniques*, **1995**, *19*, 472-480.
113. Perry-O'Keefe, H., Yao, X., Coull, J. M., Fuchs, M. and Egholm, M., *Proc. Natl. Acad. Sci. U.S.A.*, **1996**, *93*, 14670-14675.
114. Veselkov, A. G., Demidov, V. V., Nielsen, P. E. and Frank-Kamenetskii, M. D., *Nucleic Acids Res.*, **1996**, *24*, 2483-2487.
115. Carlsson, C., Jonsson, M., Norden, B., Dulay, M. T., Zare, R. N., Noolandi, J., Nielsen, P. E., Tsul, L. and Zielenski, J., *Nature*, **1996**, *380*, 207.
116. Thiede, C., Bayerdorffer, E., Blasczyk, R., Wittig, B. and Neubauer, A., *Nucleic Acids Res.*, **1996**, *24*, 983-984.
117. Hook, F., Ray, A., Norden, B. and Kasemo, B., *Langmuir*, **2001**, *17*, 8305-8312.
118. Hanvey, J. C., Pepper, N. J., Bisi, J. E., Thomson, S. A., Cadilla, R., Josey, J. A., Ricca, D. J., Hassman, F., Bonham, M. A., Karin, G. A., Carter, S. G., Bruckenstein, D. A., Boyd, A. L., Noble, S. A. and Babiss, L. E., *Science*, **1992**, *258*, 1481-1485.
119. Nielsen, P. E., Egholm, M., Berg, R. H. and Buchardt, O., *Anti-Cancer Drug Des.*, **1993**, *8*, 53-63.

CHAPTER 1 - INTRODUCTION

120. Boffa, L. C., Morris, P. L., Carpaneto, E. M., Louissaint, M. and Allfrey, V. G., *J. Biol. Chem.*, **1996**, 271, 13228-13233.
121. Nielsen, P. E., *Chem. Biodiversity*, **2010**, 7, 786-804.
122. Cheah, I. K., PhD Thesis *Antisense peptide nucleic acids as therapeutic agents for the treatment of neurodegeneration*, Monash University, **2006**.
123. Cashman, N. R., Durham, H. D., Blusztajn, J. B., Oda, K., Tabira, T., Shaw, I. T., Dahrouge, S. and Antel, J. P., *Dev. Dynam.*, **1992**, 194, 209-221.
124. Koppelhus, U., Awasthi, S. K., Zachar, V., Holst, H. U., Ebbesen, P. and Nielsen, P. E., *Antisense Nucleic Acid Drug Dev.*, **2002**, 12, 51-63.
125. Green, M. and Loewenstein, P. M., *Cell*, **1988**, 55, 1179-1188.
126. Lindgren, M., Hllbrink, M., Prochiantz, A. and Langel, U., *Trends Pharmacol. Sci.*, **2000**, 21, 99-103.
127. Schwarze, S. R., Ho, A., Vocero-Akbani, A. and Dowdy, S. F., *Science*, **1999**, 285, 1569-1572.
128. Wittung, P., Kajanus, J., Edwards, K., Nielsen, P. E., Norden, B. and Malmstrom, B. G., *FEBS Lett.*, **1995**, 365, 27-29.
129. Turner, B. J., Cheah, I. K., Macfarlane, K. J., Lopes, E. C., Petratos, S., Langford, S. J. and Cheema, S. S., *J. Neurochem.*, **2003**, 87, 752-763.
130. Koppelhus, U. and Nielsen, P. E., *Adv. Drug Delivery Rev.*, **2003**, 55, 267-280.
131. Pardridge, W. M., Boado, R. J. and Kang, Y., *Proc. Natl. Acad. Sci. U.S.A.*, **1995**, 92, 5592-5596.
132. Macfarlane, K. J., PhD Thesis, *Small molecules and peptide nucleic acids for the treatment and prevention of neurodegeneration.*, Monash University, **2004**.
133. Unthank, J., PhD thesis, *Novel 'dual-action' agents for the treatment and prevention of neurodegenerative disorders*, Monash University, **2006**.
134. Wood, L., PhD thesis, *Molecular approaches tot he treatment of motor neuron degeneration*, Monash University, **2012**.
135. Risau, W. and Wolburg, H., *Trends Neurosci.*, **1990**, 13, 174-178.
136. Rubin, L. L. and Staddon, J. M., *Annu. Rev. Neurosci.*, **1999**, 22, 11-28.
137. Reese, T. S. and Karnovsky, M. J., *J. Cell Biol.*, **1967**, 34, 207-217.
138. Dhanasekaran, M. and Polt, R., *Curr. Drug Delivery*, **2005**, 2, 59-73.
139. Pardridge, W. M., *J. Neurochem.*, **1998**, 70, 1781-1792.

CHAPTER 1 - INTRODUCTION

140. Bradbury, M. W., *Exp. Physiol.*, **1993**, 78, 453-472.
141. Pardridge, W. M., *Am. Physiological. Soc.*, **1983**, 63, 1481-1535.
142. Pardridge, W. M., *Neurochem. Res.*, **1998**, 23, 635-644.
143. Oldendorf, W. H., *Am. J. Physiol.*, **1973**, 224, 1450-1453.
144. Vannucci, S. J., Maher, F. and Simpson, I. A., *Glia*, **1997**, 21, 2-21.
145. Maresh, G. A., Kastin, A. J., Brown, T. T., Zadina, J. E. and Banks, W. A., *Brain Res.*, **1999**, 839, 336-340.
146. Ermisch, A., Brust, P., Kretzschmar, R. and Ruhle, H., *Physiol. Rev.*, **1993**, 73, 489-527.
147. Pardridge, W. M., *J. Cereb. Blood Flow Metab.*, **2012**, 32, 1959-1972.
148. Pardridge, W. M. *Brain Drug Targeting. The future of brain drug development.*; Cambridge University Press: New York, 2001.
149. Laske, D. W., Youle, R. J. and Oldfield, E. H., *Nat. Med.*, **1997**, 3, 1362-1368.
150. Neuwelt, E. A., Barnett, P. A., Bigner, D. D. and Frenkel, E. P., *Proc. Natl. Acad. Sci. U.S.A.*, **1982**, 79, 4420-4423.
151. Bodor, N. and Simpkins, J. W., *Science*, **1983**, 221, 65-67.
152. Huwyler, J., Wu, D. and Pardridge, W. M., *Proc. Natl. Acad. Sci. U.S.A.*, **1996**, 93, 14164-14169.
153. Alyautdin, R. N., Petrov, V. E., Langer, K., Berthold, A., Kharkevich, D. A. and Kreuter, J., *Pharm. Res.*, **1997**, 14, 325-328.
154. Tsuji, A. and Tamai, I., *Adv. Drug Delivery Rev.*, **1999**, 36, 277-290.
155. Wu, D., Yang, J. and Pardridge, W. M., *J. Clin. Invest.*, **1997**, 100, 1804-1812.
156. Birnbaum, M. J., Haspel, H. C. and Rosen, O. M., *Proc. Natl. Acad. Sci. U.S.A.*, **1986**, 83, 5784-5788.
157. Boado, R. J. and Pardridge, W. M., *Biochem. Biophys. Res. Commun.*, **1990**, 166, 174-179.
158. Pardridge, W. M., Boado, R. J. and Farrell, C. R., *J. Biol. Chem.*, **1990**, 265, 18035-18040.
159. Boado, R. J. and Pardridge, W. M., *Mol. Cel. Neurosci.*, **1990**, 1, 224-232.
160. Mueckler, M., Caruso, C., Baldwin, S. A., Panico, M., Blench, I., Morris, H. R., Allard, W. J., Lienhard, G. E. and Lodish, H. F., *Science*, **1985**, 229, 941-945.

CHAPTER 1 - INTRODUCTION

161. Hruz, P. W. and Mueckler, M. M., *Mol. Membr. Biol.*, **2001**, *18*, 183-193.
162. Bell, G. I., Kayano, T., Buse, J. B., Burant, C. F., Takeda, J., Lin, D., Fukumoto, H. and Seino, S., *Diabetes Care*, **1990**, *13*, 198-208.
163. Bell, G. I., Burant, C. F., Takeda, J. and Gould, G. W., *J. Biol. Chem.*, **1993**, *268*, 19161-19164.
164. Polt, R., Porreca, F., Szabo, L. Z., Bilsky, E. J., Davis, P., Abbruscato, T. J., Davis, T. P., Horvath, R., Yamamura, H. I. and Hruby, V. J., *Proc. Natl. Acad. Sci. U.S.A.*, **1994**, *91*, 7114-7118.
165. Rodriguez, R. E., Rodriguez, F. D., Sacristan, M. P., Torres, J. L., Valencia, G. and Anton, J. M. G., *Neurosci. Lett.*, **1989**, *101*, 89-94.
166. Gynther, M., Ropponen, J., Laine, K., Leppanen, J., Haapakoski, P., Peura, L., Jarvinen, T. and Rautio, J., *J. Med. Chem.*, **2009**, *52*, 3348-3353.
167. Chen, Q., Gong, T., Liu, J., Wang, X., Fu, H. and Zhang, Z., *J. Drug Target.*, **2009**, *17*, 318-328.
168. Bonina, F. P., Puglia, C., Rimoli, M. G., Melisi, D., Boatto, G., Nieddu, M., Calignano, A., La Rana, G. and De Caprariis, P., *J. Drug Target.*, **2003**, *11*, 25-36.
169. Bonina, F. P., Loredana, A., Ippolito, R., Boatto, G., Battaglia, G., Bruno, V. and de Caprariis, P., *Int. J. Pharm.*, **2000**, *202*, 79-88.
170. Eggleton, R. D., Mitchell, S. A., Huber, J. D., Palian, M. M., Polt, R. and Davis, T. P., *J. Pharm. Exp. Ther.*, **2001**, *299*, 967-972.
171. Tomatis, R., Marastoni, M., Balboni, G., Guerrini, R., Capasso, A., Sorrentino, L., Santagada, V., Caliendo, G., Lazarus, L. and Salvadori, S., *J. Med. Chem.*, **1997**, *40*, 2948-2952.
172. Negri, L., Lattanzi, R., Tabacco, F., Scolaro, B. and Rocchi, R., *Br. J. Pharmacol.*, **1998**, *124*, 1516-1522.

CHAPTER 2

GLYCOSYL ESTERS AND VITAMIN E

DERIVATIVES

Chapter 2. Glycosyl Esters and Vitamin E Derivatives

2.1. Introduction

2.1.1. Vitamin E as a Treatment for MND

In biological systems, polyunsaturated fatty acids are the most likely components to be oxidised through lipid peroxidation.¹ If unchecked, lipid peroxidation can be fatal to a cell because the oxidation of polyunsaturated fatty acids has the potential to destroy all biological membranes. Lipid peroxidation involves a free radical chain mechanism of initiation, propagation and termination (Figure 2.1). Radical initiation is caused by hydrogen abstraction from the lipid molecule. The newly formed carbon-centred radical then rapidly reacts with molecular oxygen to form a peroxy radical. This then reacts with another lipid molecule to form a new carbon-centred radical and a peroxide, and so the chain continues. The chain is broken when two lipid radicals react to form a molecular product.

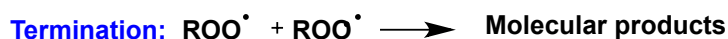
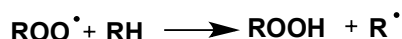
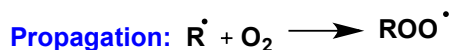


Figure 2.1: Lipid peroxidation free radical chain mechanism. In = initiator; RH = general lipid.²

Biological systems are normally protected from this destructive chain mechanism by natural antioxidants. Vitamin E is a known natural antioxidant and, as such, functions to stop free radical propagation. Figure 2.2 shows the four related structures that are referred to as vitamin E. α -Tocopherol is the most abundant form of vitamin E, and the most biologically active.¹

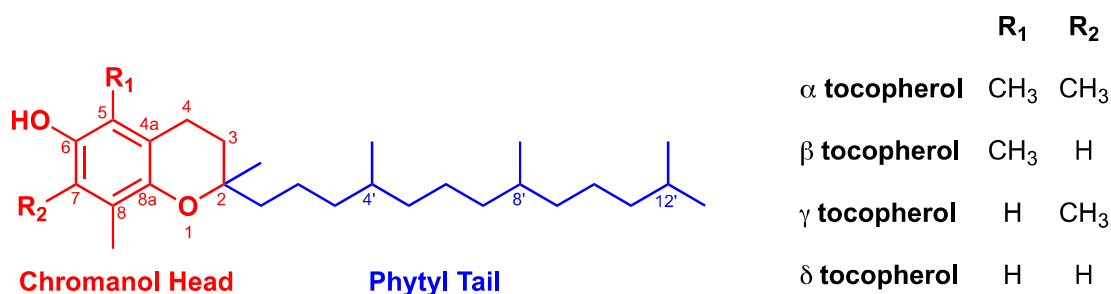


Figure 2.2: The general structure of vitamin E. This term refers to four structurally related tocopherols. α-Tocopherol is the most naturally abundant and biologically active.

Vitamin E is a lipid soluble antioxidant due to its phytyl 'tail', which allows it to be located in biological lipid membrane bilayers with the chromanol head most likely positioned towards the surface of the bilayer, and the lipophilic tail embedded in the centre of the bilayer with the hydrocarbon portions of the phospholipids.^{1,3,4} As such, it is a very efficient lipid peroxyl radical scavenger. The chromanol head of vitamin E is the moiety that gives the molecule its antioxidant ability. Abstraction of the phenolic hydrogen by a radical species results in a phenoxyl radical, which is resonance stabilized around the benzopyran unit. The oxygen of the benzopyran located in the *para* position allows for effective hydrogen donation by the phenolic group as well as contributes to canonical forms of the formed radical (Figure 2.3). The stability of the phenoxyl radical means that the radical chain is not continued.

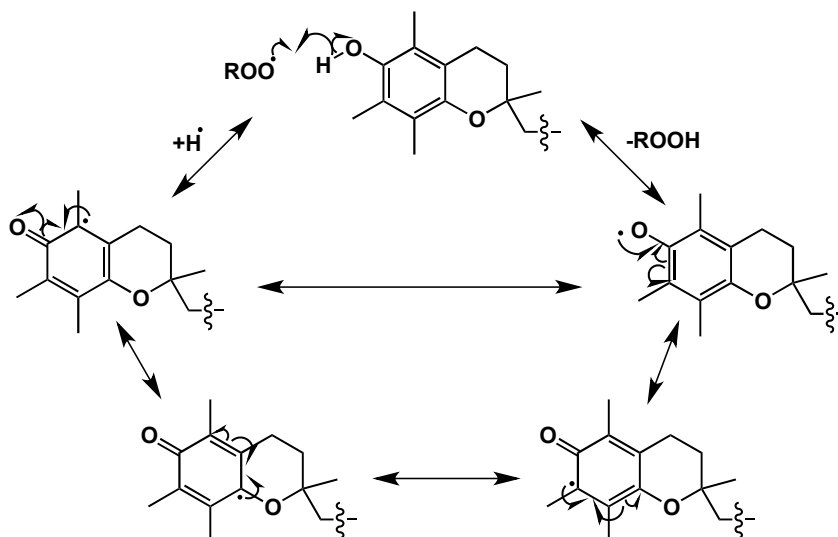


Figure 2.3: Resonance forms of vitamin E stabilise the generated radical giving rise to a potent antioxidant.

One of the possible causes of MND is oxidative stress - a result of a dysfunctional SOD1 enzyme.^{5,6} Owing to its antioxidant properties, vitamin E has been tested as a treatment for ALS. In one study, vitamin E was administered to transgenic mice carrying the mutant form of the human SOD1 gene.⁷ It was found that vitamin E significantly delayed the onset of the disease, defined as the point in time when shaking of mouse limbs occurs when it is suspended in the air by its tail, and significantly delayed the progression of the disease as measured by running in a wheel. Vitamin E, however, failed to extend survival of the transgenic mice.⁷ In human clinical trials, results have indicated that the use of natural antioxidants is not effective at increasing survival or motor function.⁸⁻¹⁰ It has been suggested that regular use of vitamin E supplements can reduce the risk of dying from ALS, with the risk decreasing with increasing time of use.¹¹

Plasma and cerebral spinal fluid (CSF) levels of vitamin E after daily oral administration have been quantified and while plasma vitamin E levels increased in a dose-dependent manner, CSF levels did not change.¹² A probable explanation for this is that vitamin E does not cross the BBB.^{12,13} It is likely that vitamin E is too lipophilic to pass through the BBB quickly and instead remains bound to the lipoproteins that transport it in the blood,¹⁴ or imbedded in membrane bilayers, restricting transbilayer movement.¹⁵ Furthermore, because vitamin E is not water soluble, it is not readily absorbed after oral administration.¹⁵ Therefore in order to utilise the efficient antioxidant properties of vitamin E to treat ALS, derivitisation is required to improve its delivery to the CNS.

2.1.2. Vitamin E Derivatives

The development of vitamin E derivatives has generally aimed to increase the water solubility of the natural, highly lipophilic antioxidant.¹⁵ Trolox (Figure 2.4) is a water soluble derivative of vitamin E first synthesised in 1974.¹⁶ Trolox does not contain the long hydrocarbon tail of vitamin E but instead a highly ionisable carboxylic acid group. It is known to be an effective antioxidant in both animal fats and vegetable oils¹⁶ and it has also been found to be more potent than α -tocopherol,¹⁷ most likely as a result of its ability to scavenge radicals in the aqueous phase.¹⁸ Further to this, it has been found that the antioxidant activity of Trolox derivatives decreased with increasing side-chain length from a methyl

group to the 16-carbon chain of α -tocopherol.³ Structure-activity relationship (SAR) analysis has revealed that the phenolic hydroxyl group of Trolox is essential for its antioxidant activity: esterification or etherification of the phenol resulted in inactive derivatives.¹⁶ The presence of the chromanol nucleus was also found to be essential for antioxidant activity.¹⁶

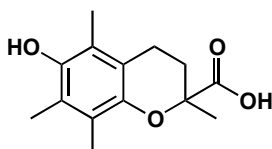


Figure 2.4: Structure of Trolox.

With the aim of improving the hydrophilicity and therefore the delivery and membrane transport of vitamin E, glycosylated vitamin E derivatives have been synthesised.^{15,19-22} A common glycosylated vitamin E derivative is shown in Figure 2.5, in which the phenolic hydroxyl group has been glycosylated.^{15,19-21}

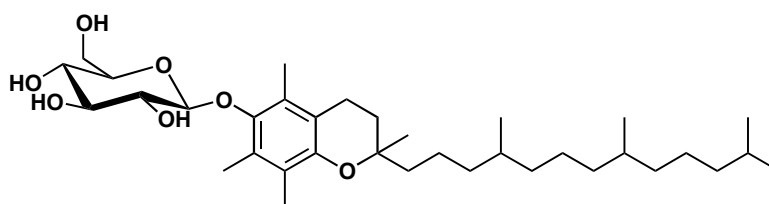


Figure 2.5: Structure of a glycosylated vitamin E derivative.

It was found that vitamin E derivatives that have been glycosylated at the phenolic position display improved membrane transport compared to vitamin E,¹⁵ and good stability in the presence of exoglycosides in various rat tissues.²² In order to be an effective antioxidant, the sugar moiety of such vitamin E derivatives would need to be cleaved *in vivo* to reveal the phenolic hydroxyl group.¹⁹

Other examples^{21,23} of glycosylated vitamin E derivatives are shown in Figure 2.6. In these examples, the sugar moiety is attached to either the *ortho* or *meta* positions relative to the phenolic hydroxyl group, leaving the phenolic hydroxyl group free, while increasing the hydrophilicity of the antioxidant.²¹ Interestingly, the parent vitamin E was a more efficient antioxidant than any of the glycosylated derivatives shown in Figure 2.6.^{21,23} This may be due to the electronic and steric effects of the sugar moiety causing the deactivation of the phenolic core, since glycosyl derivatives reacted less rapidly compared to the parent vitamin E.

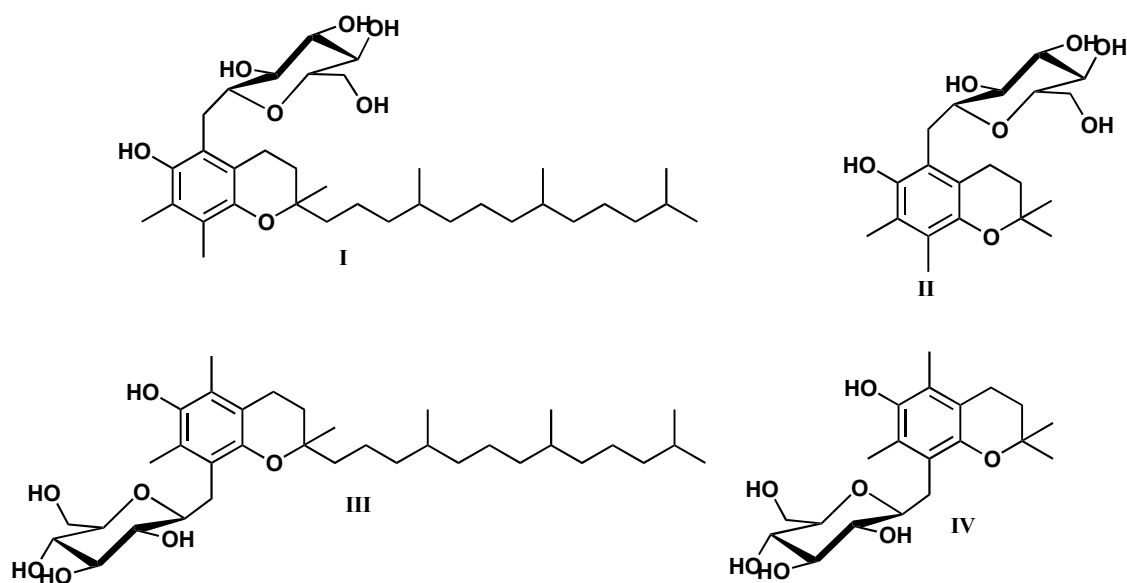


Figure 2.6: Structures of some glycosylated vitamin E derivatives with free phenolic groups.

The position of the sugar moiety was found to be the most influential factor determining antioxidant activity with *meta*-substituted derivatives (III and IV Figure 2.6) shown to be better inhibitors of lipid peroxidation than *ortho*-substituted derivatives (I and II Figure 2.6).^{21,23} While the presence or absence of the phytyl tail influenced the hydrophilicity of the antioxidant, it did not influence the antioxidant activity of the derivatives.

Yet another class of glycosylated vitamin E derivatives involves the glycosylation of the reduced form of Trolox. 2-(α -D-Glucopyranosyl)methyl-2,5,7,8-tetramethylchroman-6-ol (TMG) (Figure 2.7) was synthesised by enzymatic transglycosylation by α -glucosidase using maltose as the source of glucose.²⁴

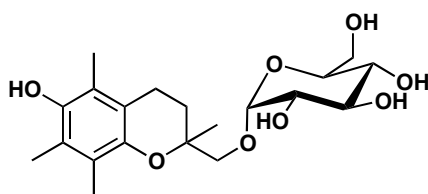


Figure 2.7: Structure of TMG.

The water solubility of TMG was found to be very high compared with other vitamin E derivatives and its free radical scavenging ability was found to be comparable to vitamin E, Trolox and ascorbic acid²⁴ and hence the sugar moiety of TMG does not affect the antioxidant ability of the chromanol core.²⁵ Furthermore, TMG has been shown to be effective against radicals in the aqueous phase.²⁵ In

subsequent studies, TMG was found to be effective in the treatment of colitis in rats²⁶ and acute lung injury.²⁷ The structure of TMG therefore appears to combine the advantages of increased hydrophilicity without sacrificing the antioxidant ability of the chromanol core. To the best of our knowledge, there have not been any studies performed to determine the activity of TMG in the CNS and hence its BBB penetrating ability.

2.1.3. Aims and Synthetic Plan

The antioxidant ability of vitamin E suggests it could be a complimentary treatment option to antisense therapies for ALS. In order for it to be effective, the hydrophilicity of the antioxidant needs to be improved to provide for increased CNS delivery. Glycosylated vitamin E derivatives have been shown to possess improved membrane penetration and good antioxidant ability.

Therefore, the overall aim of this chapter of work is to investigate synthetic routes and methodologies towards the synthesis of new glycosylated vitamin E derivatives. Continuing from the promising results of TMG, glycosylated vitamin E derivative targets in which the phytol tail of natural vitamin E is replaced with a sugar moiety are the aim of this chapter of work. Figure 2.8 depicts the general structure of the targeted glycosylated vitamin E derivative. The aim of this chapter is to explore synthetic routes and methodologies to produce the β -glycosyl ester derivatives of glucose and galactose.

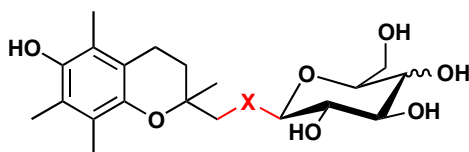


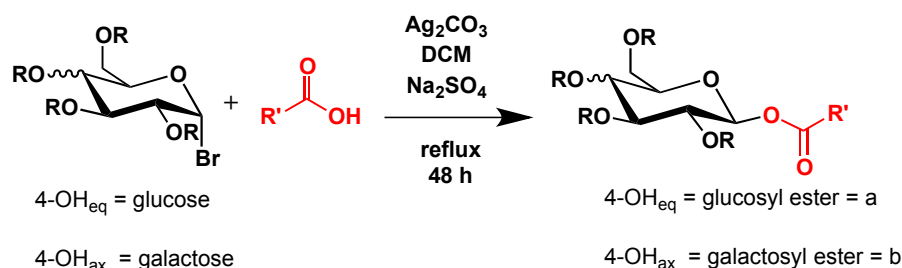
Figure 2.8: Proposed general structure of glycosylated vitamin E targets.

2.2. Results and Discussion

2.2.1. Glucosyl and Galactosyl Ester Library

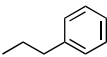
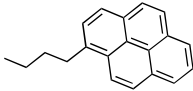
A variation of the traditional Koenigs-Knorr glycosylation method using silver carbonate as a promoter was used as the general approach explored in this chapter. Table 2.1 summarises the range of carboxylic acids coupled to either glucose or galactose to produce β -glycosyl esters, in generally good to excellent yields using this approach. A general reaction scheme for the library generated is

shown in Scheme 2.1. The carboxylic acids chosen relate to alkyl, allyl and aryl acids and purely relate to readily available compounds within our laboratory. Both acetyl and benzoyl protected sugars were employed to increase the scope of the reaction.



Scheme 2.1

Table 2.1: Results of glycosyl and galactosyl library, synthesised as shown in **Scheme 2.1**

Compound	R	R'	Yield % glycosyl ester (a)	Yield % galactosyl ester (b)
1	Ac	phenyl	98	99
2	Ac	nonyl	96	98
3	Ac		76	81
4	Ac	methyl	98	94
5	Ac		69	41
6	Ac	naphthyl	77	79
7	Ac	allyl	11	47
8	Bz	phenyl	49	60
9	Bz	nonyl	56	49

Reactions were undertaken using an excess of Ag₂CO₃. In each case, a 20 times excess of the promoter was needed to avoid a significant drop in product yield. The reaction was also better served at elevated temperatures than when the reactions were carried out at ambient temperature.

The ¹H NMR spectra of all compounds showed a consistent pattern (for example, Figure 2.9). In particular, a coupling constant of *ca.* 8 Hz was always observed for the signal attributable to the anomeric proton, indicating diaxial

coupling between the anomeric proton and the adjacent H-2 proton, consistent with β -glycoside configuration. The α -anomer was not observed.

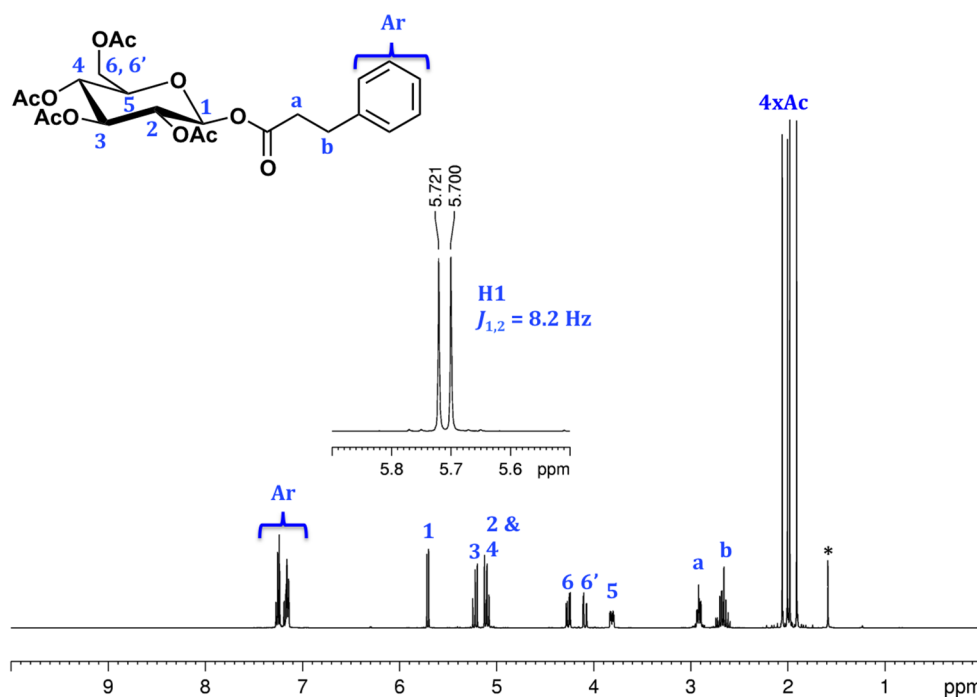


Figure 2.9: 400 MHz ^1H NMR spectrum of **3a** (CDCl_3 , 300 K). * denotes residual solvent

Single crystals of **1a** suitable for analysis were grown by vapour diffusion from dichloromethane and hexane. The solved structure (Figure 2.10) shows the expected diaxial orientation of *H*-1 and *H*-2 and, as a consequence, the β -orientation of the benzoate substituent at *C*-1.

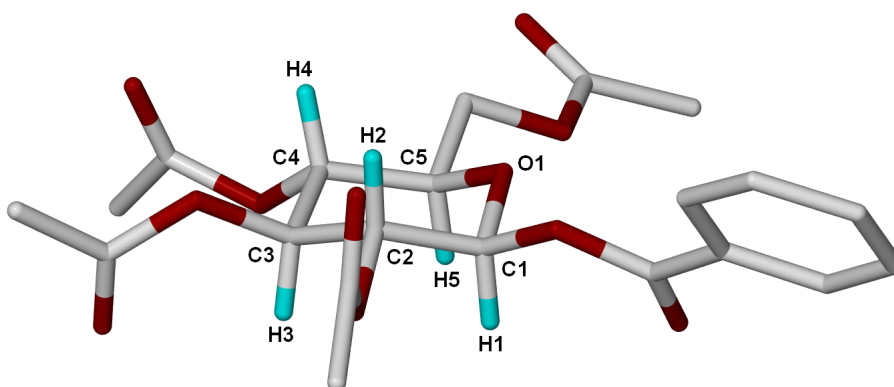
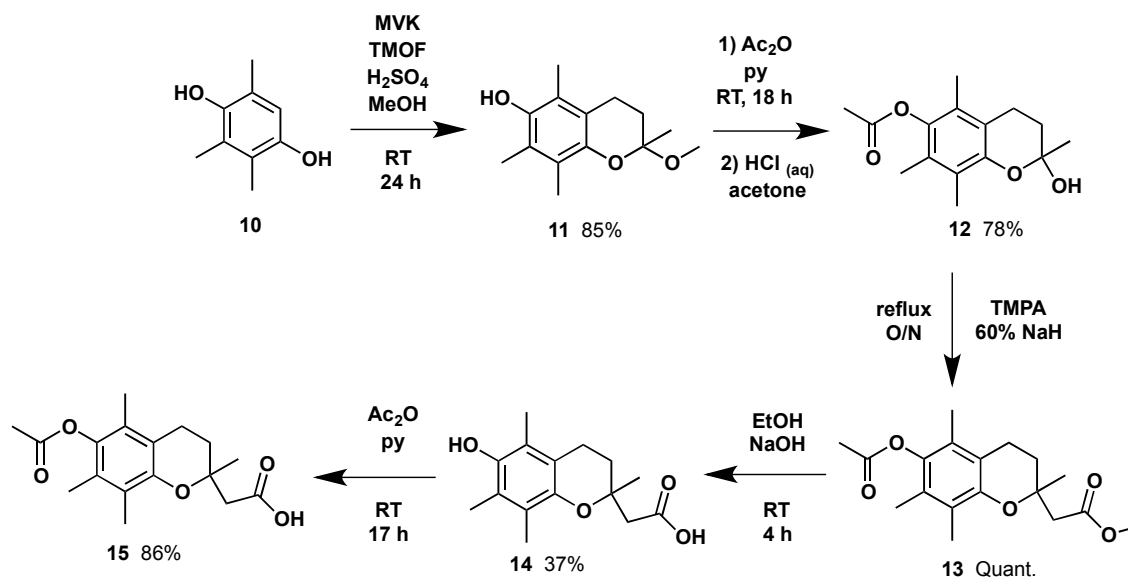


Figure 2.10: Stick representation of the X-ray structure of $\text{C}_{21}\text{H}_{24}\text{O}_{11}$. The absolute configuration of the molecule was not determined by the X-ray diffraction experiment but was inferred from the synthesis.

2.2.2. Synthesis of Novel Vitamin E Glycosyl Esters

Scheme 2.2 depicts the synthesis of a Trolox-like compound, **14**, containing an additional methylene group at the C-2 position. This synthesis is based on the total synthesis of vitamin E by Scott.²⁸



Scheme 2.2

2,3,5-Trimethylhydroquinone **10** was reacted with methyl vinyl ketone under acid-catalysed conditions to produce the methyl acetal **11** in 85% yield. One of the advantages of the conditions used is that the product precipitates from solution. ¹H NMR spectroscopy supported product formation and the presence of a set of two signals at approximately 2.6 ppm and another set of two signals at approximately 2.0 ppm, representing the adjacent pair of ring methylene protons, became characteristic for the rest of the synthetic strategy. ¹³C NMR spectroscopy also supported product formation with the presence of signals at 32.3 and 20.4 ppm indicating the presence of the ring CH₂ groups and a peak at 97.6 ppm corresponding to the quaternary acetal carbon. The ESI mass spectrum also supported product formation with a signal at *m/z* 259.2 corresponding to the [M+Na]⁺ ion. Methyl acetal **11** was produced as a mixture of enantiomers that were taken all the way to the final product **15**.

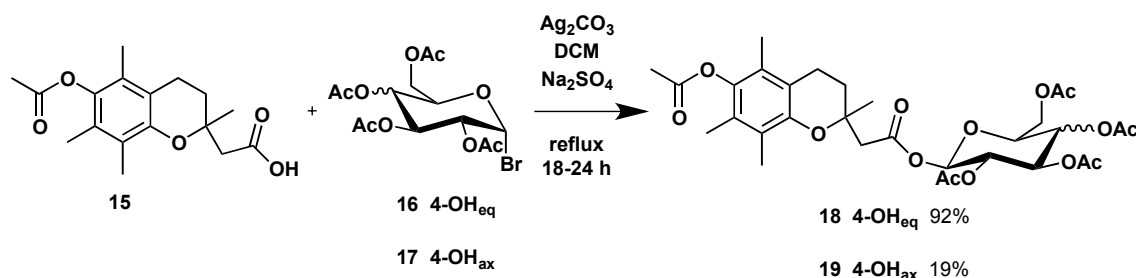
Acetylation of phenol **11** using acetic anhydride in pyridine proceeded smoothly, resulting in a yellow oil product that was clean enough to use without further purification. The ¹H NMR spectrum gave evidence for the presence of the

protecting group with a singlet at 2.33 ppm representing the acetate methyl protons. The ^{13}C NMR also supported the presence of the acetate protecting group with signals at 168.8 and 19.8 ppm. The ESI mass spectrum also supported product formation with a signal at m/z 301.2 corresponding to the $[\text{M}+\text{Na}]^+$ ion. Acid-catalysed conversion of the acetal **11** to the hemiacetal **12** was driven by the removal of the produced methanol using distillation.

A variation on the Horner-Wadsworth-Emmons reaction using trimethyl phosphonoacetate (TMPA) and sodium hydride yielded the methyl acetate **13** in quantitative yield. The yellow oil product was used in the final reaction in its crude form. ESI mass spectrometry supported product formation with a signal at m/z 343.3 corresponding to the $[\text{M}+\text{Na}]^+$ ion.

Conversion of the acetate and ester groups of **13** to the phenol and carboxylic acid groups, respectively, was accomplished simultaneously using sodium hydroxide in ethanol. Recrystallisation twice from ethanol/water gave pure **14** in 37% yield. The ^1H NMR and ^{13}C NMR spectra supported product formation with the absence of peaks representing both methyl groups as well as the carbonyl group of the acetate protecting group of **13**. The ESI mass spectrum also supported product formation with a signal at m/z 287.2 corresponding to the $[\text{M}+\text{Na}]^+$ ion. Reprotection of the phenol, so as to not complicate the esterification of the carboxylic acid group, was achieved using acetic anhydride to give **15** in 86% yield after HPLC purification. No attempt was made to prepare enantiopure **15** at this point.

Glycosylation conditions optimised in Section 2.2.1 were then used to prepare the tocopherol glycosyl ester **18** and tocopherol galactosyl ester **19** (Scheme 2.3).



Scheme 2.3

Column chromatography (silica, 1% (v/v) MeOH/DCM) was used to isolate **18** in 92% yield as a mixture of diastereomers. ^1H NMR spectroscopy shows evidence

of the presence of both diastereomers caused by the chiral centre at C-2 of vitamin E. While complicated, both ^1H and ^{13}C NMR support formation of the glycosyl ester. The J value of each of the doublets representing $H-1$ is 8.3 Hz, which is consistent with diaxial coupling between $H-1$ and $H-2$ and hence β -substitution of the glycosyl ester.

To evaluate the best purification method of the vitamin E conjugates, reverse phase HPLC, rather than column chromatography, was used to isolate **19** in 19% yield. The unusually low yield for the formation of the galactosyl ester is unknown. This reaction was not repeated in an attempt to improve the yield as a more favourable synthetic procedure was used instead, see Section 2.2.3. High resolution mass spectrometry supported product formation with a peak corresponding to the sodium adduct of **19** at m/z 659.2303. As was the case with **18**, the ^1H NMR spectrum of **19** showed evidence of the presence of both diastereomers with two overlapping doublets for the H -1 proton at 5.73 ppm and 5.71 in the ^1H NMR spectrum (Figure 2.11) and two peaks for C -1 at 92.30 and 92.26 ppm in the ^{13}C NMR spectrum.

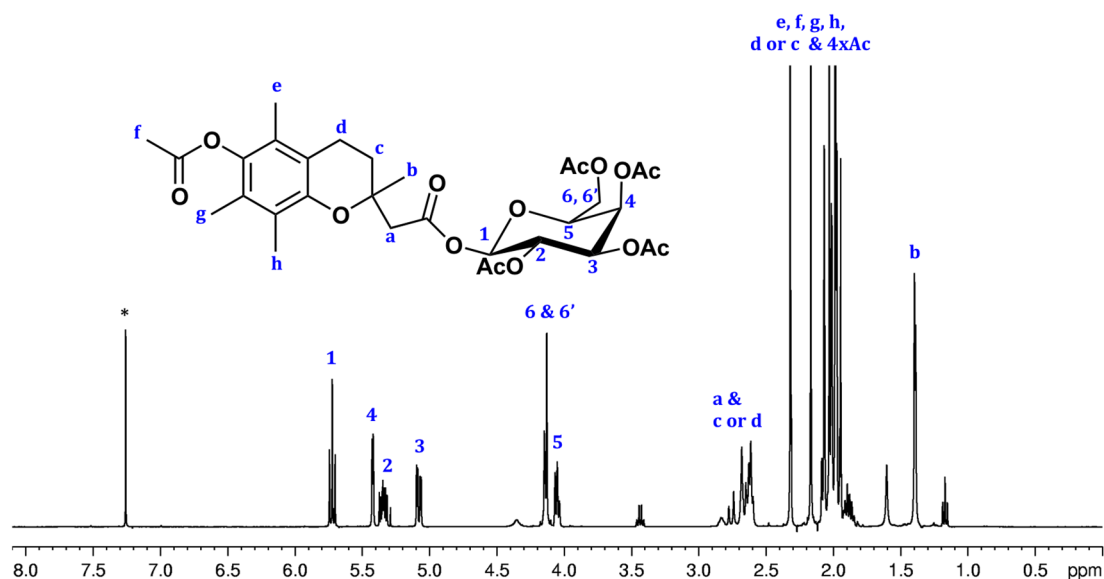
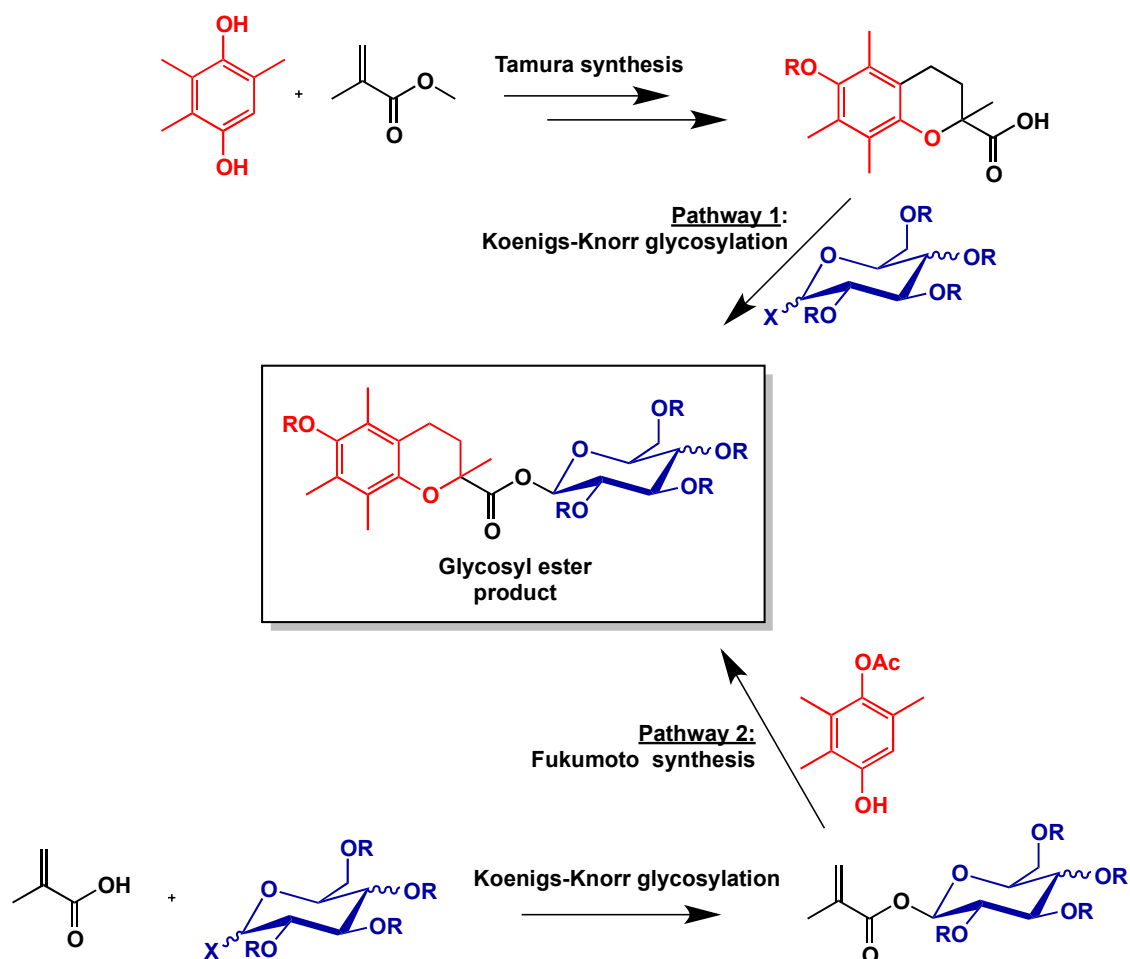


Figure 2.11: 400 MHz ^1H NMR spectrum of **19** (CDCl_3 , 300 K). * denotes residual solvent

Removal of the acetate protecting groups in **19** was attempted using triethylamine,²⁹ however as was the case with the glucosyl and galactosyl ester library, we were unable to deprotect while keeping the system intact.

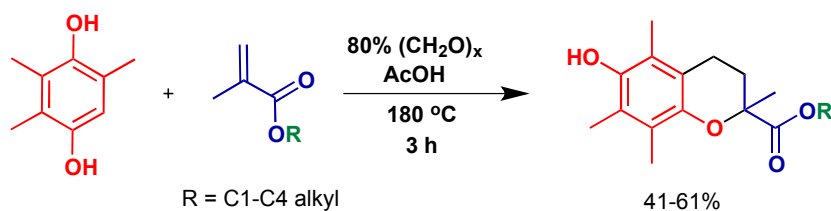
2.2.3. Alternate Synthetic Pathways to Novel Vitamin E Glycosyl Esters

Patents by Fukumoto³⁰ and Tamura³¹ describe conditions by which chromans can be synthesised in a mild one-step process that allows for variation in the substituent extending from the C-2 quaternary carbon by varying the alkene starting material. Scheme 2.4 demonstrates the two different pathways used to potentially synthesise vitamin E glycosyl esters.



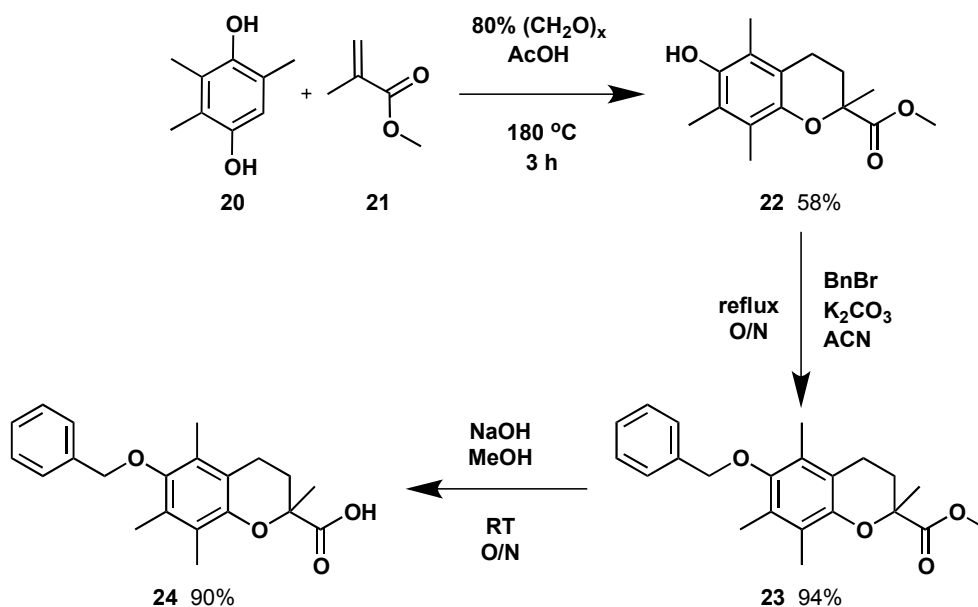
Scheme 2.4: Pathways to produce target vitamin E glycosyl esters

The method by Fukumoto³⁰ has the potential to be more versatile in that it allows a range of alkenes to be coupled with a range of substituted phenols. On the other hand, the method by Tamura³¹ is limited because only short-chain methacrylate esters can be used. It has the advantage, however, of starting with the unprotected dimethylhydroquinone. Scheme 2.5 illustrates that unlike the method used by Scott, Tamura's method produces the desired carboxylic acid-substituted chroman core in one step.

Scheme 2.5: Tamura's chroman synthesis³¹

2.2.3.1. Assessment of Pathway 1

The benzyl protected vitamin E analogue **24** bearing a carboxylic acid group at C-2, was synthesised according to the steps outlined in Scheme 2.6. Benzopyran **22** was produced in 58% yield by the reaction of methyl methacrylate **21** with the hydroquinone **20**.



Scheme 2.6

The presence of the characteristic multiplets in the regions of 2.70-2.38, 2.46-2.38 and 1.92-1.81 ppm in the ¹H NMR spectrum of **22**, representing the ring – CH₂CH₂–, supported formation of the tetrahydropyran ring. All other signals were consistent with the formation of **22**.

Benzyl protection of the phenol OH group of **22** to produce **23** proceeded smoothly using benzyl bromide and K₂CO₃. The presence of aromatic signals, as well as a two proton singlet at 4.76 ppm in the ¹H NMR spectrum of the product suggested successful protection had been achieved. The benzyl protecting group was chosen for its ability to be removed under hydrogenating conditions, which

would not interfere with the eventual glycosyl ester linkage as either acidic or basic conditions would.

The methyl ester of **23** was cleaved in aqueous NaOH in ethanol. The product **24** precipitated upon neutralisation and required no further purification. The ^1H NMR spectrum of **24** (Figure 2.12) supported product formation. In particular, the absence of the signal at 3.74 ppm correlates with the cleavage of the methyl ester.

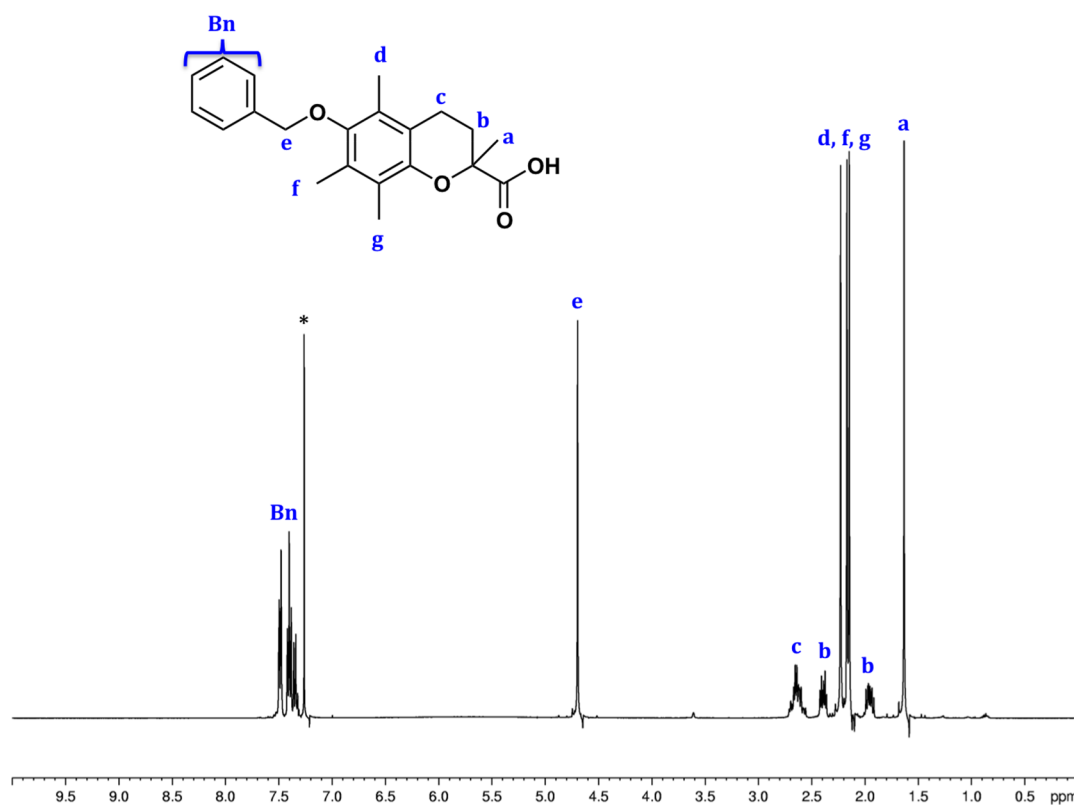
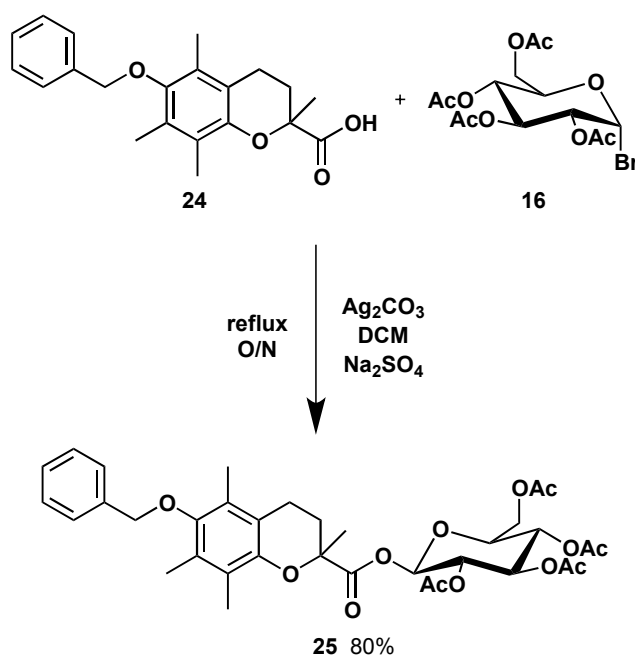


Figure 2.12: 400 MHz ^1H NMR spectrum of **24** (CDCl_3 , 300K). * denotes residual solvent

To complete Pathway 1, glycosylation of **24** was performed under Koenigs-Knorr conditions (Scheme 2.7).³² The β -anomer of **25** was exclusively formed, however both the ^1H NMR and the ^{13}C NMR spectra indicated the presence of two diastereomers, which could not be separated by flash chromatography, but resolved using HPLC purification (80% ACN/20% H_2O – 85% ACN/15% H_2O) in a ratio of 1 : 0.6. ^1H NMR analysis supported the identity of the two diastereomers of the product **25**. Mass spectrometry also supported product formation with a signal at m/z 693.2, corresponding to the $[\text{M}+\text{Na}]^+$ ion.



Scheme 2.7

As expected, the ^1H NMR spectra of the two diastereomers showed only subtle changes as a result of the positions of chirality. A representative ^1H NMR spectrum of one of the two diastereomers is shown in Figure 2.13. The coupling constant of $H-1$ is large enough in the ^1H NMR spectra of both diastereomers to indicate that the β -anomer has formed.

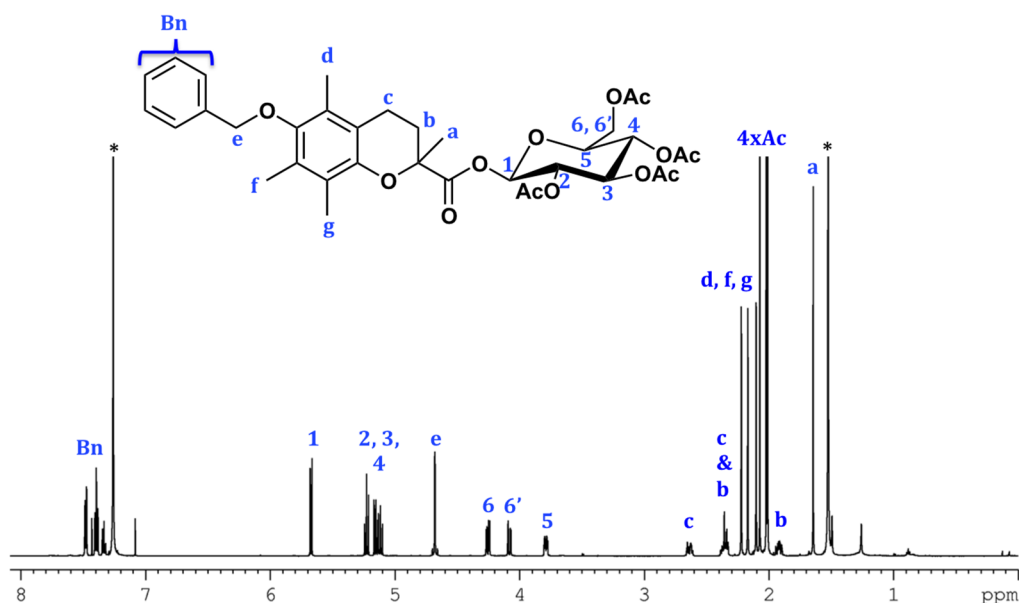


Figure 2.13: 600 MHz ^1H NMR spectrum of one diastereomer of **25** (CDCl_3 , 300K). * denotes residual solvent

In order to understand the differences in retention time better, computer modelling was used to show the in-space differences of geometry between the two diastereomers (Figure 2.14). The calculations were performed on the Gaussian 09 package.³³ All geometries were modelled and optimised using B3LYP/6-31G(d).

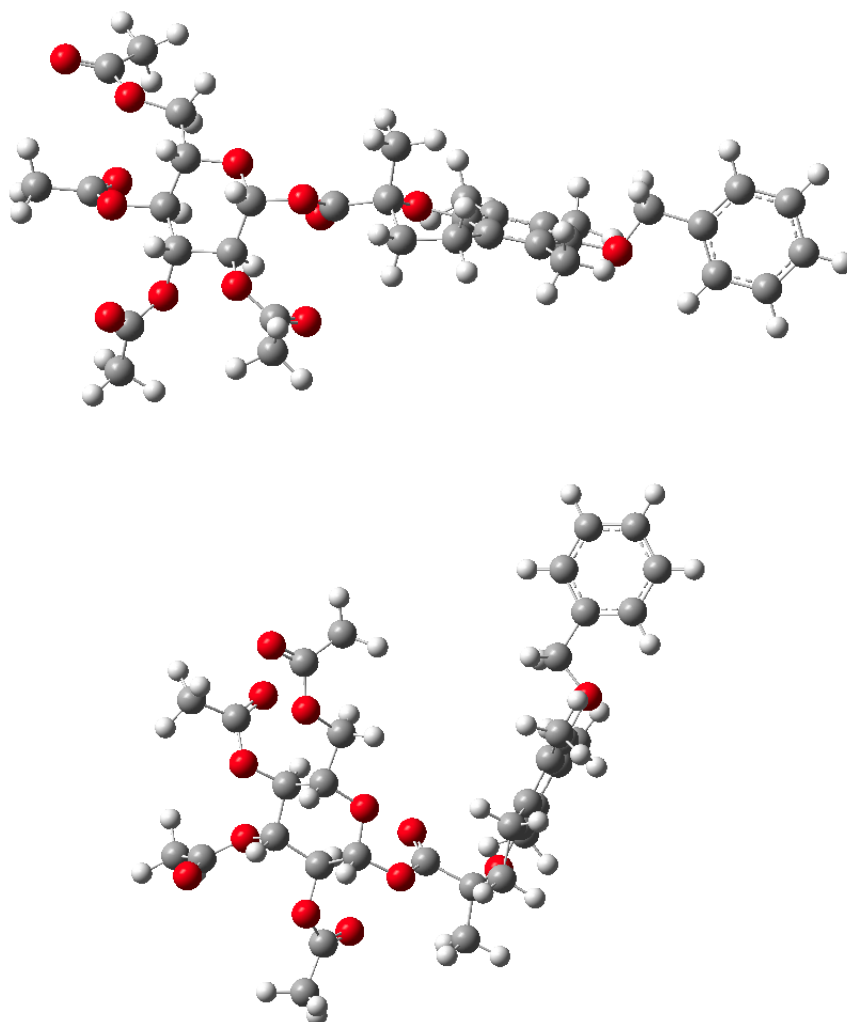
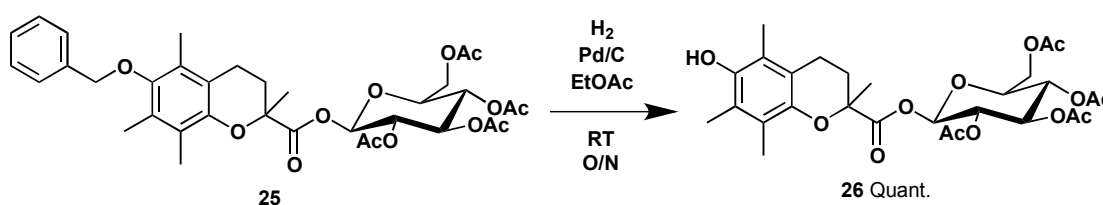


Figure 2.14: Minimised computer modeling images of the diastereomers of compound **25** using Gaussian 09.

The computer predictions of the lowest energy conformations shown in Figure 2.14 suggest that the overall three-dimensional shape is influenced greatly by the chiral centre at C-2. It can be inferred from these computer-generated models that diastereomer 1, which eluted first from the reverse-phase column, is the diastereomer pictured on top in Figure 2.14 due to its elongated structure and therefore more polar-exposed configuration, and diastereomer 2, which eluted 3 minutes later from the reverse-phase column, is the diastereomer pictured below

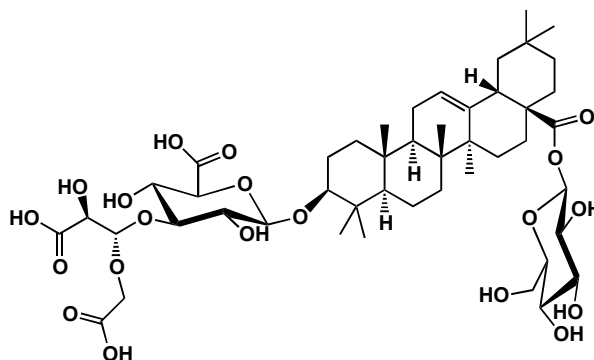
in Figure 2.14 due to its folded structure and therefore less polar-exposed configuration. With that said, confirmation by 2D-NMR techniques would be necessary to confirm the identity of each diastereomer.

The phenolic hydroxyl group of α -tocopherol derivatives is essential to antioxidant activity. The benzyl protecting group of **25** was easily removed quantitatively under hydrogenation conditions (Scheme 2.8). Both NMR spectroscopy and mass spectrometry supported formation of the product. In particular the lack of aromatic proton signals and the distinctive benzyl CH₂ signal in the ¹H NMR spectrum supported successful deprotection.



Scheme 2.8

There are numerous literature examples of the use of an aqueous solution of triethylamine,²⁹ methanolic sodium carbonate,³⁴ methanolic sodium methoxide,^{35,36} and aqueous potassium hydroxide³⁷ to cleave the acetate protecting groups of glycosyl esters, in particular, glycosylated natural products and plant saponins (Figure 2.15). The latter class of compound consists of glycosylated oleanolic acid by a monosaccharide at a hindered carboxylic acid position, as well as glycosylated at a tertiary hydroxyl group.

Figure 2.15: Deprotected glycosylated oleanolic acid.³⁶

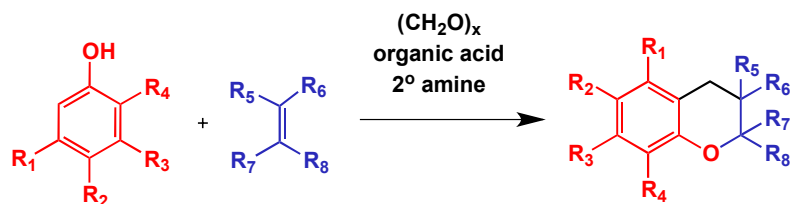
Due to the similarity of this class of compounds and **26** with respect to the hindered glycosyl ester, it was expected that the ability of small, nucleophilic bases

to cleave the acetate protecting groups while leaving the glycosyl ester intact for the saponins would be applicable to **26**.

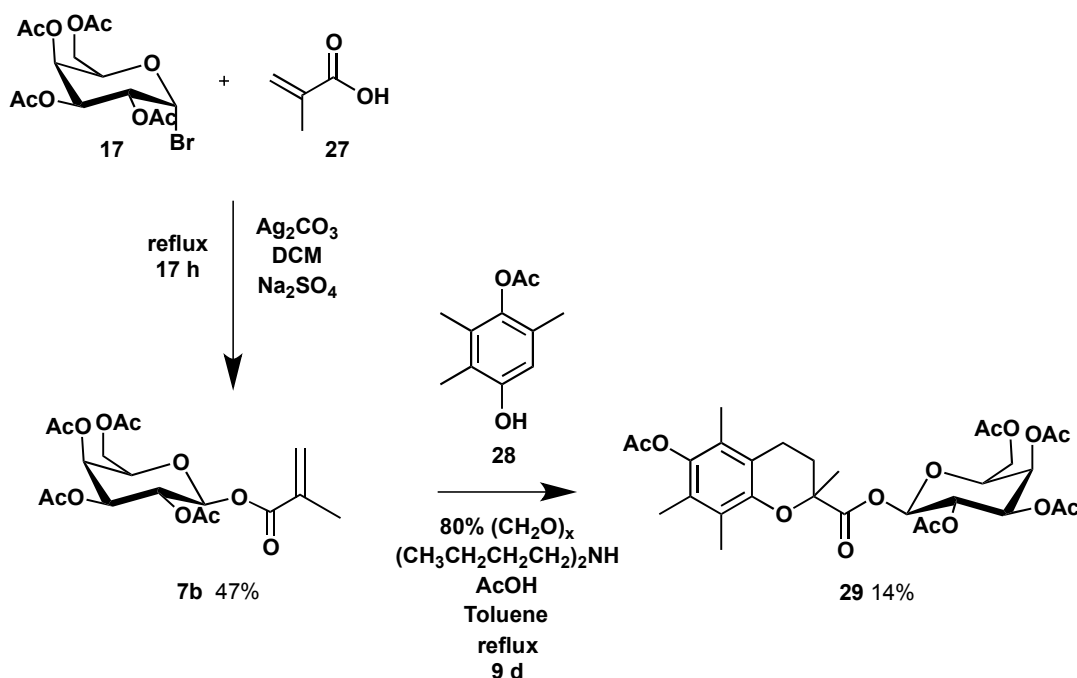
The glycosyl ester **26** was dissolved in methanol in an ice bath and treated with sodium methoxide for one hour. The ^1H NMR spectrum of the organic-soluble component of the reaction mixture displayed signals consistent with the methyl ester of **24** showing a peak at 3.69 ppm representing the new methyl group, indicating that the glycosyl ester had been cleaved. The ^1H NMR spectrum of the component of the reaction mixture that was soluble in methanol revealed the presence of a mixture of the α and β anomers of the cleaved, hydrolysed sugar moiety. These results suggest that small nucleophilic bases are not appropriate for removing acetate protecting groups from this particular glycosyl ester. A bulky base, potassium *t*-butoxide in butanol was used in a further attempt to remove the acetate protecting groups from **26**, however TLC analysis and the ESI mass spectrum did not show any change to the starting material, even under prolonged conditions.

2.2.3.2. Assessment of Pathway 2

Fukumoto's³⁰ procedure for chroman synthesis involves combining a phenol, paraformaldehyde, an unsaturated compound and catalytic amounts of a secondary amine and an organic acid, as shown generally in Scheme 2.9. The unsaturated compound must contain a carbon-carbon double bond and $\text{R}_5\text{-R}_8$ in Scheme 2.9 can be hydrogen or a linear or branched alkyl group having 1-20 carbons that can be substituted, an aryl group, carbonyl group, carboxyl group or an ester group. The difference with Fukumoto's procedure and Tamura's procedure (Pathway 1 Scheme 2.4) is that Tamura's does not use a secondary amine. As a result, the unprotected hydroquinone can be used without the risk of it being oxidised to the corresponding quinone.³¹ However a consequence of the absence of base is that only a limited range of short chain methacrylate esters can be used.

Scheme 2.9: Fukumoto's chroman synthesis³⁰

Glycosylation of methacrylic acid was achieved using silver carbonate and acetobromo galactose to form the exclusively β -orientated unsaturated compound, **7b** in 47% yield. Compound **7b** was then combined with mono acetate-protected trimethylhydroquinone **28**, paraformaldehyde and catalytic amounts of acid and base in a pressure tube (Scheme 2.10), according to the Fukumoto method.³⁰



Scheme 2.10

Purification by HPLC led to a poor yield of the desired product **29**. ^1H NMR analysis of the major fractions from HPLC revealed unreacted **7b**, and four other relatively hydrophobic major impurities. The ^1H NMR spectra of the major impurities displayed signals consistent with both a sugar moiety and a vitamin E moiety. However, the characteristic multiplets attributable to the $-\text{CH}_2\text{CH}_2-$ of the tetrahydropyran ring of the vitamin E moiety are not present. This suggests that the impurities could be the result of the sugar and vitamin E moieties reacting but the cyclisation has failed, or perhaps they are some sort of transglycosylated

product. These unidentified impurities are not surprising given the conditions used in this reaction and go some way to explain the poor yield of the desired product **29**.

Signals in the ^1H NMR spectrum attributed to **29** support successful product formation with multiplet peaks at 2.65, 2.50, 2.34 and 1.84 ppm representing the two sets of methylene rings protons as well as the typical sugar proton signals between 5.7 and 3.9 ppm. Both ^1H and ^{13}C NMR analysis show that the two possible diastereomers of this product co-eluted. Given the production of unwanted by-products, Pathway 2 appears to be an inferior pathway to Pathway 1 for the synthesis of vitamin E glycosyl esters and was not explored further.

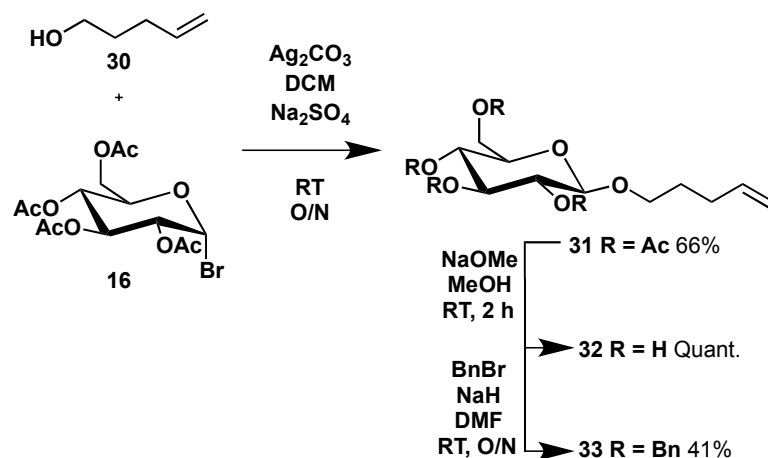
2.2.4. Benzyl Protected Glycosyl Esters

One strategy by which to overcome the susceptibility of the glycosyl ester to the conditions necessary to cleave the acetate protecting groups is to change the nature of protecting groups and hence the chemistry required to remove them. The benzyl protecting group is complementary in that it is removed by hydrogenation which does not interfere with the glycosyl ester. For an example recall the removal of the benzyl group of **25** occurred under mild conditions and high yield. Konradsson and Fraser-Reid describe the use of pent-4-enyl glycosides to produce glycosyl bromides *via* displacement by molecular bromine in dichloromethane at 0 °C.³⁸

The synthesis of benzyl-protected bromo sugar **34** started with the reaction of commercially available 2,3,4,6-tetra-O-acetyl- α -D-glucopyranosyl bromide **16**, with 4-penten-1-ol **30** to form an *O*-linkage glycoside **31** (Scheme 2.11). Silver carbonate was used as the promoter to exclusively produce the β -anomer of **31** in 66% yield. Interestingly, when boron trifluoride dietherate was used as the promoter, a mixture of the α - and β - anomers was formed. However, based on the mechanism of the conversion to the bromo sugar **34** from the pentenyl glycoside **33**, both anomers could be used to produce the desired α -bromo benzyl protected sugar.

The acetate groups of **31** were efficiently cleaved using sodium methoxide in methanol to produce **32** in quantitative yield. TLC analysis clearly indicated complete conversion. ^1H NMR analysis also showed that cleavage was complete,

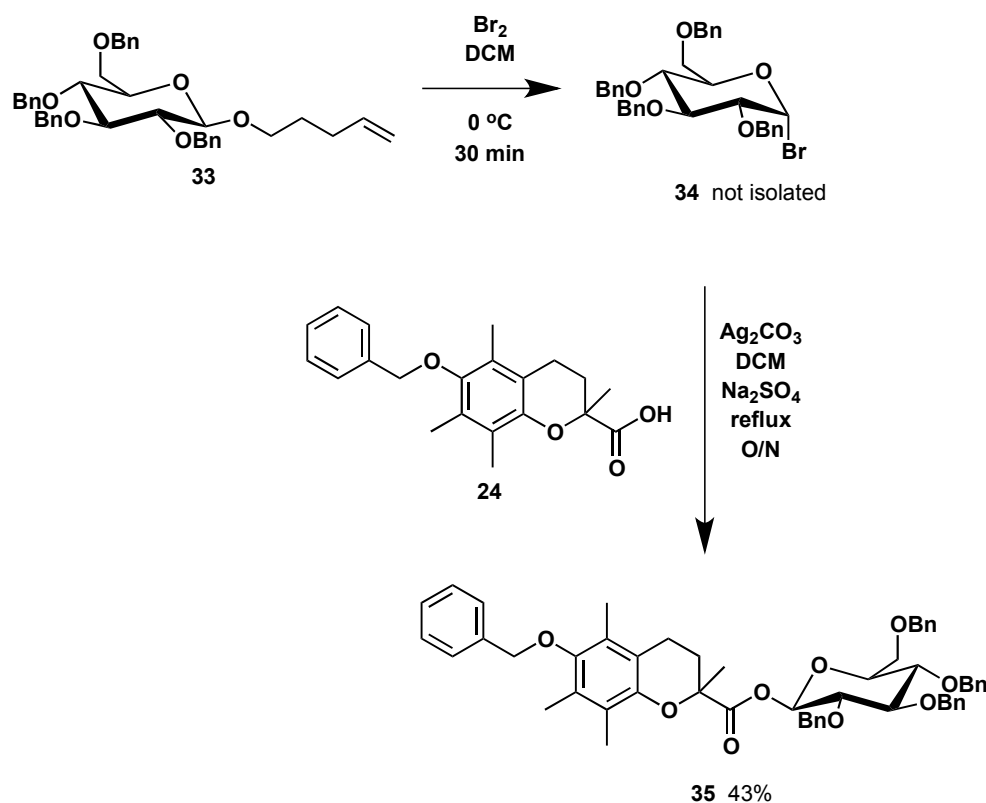
specifically by the absence of the signals corresponding to the acetate methyl protons around 2.1 ppm.



Scheme 2.11

Excess quantities of benzyl bromide and sodium hydride in DMF solution were used to benzyl protect each hydroxyl group of **32**. Purification by column chromatography separated the desired product from excess benzyl bromide and other by-products. Dichloromethane was first used to elute the benzyl bromide, followed by ethyl acetate to elute the desired benzyl protected product **33** in a modest 41% yield. The ^1H NMR and ^{13}C NMR spectra clearly indicated successful product formation with characteristic aromatic signals in the regions of 7.0–7.5 ppm and 127–128 ppm, respectively. The ESI mass spectrum supported the complete protection of **32** with a peak at m/z 631.3 corresponding to the $[\text{M}+\text{Na}]^+$ ion.

With the pent-4-enyl benzyl protected glycoside **33** in hand, its conjugation to the benzopyran was explored. Glycoside **33** was converted to the bromo sugar **34** using molecular bromine in dry DCM (Scheme 2.12). Bromo sugar **34** was not isolated although small aliquots were removed from the reaction flask in order to monitor the progress of the reaction. ^1H NMR analysis was used to monitor the disappearance of the distinctive ddt signal of the starting material at 5.87 ppm, attributable to the single proton on the non-terminal end of the double bond. Mass spectrometry was also used to monitor the disappearance of the starting material.



Scheme 2.12

Once the starting material had been converted, the solvent was removed *in vacuo*. Vitamin E analogue **24**, silver carbonate, drying agents (molecular sieves and Na_2SO_4) and freshly distilled dichloromethane were then immediately added to the same reaction flask. The glycosylation reaction was heated to reflux and allowed to react overnight (Scheme 2.12). Upon workup of the reaction mixture, column chromatography was attempted, however as was the case with **25**, HPLC was needed to completely separate all components of the reaction mixture.

Due to the non-polar nature of **35** (as a consequence of five benzyl rings), the desired product eluted at 52 minutes and 55 minutes with the solvent at 100% acetonitrile on the reverse phase column. These two peaks correspond to the two possible diastereomers of the product in a ratio of 0.5 : 1.

The ^1H NMR spectra of the two diastereomers indicate that the β -anomer was formed in both cases with $J = 7.8\text{--}8.0\text{ Hz}$ for H-1. Figure 2.16 shows the ^1H NMR spectrum of the major diastereomer of **35**.

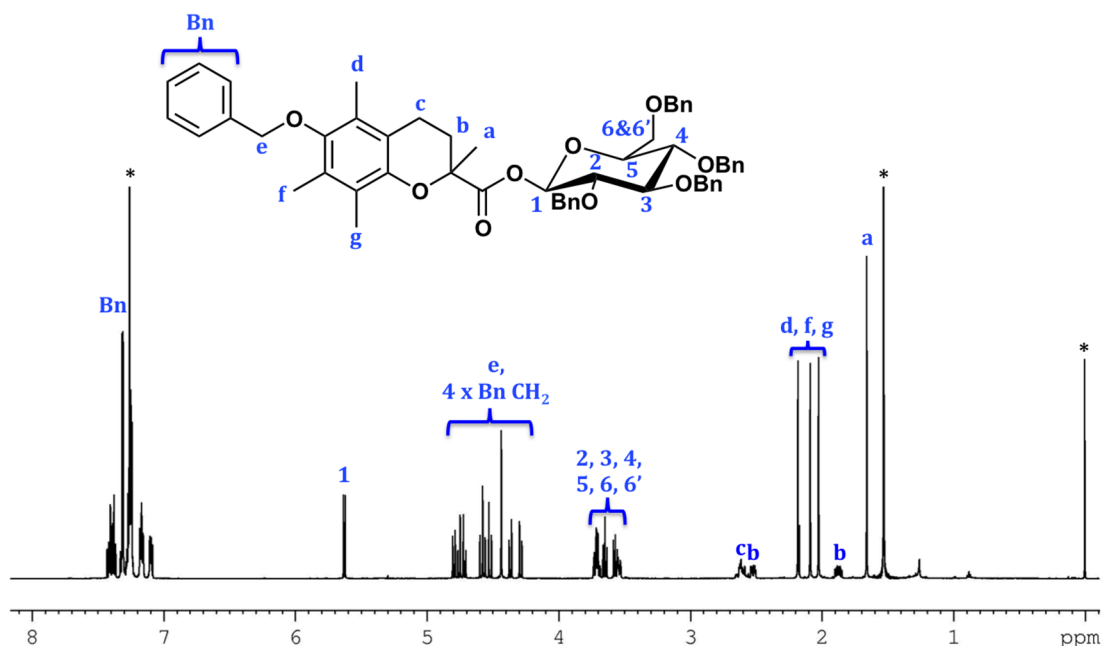


Figure 2.16: 600 MHz ^1H NMR spectrum of **35** – major diastereomer (CDCl_3 , 300K).

* denotes residual solvent

2.3. Conclusions and Future Directions

This chapter of work focussed on an alternative preparation of vitamin E derivatives. As a known antioxidant, vitamin E has the potential to treat MND or perhaps work as a complementary therapeutic. Natural vitamin E is very lipid soluble and does not cross the BBB and therefore more hydrophilic analogues are required for the treatment of MND. Glycosylated vitamin E analogues have been reported to possess improved BBB penetration ability.

A library of glycosyl ester derivatives was prepared to explore the use of silver carbonate in carbohydrate conjugation. Compounds **1-9** (**a** and **b**; glucose and galactose derivatives) were prepared in moderate to excellent yields and the β -anomer was exclusively formed in each case. The acetate protecting groups however could not be removed while maintaining the glycosyl ester linkage.

The use of silver carbonate to form β -orientated glycosyl esters was transferred to the production of glycosylated vitamin E derivatives. Initially, a six-step synthesis was used to produce a Trolox-like vitamin E derivative, **15** that contained carboxylic functionality from which a glycosyl ester could be formed. Glucosyl ester **18** and galactosyl ester **19** vitamin E derivatives were produced

however again, the sugar acetate protecting groups could not be removed while maintaining the glycosyl ester linkage.

Alternate syntheses of glycosyl ester vitamin E derivatives were explored. Pathway 1 involved the synthesis of vitamin E carboxylic acid derivative **24** in a more efficient 3 steps. Glucosyl ester vitamin E derivative **25** was produced from the silver carbonate glycosylation of **24**. The two possible diastereomers of **25** were successfully isolated and characterised. Computational modelling was used to explain the large difference in elution time of the two diastereomers. Distinctly different three-dimensional shapes (elongated and folded) were found to result from the inversion of the one stereocentre. Neither small nucleophilic bases nor bulky bases were successful in removing the sugar acetate protecting groups. Hydrogenation successfully removed the phenol benzyl protecting group to produce **26**.

Pathway 2 involved the formation of the glycosylated allyl moiety **7b** first, followed by the formation of the vitamin E chromanol structure, to produce galactosyl ester vitamin E derivative **29**. This synthetic route however produced many undesired by-products and was therefore considered an inferior pathway.

An alternative synthetic strategy involved the use of benzyl protecting groups on the sugar and phenol. This required the preparation of the benzyl bromide sugar **34** *in situ* from the benzyl 4-pentenyl sugar **33**. Glucosyl ester vitamin E derivative **35** was produced from the silver carbonate glycosylation of **24**. HPLC purification successfully isolated the two possible stereoisomers of **35**.

The most immediate future work in this area of research would be to successfully carry out the hydrogenation of the benzyl protected glucosyl ester vitamin E derivative **35**. It is assumed that this would be a facile reaction and readily produce the desired unprotected glucosyl ester vitamin E derivative. Of the various synthetic strategies explored in this study to produce a glycosyl ester vitamin E derivative, the benzyl protected sugar strategy appears to be the most likely to successfully produce an unprotected final product.

Further necessary work would be to conduct biological assays to assess the ability of the glycosylated vitamin E derivatives to act as antioxidants, and penetrate the BBB. It is possible that the acetate protecting groups of **26** would be cleaved *in vivo* before they reached the BBB. If that were the case, Pathway 1

would be favoured over the benzyl protected sugar strategy due to the readily available starting aceto sugar.

2.4. Experimental Details

2.4.1. General Experimental Methods

All solvents used were AR grade or HPLC grade. All experiments were conducted under N₂ unless otherwise stated. Acetonitrile was dried by storage over 4A molecular sieves before use. Dichloromethane was dried over CaH₂ prior to distillation.

Melting points (MP) were measured on a Stuart Scientific SMP 3 melting point apparatus.

Analytical thin layer chromatography (TLC) was performed on metal plates coated in silica gel (Silica 60 F₂₅₄). Column chromatography was conducted using Merck silica gel 60, with a pore size between 0.063 and 0.200 mm. The eluent conditions are expressed as volume (v/v) ratios. Components were detected by fluorescence under 254 nm ultraviolet irradiation and/or after coating in vanillin stain and heated (sugar moieties).

High performance liquid chromatography (HPLC) was conducted using Waters 600 gradient controller with a C₁₈ column, Waters 996 photo diode array and Waters Millennium 32 software. A Jupiter C₁₈ column (10 mm diameter, 250 mm length, 10 µm particle size) was used for analytical runs, while a Delta Pak C₁₈ column (19 mm diameter, 300 mm length, 15 µm particle size) was used for preparative runs.

¹H NMR spectra were recorded using Bruker AV200 MHz, DPX 300 MHz, DRX 400 MHz, Bruker Avance III 400 MHz or Bruker Avance III 600 MHz spectrometers. All ¹H NMR spectra were obtained in solutions using deuterated chloroform (CDCl₃) as the solvent and calibrated to the residual solvent resonance (7.26 ppm). All resonance peaks were assigned with the following format: chemical shift measured in parts per million (ppm), multiplicity (denoted as s (singlet), d (doublet), t (triplet), q (quartet), m (multiplet), doublet of doublets (dd) or doublet of doublet of triplets (ddt), and prefixed broad (br) where applicable.), observed coupling constants (*J* Hz), number of protons and assignment. Most ¹H NMR and ¹³C NMR spectra were assigned from COSY and HMQC experiments.

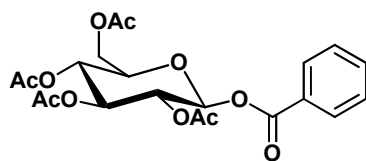
JMOD ^{13}C NMR spectra were recorded using a Bruker DPX, DRX or Advance III spectrometer, at 75 MHz, 100 MHz or 150 MHz respectively. All ^{13}C NMR spectra were obtained in solutions using deuterated chloroform (CDCl_3) as the solvent and calibrated to the residual solvent resonance (77.36 ppm).

Mass spectrometry (MS) results were obtained by Sally Duck, School of Chemistry, Monash University. Low-resolution electrospray ionisation (ESI) spectra were recorded on a Micromass Platform (QMS-quadrupole mass electrospray) or a Micromass ZMD mass spectrometer. High-resolution ESI spectra were recorded on an Agilent Technologies 6220 Accurate-Mass TOF LC/MS mass spectrometer, or on a Bruker BioApex 47e Fourier Transform mass spectrometer. The predominant ion peaks (m/z) were recorded. $[\text{M}]^+$ denotes the molecular ion.

X-ray crystallography results were obtained by Kristina Konstas and Craig Forsyth, School of Chemistry, Monash University. X-ray crystal diffraction patterns were determined using a Bruker Kappa Apex II diffractometer with graphite monochromated $\text{MoK}\alpha$ radiation at 123 K. The crystal data was solved and refined using SHELXS-97³⁹ and SHELXL-97⁴⁰ suite of programs with the graphical interface X-seed v2.0.⁴¹

2.4.2. Synthesis of Glucosyl and Galactosyl Ester Library

Synthesis of 1a



Tetraacetyl bromo- α -D-glucopyranose (50 mg, 0.12 mmol), benzoic acid (22 mg, 0.18 mmol), silver carbonate (711 mg, 2.58 mmol) and sodium sulfate (1.4 g, 9.9 mmol) were stirred in DCM (15 mL) at reflux, under an atmosphere of nitrogen for 24 h. The reaction mixture was then filtered through celite, the organic layer washed with sat. NaHCO_3 (aq) (2 x 20 mL) and H_2O (20 mL), dried (MgSO_4) and the solvent removed under reduced pressure to leave **1a** as a white solid (53.9 mg, 98%).

^1H NMR (400 MHz): δ 8.03 (d, 2H, $J = 7.3$ Hz, Ar H); 7.60 (tt, 1H, $J = 7.3, 1.3$ Hz, Ar H); 7.45 (t, 2H, $J = 7.3$ Hz, Ar H); 5.92 (m, 1H, $H-1$); 5.33 (m, 2H, $H-3$ & $H-2$ or $H-4$);

5.19 (m, 1H, *H*-2 or *H*-4); 4.32 (dd, 1H, *J* = 12.5, 4.5, *H*-6); 4.14 (dd, 1H, *J* = 12.5, 2.2, *H*-6'); 3.94 (ddd, 1H, *J* = 10.0, 4.5, 2.3, *H*-5); 2.06 (s, 3H, Ac *CH*₃); 2.04 (s, 3H, Ac *CH*₃); 2.04 (s, 3H, Ac *CH*₃); 1.98 (s, 3H, Ac *CH*₃).

¹³C NMR (100 MHz): δ 170.9, 170.4, 169.8, 169.7, 164.9, 134.3, 130.5, 129.0, 128.8, 92.7, 73.2, 73.0, 70.6, 69.0, 61.9, 21.0, 20.9, 20.9, 20.9.

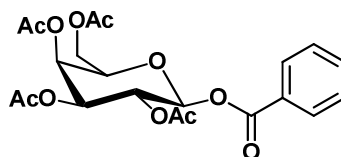
MS (ESI, +ve): *m/z* 475.2 [M+Na]⁺.

HRMS (ESI, +ve): *m/z* 475.1219 [M+Na]⁺, C₂₁H₂₄O₁₁Na required *m/z* 475.1211.

MP: 140–141 °C (Literature⁴²: 146–148 °C).

X-ray crystallography: For data, see Appendix.

Synthesis **1b**



Tetraacetyl bromo-α-D-galactopyranose (50 mg, 0.12 mmol), benzoic acid (22 mg, 0.18 mmol), silver carbonate (711 mg, 2.58 mmol) and sodium sulfate (1.4 g, 9.9 mmol) were stirred in DCM (15 mL) at reflux, under an atmosphere of nitrogen for 24 h. The reaction mixture was then filtered through celite, the organic layer washed with sat. NaHCO₃ (aq) (2 x 20 mL) and H₂O (20 mL), dried (MgSO₄) and the solvent removed under reduced pressure to leave **1b** as a white solid (54.5 mg, 99%).

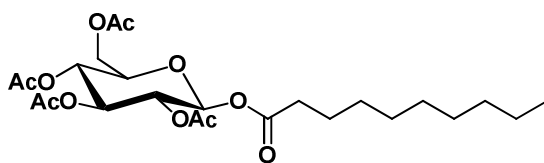
¹H NMR (400 MHz): δ 8.05 (dd, 2H, *J* = 8.3, 1.2 Hz, Ar *H*); 7.60 (tt, 1H, *J* = 7.5, 1.5 Hz, Ar *H*); 7.45 (t, 2H, *J* = 7.7 Hz, Ar *H*); 5.90 (d, 1H, *J* = 8.3 Hz, *H*-1); 5.53 (dd, 1H, *J* = 10.5, 8.3 Hz, *H*-2); 5.48 (d, 1H *J* = 3.3 Hz, *H*-4); 5.16 (dd, 1H, *J* = 10.5, 3.4 Hz, *H*-3); 4.16 (m, 3H, *H*-5, *H*-6 & *H*-6'), 2.19 (s, 3H, Ac *CH*₃); 2.04 (s, 3H, Ac *CH*₃); 2.01 (s, 3H, Ac *CH*₃); 1.98 (s, 3H, Ac *CH*₃).

¹³C NMR (100 MHz): δ 170.7, 170.5, 170.3, 169.8, 164.9, 134.3, 130.5, 128.9, 128.8, 93.2, 72.2, 71.1, 68.2, 67.3, 61.4, 21.0, 20.9.

MS (ESI, +ve) *m/z* 475.1 [M+Na]⁺.

HRMS (ESI, +ve) *m/z* 475.1216 [M+Na]⁺, C₂₁H₂₄O₁₁Na required *m/z* 475.1211.

MP: 119–121 °C.

Synthesis 2a

Tetraacetyl bromo- α -D-glucopyranose (50 mg, 0.12 mmol), decanoic acid (25 mg, 0.14 mmol), silver carbonate (711 mg, 2.57 mmol) and sodium sulfate (1.4 g, 9.9 mmol) were stirred in DCM (15 mL) at reflux, under an atmosphere of nitrogen for 6 d. The reaction mixture was then filtered through celite, the organic layer washed with sat. NaHCO_3 (aq) (1 x 20 mL) and water (1 x 20 mL), dried (MgSO_4) and the solvent removed under reduced pressure. Purification by flash chromatography (2:1 hexane:ethyl acetate; R_f = 0.22). The solvent was removed under reduced pressure to leave **2a** as a white solid (58.4 mg, 96%).

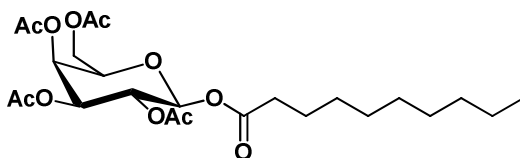
^1H NMR (400 MHz): δ 5.72 (d, 1H, J = 8.3 Hz, H -1); 5.25 (t, 1H, J = 9.6 Hz, H -3); 5.13 (m, 2H, H -2 & H -4); 4.28 (dd, 1H, J = 12.5, 4.4 Hz, H -6); 4.10 (dd, 1H, J = 12.4, 1.9 Hz, H -6'); 3.83 (dt, 1H, J = 7.7, 2.2 Hz, H -5); 2.34 (td, 2H, J = 7.5, 1.7 Hz, $-\text{CH}_2\text{COO}-$); 2.07 (s, 3H, Ac CH_3); 2.02 (s, 3H, Ac CH_3); 2.01 (s, 3H, Ac CH_3); 2.00 (s, 3H, Ac CH_3); 1.59 (bs, 2H, $-\text{CH}_2-$); 1.25 (bs, 12H, 6 x $-\text{CH}_2-$); 0.87 (t, 3H, J = 6.7 Hz, $-\text{CH}_3$).

^{13}C NMR (100 MHz): δ 172.2, 171.0, 170.9, 170.5, 169.7, 91.9, 73.1, 73.0, 70.6, 68.1, 61.8, 34.4, 32.2, 29.7, 29.6, 29.5, 29.3, 24.9, 23.0, 21.0, 20.9, 20.9, 8.6.

MS (ESI, +ve) m/z 525.1 $[\text{M}+\text{Na}]^+$.

HRMS (ESI, +ve) m/z 525.2313 $[\text{M}+\text{Na}]^+$, $\text{C}_{24}\text{H}_{38}\text{O}_{11}\text{Na}$ required m/z 525.2306.

MP: 53–56 °C.

Synthesis of 2b

Tetraacetyl bromo- α -D-galactopyranose (40 mg, 0.10 mmol), decanoic acid (20 mg, 0.12 mmol), silver carbonate (568 mg, 2.06 mmol) and sodium sulfate (1.1 g, 7.9 mmol) were stirred in DCM (10 mL) at reflux under an atmosphere of nitrogen for 2 d. The reaction mixture was then filtered through celite, the organic

layer washed with sat. NaHCO_3 (aq) (20 mL) and water (20 mL), dried (MgSO_4) and the solvent removed under reduced pressure. Purification by flash chromatography (2:1 hexane:ethyl acetate; $R_f = 0.28$). The solvent was removed under reduced pressure to leave **2b** as a colourless oil (48.1 mg, 98%).

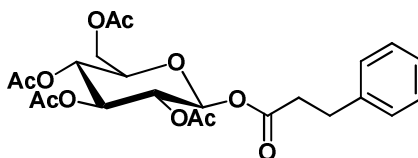
^1H NMR (400 MHz): δ 5.70 (d, 1H, $J = 8.3$ Hz, $H-1$); 5.42 (dd, 1H, $J = 3.4, 0.9$ Hz, $H-4$); 5.33 (dd, 1H, $J = 10.5, 8.3$ Hz, $H-2$); 5.07 (dd, 1H, $J = 10.4, 3.4$ Hz, $H-3$); 4.12 (m, 2H, $H-6$ & $H-6'$); 4.05 (td, 1H, $J = 6.6, 1.0$, $H-5$); 2.36 (td, 2H, $J = 7.6, 1.6$ Hz, $-\text{CH}_2\text{COO}-$); 2.16 (s, 3H, Ac CH_3); 2.04 (s, 3H, Ac CH_3); 2.03 (s, 3H, Ac CH_3); 2.00 (s, 3H, Ac CH_3); 1.61 (m, 2H, $-\text{CH}_2-$); 1.26 (m, 12H, 6 x $-\text{CH}_2-$); 0.88 (t, 3H, $J = 6.8$ Hz, $-\text{CH}_3$).

^{13}C NMR (100 MHz): δ 172.2, 170.7, 170.5, 170.3, 169.7, 92.3, 72.0, 71.2, 68.2, 67.1, 61.3, 34.4, 32.2, 29.7, 29.6, 29.5, 29.2, 24.9, 23.0, 21.0, 20.9, 8.8.

MS (ESI, +ve) m/z 525.1 $[\text{M}+\text{Na}]^+$.

HRMS (ESI, +ve) m/z 525.2310 $[\text{M}+\text{Na}]^+$, $\text{C}_{24}\text{H}_{38}\text{O}_{11}\text{Na}$ required m/z 525.2306.

Synthesis of **3a**



Tetraacetyl bromo- α -D-glucopyranose (30 mg, 0.07 mmol), hydrocinnamic acid (16 mg, 0.11 mmol), silver carbonate (427 mg, 1.55 mmol) and sodium sulfate (842 mg, 5.93 mmol) were stirred in DCM (10 mL) at reflux, under an atmosphere of nitrogen in the dark for 2 d. The reaction mixture was then filtered through celite, the organic layer washed with sat. NaHCO_3 (aq) (20 mL) and water (20 mL), dried (MgSO_4) and the solvent removed under reduced pressure. Purification by flash chromatography (5% methanol/DCM; $R_f = 0.58$). The solvent was removed under reduced pressure to leave **3a** as a white solid (27.8 mg, 79%).

^1H NMR (400 MHz): δ 7.26 (m, 2H, Ar H); 7.16 (m, 3H, Ar H); 5.71 (d, 1H, $J = 8.2$ Hz, $H-1$); 5.22 (t, 1H, $J = 9.4$ Hz, $H-3$); 5.10 (m, 2H, $H-2$ & $H-4$); 4.26 (dd, 1H, $J = 12.5, 4.6$ Hz, $H-6$); 4.09 (dd, 1H, $J = 6.2, 2.2$ Hz, $H-6'$); 3.81 (ddd, 1H, $J = 10.0, 4.5, 2.2$ Hz, $H-5$); 2.92 (m, 2H, $-\text{CH}_2\text{CH}_2-$); 2.67 (m, 2H, $-\text{CH}_2\text{CH}_2-$); 2.06 (s, 3H, Ac CH_3); 2.01 (s, 3H, Ac CH_3); 1.98 (s, 3H, Ac CH_3); 1.91 (s, 3H, Ac CH_3).

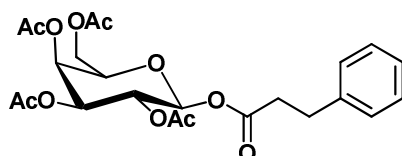
^{13}C NMR (100 MHz): δ 171.2, 170.9, 170.4, 169.7, 169.5, 140.2, 128.9, 128.6, 126.8, 92.1, 73.1, 73.1, 70.6, 68.2, 61.8, 35.8, 30.7, 21.0, 20.9, 20.8.

MS (ESI, +ve) m/z 503.1 $[\text{M}+\text{Na}]^+$.

HRMS (ESI, +ve) m/z 503.1529 $[\text{M}+\text{Na}]^+$, $\text{C}_{23}\text{H}_{28}\text{O}_{11}\text{Na}$ required m/z 503.1524.

MP: 120–122 °C.

Synthesis of **3b**



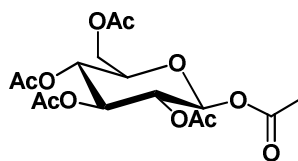
Tetraacetyl bromo- α -D-galactopyranose (30 mg, 0.07 mmol), hydrocinnamic acid (16 mg, 0.11 mmol), silver carbonate (427 mg, 1.55 mmol) and sodium sulfate (842 mg, 5.93 mmol) were stirred in DCM (10 mL) at reflux, under an atmosphere of nitrogen in the dark for 2 d. The reaction mixture was then filtered through celite, the organic layer washed with sat. NaHCO_3 (aq) (20 mL) and water (20 mL), dried (MgSO_4) and the solvent removed under reduced pressure. Purification by flash chromatography (5% methanol/DCM; R_f = 0.69). The solvent was removed under reduced pressure to leave **3b** as a colourless oil (28.4 mg, 81%).

^1H NMR (400 MHz): δ 7.25 (m, 2H, Ar H); 7.17 (m, 3H, Ar H); 5.69 (d, 1H, J = 8.3 Hz, H -1) 5.40 (dd, 1H, J = 3.4, 1.0 Hz, H -4); 5.30 (dd, 1H, J = 10.4, 8.3 Hz, H -2); 5.05 (dd, 1H, J = 10.4, 3.4 Hz, H -3); 4.12 (m, 2H, H -6 & H -6'); 4.02 (t, 1H, J = 6.6 Hz, H -5); 2.92 (m, 2H, $-\text{CH}_2\text{CH}_2-$); 2.68 (m, 2H, $-\text{CH}_2\text{CH}_2-$); 2.14 (s, 3H, Ac CH_3); 2.01 (s, 3H, Ac CH_3), 1.96 (s, 3H, Ac CH_3); 1.91 (s, 3H, Ac CH_3).

^{13}C NMR (100 MHz): δ 171.2, 170.6, 170.4, 170.3, 169.6, 140.2, 128.9, 128.6, 126.8, 92.6, 72.1, 71.2, 68.2, 67.2, 61.3, 35.8, 30.7, 21.0, 20.9, 20.9, 20.8.

MS (ESI, +ve) m/z 503.1 $[\text{M}+\text{Na}]^+$.

HRMS (ESI, +ve) m/z 503.1524 $[\text{M}+\text{Na}]^+$, $\text{C}_{23}\text{H}_{28}\text{O}_{11}\text{Na}$ required m/z 503.1524.

Synthesis of 4a

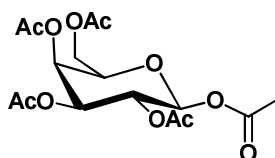
To a stirred solution of acetic acid (0.004 mL, 0.073 mmol) in acetic anhydride (0.003 mL, 0.036 mmol), was added tetraacetyl bromo- α -D-glucopyranose (30 mg, 0.07 mmol), silver carbonate (427 mg, 1.55 mmol) and sodium sulfate (842 mg, 5.93 mmol) and DCM (10 mL). The reaction mixture was heated to reflux and allowed to stir under an atmosphere of nitrogen in the dark for 2 d. The reaction mixture was then filtered through celite, the organic layer washed with sat. NaHCO_3 (aq) (20 mL) and water (20 mL), dried (MgSO_4) and the solvent removed under reduced pressure. Purification by flash chromatography (5% methanol/DCM; R_f = 0.66). The solvent was removed under reduced pressure to leave **4a** as a white solid (27.9 mg, 98%).

^1H NMR (400 MHz): δ 5.72 (d, 1H, J = 7.0 Hz, H -1); 5.25 (t, 1H, J = 9.4 Hz, H -3); 5.13 (m, 2H, H -2 & H -4); 4.28 (dd, 1H, J = 12.5, 4.6 Hz, H -6); 4.11 (dd, 1H, J = 12.5, 2.3 Hz, H -6'); 3.84 (ddd, 1H, J = 9.8, 4.4, 2.2 Hz, H -5); 2.11 (s, 3H, Ac CH_3); 2.06 (s, 3H, Ac CH_3); 2.03 (s, 6H, 2 x Ac CH_3); 2.01 (s, 3H, Ac CH_3).

^{13}C NMR (50 MHz) δ : 170.9, 170.4, 169.7, 169.6, 169.3, 92.1, 73.1, 73.1, 70.6, 68.1, 61.8, 21.1, 21.0, 20.9.

MS (ESI, +ve): m/z 413.1 $[\text{M}+\text{Na}]^+$.

MP: 130–131 $^\circ\text{C}$ (Literature⁴³: 131–132 $^\circ\text{C}$).

Synthesis of 4b

To a stirred solution of acetic acid (0.004 mL, 0.073 mmol) in acetic anhydride (0.003 mL, 0.036 mmol), was added tetraacetyl bromo- α -D-galactopyranose (30 mg, 0.07 mmol), silver carbonate (427 mg, 1.55 mmol) and sodium sulfate (842 mg, 5.93 mmol) and DCM (10 mL). The reaction mixture was heated to reflux and

allowed to stir under an atmosphere of nitrogen in the dark for 2 d. The reaction mixture was then filtered through celite, the organic layer washed with sat. NaHCO_3 (aq) (20 mL) and water (20 mL), dried (MgSO_4) and the solvent removed under reduced pressure. Purification by flash chromatography (5% methanol/DCM; R_f = 0.58). The solvent was removed under reduced pressure to leave **4b** as a white solid (26.7 mg, 94%).

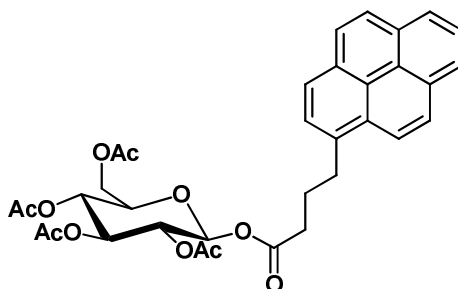
^1H NMR (300 MHz) δ : 5.69 (d, 1H, J = 8.3 Hz, H-1); 5.41 (dd, 1H, J = 3.4, 1.1 Hz, H-4); 5.32 (dd, 1H, J = 10.4, 8.3 Hz, H-2); 5.10 (dd, 1H, J = 10.4, 3.4 Hz, H-3); 4.14 (m, 2H, H-6 & H-6'); 4.05 (t, 1H, J = 6.7 Hz, H-5) 2.16 (s, 3H, Ac CH_3); 2.11 (s, 3H, Ac CH_3); 2.03 (s, 6H, 2 x Ac CH_3); 1.98 (s, 3H, Ac CH_3).

^{13}C NMR (75 MHz) δ : 170.7, 170.5, 170.2, 169.75, 169.2, 92.5, 72.0, 71.2, 68.2, 67.2, 61.3, 21.1, 20.9, 20.9, 20.8.

MS (ESI, +ve): m/z 413.1 $[\text{M}+\text{Na}]^+$.

MP: 148–150 °C (Literature⁴⁴: 142 °C).

Synthesis of **5a**



Tetraacetyl bromo- α -D-glucopyranose (40 mg, 0.10 mmol), pyrenebutyric acid (42 mg, 0.15 mmol), silver carbonate (567 mg, 2.06 mmol) and sodium sulfate (1.1 g, 7.9 mmol) were stirred in DCM (20 mL) at reflux, under an atmosphere of nitrogen in the dark for 2 d. The reaction mixture was then filtered through celite, the organic layer washed with sat. NaHCO_3 (aq) (20 mL) and water (20 mL), dried (MgSO_4) and the solvent removed under reduced pressure. Purification by flash chromatography (5% methanol/DCM; R_f = 0.70). The solvent was removed under reduced pressure to leave **5a** as a yellow solid (41.4 mg, 69%).

^1H NMR (400 MHz): δ 8.27 (d, 1H, J = 9.2 Hz, Ar H); 8.17 (m, 2H, Ar H); 8.12 (d, 1H, J = 9.3 Hz, Ar H); 8.11 (d, 1H, J = 7.8 Hz, Ar H) 8.03 (s, 2H, Ar H); 8.00 (t, 1H, J = 7.6 Hz, Ar H); 7.84 (d, 1H, J = 7.8, Ar H); 5.79 (d, 1H, J = 8.3 Hz, H-1); 5.27 (t, 1H, J = 9.3

Hz, *H*-3); 5.16 (m, 2H, *H*-2 & *H*-4); 4.30 (dd, 1H, *J* = 12.5, 4.6 Hz, *H*-6); 4.13 (dd, 1H, *J* = 12.5, 2.2 Hz, *H*-6'); 3.87 (ddd, 1H, *J* = 7.8, 4.5, 2.2 Hz, *H*-5); 3.38 (t, 2H, *J* = 7.7 Hz, -CH₂COO-); 2.52 (m, 2H, -CH₂CH₂-); 2.20 (m, 2H, -CH₂CH₂-); 2.06 (s, 3H, Ac CH₃); 2.04 (s, 3H, Ac CH₃); 2.01 (s, 3H, Ac CH₃); 1.96 (s, 3H, Ac CH₃).

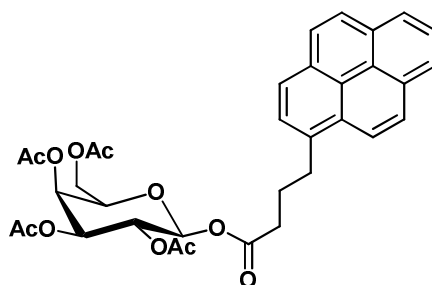
¹³C NMR (100 MHz): δ 171.9, 170.9, 169.7, 169.5, 135.5, 131.8, 131.2, 130.5, 129.1, 127.9, 127.8, 127.6, 127.2, 126.2, 125.5, 125.4, 125.2, 123.5, 92.1, 73.2, 73.1, 70.7, 68.2, 61.9, 33.9, 32.8, 26.7, 21.1, 21.0, 20.9, 20.9.

MS (ESI, +ve): *m/z* 641.1 [M+Na]⁺.

HRMS (ESI, +ve) *m/z* 641.1996 [M+Na]⁺, C₃₄H₃₄O₁₁Na required *m/z* 641.1993.

MP: 79–81 °C.

Synthesis of **5b**



Tetraacetyl bromo-α-D-galactopyranose (40 mg, 0.10 mmol), pyrenebutyric acid (42 mg, 0.15 mmol), silver carbonate (567 mg, 2.06 mmol) and sodium sulfate (1.1 g, 7.9 mmol) were stirred in DCM (20 mL) at reflux, under an atmosphere of nitrogen in the dark for 2 d. The reaction mixture was then filtered through celite, the organic layer washed with sat. NaHCO₃ (aq) (20 mL) and water (20 mL), dried (MgSO₄) and the solvent removed under reduced pressure. Purification by flash chromatography (5% methanol/DCM; *R_f* = 0.56). The solvent was removed under reduced pressure to leave **5b** as a white solid (24.5 mg, 41%).

¹H NMR (300 MHz): δ 8.28 (d, 1H, *J* = 9.3 Hz, Ar *H*); 8.18 (m, 2H, Ar *H*); 8.13 (d, 2H, *J* = 9.3 Hz, Ar *H*); 8.11 (d, 1H, *J* = 7.8 Hz, Ar *H*); 8.03 (s, 2H, Ar *H*); 7.99 (t, 1H, *J* = 7.6 Hz, Ar *H*); 7.84 (d, 1H, *J* = 7.8 Hz, Ar *H*); 5.79 (d, 1H, *J* = 8.3 Hz, *H*-1); 5.44 (dd, 1H, *J* = 3.4, 1.0 Hz, *H*-4); 5.36 (dd, 1H, *J* = 10.4, 8.3 Hz, *H*-2); 5.10 (dd, 1H, *J* = 10.4, 3.4 Hz, *H*-3); 4.11 (m, 3H, *H*-5, *H*-6 & *H*6'); 3.39 (t, 2, *J* = 7.7 Hz, -CH₂COO-); 2.53 (td, 2H, *J* = 7.3, 3.1 Hz, -CH₂CH₂-); 2.20 (m, 2H, -CH₂CH₂-); 2.17 (s, 3H, Ac CH₃); 2.03 (s, 3H, Ac CH₃); 2.00 (s, 3H, Ac CH₃); 1.97 (s, 3H, Ac CH₃).

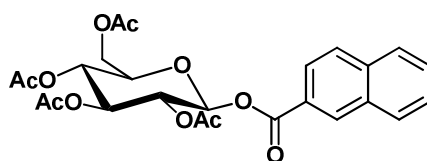
¹³C NMR (75 MHz) δ : 171.9, 170.4, 170.3, 169.7, 135.6, 131.8, 131.2, 130.4, 129.1, 127.9, 127.8, 127.6, 127.2, 126.2, 125.3, 125.2, 123.5, 92.6, 72.1, 71.2, 68.3, 67.2, 61.4, 34.0, 32.8, 26.8, 21.0, 21.0.

MS (ESI, +ve): m/z 641.0 [M+Na]⁺.

HRMS (ESI, +ve) m/z 641.1998 [M+Na]⁺, C₃₄H₃₄O₁₁Na required m/z 641.1993.

MP: 67–71 °C.

Synthesis of **6a**



Tetraacetyl bromo- α -D-glucopyranose (40 mg, 0.10 mmol), 2-naphthoic acid (25 mg, 0.15 mmol), silver carbonate (567 mg, 2.06 mmol) and sodium sulfate (1.1 g, 7.9 mmol) were stirred in DCM (20 mL) at reflux, under an atmosphere of nitrogen in the dark for 2 d. The reaction mixture was then filtered through celite, the organic layer washed with sat. NaHCO₃ (aq) (20 mL) and water (20 mL), dried (MgSO₄) and the solvent removed under reduced pressure. Purification by flash chromatography (5% methanol/DCM; R_f = 0.67). The solvent was removed under reduced pressure to leave **6a** as a cream solid (37.5 mg, 77%).

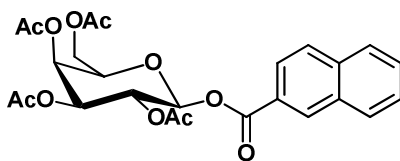
¹H NMR (400 MHz): δ 8.62 (s, 1H, Ar *H*); 8.03 (dd, 1H, J = 8.6, 1.7 Hz, Ar *H*); 7.97 (d, 1H, J = 8.0 Hz, Ar *H*); 7.89 (d, 1H, J = 8.7 Hz, Ar *H*); 7.87 (d, 1H, J = 8.1 Hz, Ar *H*); 7.60 (m, 2H, Ar *H*); 6.00 (d, 1H, J = 7.9 Hz, *H*-1); 5.37 (m, 2H, *H*-3 & *H*-2); 5.23 (t, 1H, J = 9.6 Hz, *H*-4); 4.34 (dd, 1H, J = 12.6, 4.5 Hz, *H*-6); 4.15 (dd, 1H, J = 12.5, 2.1, *H*-6'); 3.98 (ddd, 1H, J = 10.0, 4.5, 2.2, *H*-5); 2.07 (s, 3H, Ac CH₃); 2.06 (s, 3H, Ac CH₃); 2.05 (s, 3H, Ac CH₃); 1.98 (s, 3H, Ac CH₃).

¹³C NMR (100 MHz) δ : 170.9, 170.4, 169.8, 169.7, 165.0, 136.3, 132.8, 132.5, 130.0, 129.2, 128.8, 128.1, 127.2, 125.5, 92.8, 73.2, 73.1, 71.4, 70.6, 68.3, 61.9, 21.0, 20.9, 20.9, 20.9.

MS (ESI, +ve): m/z 525.0 [M+Na]⁺.

HRMS (ESI, +ve) m/z 525.1371 [M+Na]⁺, C₂₅H₂₆O₁₁Na required m/z 525.1367.

MP: 123–125 °C.

Synthesis of 6b

Tetraacetyl bromo- α -D-galactopyranose (40 mg, 0.10 mmol), 2-naphthoic acid (25 mg, 0.15 mmol), silver carbonate (567 mg, 2.06 mmol) and sodium sulfate (1.1 g, 7.9 mmol) were stirred in DCM (20 mL) at reflux, under an atmosphere of nitrogen in the dark for 2 d. The reaction mixture was then filtered through celite, the organic layer washed with sat. NaHCO_3 (aq) (20 mL) and water (20 mL), dried (MgSO_4) and the solvent removed under reduced pressure. Purification by flash chromatography (5% methanol/DCM; R_f = 0.62). The solvent was removed under reduced pressure to leave **7b** as an orange solid (38.7 mg, 79%).

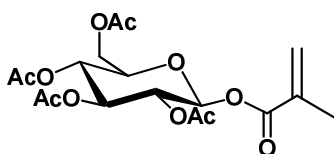
^1H NMR (400 MHz): δ 8.65 (s, 1H, Ar H); 8.05 (dd, 1H, J = 8.6 Hz, 1.7 Hz, Ar H); 7.98 (d, 1H, J = 8.0 Hz, Ar H); 7.89 (d, 1H, J = 8.7 Hz, Ar H); 7.87 (d, 1H, J = 8.2 Hz, Ar H); 7.58 (m, 2H, Ar H); 5.98 (d, 1H, J = 8.3 Hz, H -1); 5.60 (dd, 1H, J = 10.5, 8.3 Hz, H -2); 5.50 (d, 1H, J = 3.4 Hz, H -4); 5.20 (dd, 1H, J = 10.5, 3.4 Hz, H -3); 4.19 (m, 3H, H -5, H -6 & H 6'); 2.21 (s, 3H, Ac CH_3); 2.05 (s, 3H, Ac CH_3); 2.03 (s, 3H, Ac CH_3); 1.98 (s, 3H, Ac CH_3).

^{13}C NMR (100 MHz): δ 170.3, 170.2, 170.0, 169.5, 164.8, 136.0, 132.4, 132.2, 129.7, 128.8, 128.5, 127.8, 126.9, 125.7, 125.3, 93.0, 71.9, 70.8, 67.9, 67.0, 61.1, 20.7, 20.6.

MS (ESI, +ve): m/z 525.0 $[\text{M}+\text{Na}]^+$.

HRMS (ESI, +ve) m/z 525.1366 $[\text{M}+\text{Na}]^+$, $\text{C}_{25}\text{H}_{26}\text{O}_{11}\text{Na}$ required m/z 525.1367.

MP: 73–75 °C.

Synthesis of 7a

Tetraacetyl bromo- α -D-glucopyranose (100 mg, 0.243 mmol), methacrylic acid (0.025 mL, 0.292 mmol), silver carbonate (1.42 g, 5.15 mmol) and sodium sulfate (2.80 g, 19.7 mmol) were stirred in DCM (20 mL) at reflux, under an atmosphere of nitrogen in the dark for 17 h. The reaction mixture was then

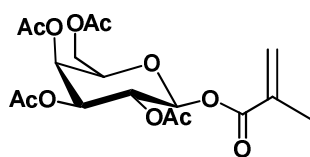
filtered through celite, the organic layer washed with sat. NaHCO_3 (aq) (20 mL) and water (20 mL), dried (MgSO_4) and the solvent removed under reduced pressure. Purification by flash chromatography (2.5% methanol/DCM; $R_f = 0.71$). The solvent was removed under reduced pressure to leave **7a** as a colourless oil (11.5 mg, 11%).

^1H NMR (300 MHz): δ 6.19 (m, 1H, $H\text{-b}$); 5.74 (d, 1H, $J = 7.7$ Hz, $H\text{-1}$); 5.69 (m, 1H, $H\text{-a}$); 5.22 (m, 3H, $H\text{-2}$, $H\text{-3}$ & $H\text{-4}$); 4.30 (dd, 1H, $J = 12.5, 4.5$ Hz, $H\text{-6}$); 4.12 (dd, 1H, $J = 12.5, 2.3$ Hz, $H\text{-6'}$); 3.88 (ddd, 1H, $J = 10.0, 4.5, 2.3$ Hz, $H\text{-5}$); 2.08 (s, 3H, Ac CH_3); 2.04 (s, 3H, Ac CH_3); 2.02 (s, 3H, Ac CH_3); 2.01 (s, 3H, Ac CH_3); 1.94 (m, 3H, CH_3).

^{13}C NMR (100 MHz): δ 170.7, 170.1, 169.5, 169.3, 165.1, 134.8, 128.4, 92.2, 72.7, 72.6, 70.1, 67.9, 61.6, 20.8, 20.6, 20.6, 18.1.

MS (ESI, +ve) m/z 439.1 $[\text{M}+\text{Na}]^+$.

Synthesis of **7b**



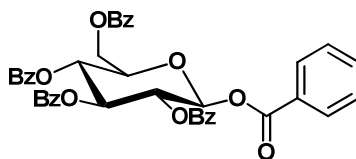
Tetraacetyl bromo- α -D-galactopyranose (100 mg, 0.243 mmol), methacrylic acid (0.025 mL, 0.292 mmol), silver carbonate (1.42 g, 5.15 mmol) and sodium sulfate (2.80 g, 19.7 mmol) were stirred in DCM (20 mL) at reflux, under an atmosphere of nitrogen in the dark for 17 h. The reaction mixture was then filtered through celite, the organic layer washed with sat. NaHCO_3 (aq) (20 mL) and water (20 mL), dried (MgSO_4) and the solvent removed under reduced pressure. Purification by flash chromatography (2.5% methanol/DCM; $R_f = 0.71$). The solvent was removed under reduced pressure to leave **7b** as a colourless oil (47.8 mg, 47%).

^1H NMR (400 MHz): δ 6.20 (m, 1H, $H\text{-b}$); 5.69 (d, 1H, $J = 8.4$ Hz, $H\text{-1}$); 5.67 (m, 1H, $H\text{-a}$); 5.42 (dd, 1H, $J = 3.6, 0.8$ Hz, $H\text{-4}$); 5.39 (dd, 1H, $J = 10.6, 8.2$ Hz, $H\text{-2}$); 5.10 (dd, 1H, $J = 10.4, 3.6$ Hz, $H\text{-3}$); 4.15 (m, 3H, $H\text{-5}$, $H\text{-6}$ & $H\text{-6'}$); 2.15 (s, 3H, Ac CH_3); 2.02 (s, 3H, Ac CH_3); 2.00 (s, 3H, Ac CH_3); 1.98 (s, 3H, Ac CH_3); 1.93 (m, 3H, CH_3).

^{13}C NMR (100 MHz): δ 170.6, 170.4, 170.2, 169.7, 165.4, 135.2, 128.5, 93.0, 72.1, 71.0, 68.1, 67.2, 61.3, 20.9, 20.9, 20.8, 18.3.

HRMS (ESI, +ve) m/z 439.1218 $[M+Na]^+$, $C_{18}H_{24}O_{11}Na$ required m/z 439.1211.

Synthesis of **8a**



Tetrabenzoyl bromo- α -D-glucopyranose (80 mg, 0.12 mmol), benzoic acid (28 mg, 0.23 mmol), silver carbonate (707 mg, 2.57 mmol) and sodium sulfate (1.75g, 12.3 mmol) were stirred in DCM (20 mL) at reflux, under an atmosphere of nitrogen in the dark for 2 d. The reaction mixture was then filtered through celite, the organic layer washed with sat. $NaHCO_3$ (aq) (20 mL) and water (20 mL), dried ($MgSO_4$) and the solvent removed under reduced pressure. Purification by flash chromatography (5% methanol/DCM; R_f = 0.81). The solvent was removed under reduced pressure to leave **8a** as a white solid (41.4 mg, 49%).

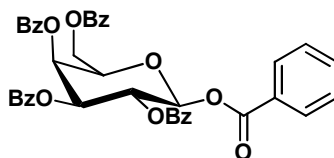
1H NMR (400 MHz): δ 8.06 – 7.86 (m, 10H, Ar H); 7.55 – 7.28 (m, 15H, Ar H); 6.32 (d, 1H, J = 8.0 Hz, H -1); 6.06 (t, 1H, J = 9.4 Hz, H -3); 5.90 – 5.82 (m, 2H, H -2 & H -4); 4.67 (dd, 1H, J = 12.3, 2.9 Hz, H -6); 4.52 (dd, 1H, J = 12.3, 4.7 Hz, H -6'); 4.44 (m, 1H, H -5).

^{13}C NMR (100 MHz): δ 166.4, 166.0, 165.5, 164.9, 134.2, 133.8, 133.8, 133.7, 133.4, 130.5, 130.2, 130.2, 130.3, 129.9, 129.1, 129.1, 129.1, 128.9, 128.8, 128.8, 128.7, 93.1, 73.6, 73.2, 71.2, 69.5, 63.1.

MS (ESI, +ve): m/z 722.9 $[M+Na]^+$.

MP: 186-187 °C.

Synthesis of **8b**



Tetrabenzoyl bromo- α -D-galactopyranose (80 mg, 0.12 mmol), benzoic acid (28 mg, 0.23 mmol), silver carbonate (889 mg, 3.20 mmol) and sodium sulfate (1.75g, 12.3 mmol, 81.2 equ) were stirred in DCM (20 mL) at reflux, under an atmosphere of nitrogen in the dark for 2 d. The reaction mixture was then filtered

through celite, the organic layer washed with sat. NaHCO_3 (aq) (20 mL) and water (20 mL), dried (MgSO_4) and the solvent removed under reduced pressure. Purification by flash chromatography (5% methanol/DCM; R_f = 0.72) and then by gravity chromatography (5% methanol/DCM). The solvent was removed under reduced pressure to leave **8b** as a white solid (51.2 mg, 60%).

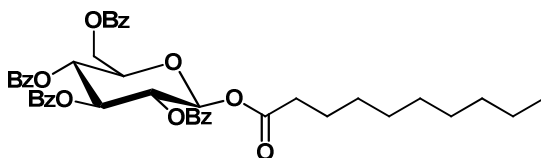
^1H NMR (400 MHz): δ 8.14-7.80 (m, 10H, Ar H); 7.64-7.24 (m, 15H, Ar H); 6.32 (d, 1H, J = 8.0 Hz, H -1); 6.11 (m, 2H, H -2 & H -4); 5.80 (dd, 1H, J = 10.4, 3.5 Hz, H -3); 4.68 (dd, 1H, J = 11.0, 6.4 Hz, H -6); 4.60 (td, 1H, J = 6.4, 1.0 Hz, H -5); 4.47 (dd, 1H, J = 11.0, 6.4 Hz, H -6').

^{13}C NMR (100 MHz): δ 166.3, 165.8, 165.8, 165.7, 165.0, 134.2, 134.0, 133.8, 133.7, 133.6, 130.6, 130.4, 130.2, 130.1, 130.1, 129.7, 129.4, 129.2, 129.1, 129.0, 128.9, 128.9, 128.8, 128.8, 128.7, 93.4, 72.8, 71.9, 69.2, 68.3, 62.1.

MS (ESI, +ve): m/z 722.9 $[\text{M}+\text{Na}]^+$.

MP: 166-167 °C

Synthesis of **9a**



Tetrabenzoyl bromo- α -D-glucopyranose (80 mg, 0.12 mmol), decanoic acid (31 mg, 0.18 mmol), silver carbonate (707 mg, 2.57 mmol) and sodium sulfate (1.40 g, 142 mmol) were stirred in DCM (10 mL) at reflux, under an atmosphere of nitrogen in the dark for 2 d. The reaction mixture was then filtered through celite, the organic layer washed with sat. NaHCO_3 (aq) (20 mL) and water (20 mL), dried (MgSO_4) and the solvent removed under reduced pressure. Purification by flash chromatography (10% methanol/DCM; R_f = 0.98). The solvent was removed under reduced pressure to leave **9a** as a colourless oil (50.7 mg, 56%).

^1H NMR (400 MHz): δ 8.04 (d, 2H, J = 7.8 Hz, Ar H); 7.94 (d, 2H, J = 7.8 Hz, Ar H); 7.90 (d, 2H, J = 7.8 Hz, Ar H); 7.84 (d, 2H, J = 7.8 Hz, Ar H); 7.57-7.29 (m, 12H, Ar H); 6.12 (d, 1H, J = 8.2 Hz, H -1); 5.96 (t, 1H, J = 9.6 Hz, H -3); 5.75 (t, 1H, J = 9.6 Hz, H -4); 5.68 (t, 1H, J = 9.0 Hz, H -2); 4.63 (dd, 1H, J = 12.2, 2.9 Hz, H -6); 4.49 (dd, 1H, J

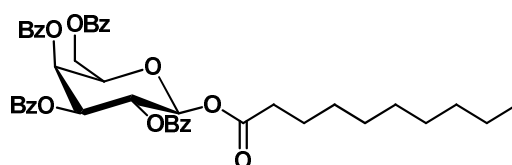
= 12.2, 4.8 Hz, *H*-6'); 4.31 (m, 1H, *H*-5); 2.31 (m, 2H, -CH₂COO-); 1.49 (m, 2H, -CH₂-); 1.27 – 1.10 (m, 12H, 6 x -CH₂), 0.87 (t, 3H, *J* = 7.1 Hz, -CH₃).

¹³C NMR (100 MHz): δ 172.2, 166.4, 166.0, 165.4, 165.3, 133.8, 133.8, 133.6, 133.4, 130.2, 130.1, 130.1, 129.9, 129.1, 129.1, 129.0, 128.8, 128.8, 128.7, 128.6, 92.3, 73.5, 73.2, 71.2, 69.5, 61.1, 34.4, 32.1, 29.5, 29.5, 29.4, 29.1, 24.9, 22.9, 14.4.

MS (ESI, +ve): *m/z* 772.8 [M+Na]⁺.

HRMS (ESI, +ve) *m/z* 768.3377 [M+NH₄]⁺, C₄₄H₄₆O₁₁NH₄ required *m/z* 768.3378.

Synthesis of **9b**



Tetrabenzoyl bromo-α-D-galactopyranose (80 mg, 0.12 mmol), decanoic acid (31 mg, 0.18 mmol), silver carbonate (707 mg, 2.57 mmol) and sodium sulfate (1.40 g, 142 mmol) were stirred in DCM (10 mL) at reflux, under an atmosphere of nitrogen in the dark for 2 d. The reaction mixture was then filtered through celite, the organic layer washed with sat. NaHCO₃ (aq) (20 mL) and water (20 mL), dried (MgSO₄) and the solvent removed under reduced pressure. Purification by flash chromatography (10% methanol/DCM; *R_f* = 0.82) and then by gravity chromatography (5% methanol/DCM). The solvent was removed under reduced pressure to leave **9b** as a colourless oil (44.3 mg, 49%).

¹H NMR (400 MHz): δ 8.10 (m, 2H, Ar *H*); 8.00 (m, 2H, Ar *H*); 7.92 (m, 2H, Ar *H*); 7.78 (m, 2H, Ar *H*); 7.64–7.35 (m, 10H, Ar *H*); 7.24 (m, 2H, Ar *H*); 6.11 (d, 1H, *J* = 8.3 Hz, *H*-1); 6.04 (dd, 1H, *J* = 3.4, 0.9 Hz, *H*-4); 5.92 (dd, 1H, *J* = 10.3, 8.3 Hz, *H*-2); 5.67 (dd, 1H, *J* = 10.3, 3.4 Hz, *H*-3); 4.64 (dd, 1H, *J* = 10.8, 6.1 Hz, *H*-6); 4.49 (td, 1H, *J* = 6.5, 0.9 Hz, *H*-5); 4.42 (dd, 1H, *J* = 10.8, 6.5 Hz, *H*-6'); 2.34 (td, 2H, *J* = 7.5, 2.4 Hz, -CH₂COO-); 1.52 (m, 2H, -CH₂-); 1.31–1.09 (m, 12H, 6 x -CH₂-); 0.87 (t, 3H, *J* = 7.1 Hz, -CH₃).

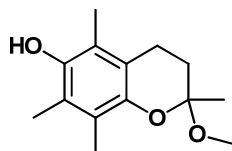
¹³C NMR (100 MHz): δ 172.2, 166.3, 165.8, 165.5, 134.0, 133.8, 133.7, 133.6, 130.4, 130.2, 130.2, 130.1, 129.7, 129.4, 129.2, 129.1, 129.0, 128.8, 128.8, 128.7, 92.6, 72.8, 72.0, 69.2, 68.3, 62.2, 34.5, 32.2, 29.6, 29.5, 29.4, 29.2, 27.8, 25.0, 14.4.

MS (ESI, +ve): *m/z* 772.8 [M+Na]⁺.

HRMS (ESI, +ve) m/z 768.3375 $[M+NH_4]^+$, $C_{44}H_{46}O_{11}NH_4$ required m/z 768.3378.

2.4.3. Synthesis of Vitamin E Derivatives

Synthesis of 11



Trimethylhydroquinone (20.0 g, 131 mmol) and trimethyl orthoformate (20.0 mL, 183 mmol) were dissolved in degassed methanol (80 mL). The mixture was cooled in ice under an atmosphere of nitrogen. Concentrated sulfuric acid (20 drops) was added followed by dropwise addition of methyl vinyl ketone (22.4 mL, 270 mmol). The reaction mixture was wrapped in foil and stirred at room temperature for 26 h after which time water (20 mL) was added. The resulting solid was filtered and washed with water (20 mL) to give **11** as a tan solid product (26.5 g, 85%) that could be used in subsequent reactions without further purification.

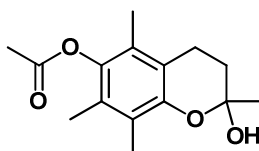
1H NMR (400 MHz) δ : 4.23 (s, 1H -OH); 3.21 (s, 3H, -OCH₃); 2.73/2.57 (ddd/ddd, 1H/1H, J = 16.6, 12.3, 6.6/16.4, 6.5, 2.1 Hz, -CH₂CH₂-); 2.17 (3H, Ar-CH₃); 2.16 (3H, Ar-CH₃); 2.11 (s, 3H, Ar-CH₃); 2.10/1.80 (ddd/ddd, 1H/1H, J = 13.4, 6.8, 2.2/13.4, 12.5, 6.6 Hz, -CH₂CH₂-); 1.54 (3H, -CH₃).

^{13}C NMR (100 MHz) δ : 145.8, 144.1, 122.6, 121.2, 118.9, 118.8, 97.6, 49.2, 32.3, 23.5, 20.4, 12.5, 11.9, 11.6.

MS (ESI, +ve): m/z 259.2 $[M+Na]^+$.

MP: 125–128 °C (Literature²⁸: 125–126 °C).

Synthesis of 12



Acetic anhydride (43 mL) was added to a mixture of **11** (5.0 g, 21 mmol) in pyridine (29 mL). The yellow solution was degassed for 45 minutes and allowed to stir at room temperature for 19 h. Ice water (120 mL) was then added and the

resultant oily suspension left to stir for 3 h at room temperature. The product was extracted into dichloromethane, washed with water (20 mL), 2M HCl (20 mL) and sat. NaHCO₃ (aq) (20 mL), dried (MgSO₄), filtered and solvent removed under reduced pressure to give the product (5.8 g, 98%) as a yellow oil. This product was used in the subsequent reaction without further purification.

¹H NMR (300 MHz) δ : 3.21 (s, 3H, -OCH₃); 2.71/2.54 (m/ddd, 1H/1H, J = 16.4, 6.3, 2.1 Hz, -CH₂CH₂-); 2.33 (s, 3H, CH₃CO₂-); 2.14 (s, 3H, Ar-CH₃); 2.07/1.79, m/td, 1H/1H, J = 12.9, 6.4 Hz, -CH₂CH₂-); 2.03 (s, 3H, Ar-CH₃); 1.98 (s, 3H, Ar-CH₃); 1.54 (s, 3H, -CH₃).

¹³C NMR (100 MHz) δ : 168.8, 147.4, 141.4, 126.4, 124.7, 122.2, 118.6, 97.2, 48.3, 31.4, 22.6, 19.8, 19.6, 12.5, 11.5, 11.2.

MS (ESI, +ve): m/z 301.2 [M+Na]⁺.

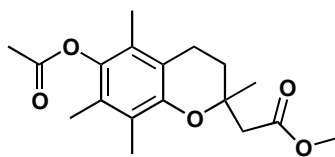
2-Hydroxy-2,5,7,8-tetramethyl-3,4-dihydro-2*H*-chromen-6-yl acetate (5.8 g, 21 mmol) was dissolved in acetone (28 mL) and water (15 mL) with concentrated HCl (10 drops). Acetone was removed at reflux until the distilling head reached 92 °C. The heat source was removed and acetone (60 mL) added when the temperature of the solution decreased to 70 °C. After cooling to 30 °C, the remaining acetone was removed under reduced pressure, leaving a bright yellow solid product. Cold water was added to the solid before it was filtered and washed with water. The solid was recrystallised from acetone/water to give the product, **12** (4.4 g, 80%) as a bright yellow solid.

¹H NMR (400 MHz) δ : 2.77/2.63 (m/ddd, 1H/1H, J = 16.7, 6.4, 3.2 Hz, -CH₂CH₂-); 2.4 (bs, 1H, -OH); 2.33 (s, 3H, CH₃CO₂-); 2.11 (s, 3H, Ar-CH₃); 2.09/1.84, m/m, 1H/1H, -CH₂CH₂-); 2.02 (s, 3H, Ar-CH₃); 2.00 (s, 3H, Ar-CH₃); 1.63 (s, 3H, -CH₃).

¹³C NMR (75 MHz) δ : 169.9, 148.3, 141.6, 127.2, 125.2, 123.1, 118.1, 95.8, 31.6, 29.8, 20.7, 20.3, 13.3, 12.7, 12.3.

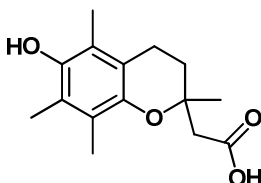
MS (ESI, +ve): m/z 287.2 [M+Na]⁺.

MP: 124-129 °C (Literature²⁸: 124-126 °C).

Synthesis of 13

Sodium hydride (1.6 g, 60% formulation, 39 mmol) was stirred in dry tetrahydrofuran (44 mL). Trimethyl phosphonoacetate (6.3 mL, 38 mmol) was added slowly (gas evolution and solid formation) and the mixture was stirred for 30 m. **12** (4.3 g, 16 mmol), pre-dissolved in dry tetrahydrofuran (34 mL) was then added slowly. The solution was stirred at room temperature overnight and then at reflux (~ 90 °C) for 4 h. The solvent was then removed under reduced pressure and the product dissolved in ether, washed with HCl (2M, 20 mL) and water (20 mL), dried (MgSO₄), filtered and the solvent removed to leave **13** (5.2 g, assumed 16.24 mmol) as a dark yellow oil. This product was used crude in subsequent reactions.

MS (ESI, +ve): m/z 343.3 [M+Na]⁺.

Synthesis of 14

Crude **13** (5.2 g, assumed 16 mmol) was dissolved in ethanol (30 mL). NaOH pellets (1.3 g, 33 mmol) pre-dissolved in water (30 mL) were added and the black-brown solution stirred at room temperature for 5 h. The solution was washed with hexane (2 x 30 mL) and then diluted with ice water (80 mL). Concentrated HCl (20 mL) was added drop wise to produce a dark red solid. The solid was filtered, washed with water and recrystallised twice from ethanol/water to give **13** (1.57 g, 37%) as a light tan fine solid.

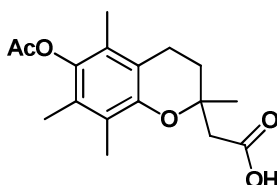
¹H NMR (400 MHz) δ : 2.67, (s, 2H, -CH₂CO₂H); 2.62 (m, 2H, -CH₂CH₂); 2.16 (s, 3H, Ar-CH₃); 2.11 (s, 3H, Ar-CH₃); 2.10 (s, 3H, Ar-CH₃); 1.95 (m, 2H, -CH₂CH₂); 1.44 (s, 3H, -CH₃).

¹³C NMR (75 MHz) δ : 175.1, 145.7, 144.7, 123.2, 121.8, 119.1, 117.3, 73.7, 44.3, 31.7, 24.7, 20.9, 12.6, 12.1, 11.6.

MS (ESI, +ve): m/z 287.2 [M+Na]⁺.

MP: 172-174 °C (Literature²⁸: 180–182 °C).

Synthesis of **15**

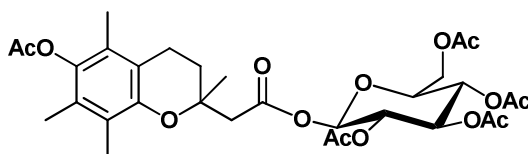


Acetic anhydride (30 mL) was added to a mixture of **14** (0.50 g, 1.9 mmol) in pyridine (20 mL). The yellow solution was degassed and allowed to stir at room temperature for 17 h. Ice water (120 mL) was then added and the resultant oily suspension left to stir for 5 h at room temperature. The product was extracted into dichloromethane (100 mL), washed with water (100 mL), HCl (2M, 100 mL) and sat. NaHCO₃ (aq) (100 mL), dried (MgSO₄), filtered and solvent removed under reduced pressure. Purification was by reverse phase HPLC on a C₁₈ Delta Pak column with a flow rate of 5 mL/minute. The solvent system used was 40:60 H₂O:ACN for 5 minutes then a gradual change to 20:80 H₂O:ACN for 10 minutes followed by a gradual change to 10:90 H₂O:ACN over 5 minutes and held for 10 minutes. The desired product eluted at approximately 25 minutes as detected at 256 nm absorbance. The solvent was removed under reduced pressure to leave **15** as a purple coloured oil product (498 mg, 86%).

¹H NMR (400 MHz) δ : 2.65 (m, 4H, -CH₂-CO₂H & -CH₂CH₂-); 2.34 (s, 3H, Ac CH₃); 2.09 (s, 3H, Ar-CH₃); 2.15/1.92 (m/m, 1H/1H, -CH₂CH₂-); 2.03 (s, 3H, Ar-CH₃); 1.99 (s, 3H, Ar-CH₃); 1.46 (s, 3H, -CH₃).

¹³C NMR (75 MHz) δ : 175.4, 170.0, 148.7, 141.6, 127.5, 125.6, 123.6, 117.4, 74.1, 53.7, 31.2, 24.7, 20.8, 20.8, 13.3, 12.4, 12.1.

MS (ESI, +ve): m/z 329.1 [M+Na]⁺.

Synthesis of 18

Tetraacetyl bromo- α -D-glucopyranose (465 mg, 1.13 mmol), **15** (519.0 mg, 1.70 mmol), silver carbonate (6.60 g, 24.0 mmol) and sodium sulfate (3.0 g, 21 mmol) were stirred in DCM (20 mL) at reflux, under an atmosphere of nitrogen in the dark for 18 h. The reaction mixture was then filtered through celite, the organic layer washed with sat. NaHCO₃ (aq) (20 mL) and water (20 mL), dried (MgSO₄) and the solvent removed under reduced pressure. Purification by flash chromatography (1% methanol/DCM; R_f = 0.70). The solvent was removed under reduced pressure to leave **18** as a yellow solid (662 mg, 92%).

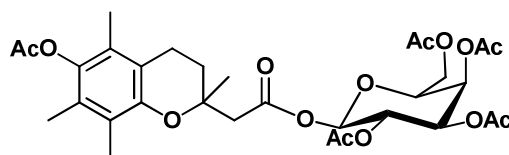
¹H NMR* (300 MHz) δ : 5.74 & 5.72 (d, 1H, J = 8.3 Hz, H -1); 5.24 – 5.08 (m, 3H, H -2, H -3 & H -4); 4.27 (dd, 1H, J = 12.5, 4.5 Hz, H -6); 4.09 (dd, 1H, J = 12.4, 2.2 Hz, H -6'); 3.83 (ddd, 1H, J = 9.9, 4.5, 2.3, H -5); 2.60 (m, 4H, -CH₂-CO₂- & -CH₂CH₂-); 2.30 (s, 3H, Ph Ac CH₃); 2.07 (m, 1H, -CH₂CH₂-); 2.05 (s, 3H, Ac CH₃); 2.04 (s, 3H, Ar CH₃); 2.01 (s, 3H, Ac CH₃); 1.99 (s, 3H, Ar CH₃); 1.98 (s, 3H, Ac CH₃); 1.95 (s, 3H, Ac CH₃); 1.92 (s, 3H, Ar CH₃); 1.83 (m, 1H, -CH₂CH₂-); 1.37 (s, 3H, -CH₃).

¹³C NMR* (75 MHz) δ : 170.8, 170.4, 170.4, 169.9, 169.6, 169.5, 169.4, 168.7, 148.7, 141.5, 127.5, 127.5, 125.5, 125.4, 123.7, 123.7, 117.3, 117.1, 92.0, 91.9, 73.8, 73.8, 70.5, 68.2, 68.2, 61.8, 31.3, 31.0, 30.0, 23.9, 21.0, 21.0, 20.8, 20.8, 20.7, 20.7, 20.7, 13.2, 12.4, 12.1.

MS (ESI, +ve): m/z 659.23 [M+Na]⁺.

MP: 142-145 °C.

* Both diastereomers present.

Synthesis of 19

Tetraacetyl bromo- α -D-galactopyranose (156 mg, 0.38mmol), **15** (141 mg, 1.70 mmol), silver carbonate (2.20 g, 8.06 mmol) and sodium sulfate (4.38 g, 30.9

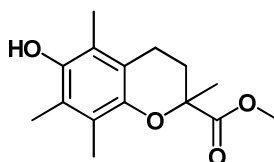
mmol) were stirred in DCM (20 mL) at reflux, under an atmosphere of nitrogen in the dark for 24 h. The reaction mixture was then filtered through celite, the organic layer washed with sat. NaHCO_3 (aq) (20 mL) and water (20 mL), dried (MgSO_4) and the solvent removed under reduced pressure. Purification was by reverse phase HPLC on a C_{18} Delta Pak column with a flow rate of 5 mL/minute. The solvent system used was 40:60 H_2O :ACN for 5 minutes then a gradual change to 20:80 H_2O :ACN for 10 minutes followed by a gradual change to 10:90 H_2O :ACN over 5 minutes and held for 10 minutes. The desired product eluted at approximately 33 minutes as detected at 256 nm absorbance. The solvent was removed under reduced pressure to leave **19** as a colourless oil (44.9 mg, 19%).

^1H NMR (400 MHz) δ : 5.72 (t, 1H, $J = 8.4$ Hz, $H-1$); 5.42 (dd, 1H, $J = 3.2, 0.8$ Hz, $H-4$); 5.34 (m, 1H, $H-2$); 5.08 (dd, 1H, $J = 10.4, 3.6$ Hz, $H-3$); 4.15 (m, 2H, $H-6$ & $H-6'$); 4.05 (m, 1H, $H-5$); 2.88–2.59 (m, 4H, $-\text{CH}_2\text{-CO}_2-$ & $-\text{CH}_2\text{CH}_2-$); 2.32 (s, 3H, Ph Ac CH_3); 2.17 (s, 3H, Ac CH_3); 2.09 (m, 1H, $-\text{CH}_2\text{CH}_2-$); 2.07 (s, 3H, Ar CH_3); 2.03 (s, 3H, Ac CH_3); 2.02 (s, 3H, Ac CH_3); 1.99 (s, 3H, Ac CH_3); 1.97 (s, 3H, Ar CH_3); 1.95 (s, 3H, Ar CH_3); 1.39 (s, 3H, CH_3).

^{13}C NMR (75 MHz) δ : 170.5, 170.3, 170.1, 170.1, 169.8, 169.5, 169.4, 168.7, 168.6, 148.6, 141.4, 127.4, 127.3, 125.3, 125.3, 123.6, 123.6, 117.2, 117.0, 92.3, 92.3, 73.7, 73.7, 71.9, 71.9, 71.2, 71.1, 67.9, 67.0, 61.1, 44.4, 31.2, 30.8, 24.8, 20.8, 20.7, 20.6, 20.6, 13.1, 12.3, 12.0.

HRMS (ESI, +ve) m/z 659.2303 $[\text{M}+\text{Na}]^+$, $\text{C}_{31}\text{H}_{40}\text{O}_{14}\text{Na}$ required m/z 659.2310.

Synthesis of **22**



Trimethylhydroquinone (1.0 g, 6.6 mmol), methyl methacrylate (3.5 mL, 33 mmol), 80% paraformaldehyde (494.0 mg, 13.2 mmol) and glacial acetic acid (190 μL , 3.40 mmol) were combined in a pressure tube and degassed for 10 min. The pressure tube was then sealed and heated to 180 $^\circ\text{C}$ for 3 h with constant stirring. After this time the tube was removed from heat. A cream coloured solid formed

upon cooling and was filtered and washed with cold methanol (10 mL) to afford **22** as a cream solid (1.03 g, 58%).

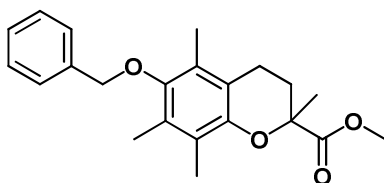
¹H NMR (300 MHz): δ 4.20 (s, 1H, -OH); 3.67 (s, 3H, -OCH₃); 2.70–2.38 (m, 2H, -CH₂CH₂-); 2.46–2.38 (m, 1H, -CH₂CH₂-); 2.18 (s, 3H, Ar CH₃); 2.16 (s, 3H, Ar CH₃); 2.07 (s, 3H, Ar CH₃); 1.92–1.81 (m, 1H, -CH₂CH₂-); 1.60 (s, 3H, CH₃).

¹³C NMR (75 MHz): δ 174.6, 145.7, 145.4, 122.7, 121.4, 118.5, 117.0, 77.4, 52.4, 30.8, 25.5, 21.1, 16.7, 12.3, 11.9, 11.3.

MS (ESI, +ve) m/z 265.3 [M+H]⁺, 287.3 [M+Na]⁺.

MP: 162–163 °C (Literature⁴⁵: 162–164 °C).

Synthesis of **23**

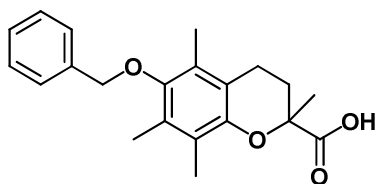


Compound **22** (300 mg, 1.13 mmol), benzyl bromide (0.54 mL, 4.5 mmol), potassium carbonate (628 mg, 4.54 mmol) were combined in ACN (20 mL) and allowed to stir under an atmosphere of nitrogen at reflux for 5 h. The reaction mixture was then filtered and the solvent removed under reduced pressure to leave a viscous yellow oil. The crude material was purified by column chromatography (DCM). The solvent was removed from the appropriate fraction under reduced pressure to leave **23** as a yellow oil (376 mg, 94%).

¹H NMR (400 MHz): δ 7.58–7.34 (m, 5H, Ar H); 4.76 (s, 2H, Bn CH₂); 3.74 (s, 3H, -OCH₃); 2.75–2.66 (m, 1H, -CH₂CH₂-); 2.63–2.48 (m, 2H, -CH₂CH₂-); 2.31 (s, 3H, Ar CH₃); 2.28 (s, 3H, Ar CH₃); 2.21 (s, 3H, Ar CH₃); 1.98–1.91 (m, 1H, -CH₂CH₂-); 1.70 (s, 3H, CH₃).

¹³C NMR (100 MHz): δ 174.3, 149.0, 148.0, 138.1, 128.4, 128.3, 127.8, 127.7, 126.0, 123.0, 117.3, 77.2, 74.7, 52.4, 30.6, 25.5, 21.0, 13.0, 12.0, 12.0.

MS (ESI, +ve) m/z 355.2 [M+H]⁺, 377.1 [M+Na]⁺.

Synthesis of 24

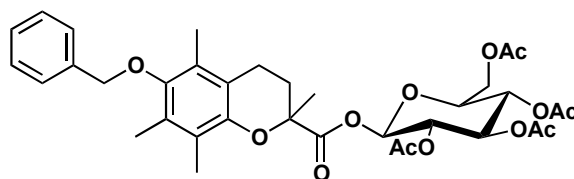
Compound **23** (2.3 g, 6.7 mmol) was stirred in ethanol (15 mL) and sodium hydroxide solution (3M, 12 mL) over night. The reaction mixture was then washed with hexane (20 mL) and the aqueous layer was acidified with concentrated hydrochloric acid (~ 10 mL). The white solid product **24** was filtered and washed with water (2.05 g, 90 %).

¹H NMR (400 MHz): δ 7.52–7.31 (m, 5H, Ar *H*); 4.70 (s, 2H, Bn *CH*₂); 2.71–2.56 (m, 2H, -*CH*₂*CH*₂-); 2.42–2.36 (m, 1H, -*CH*₂*CH*₂-); 2.23 (s, 3H, Ar *CH*₃); 2.17 (s, 3H, Ar *CH*₃); 2.15 (s, 3H, Ar *CH*₃); 1.99–1.92 (m, 1H, -*CH*₂*CH*₂-); 1.63 (s, 3H, *CH*₃).

¹³C NMR (100 MHz): δ 177.8, 149.4, 147.1, 137.9, 128.7, 128.6, 128.0, 127.9, 126.4, 123.0, 117.5, 77.3, 74.8, 30.1, 24.8, 20.7, 13.0, 12.2, 12.1.

MS (ESI, +ve) *m/z* 341.1 [M+H]⁺, 363.0 [M+Na]⁺, 379.0 [M+K]⁺; (ESI, -ve) *m/z* 339.0 [M-H]⁻.

MP: 148-150 °C.

Synthesis of 25

Compound **24** (200 mg, 0.59 mmol) was combined with tetraacetyl bromo- α -D-glucopyranose (363 mg, 0.88 mmol), silver carbonate (3.44 g, 12.5 mmol) and sodium sulfate (6.78 g, 47.8 mmol) in dry DCM (20 mL) with molecular sieves. The reaction was left to reflux under an atmosphere of nitrogen and in the dark over night. The reaction mixture was then filtered (celite), washed with sat. NaHCO₃ (aq) (2 x 20 mL), water (20 mL), dried (MgSO₄) and the solvent removed under reduced pressure to leave a thick oily crude mixture. Purification was by column chromatography (diethyl ether), the solvent removed from the appropriate fractions to leave **25** as a white solid (315 mg, 80%)

Reverse phase HPLC was then used on a small amount of the product in order to separate the diastereomers. A C₁₈ Delta Pak column with a flow rate of 5 mL/minute was used. The solvent system used was 20:80 H₂O:ACN for 10 minutes then a gradual change to 15:85 H₂O:ACN for 10 minutes. The desired product eluted at approximately 45 and 48 minutes as detected at 256 nm absorbance. The solvent was removed under reduced pressure to leave the colourless oil product (diastereomer 1: diastereomer 2 = 1:0.6).

Diastereomer 1

¹H NMR (600 MHz): δ 7.48 (m, 2H, Ar *H*); 7.40 (m, 2H, Ar *H*); 7.36 (m, 1H, Ar *H*); 5.67 (d, 1H, *J* = 8.0 Hz, *H*-1); 5.38–5.04 (m, 3H, *H*-2, *H*-3 & *H*-4); 4.68 (s, 2H, Bn CH₂); 4.25 (dd, 1H, *J* = 12.4, 4.4 Hz, *H*-6); 4.08 (dd, 1H, *J* = 12.4, 2.4 Hz, *H*-6'); 3.79 (ddd, 1H, *J* = 9.9, 4.8, 2.4 Hz, *H*-5); 2.66–2.61 (m, 1H, -CH₂CH₂-); 2.40–2.33 (m, 2H, -CH₂CH₂-); 2.22 (s, 3H, Ar CH₃); 2.17 (s, 3H, Ar CH₃); 2.10 (s, 3H, Ar CH₃); 2.07 (s, 3H, Ac CH₃); 2.02 (s, 3H, Ac CH₃); 2.01 (s, 3H, Ac CH₃); 2.01 (s, 3H, Ac CH₃); 1.93–1.89 (m, 1H, CH₂CH₂-); 1.64 (s, 3H, CH₃).

¹³C NMR (150 MHz): δ 171.6, 170.7, 170.2, 169.5, 169.1, 149.3, 147.7, 138.1, 128.8, 128.6, 128.0, 127.9, 125.9, 123.4, 116.8, 92.4, 74.8, 73.0, 72.9, 70.3, 68.1, 61.6, 30.3, 25.0, 20.9, 20.8, 20.7, 20.6, 13.0, 12.1, 11.9.

MS (ESI, +ve) *m/z* 693.2 [M+Na]⁺.

HRMS (ESI, +ve) *m/z* 693.2520 [M+Na]⁺, C₃₅H₄₂O₁₃Na required *m/z* 693.2518.

MP: 115–117 °C.

Diastereomer 2

¹H NMR (600 MHz): δ 7.47 (m, 2H, Ar *H*); 7.39 (m, 2H, Ar *H*); 7.34 (m, 1H, Ar *H*); 5.65 (d, 1H, *J* = 7.2 Hz, *H*-1); 5.21–4.99 (m, 3H, *H*-2, *H*-3 & *H*-4); 4.66 (s, 2H, Bn CH₂); 4.29 (dd, 1H, *J* = 12.4, 4.8 Hz, *H*-6); 4.07 (dd, 1H, *J* = 12.4, 2.4 Hz, *H*-6'); 3.78 (ddd, 1H, *J* = 9.9, 4.8, 2.4 Hz, *H*-5); 2.67–2.60 (m, 1H, -CH₂CH₂-); 2.55–2.46 (m, 2H, -CH₂CH₂-); 2.22 (s, 3H, Ar CH₃); 2.15 (s, 3H, Ar CH₃); 2.12 (s, 3H, Ar CH₃); 2.05 (s, 3H, Ac CH₃); 2.02 (s, 3H, Ac CH₃); 1.98 (s, 3H, Ac CH₃); 1.91–1.81 (m, 1H, CH₂CH₂-); 1.76 (s, 3H, Ac CH₃); 1.61 (s, 3H, CH₃).

¹³C NMR (150 MHz): δ 172.1, 170.5, 170.1, 169.3, 168.8, 149.1, 147.5, 137.9, 128.5, 128.5, 127.8, 127.7, 125.9, 123.2, 117.0, 91.9, 74.6, 72.9, 72.8, 69.8, 68.0, 61.5, 30.1, 25.3, 20.6, 20.5, 20.0, 12.8, 11.9, 11.8.

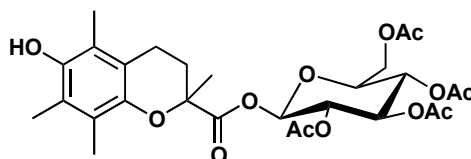
MS (ESI, +ve) m/z 693.2 $[M+Na]^+$.

HRMS (ESI, +ve) m/z 693.2520 $[M+Na]^+$, $C_{35}H_{42}O_{13}Na$ required m/z 693.2518.

MP: 115–117 °C.

Computational modelling: Calculations performed on the Gaussian 09 package. All geometries were modelled and optimised using B3LYP/6-31G(d). There were no imaginary frequencies.

Synthesis of **26**



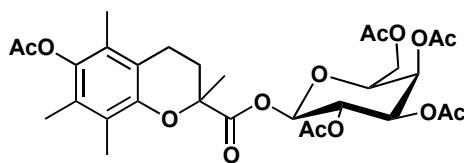
Compound **25** (20 mg, 0.03 mmol) was dissolved in ethyl acetate (3 mL) and the solution degassed with nitrogen before Pd/C (5%, 10 mg) was added and hydrogenated with a balloon of hydrogen gas at room temperature for 21 h. The solution was filtered through celite and the solvent removed under reduced pressure to give **26** as a colourless oil (17 mg, quant.).

1H NMR* (400 MHz): δ 5.65 & 5.64 (d, 1H, J = 8.0 Hz, H -1); 5.25–5.05 (m, 3H, H -2, H -3 & H -4); 4.28 & 4.22 (dd, 1H, J = 12.4, 4.8 Hz, H -6); 4.06 (dd, 1H, J = 12.6, 2.2 Hz, H -6'); 3.72 (m, 1H, H -5); 2.65 (m, 1H, $-CH_2CH_2-$); 2.35 (m, 2H, $-CH_2CH_2-$); 2.17 (s, 3H, CH_3); 2.15 & 2.15 (s, 3H, CH_3); 2.07 (s, 3H, CH_3); 2.05–1.98 (m, 12H, 4 x CH_3); 1.87 (m, 1H, $-CH_2CH_2-$); 1.62 & 1.59 (s, 3H, $-CH_3$).

^{13}C NMR* (100 MHz): δ 171.7, 170.7, 170.7, 170.2, 170.2, 169.5, 169.5, 169.1, 168.9, 145.7, 145.6, 145.5, 145.4, 123.0, 123.0, 121.6, 121.5, 118.5, 118.4, 116.8, 116.6, 92.3, 91.9, 77.0, 73.1, 73.0, 73.0, 72.9, 70.3, 70.0, 68.1, 61.7, 30.5, 29.8, 25.5, 25.1, 21.0, 20.8, 20.8, 20.7, 20.7, 20.6, 20.1, 12.3, 12.3, 11.9, 11.8, 11.4, 11.3.

MS (ESI, +ve) m/z 603.1 $[M+Na]^+$.

* Both diastereomers present

Synthesis of 29

Monoacetate trimethyl hydroquinone (41 mg, 0.21 mmol) was combined in a pressure tube with **7b** (44 mg, 0.11 mmol) and 80% paraformaldehyde (12 mg, 0.32 mmol) in toluene (2 mL) and degassed before dibutylamine (1.87 μ L, 0.01 mmol) and acetic acid (3.03 μ L, 0.05 mmol) were added and the pressure tube sealed and the reaction temperature set to reflux. Six d later, more paraformaldehyde (20 mg) and mono-protected hydroquinone (40 mg) were added. Three d later, the reaction mixture was allowed to cool before being washed with sat. NaHCO_3 (aq) (2x 20 mL), water (20 mL), dried (MgSO_4) and the solvent removed under reduced pressure. Purification by column chromatography (diethyl ether) failed to completely separate the components of the reaction. Reverse phase HPLC was then used on a C_{18} Delta Pak column with a flow rate of 5 mL/minute. The solvent system used was 20: 80 H_2O :ACN for 10 minutes then a gradual change to 15:85 H_2O :ACN for 10 minutes. The desired product eluted at 26 minutes as detected at 256 nm absorbance. The solvent was removed under reduced pressure to leave **29** as a colourless oil (8.9 mg, 14%).

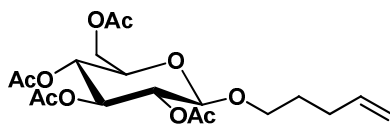
$^1\text{H NMR}^*$ (400 MHz): δ 5.64 (d, 1H, J = 8.4 Hz, H -1); 5.43 (t, 1H, J = 2.4 Hz, H -4); 5.34 (dd, 1H, J = 8.4, 10.4 Hz, H -2); 5.06 (ddd, 1H, J = 3.6, 10.4, 13.5 Hz, H -3); 4.13 (m, 2H, H -6 & H -6'); 4.02 (m, 1H, H -5); 2.66 (m, 1H, $-\text{CH}_2\text{CH}_2-$); 2.50 (m, 1H, $-\text{CH}_2\text{CH}_2-$); 2.34 (m, 1H, $-\text{CH}_2\text{CH}_2-$); 2.34 & 2.33 (s, 3H, CH_3); 2.19 & 2.18 (s, 3H, CH_3); 2.17 & 2.15 (s, 3H, CH_3); 2.03 (s, 3H, CH_3); 1.20 (s, 3H, CH_3); 1.99 & 1.97 (s, 3H, CH_3); 1.94 & 1.93 (s, 3H, CH_3); 1.85 (m, 1H, $-\text{CH}_2\text{CH}_2-$); 1.81 (s, 3H, CH_3); 1.64 & 1.60 (s, 3H, CH_3).

$^{13}\text{C NMR}^*$ (75 MHz): δ 170.4, 170.3, 170.3, 170.1, 170.0, 141.7, 127.5, 127.5, 125.1, 124.9, 123.5, 117.0, 116.8, 92.8, 92.5, 72.0, 71.9, 71.0, 70.9, 67.9, 67.4, 66.9, 66.8, 29.9, 25.4, 25.0, 20.8, 20.8, 20.7, 20.7, 20.6, 20.3, 13.1, 13.1, 12.2, 12.2, 11.9, 11.9.

MS (ESI, +ve) m/z 645.1 $[\text{M}+\text{Na}]^+$, 661.1 $[\text{M}+\text{K}]^+$.

HRMS (ESI, +ve) m/z 640.2600 $[\text{M}+\text{NH}_4]^+$, $\text{C}_{30}\text{H}_{42}\text{O}_{14}\text{N}$ required m/z 640.2600.

*Both diastereomers present

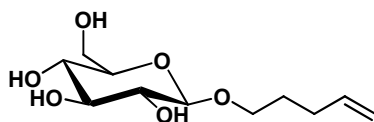
Synthesis of 31

Tetraacetyl bromo- α -D-glucopyranose (50 mg, 0.12 mmol), silver carbonate (413 mg, 2.59 mmol) and sodium sulfate (1.4 g, 9.9 mmol) were combined in freshly distilled DCM (5 mL) and 4-penten-1-ol (0.03 mL, 0.24 mmol) was then added. The reaction mixture was allowed to stir at room temperature for 24 h before it was filtered through celite. The organic layer was washed with water (2 x 20 mL), dried (MgSO_4) and the solvent removed under reduced pressure to leave a viscous colourless oil. Purification by flash chromatography (1% MeOH/DCM) to leave **31** as a clear colourless oil (34 mg, 66%).

^1H NMR (400 MHz): δ 5.77 (ddt, 1H, $J = 17.1, 10.3, 6.7$ Hz, $\text{CH}=\text{CH}_2$); 5.19 (t, 1H, $J = 9.6$ Hz, $H-3$); 5.06 (t, 1H, $J = 9.6$ Hz, $H-4$); 5.02–4.94 (m, 3H, $\text{CH}=\text{CH}_2$ & $H-2$); 4.48 (d, 1H, $J = 8.0$ Hz, $H-1$); 4.25 (dd, 1H, $J = 12.0, 4.8$ Hz, $H-6$); 4.12 (dd, 1H, $J = 12.0, 2.4$ Hz, $H-6'$); 3.86 (dt, 1H, $J = 9.6, 6.0$ Hz, $-\text{OCH}_2-$); 3.68 (ddd, 1H, $J = 9.8, 4.8, 2.4$ Hz, $H-5$); 3.49 (dt, 1H, $J = 9.6, 6.6$ Hz, $-\text{OCH}_2-$); 2.11 – 2.04 (m, 2H, $-\text{OCH}_2\text{CH}_2\text{CH}_2-$); 2.07 (s, 3H, Ac CH_3); 2.03 (s, 3H, Ac CH_3); 2.01 (s, 3H, Ac CH_3); 1.99 (s, 3H, Ac CH_3); 1.74–1.59 (m, 2H, $-\text{OCH}_2\text{CH}_2\text{CH}_2-$).

^{13}C NMR (100 MHz): δ 170.6, 170.3, 169.4, 169.3, 137.8, 115.1, 100.9, 72.9, 69.3, 68.6, 62.1, 29.9, 28.6, 20.7, 20.7, 20.6, 20.6.

MS (ESI, +ve) m/z 439.0 $[\text{M}+\text{Na}]^+$.

Synthesis of 32

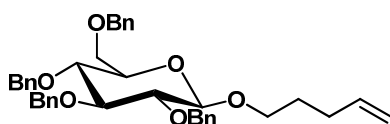
Compound **31** (34 mg, 0.08 mmol) was dissolved in methanol (5 mL) and sodium methoxide (10 mg) was added and allowed to stir at room temperature for 1 hour. Amberlite IR 120 was then added and the reaction mix was stirred for a further 30 minutes. It was then filtered and the filtrate was removed under reduced pressure to leave **32** as a white solid (20.3 mg, quant.).

¹H NMR (300 MHz): δ 5.79 (ddt, 1H, J = 17.1, 10.3, 6.7 Hz, CH=CH₂); 5.02–4.87 (m, 2H, CH=CH₂); 4.21 (d, 1H, J = 7.8 Hz, H-1); 3.91–3.79 (m, 2H, H-6 & -OCH₂-); 3.65 (dd, 1H, J = 5.3, 11.9 Hz, H-6'); 3.51 (dt, 1H, J = 9.6, 6.7 Hz, -OCH₂-); 3.27 (m, 3H, H-2, H-3, & H-4); 3.14 (m, 1H, H-5); 2.10 (m, 2H, -OCH₂CH₂CH₂-); 1.67 (m, 2H, -OCH₂CH₂CH₂-).

¹³C NMR (100 MHz): δ 138.9, 115.2, 103.9, 77.4, 77.2, 74.5, 71.1, 70.0, 62.2, 30.8, 29.6.

MS (ESI, +ve) m/z 271.1 [M+Na]⁺.

Synthesis of **33**

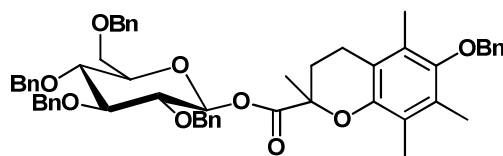


Compound **32** (31 mg, 0.12 mmol) was dissolved in DMF (2 mL) and NaH (60% dispersion in oil, 39 mg, 0.98 mmol) was added while in an ice bath. Benzyl bromide (0.13 mL, 1.1 mmol) was then slowly added and the reaction stirred at room temperature for 7 hours. Methanol (5 mL) was then added, followed by DCM (10 mL). The mixture was then washed with water (2 x 20 mL), dried (MgSO₄) and the solvent was removed under reduced pressure to leave a thick oil. This was purified by column chromatography (DCM then EtOAc), the solvent removed from the appropriate fractions to leave **33** as a white solid (30.8 mg, 41%).

¹H NMR (300 MHz): δ 7.41–7.15 (m, 20H, Ar H); 5.87 (ddt, 1H, J = 17.1, 10.3, 6.7 Hz, CH=CH₂); 5.12–4.57 (m, 10H, 4xBn CH₂, CH=CH₂); 4.44 (d, 1H, J = 7.8 Hz, H-1); 4.02 (dt, 1H, J = 9.5, 6.4 Hz, -OCH₂-); 3.83–3.47 (m, 7H, -OCH₂-, H-2, H-3, H-4, H-5, H-6 & H-6'); 2.23 (m, 2H, -OCH₂CH₂CH₂-); 1.82 (m, 2H, -OCH₂CH₂CH₂-).

¹³C NMR (100 MHz): δ 138.8, 138.6, 138.4, 138.3, 138.2, 128.5, 128.5, 128.3, 128.1, 128.0, 128.0, 127.9, 127.9, 127.8, 127.7, 115.0, 103.8, 84.9, 82.4, 78.1, 75.8, 75.1, 75.0, 75.0, 73.6, 69.5, 69.2, 30.4, 29.1.

MS (ESI, +ve) m/z 631.3 [M+Na]⁺.

Synthesis of 35

Glycosylated pentenyl ether **33** (31 mg, 0.05 mmol) was dissolved in DCM (2 mL) in an ice bath with molecular sieves. Br₂ (in DCM, 2.59 μ L, 0.05 mmol) was then added very slowly to the reaction. 90 min later, more Br₂ (1.30 μ L, 0.026 mmol) was slowly added to the reaction. 30 min later, the solvent was removed under reduced pressure. To the same flask, **24** (19 mg, 0.06 mmol), silver carbonate (298 mg, 1.10 mmol) and sodium sulfate (588 mg, 4.10 mmol) were added with fresh dry DCM (5 mL). The reaction temperature was set to reflux under an atmosphere of nitrogen, in the dark for 24 hours. The reaction mixture was then filtered (celite), washed with saturated sodium hydrogen carbonate (2 x 20 mL), water (20 mL), dried (MgSO₄) and the solvent removed under reduced pressure. Purification was attempted with column chromatography (various conditions: diethyl ether; DCM; 9:1 Hexane:EtOAc), however complete separation was not achieved. Reverse phase HPLC was then used on a C₁₈ Delta Pak column with a flow rate of 5 mL/minute using 100% ACN. The desired product eluted at approximately 52 and 55 minutes as detected at 256 nm absorbance. The solvent was removed under reduced pressure to leave the colourless oil product (11.9 mg, 43%, diastereomer 1: diastereomer 2 = 0.5:1.0).

Diastereomer 1

¹H NMR (400 MHz): δ 7.52–7.15 (m, 25H, Ar *H*), 5.57 (d, 1H, *J* = 8.0 Hz, *H*-1); 4.86–4.73 (m, 5H, Bn CH₂); 4.63 (s, 2H, Bn CH₂); 4.58–4.46 (m, 3H, Bn CH₂); 3.75–3.50 (m, 6H, *H*-2, *H*-3, *H*-4, *H*-5, *H*-6 & *H*-6'); 2.48–2.43 (m, 2H, -CH₂CH₂-); 2.41–2.35 (m, 1H, -CH₂CH₂-); 2.18 (s, 3H, Ar CH₃); 2.14 (s, 3H, Ar CH₃); 1.98 (s, 3H, Ar CH₃); 1.93–1.86 (m, 1H, -CH₂CH₂-); 1.66 (s, 3H, CH₃).

MS (ESI, +ve) *m/z* 885.3 [M+Na]⁺.

HRMS (ESI, +ve) *m/z* 885.3975 [M+Na]⁺, C₅₅H₅₈O₉Na required *m/z* 885.3973.

Diastereomer 2

¹H NMR (600 MHz): δ 7.41–7.10 (m, 25H, Ar H), 5.62 (d, 1H, J = 8.0 Hz, H-1); 4.81–4.73 (m, 3H, Bn CH₂); 4.61–4.50 (m, 3H, Bn CH₂); 4.43 (s, 2H, Bn CH₂); 4.38–4.27 (m, 2H, Bn CH₂); 3.72–3.55 (m, 6H, H-2, H-3, H-4, H-5, H-6 & H-6'); 2.68–2.56 (m, 2H, -CH₂CH₂-); 2.55–2.45 (m, 1H, -CH₂CH₂-); 2.18 (s, 3H, Ar CH₃); 2.09 (s, 3H, Ar CH₃); 2.03 (s, 3H, Ar CH₃); 1.93–1.81 (m, 1H, -CH₂CH₂-); 1.66 (s, 3H, CH₃).

¹³C NMR (150 MHz): 172.9, 149.2, 147.8, 138.5, 138.3, 138.2, 138.2, 138.1, 128.6, 128.5, 128.5, 128.5, 128.1, 128.0, 128.0, 128.0, 127.9, 127.8, 127.8, 127.6, 126.3, 122.9, 117.3, 95.1, 84.8, 81.1, 76.0, 75.7, 75.1, 74.6, 74.4, 73.7, 68.4, 30.4, 25.7, 20.8, 12.9, 12.1, 12.0.

MS (ESI, +ve) m/z 885.3 [M+Na]⁺.

HRMS (ESI, +ve) m/z 885.3975 [M+Na]⁺, C₅₅H₅₈O₉Na required m/z 885.3973.

2.5. References

1. Burton, G. W. and Ingold, K. U., *Acc. Chem. Res.*, **1986**, *19*, 194-201.
2. Porter, N. A., Caldwell, S. E. and Mills, K. A., *Lipids*, **1995**, *30*, 277-290.
3. Kagan, V. E., Serbinova, E. A., Bakalova, R. A., Stoytchev, T. S., Erin, A. N., Prilipko, L. L. and Evstigneeva, R. P., *Biochem. Pharmacol.*, **1990**, *40*, 2403-2413.
4. Serbinova, E., Kagan, V., Han, D. and Packer, L., *Free Radical Biol. Med.*, **1991**, *10*, 263-275.
5. Rowland, L. P. and Shneider, N. A., *N. Engl. J. Med.*, **2001**, *344*, 1688-1700.
6. Wiedau-Pazos, M., Goto, J. J., Rabizadeh, S., Gralla, E. B., Roe, J. A., Lee, M. K., Valentine, J. S. and Bredesen, D. E., *Science*, **1996**, *271*, 515-518.
7. Grurney, M. E., Cutting, F. B., Zhai, P., Doble, A., Taylor, C. P., Andrus, P. K. and Hall, E. D., *Ann. Neurol.*, **1996**, *39*, 147-157.
8. Desnuelle, C., Dib, M., Garrel, C. and Favier, A., *Amyotroph. Lateral Sc.*, **2001**, *2*, 9-18.
9. Graf, M., Ecker, D., Horowski, R., Kramer, B., Riederer, P., Gerlach, M., Hager, C. and Ludolph, A. C., *J. Neural. Transm.*, **2005**, *112*, 649-660.
10. Galbussera, A., Tremolizzo, L., Brighina, L., Testa, D., Lovati, R., Ferrarese, C., Cavaletti, G. and Filippini, G., *J. Neurol. Sci.*, **2006**, *27*, 190-193.
11. Ascherio, A., Weisskopf, M. G., O'Reilly, E. J., Jacobs, E. J., McCullough, M. L., Calle, E. E., Cudkowicz, M. and Thun, M. J., *Ann. Neurol.*, **2005**, *57*, 104-110.

12. Pappert, E. J., Tangney, C. C., Goetz, C. G., Ling, Z. D., Lipton, J. W., Stebbins, G. T. and Carvey, P. M., *Neurology*, **1996**, *47*, 1037-1042.
13. Gilgun-Sherki, Y., Melamed, E. and Offen, D., *Neuropharmacology*, **2001**, *40*, 959-975.
14. Adams, J. D. and Wang, B., *J. Cereb. Blood Flow Metab.*, **1994**, *14*, 362-363.
15. Bonina, F., Lanza, M., Montenegro, L., Salerno, L., Smeriglio, P., Trombetta, D. and Saija, A., *Pharm. Res.*, **1996**, *13*, 1343-1347.
16. Scott, J. W., Cort, W. M., Harley, H., Parrish, D. R. and Saucy, G., *J. Am. Oil Chem. Soc.*, **1974**, *51*, 200-203.
17. Cort, W. M., Scott, J. W., Araujo, M., Mergens, W. J., Cannalunga, M. A., Osadca, M., Harley, H., Parrish, D. R. and Pool, W. R., *J. Am. Oil Chem. Soc.*, **1975**, *52*, 174-178.
18. Sagach, V. F., Scrosati, M., Fielding, J., Rossoni, G., Galli, C. and Visioli, F., *Pharmacol. Res.*, **2002**, *45*, 435-439.
19. Praly, J., He, L., Qin, B. B., Tanoh, M. and Chen, G., *Tetrahedron Lett.*, **2005**, *46*, 7081-7085.
20. Spivak, A. Y., Knyshenko, O. V., Ivanova, O. V., Mallyabaeva, M. I., Murtazina, E. S., Ponedel'kina, I. Y. and Odinokov, V. N., *Russ. Chem. Bull., Int. Ed.*, **2007**, *56*, 2487-2490.
21. He, L., Galland, S., Dufour, C., Chen, G., Dangles, O., Fenet, B. and Praly, J., *Eur. J. Org. Chem.*, **2008**, 1869-1883.
22. Knas, M., Walejko, P., Maj, J., Hryniewicka, A., Witkowski, S., Borzym-Kluczyk, M., Dudzik, D. and Zwierz, K., *Toxicol. Mech. Methods*, **2008**, *18*, 491-496.
23. Chen, G. and Praly, J., *C. R. Chimie*, **2008**, *11*, 19-28.
24. Murase, H., Yamauchi, R., Kato, K., Kunieda, T. and Terao, J., *Lipids*, **1997**, *32*, 73-78.
25. Murase, H., Moon, J., Yamauchi, R., Kato, K., Kunieda, T., Yoshikawa, T. and Terao, J., *Free Radical Biol. Med.*, **1998**, *24*, 217-225.
26. Yoshida, N., Yoshikawa, T., Yamaguchi, T., Naito, Y., Tanigawa, T., Murase, H. and Kondo, M., *Antioxid. Redox Signaling.*, **1999**, *1*, 555-562.
27. Ochiai, J., Takano, H., Ichikawa, H., Naito, Y., Yoshida, N., Yanagisawa, R., Yoshino, S., Murase, H. and Yoshikawa, T., *Shock*, **2002**, *18*, 580-584.
28. Scott, J. W., Bizzarro, F. T., Parrish, D. R. and Saucy, G., *Helv. Chim. Acta*, **1976**, *59*, 290-306.

29. Bliard, C., Massiot, G. and Nazabadioko, S., *Tetrahedron Lett.*, **1994**, 35, 6107-6108.
30. Fukumoto, E., Torihara, M. & Tamai, Y., *Process for Producing Chroman*, US Patent 5,495,026, **1996**.
31. Tamura, Y., *Method for Producing 6-hydroxy-2,5,7,8-tetramethylchroman-2-carboxylic acid ester*, Patent number 2001-348619, **2003**.
32. Koenigs, W. and Knorr, E., *Ber. Dtsch. Chem. Ges.*, **1901**, 34, 957-981.
33. Frisch, M. J., Trucks, G. W., Schlegel, H. B., Scuseria, G. E., Robb, M. A., Cheeseman, J. R., Scalmani, G., Barone, V., Mennucci, B., Petersson, G. A., Nakatsuji, H., Caricato, M., Li, X., Hratchian, H. P., Izmaylov, A. F., Bloino, J., Zheng, G., Sonnenberg, J. L., Hada, M., Ehara, M., Toyota, K., Fukuda, R., Hasegawa, J., Ishida, M., Nakajima, T., Honda, Y., Kitao, O., Nakai, H., Vreven, T., Montgomery, J. J. A., Peralta, J. E., Ogliaro, F., Bearpark, M., Heyd, J. J., Brothers, E., Kudin, K. N., Staroverov, V. N., Kobayashi, R., Normand, J., Raghavachari, K., Rendell, A., Burant, J. C., Iyengar, S. S., Tomasi, J., Cossi, M., Rega, N., Millam, N. J., Klene, M., Knox, J. E., Cross, J. B., Bakken, V., Adamo, C., Jaramillo, J., Gomperts, R., Stratmann, R. E., Yazyev, O., Austin, A. J., Cammi, R., Pomelli, C., Ochterski, J. W., Martin, R. L., Morokuma, K., Zakrzewski, V. G., Voth, G. A., Salvador, P., Dannenberg, J. J., Dapprich, S., Daniels, A. D., Farkas, Ö., Foresman, J. B., Ortiz, J. V., Cioslowski, J. and Fox, D. J. *Gaussian 09* Wallingford CT, 2009.
34. Takabe, S., Takeda, T. and Ogihara, Y., *Carbohydr. Res.*, **1979**, 76, 101-108.
35. Ogawa, T., Nozaki, M. and Matsui, M., *Carbohydr. Res.*, **1978**, 60, c7 - c10.
36. Zhu, S., Li, Y. and Yu, B., *J. Org. Chem.*, **2008**, 73, 4978-4985.
37. Gauthier, C., Legault, J., Rondeau, S. and Pichette, A., *Tetrahedron Lett.*, **2009**, 50, 988-991.
38. Konradsson, P. and B., F.-R., *J. Chem. Soc., Chem. Commun.*, **1989**, 1124-1125.
39. Sheldrick, G. M., *Acta Crystallogr.*, **1990**, A46, 467-473.
40. Sheldrick, G. M., *Computer program for crystal structure refinement*, **1997**, University of Gottingen: Gottingen, Germany.
41. Barbour, L. J., *J. Supramol. Chem.*, **2001**, 1, 189-191.
42. Yu, C., Li, Z. and Cai, M., *Synth. Commun.*, **1990**, 20, 943-948.
43. Furniss, B. S., Hannaford, A. J., Smith, P. W. G. and Tatchell, A. R. *Vogel's Textbook of Practical Organic Chemistry, 5th edition*; Addison Wesley Longman Limited: England, 1996, p 438.
44. Wolfrom, M. L., *J. Am. Chem. Soc.*, **1930**, 52, 2464-2473.

45. Palozza, P., Piccioni, E., Avanzi, L., Vertuani, S., Calviello, G. and Manfredini, S., *Free Radical Biol. Med.*, **2002**, 33, 1724-1735.

CHAPTER 3

FUNCTIONAL PNA MONOMERS

Chapter 3. Functional PNA Monomers

3.1. Introduction

3.1.1. Modified Peptide Nucleic Acids

The many benefits of PNAs over other classes of nucleic acid molecules have long been known (see Chapter 1).¹⁻⁴ The unnatural, achiral PNA backbone is the structural feature that contributes most to the benefits of high sequence selectivity, strong DNA binding and resistance to nucleases and proteases. These benefits combine to produce a very useful class of molecule.⁵

To expand the potential application of PNA, many modified structures have been prepared.^{6,7} Modifications include conjugating a group to the *N* or *C* terminus of the PNA sequence,^{8,9} derivatising the natural nucleobases,^{10,11} changing the nucleobase linker,¹² substituting the PNA backbone^{13,14} and replacing the nucleobase with another useful moiety.^{15,16} Figure 3.1 summarises these points of modification on the structure of a PNA oligomer and compares the modifications with an unmodified PNA oligomer. Examples of some of the above modifications and the applications to which they relate are summarised below.

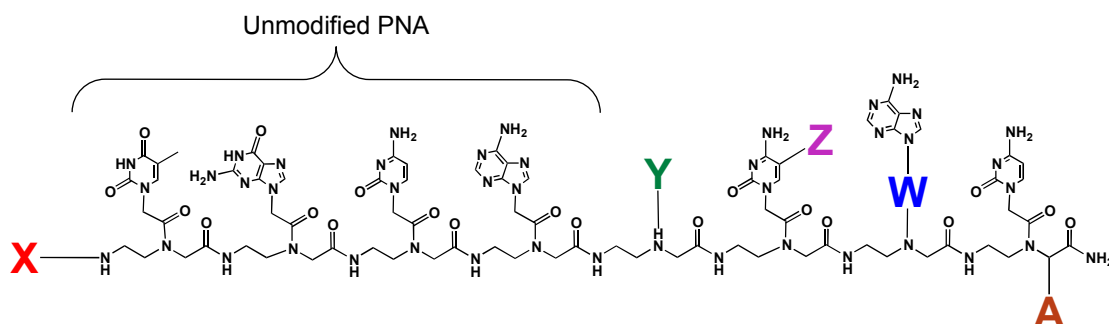


Figure 3.1: Representative PNA structure showing a section of unmodified PNA (left) in a sequence and also indicating potential positions for modification (right): X = N terminal conjugation of useful group; Y = Nucleobase replacement with useful group; Z = Nucleobase derivatisation; W = Substitution or derivatisation of linker; A = Substitution of PNA backbone.

In the field of antisense biosensors, Gasser *et al.* have synthesised modified PNA monomers containing a ferrocenyl moiety for use as a redox sensor for specific DNA/RNA sequences.^{17,18} In one variation, the ferrocenyl moiety was attached to the uracil nucleobase¹⁷ (Figure 3.2, left) of the monomer while in

another it was attached *via* a linker directly to the PNA monomer backbone¹⁸ (Figure 3.2, right), demonstrating the synthetic and derivatisable versatility of the PNA monomer. The purpose of the ferrocenyl-derivatised monomers was to provide an improved redox biosensor by incorporating multiple derivatised monomers in a single PNA oligomer. The benefit of the second derivative in which the ferrocenyl moiety is attached *via* a linker directly to the PNA monomer backbone, lies in the synthetic strategy used to prepare it. To protect the sensitive ferrocenyl moiety from the harsh conditions of PNA oligomer synthesis, this monomer is initially prepared as an alkyne-substituted monomer that is incorporated into the PNA oligomer. The ferrocenyl is then introduced to the completed PNA oligomer *via* a click reaction with an azidoferrocene. This synthetic strategy is not available to the first derivative in which the ferrocenyl moiety is attached to the uracil nucleobases prior to incorporation into the PNA oligomer.

Furthermore, the same group have prepared a bimetallic monomer in which the *C* terminus is attached to a platinum moiety and the *N* terminus is attached to a ferrocene moiety¹⁹ as well as most recently, modified PNA monomers with various ruthenium-containing complexes replacing the nucleobase for biosensing.²⁰

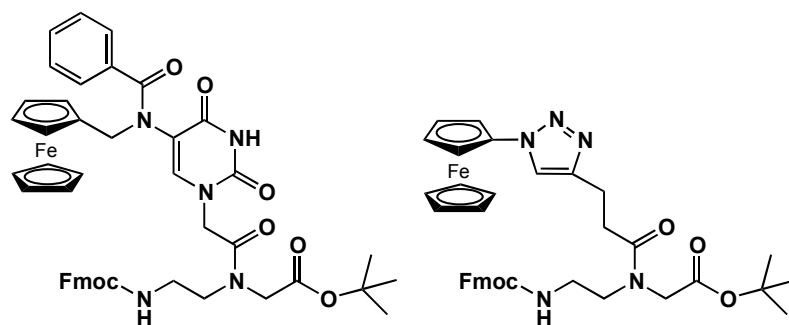


Figure 3.2: Ferrocenyl moiety attached to uracil nucleobase (left) and ferrocenyl moiety replacing the nucleobase (right).¹⁷

Modified PNA monomers have also been prepared with pyrene and acetate respectively replacing the nucleobase.²¹ Using varying numbers and combinations of the two modified monomers, oligomers were synthesised for potential use as polyintercalators with DNA (Figure 3.3). While various bisintercalators had been reported,²² there were fewer reports of tris- or higher intercalators due to the complexity in design and synthesis of polyintercalators including the requirement

of balance between a pre-organised arrangement and sufficient flexibility to follow changes in DNA conformation.²¹ Therefore the synthesis of modified PNA monomers was undertaken with the aim of addressing such obstacles to synthesise DNA polyintercalators.

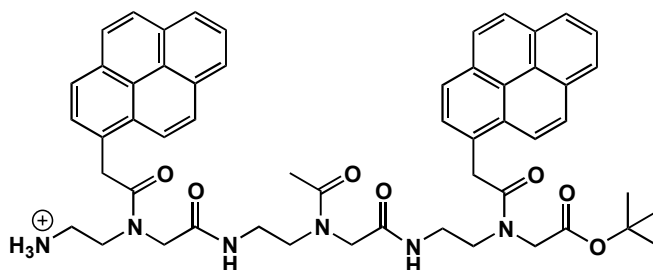


Figure 3.3: Structure of pyrene replacing the nucleobase to form a DNA polyintercalator.²¹

As an extension, “universal bases” have been prepared with a selection of polycyclic aromatic hydrocarbons such as 1-anthracene, 2-anthracene, 4-biphenyl and 5-acenaphthene replacing the nucleobases of the PNA monomer.²³ Universal PNA bases are PNA monomers that are able to pair equally well with any of the natural bases and therefore can be included in a sequence without destabilising a consequential duplex.²³ These “universal bases” may find potential application in PNA probe molecules to hybridise with various DNA targets.

Fluoroaromatic-substituted PNA monomers containing a 2,4-difluoro-5-methylphenyl moiety¹⁶ are a further development of aromatic-substituted nucleobases. When incorporated into oligomers, these modified monomers could find potential applications as probes for the study of hydrophobic and stacking interactions.¹⁶

Manicardi *et al.* have recently prepared uracil monomers modified with an azide group at the C5 position¹¹ as an access point for further modification (Figure 3.4). For reviews specifically on nucleobases modification in PNAs, see Wojciechowski and Hudson²⁴ and Pensato *et al.*⁶

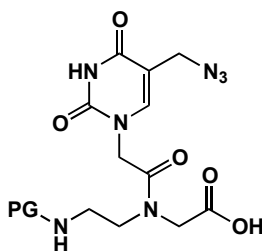


Figure 3.4: Structure of Manicardi's modified nucleobase.¹¹

3.1.2. PNA Modifications for Increased Solubility and Cell Penetration

While the properties of PNAs make them highly suitable as antisense diagnostic/probe molecules, unmodified PNAs are less successful as antisense therapeutic molecules.²⁵ The limited ability of unmodified PNA molecules to cross biological membranes²⁶ results in limited bioavailability of PNA molecules *in vivo*.^{25,27}

In order to improve the physicochemical properties of PNAs, there are many examples in the literature of modified PNA oligomers and monomers that aim to increase the solubility and cell-penetrating ability of PNAs. For example, the positively charged amino acid, lysine, has been added to PNA oligomers to increase their aqueous solubility.¹ Due to its positive charge, lysine also imparts electrostatic attraction to the otherwise neutral PNA. It is therefore likely that the lysine causes nonspecific DNA attraction.¹ The disadvantage of such a modification to the PNA oligomer is that it introduces a site of reactivity, which could also be a source of complication during synthesis.²⁸

Conjugation of PNA sequences has previously been shown to increase cellular up-take and overcome their poor membrane permeability.²⁹ Such molecules include cell-penetrating (or “Trojan”) peptides such as Tat, Penetratin and Transportan,^{30,31} lipids such as adamantly acetic acid,⁹ insulin-like growth factor peptide analogue,⁸ and even oligonucleotides.³²

The solubility of PNAs has successfully been enhanced by modified monomers.²⁸ Incorporation of the modified PNA monomers shown in Figure 3.5 into previously insoluble PNA oligomers resulted in the complete solubilisation of the oligomers, leading to improved synthesis, purification and use as probes. When the solubility enhancers were added to the *C* and/or *N* termini of PNA oligomers, in varying quantities, hybridisation to complementary nucleic acids was not affected.²⁸

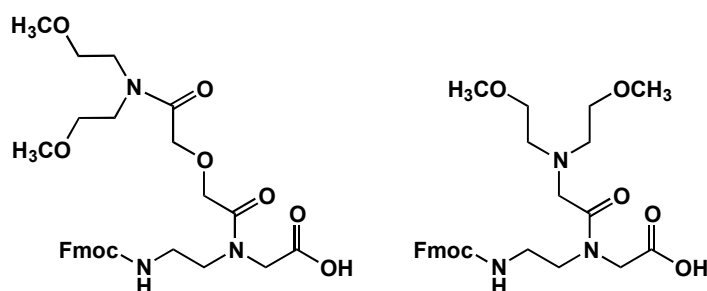


Figure 3.5: PNA solubility enhancers by Gildea *et al.*²⁸

There are a limited number of examples of PNA modifications involving sugars as solubilising agents. These modifications have been made to the PNA backbone in order to alter the pharmacokinetic properties of the PNA oligomer. In one example, modified thymine monomers substituted at the backbone “C” position with galactosyl, mannosyl, fucosyl, *N*-acetylgalactosaminyl, and *N*-acetylglucosaminyl substituents have been made.³³ Incorporation of each of the modified glycosylated monomers into a PNA oligomer resulted in a decrease in thermal stability of the corresponding PNA-RNA duplex.³³ The biodistribution of the resultant glycosylated PNA oligomers was altered significantly compared to unmodified oligomers with the *N*-acetylgalactosaminyl-substituted oligomer, in particular, displaying high affinity for the liver.³³

In a further development, a glycosylated PNA monomer has been prepared by forming a carbon-carbon bond with the “C” position of the backbone of a thymine nucleobase monomer (Figure 3.6) with a more efficient synthesis.³⁴ The purpose of this modified PNA monomer was to improve the biodistribution of the PNA sequence it is incorporated into, leading to increased water solubility without DNA binding hinderance.³⁴ The benefit of glycosylating a thymine monomer, rather than attaching a sugar moiety to the *N*-terminus of the sequence, is that the number and position of sugars can be varied, at least within the confines of sequence identity.

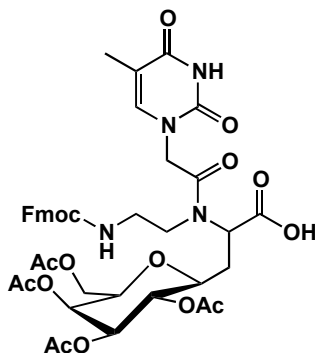


Figure 3.6: A glycosylated PNA thymine monomer.³⁴

3.1.3. Aims and Synthetic Plan

The over-arching aim of this Chapter is to develop new methods of incorporating glycosylated building blocks into PNA sequences in order to improve the physicochemical properties of the PNA and more specifically, enhance the BBB penetrating abilities of the PNA sequences. We have decided to explore two points of modification that have not yet been explored in the literature: *N* terminal conjugation (modification “X” in Figure 3.1) and nucleobases replacement (modification “Y” in Figure 3.1).

The general structure of modification “X” is shown in Figure 3.7. The use of two different linker groups, will be explored: the chiral amino acid serine and the achiral molecule 4-(hydroxymethyl)benzoic acid. These selected linker groups possess the required hydroxyl group to which the sugar moiety can be attached. They also possess the required carboxylic acid functionality to allow conjugation to the *N*-terminus of the PNA sequence *via* peptide bond formation.

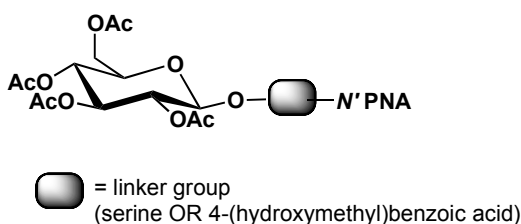


Figure 3.7: Structure of modification “X”: sugar moiety attached to a linker group to be conjugated to the *N* terminal of a PNA sequence.

The general structure of modification “Y” is shown in Figure 3.8. The synthesis of the modified glycosylated PNA monomer using three different types of linkers,

being rigid aromatic linkers, succinic anhydride linkers and alkyl linkers, will be explored.

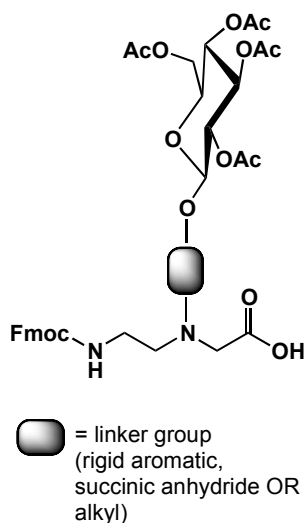


Figure 3.8: Structure of modification “Y”: sugar moiety replaces nucleobase and attached to PNA backbone by various linkers.

The synthesis of the glycosylated building blocks, using various linkers at both points of modification will focus on the optimisation of synthetic conditions to produce β -O-linked glycosides. The sugars to be used are glucose and galactose. The influence, if any, that the structural difference between these sugars has on transport and binding will be studied in Chapter 4.

3.2. Results and Discussion

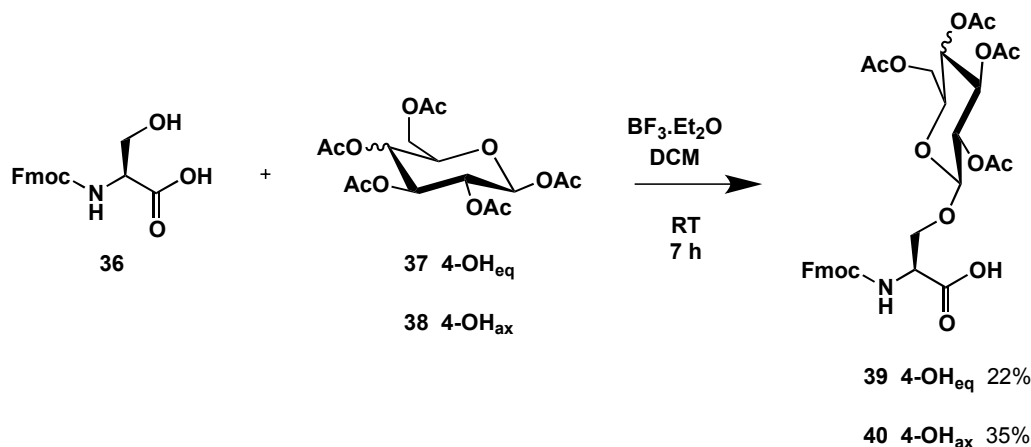
3.2.1. Design and Synthesis of Glycosylated Building Blocks for *N*-Terminal Conjugation

3.2.1.1. Chiral Glycosylated Building Blocks

The simplest approach to the addition of a carbohydrate to the PNA backbone would be to generate an appropriate glycosylated amino acid. Typical approaches use a pentaacetate of the sugar with the appropriate amino acid in the presence of a Lewis acid (Scheme 3.1).^{35,36}

Amino acids conferring hydroxyl groups such as serine, threonine and tyrosine, are appropriate with which to undergo glycosylation in a chemoselective way leaving the amino acid’s amine and carboxylic acid free for conjugation to the

backbone of a PNA. Owing to its simple structure, L-serine, **36**, was used in this project.



Scheme 3.1

The synthesis of compounds **39** and **40** proceeded smoothly with predictable elution times by RP-HPLC purification (eluent (v/v): 60% H₂O/40% ACN to 40% H₂O/60% ACN; C₁₈ column). ¹H NMR spectroscopy (Figure 3.9) supported product formation in both cases. Easily identifiable are the four singlets at 2.1 ppm representing the remaining four acetyl methyl groups of the product, indicating the fifth had been displaced. The coupling constant of the anomeric proton H-1 in each of these compounds was of the order 7-8 Hz, consistent with diaxial coupling between H-1 and H-2 and hence the β-anomer of the conjugate.

Mass spectrometry also supported the formation of each of these conjugates with [M+Na]⁺ signals identified in each case. While this method of conjugate synthesis was able to produce the desired product, it only did so in very low yields. Attempts to improve yield through increases in stoichiometry, elevated temperature, or longer reaction time failed to increase yields significantly. Low to moderate yields of glycosylated amino acids, with the galactose product forming in higher yield than the glucose product, have been reported previously.³⁶ The formation of undesired glycosylated by-products seems to be responsible for the low yields. Glycosylated building blocks **39** and **40** will be used in Chapter 4 to prepare novel PNAs.

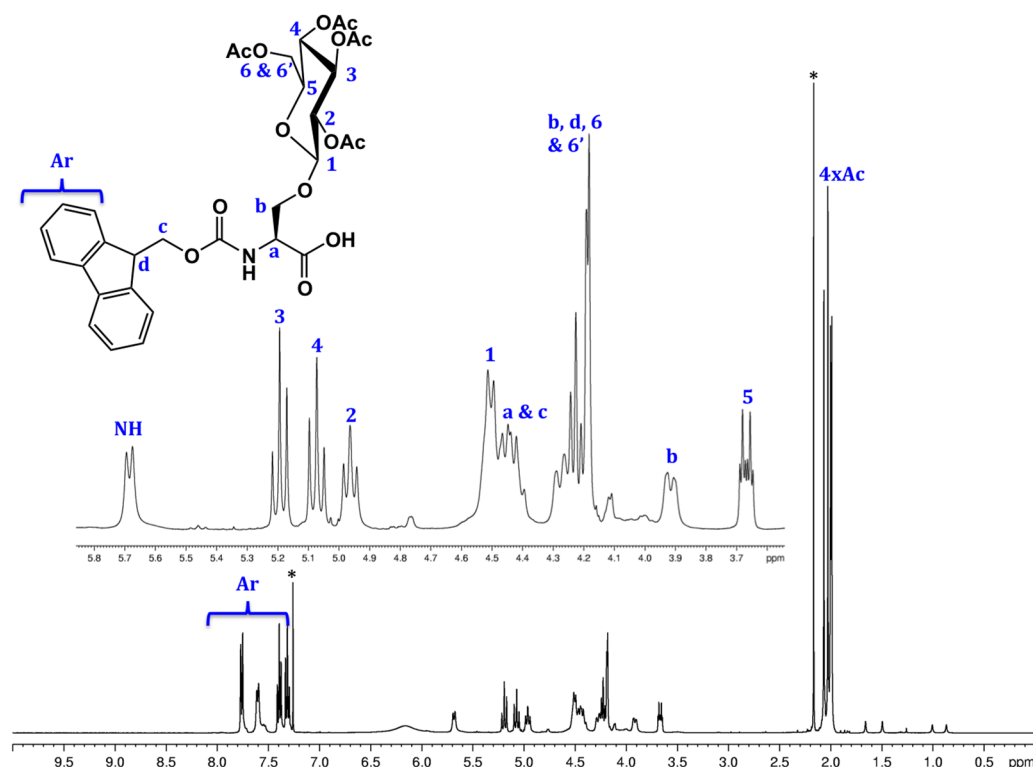


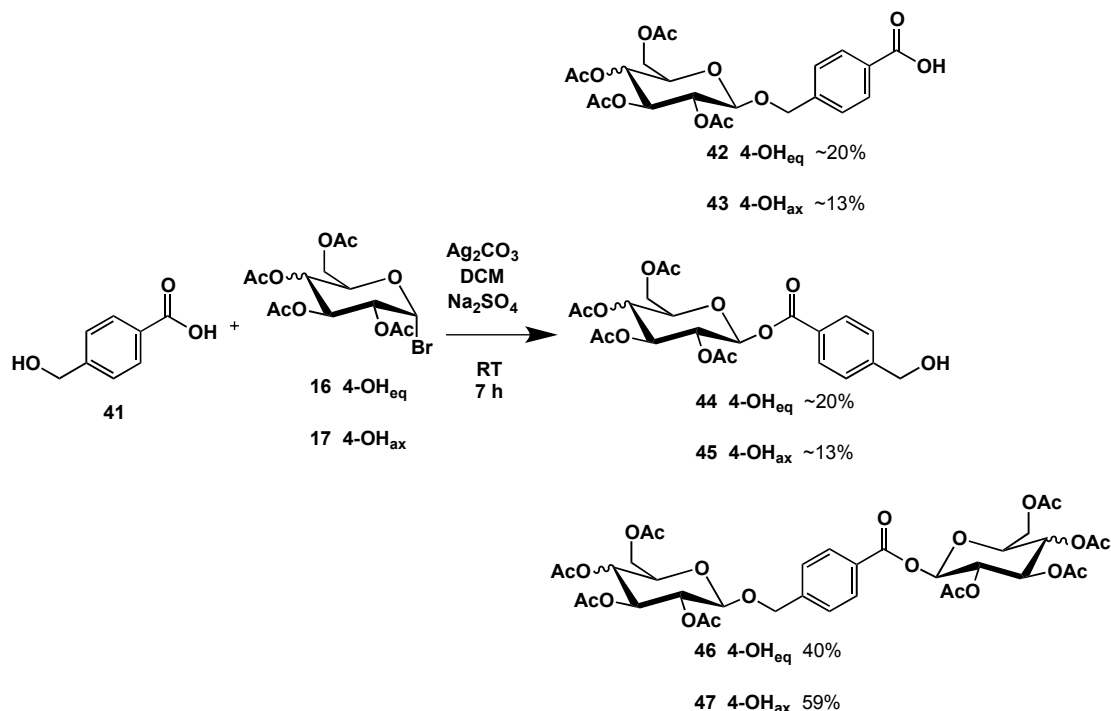
Figure 3.9: 400 MHz ^1H NMR spectrum of **39** (CDCl_3 , 300 K). * denotes residual solvent

3.2.1.2. Achiral Glycosylated Building Blocks

While the synthesis of glycosylated amino acids is a straightforward single step reaction and convenient way to couple sugars to a linker molecule so that they can be conjugated to PNA sequences, this method also produces chiral glycoconjugates from the chiral amino acid. This is potentially undesirable as the glycoconjugate may be recognised by endogenous peptidases *in vivo* and consequently degraded. One way of improving the biological stability of sugar conjugates is to produce achiral and hence less biologically recognisable conjugates.^{37,38}

In order to satisfy our conditions of glycosylation and functionalisation to the PNA backbone, 4-(hydroxymethyl)benzoic acid was seen as a suitable linker. While the use of $\text{BF}_3 \cdot \text{Et}_2\text{O}$ for glycosylation was low yielding in this case, silver carbonate was also investigated to facilitate the glycosylation. Here, as was seen with the use of L-serine, we expected that reaction was more likely to occur at the hydroxy group of 4-(hydroxymethyl)benzoic acid and the carboxylic acid could conjugate to the PNA backbone through peptide bond formation at a later stage. Reaction of 4-(hydroxymethyl) benzoic acid, **41**, with either acetobromoglucose,

16, or acetobromogalactose, **17**, in the presence of silver carbonate (Scheme 3.2), however, yielded a number of interesting products.



Scheme 3.2

Purification of the reaction mixtures by RP-HPLC led to the elution of two major fractions at 35 and 62 minutes (eluent (v/v): 60% H₂O/40% ACN to 40% H₂O/60% ACN; C₁₈ column). ¹H NMR analysis of the faster fraction indicated the presence of two products in equal proportions for both sugar forms. Clearly evident were two distinct ABq resonances between 7-8 ppm and a multiplication of overlapping signals for sugar, benzylic and acetate methyl protons, all integrating to double the expected amount.

The ESI mass spectrum of the 35 minute fraction for both the glucose and galactose derivative has a single peak at *m/z* 505.1, corresponding to the [M+Na]⁺ ion, which supports the theory that the two products present in the 35 minute HPLC fraction are regioisomers (**42** and **44** for glucose and **43** and **45** for galactose). The ¹H NMR spectra of the glucose and galactose mixtures indicate that the β-anomer of each isomer has formed, with each H-1 signal displaying a coupling constant of ~8 Hz at a chemical shift of 5.90 ppm for the esters **44** and **45** and a chemical shift of 4.56 ppm for the ethers **42** and **43**. As these two isomers eluted at the same time on a reverse phase column, no further attempt was made

to separate the isomers. Further NMR analysis allowed us to conclude the presence of the glycosyl ester and the glucoside/galactoside. ^1H NMR and ^{13}C NMR analyses of the slower eluting product for both glucose and galactose derivatives supported formation of the bis-sugar product **46** and **47**. Each glycosylated product was formed in approximate statistical yield, as expected.

^1H NMR spectroscopic evidence for the formation of products **46** and **47** include one AA'MM' system in the aromatic region between 7-8 ppm, signals for sugar protons integrating to that required for two sugar residues, one benzylic group signal only and 8 distinct singlets at approximately 2 ppm representing the acetyl methyl groups. ^{13}C NMR (jmod) spectroscopic evidence for the formation of products **46** and **47**, as distinct from the formation of two separate products, include the presence of three CH_2 signals in the region between 60-70 ppm representing two C-6 carbons and one benzylic carbon; 9 carbonyl carbon peaks and 2 aromatic CH peaks. The ESI mass spectrum also supports the formation of a bis-sugar product for both sugars with a signal at m/z 835.0, corresponding to the $[\text{M}+\text{Na}]^+$ ion.

While products **46** and **47** are of no use in the current project, the ability to make such products may be useful in the future.

3.2.2. Design and Synthesis of Glycosylated PNA Monomers – Replacing the Nucleobase

3.2.2.1. The PNA Monomer Backbone

The synthesis of *N*-functionalised 2-aminoethylglycine, has been reported previously.³⁹ The general utility of the PNA monomer is its amino acid structure, meaning it is amenable to the same peptide chemistry as other amino acids. The general structure of the 2-aminoethylglycine PNA monomer (Figure 3.10) contains a primary amine at one end of the backbone, that is often Fmoc protected, and a free carboxylic acid at the other. These functionalities allow amide bonds to form between monomers to produce a PNA sequence using solid-phase synthesis (SPS) methods. The tertiary nitrogen of the backbone is linked to the nucleobase (adenine, cytosine, guanine or thymine) *via* an amide link. Hence the identity of the PNA sequence depends upon the order of A, C, G and T, as with DNA. The

achiral and unnatural nature of PNA monomers gives rise to the increased biological stability of PNA oligomer compared to native DNA sequences.^{3,40}

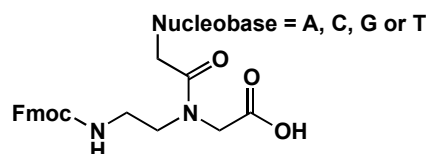
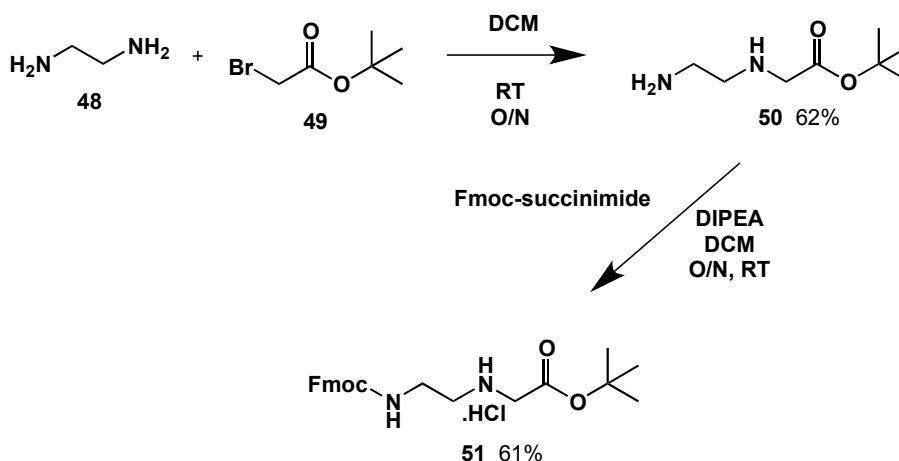


Figure 3.10: General structure of the PNA monomer backbone.

In order to synthesise glycosylated PNA monomers in which the nucleobase is replaced with a sugar, compound **51** was initially prepared (Scheme 3.3).

A protected form of 2-aminoethylglycine was synthesised in 2 steps. Ethylenediamine, **48**, was reacted with *t*-butyl bromoacetate, **49**, in a dropwise fashion, keeping the diamine in excess. Separation of the desired product by an aqueous wash from the statistical mix led to an expected yield of close to 50% as an orange oil. The product obtained had an indicative signal in the ¹H NMR spectrum at 1 ppm integrating to 9 protons representing the *t*-butyl group. The ESI mass spectrum of **50** supported product formation with a signal at *m/z* 175.17 corresponding to the [M+Na]⁺ ion.



Scheme 3.3

Reaction of **50** with the succinimidyl ester of Fmoc gave rise to the fully protected PNA monomer backbone **51** in 61% yield as the HCl salt, in slightly higher yield than previously reported.³⁹ The product was obtained as the hydrochloride salt white solid that precipitated out of a yellow solution at -20 °C in three crops. The product is more easily stored as the hydrochloride salt and only

converted to the free base immediately prior to use. The product obtained had indicative signals in the ^1H NMR spectrum (Figure 3.11) attributable to the Fmoc signals and a new downfield broad signal representing the NH of the newly formed amide bond.

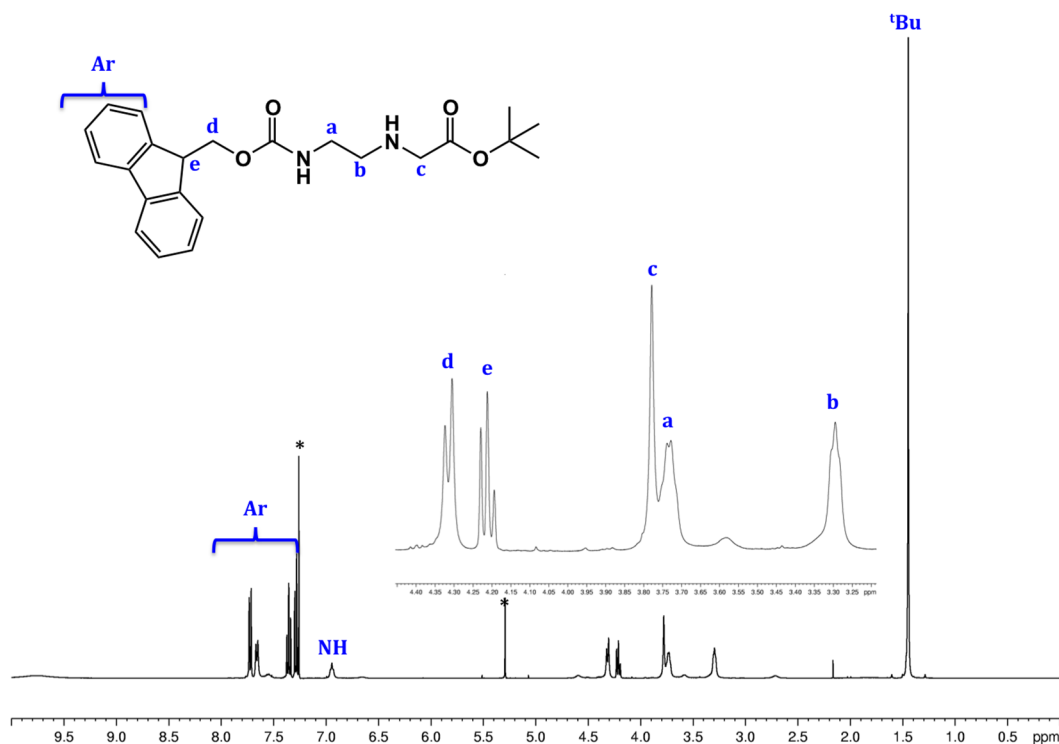
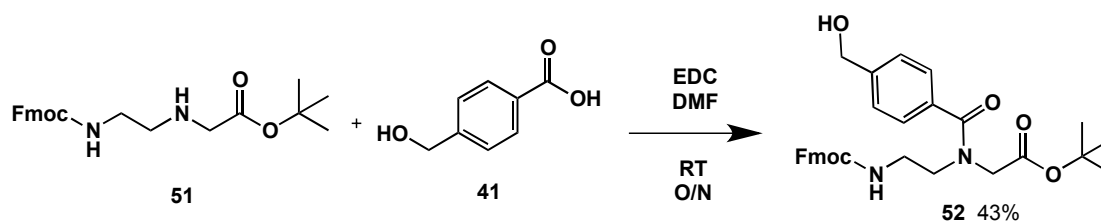


Figure 3.11: 400 MHz ^1H NMR spectrum of **51** (CDCl_3 , 300 K). * denotes residual solvent.

3.2.2.2. Rigid-Linked Glycosylated Monomers

The original approach undertaken to the synthesis of our target sugar conjugates employs a rigid spacer between the backbone and sugar groups, thereby directing the sugar away from the backbone. We chose to begin our studies with **41** bearing both alcohol and acid groups. In order to overcome the problems associated with the production of undesired products **44-47** (Scheme 3.2), we decided to amide couple to the backbone first, in place of the nucleobases, so that glycosylation of the benzylic alcohol could proceed without complication.

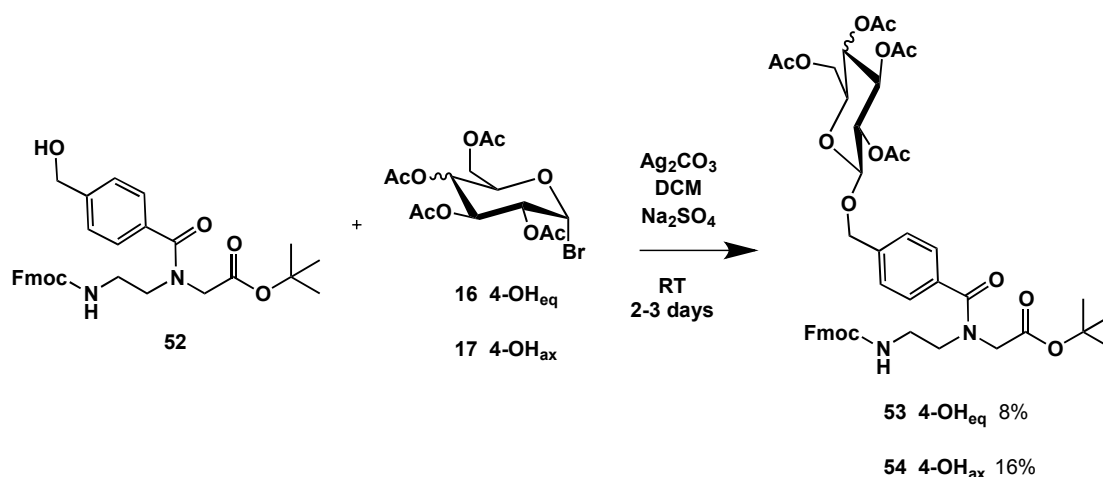
The coupling of **41** with the 2-aminoethylglycine derivative **51** using the coupling reagent 1-ethyl-3-(3-dimethylaminopropyl)carbodiimide (EDC) hydrochloride led to the formation of **52** in 43% yield (Scheme 3.4).



Scheme 3.4

The reaction was monitored by TLC analysis and ceased when no starting material was observed in the reaction mixture. Column chromatography (5% MeOH/DCM) was used to purify **52** and ESI mass spectrometry supported product formation with a signal at m/z 531.6 corresponding to the $[M+H]^+$ ion. The presence of four extra aromatic proton signals, yielding an AA'MM' system, in the ^1H NMR spectrum of **52** compared to that of **41** supported the successful coupling of 4-(hydroxymethyl)benzoic acid to the backbone. There are some interesting issues with this spectrum that have plagued much of the following characterisation. The coupling of **41** has caused the methylene proton signals of **52** to broaden considerably. Also, the signal corresponding to the *t*-butyl methyl protons is represented by two broad singlets, whereas in the spectrum of **51**, it appears as one sharp singlet. Restricted rotation about the tertiary amide bond of the backbone can lead to two rotamers.⁴¹ Therefore the broadening of signals and duplication of some signals are attributed to the likely result of the product existing in two rotamer forms. This will be discussed further in later sections of this chapter. The ^{13}C NMR spectrum for **52** supports product formation with an additional carbonyl carbon peak at 173 ppm (amide bond), additional aromatic carbon peaks and an extra CH_2 peak at 63.9 ppm corresponding to the methylene next to the OH group of 4-(hydroxymethyl)benzoic acid.

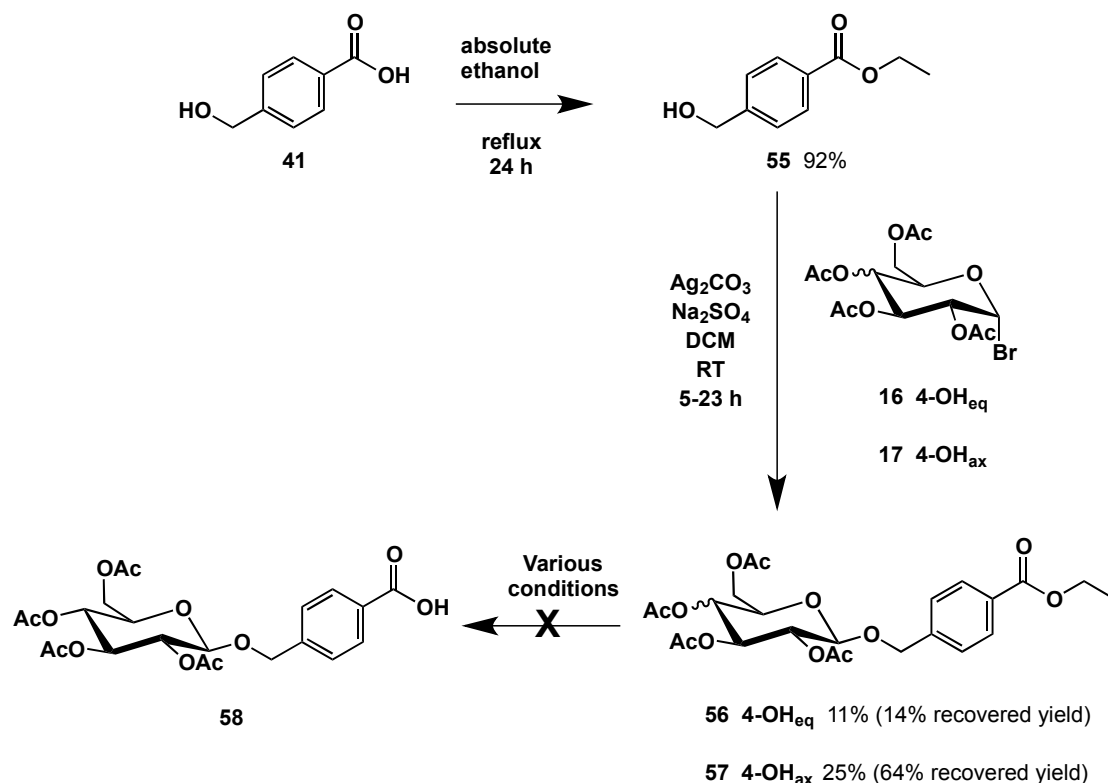
While this reaction did produce the desired substituted backbone product, it proceeded in moderate yields at best (43%) with tedious purification required to remove impurities and side products. Nevertheless, with **52** in hand, glycosylation with glucose or galactose using silver carbonate as the promoter was undertaken (Scheme 3.5).



Scheme 3.5

While silica column chromatography (5% v/v MeOH/DCM) was unable to separate the products from other impurities, RP-HPLC gave the desired conjugates in a highly purified form, albeit low yield. The ¹H NMR spectra of **53** and **54** both displayed very broad signals, as seen in **52**. Normally the size of the coupling constant of H-1 is used to determine the orientation of the glycosidic bond. However due to the broad, undefined peaks in these spectra, no coupling is determinable. The ¹³C NMR spectra, however, of **53** and **54** clearly show the peaks corresponding to C-1 have chemical shifts of 100.0 ppm and 97.7 ppm respectively. While different glycosides exhibit different anomeric chemical shifts, it has been observed throughout this work with various glycosyl ethers that a chemical shift towards 100 ppm for the C-1 carbon is indicative of the presence of the β-anomer, whereas a chemical shift closer to 90 ppm suggests the α-anomer.

While achievable, the overall yields for this sequence were low, despite attempts to optimise the reaction conditions. A new synthetic approach began by protecting the carboxylic acid of 4-(hydroxymethyl)benzoic acid (Scheme 3.6) to produce **55** in excellent yield. This simple esterification was carried out using acidified absolute ethanol. The characteristic triplet and quartet signals in the ¹H NMR spectrum of **55** at 1.38 and 4.35 ppm, respectively, are indicative of the ethyl protecting group, supporting successful product formation.



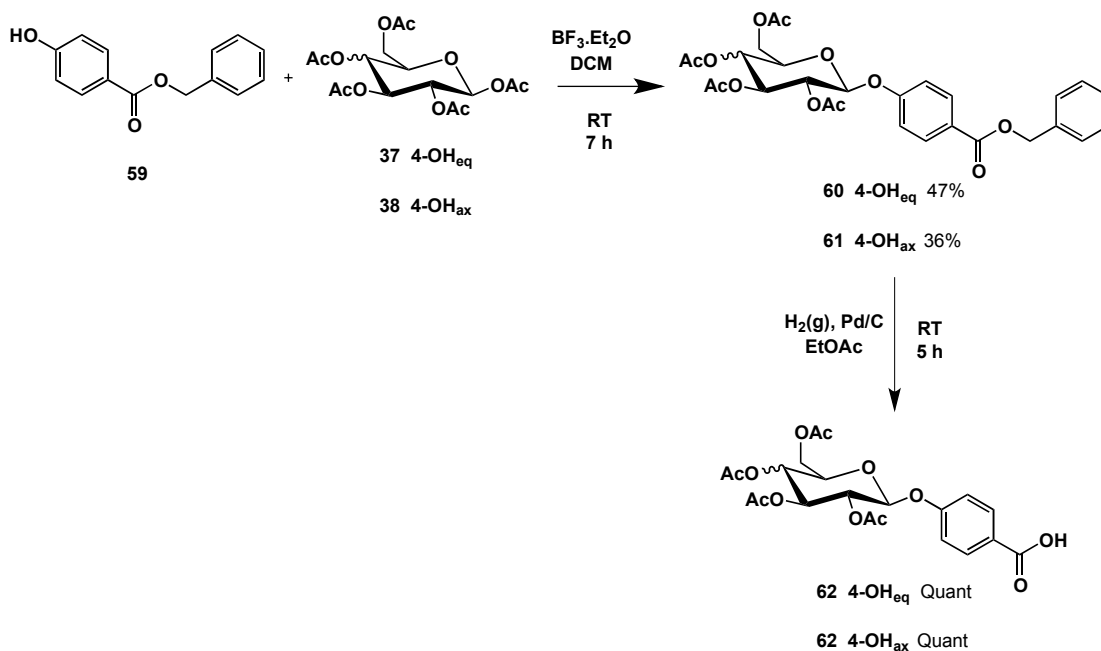
Scheme 3.6

The ester **55** was glycosylated using silver carbonate as the promoter to give compounds **56** and **57** (glucose and galactose conjugate, respectively). Reverse phase HPLC was used to purify both conjugates. The ¹H NMR spectra of these compounds, and in particular the H-1 coupling constants, both indicate that the β-glycoside was formed (*J* 7.7 Hz and 7.9 Hz for **56** and **57**, respectively). ESI mass spectrometry yielded peaks corresponding to the sodium adduct of the glucose and galactose conjugate at *m/z* 533.0 and 533.2, respectively.

Various conditions were attempted including lithium hydroxide, aqueous hydrochloric acid, enzymatic cleavage with Pancreatin and sodium hydroxide, however none of these conditions successfully cleaved the ethyl ester while leaving the sugar acetate protecting groups intact.

Despite success in coupling, and with the ethyl ester not being able to be cleaved successfully, an adaptation of the protocol to allow hydrogenation of the protected linker group was undertaken. Scheme 3.7 shows the reaction of benzyl 4-hydroxybenzoate, **59** with glucose or galactose. After the trial of AgOTf, Ag₂CO₃ and BF₃.Et₂O at various temperatures, reaction times and ratios of reactants and promoters, it was found that BF₃.Et₂O gave the highest conversion of starting

material to product. The β -anomer was the major anomer produced and could be separated from the α -anomer by RP-HPLC, with the former eluting first. It was found that a reaction time of only one hour gave the highest yield of the desired β -anomer in the case of the galactose conjugate. The glucose conjugate was consistently produced in a higher β to α ratio (1 : 0.026) than the galactose conjugate (1 : 0.26).



Scheme 3.7

For both **60** and **61**, the ^1H NMR (Figure 3.12, Figure 3.13 and Figure 3.14) and ^{13}C NMR spectra can distinguish between the α and β anomers. The signals corresponding to the acetate protons, H -1, H -2, H -3 and H -4 in the ^1H NMR spectra are the most significantly different for the two anomers.

The cleavage of the benzyl ester for both **60** and **61** was extremely facile. When TLC analysis had shown that all starting material had been cleaved, the reaction mixture was filtered through celite to remove the Pd/C catalyst and the solvent removed to leave the products as a white solid with no need for purification in quantitative yields. The absence of signals in the ^1H NMR spectra corresponding to the benzyl protecting group (multiplet integrating to five protons at 7.37 ppm and the singlet at 5.35 ppm integrating to two) supported formation of **62** and **63**.

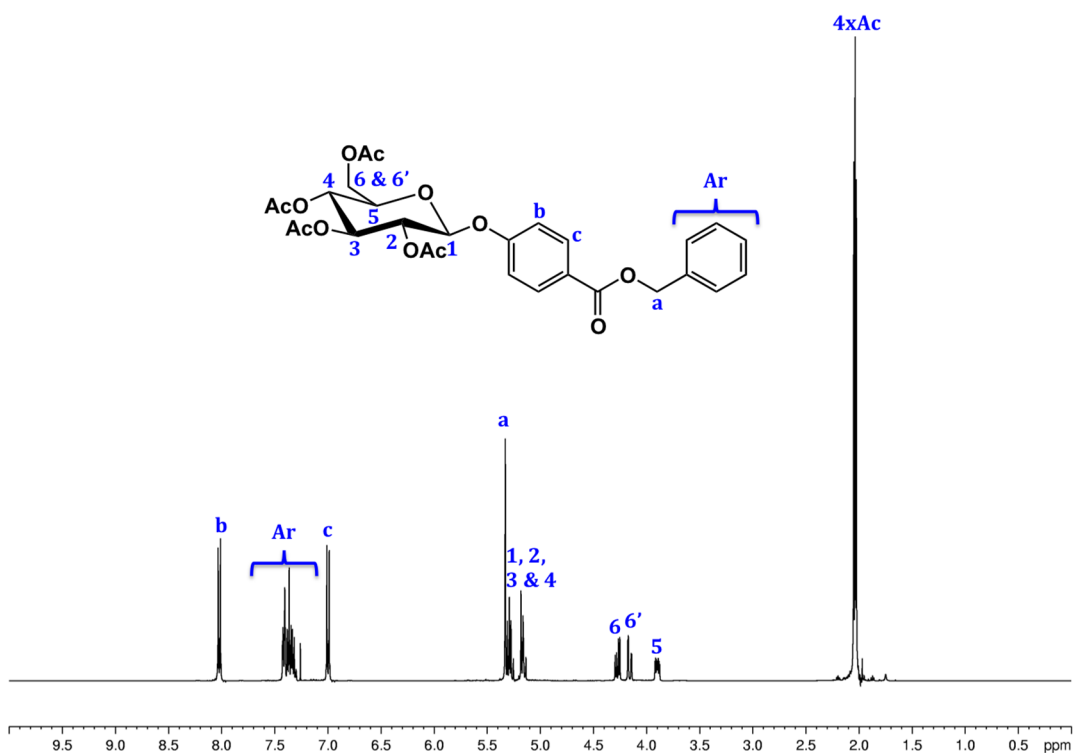


Figure 3.12: 400 MHz ^1H NMR spectrum of **60**, β -anomer (CDCl_3 , 300 K).

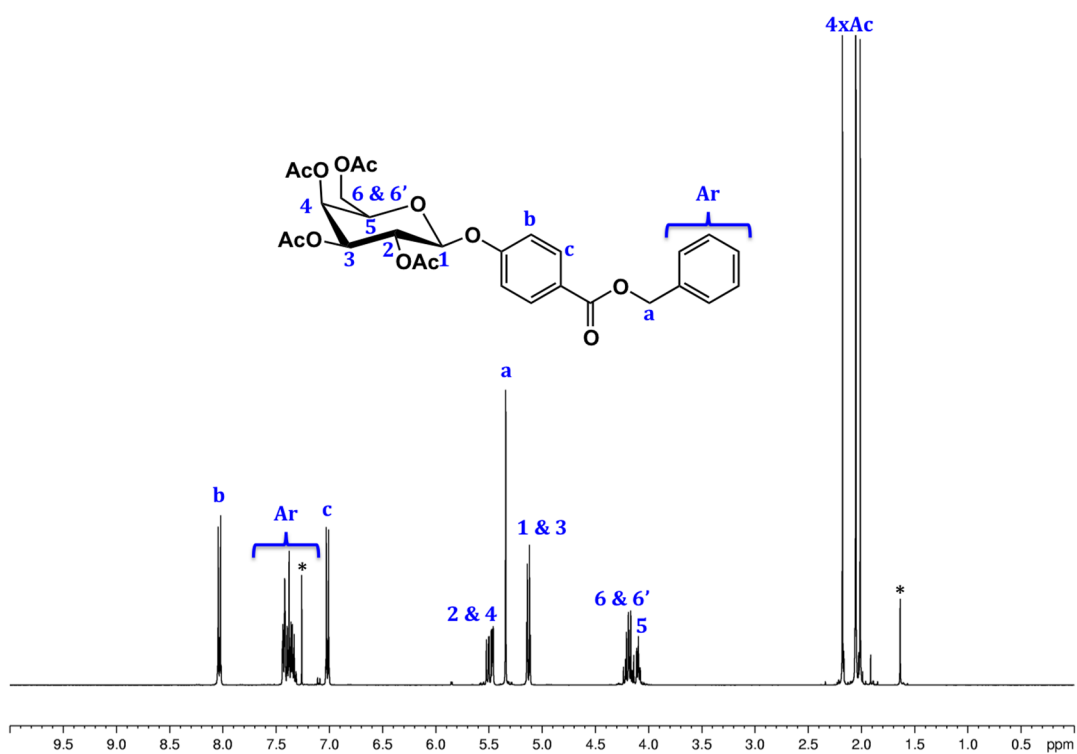


Figure 3.13: 400 MHz ^1H NMR spectrum of **61**, β -anomer (CDCl_3 , 300 K). * denotes residual solvent

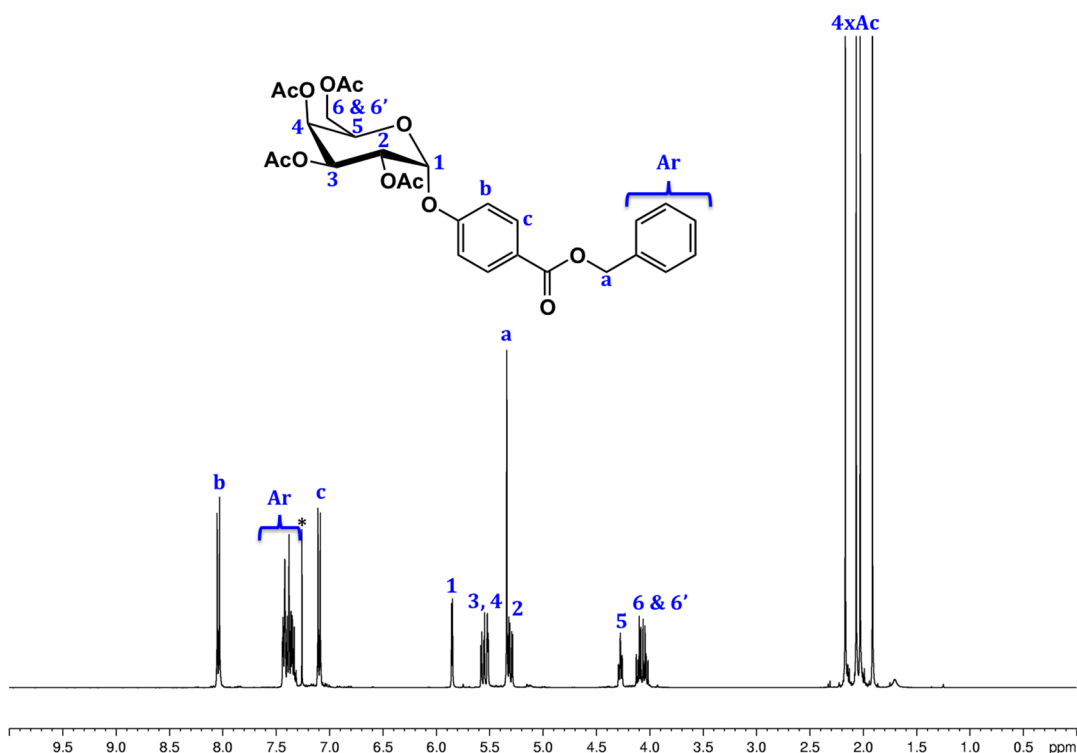
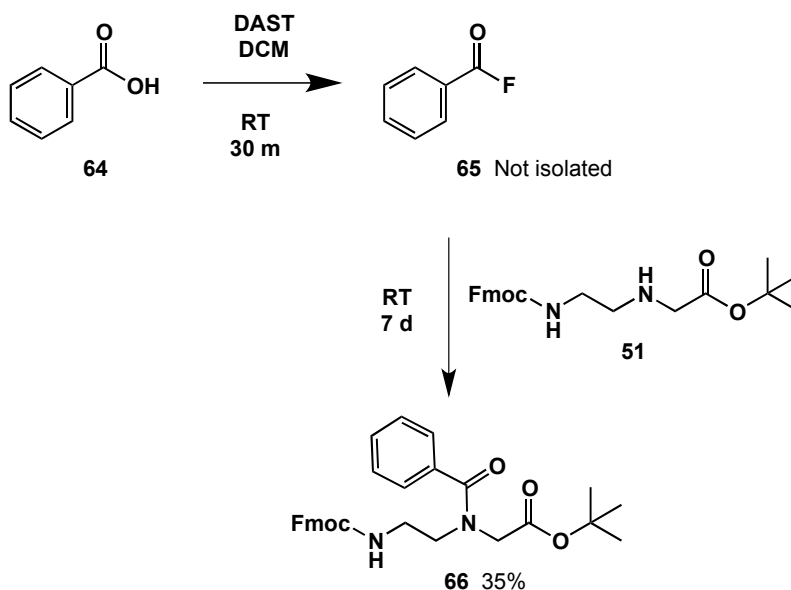


Figure 3.14: 400 MHz ^1H NMR spectrum of **61**, α -anomer (CDCl_3 , 300 K). * denotes residual solvent

Test reaction trials were undertaken to determine appropriate conditions for the formation of an amide bond with the secondary amine of the PNA backbone monomer **51**. Benzoic acid **64** was used rather than acids **62** and **63** for trials (Scheme 3.8). Conditions trialled include EDC (in DCM and DMF), triethylacetyl chloride and triethylamine, the pentafluoroester with HOBt, DCC with HOBt and formation of the acid fluoride. All conditions failed to produce the desired phenyl amide substituted PNA monomer **66** with the exception being (diethylamino)sulfur trifluoride (DAST), yielding the product in 35% yield.⁴² An advantage of the use of DAST as a fluorinating agent is that the reaction by-products produced by using DAST are water soluble and so can be removed by a simple wash before the amine component is added.⁴²

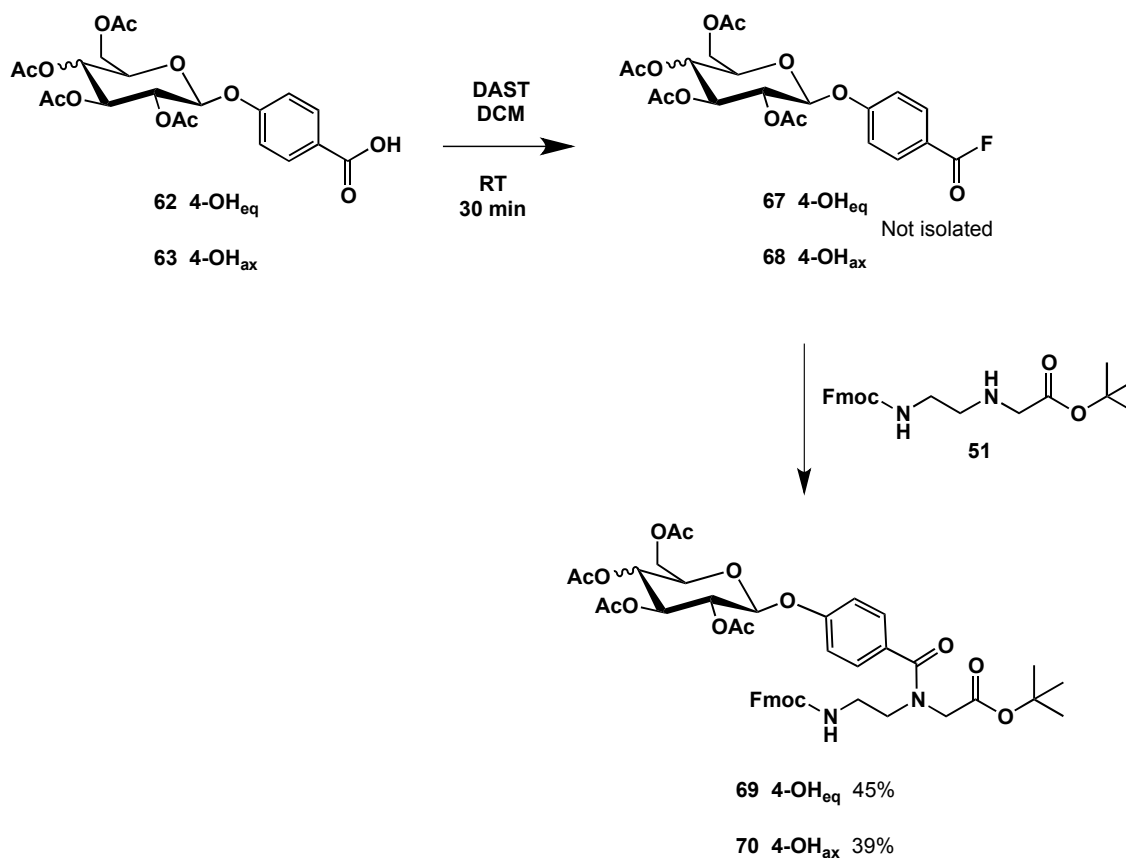


Scheme 3.8

The successful formation of **66** was supported by the ^1H NMR spectrum in which signals representing the coupled aromatic ring were apparent between 7-8 ppm. The methylene protons of the backbone are each represented by broad singlets in the ^1H NMR spectrum of **66**, whereas in the ^1H NMR spectrum of **51**, each pair of methylene protons are represented by a multiplet or singlet. This difference suggests that the presence of the aromatic ring creates a different chemical environment for each proton in the methylene groups of the backbone. Furthermore, the *t*-butyl group is represented by a singlet in the spectrum of **51**, but is represented by 2 singlets in the spectrum of **66**. This has been reported previously for PNA monomers containing aromatic rings.^{18,21,23} It appears that, again, the two different rotamers caused by the restricted rotation about the tertiary amide bond, display different chemical shifts for some signals due to the presence of an aromatic ring that causes the chemical environment of two different rotamers of the product to differ.

Following the successful formation of **66** *via* the acid fluoride, DAST was used in the synthesis of the targeted rigid linked glycosylated monomers (Scheme 3.9). Sugar acids **62** and **63** were independently combined with DAST to produce the corresponding acid fluorides **67** and **68** before the PNA monomer backbone **51** was added to form the desired glycosylated PNA monomers **69** and **70**. The products were isolated after HPLC purification although only in modest yields

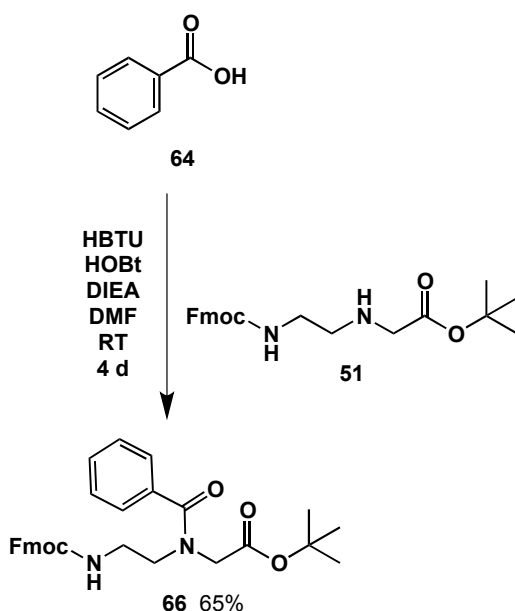
(glucose 45%; galactose 39%) commensurate with the model reaction. The ^1H NMR spectra of **69** and **70** displayed similar broadening effects as seen in the spectrum of **66**. The region between 3–6 ppm integrated to the correct number of protons expected (3 for Fmoc, 6 for backbone and 7 for sugar) indicating that the sugar was conjugated to the backbone in each case. The high resolution ESI mass spectra of both conjugates display peaks corresponding to the proton adduct (m/z 847.3281 and 847.3283) as well as the sodium adduct (m/z 869.3105 and 869.3101), further support product formation.



Scheme 3.9

While the formation of the acid fluorides using DAST and the subsequent successful peptide coupling to the PNA monomer backbone resulted in the desired rigid linked glycosylated monomers, the moderate yields of this reaction prompted another series of test reactions to examine other coupling conditions. When HATU was used as the activator in conjugation with HOBt,²¹ the desired coupled product was produced in 36% yield. Gasser *et al.*^{17,18} found that the use of *N*-methylmorpholine, HOBt and HBTU in dry DMF worked best to produce their

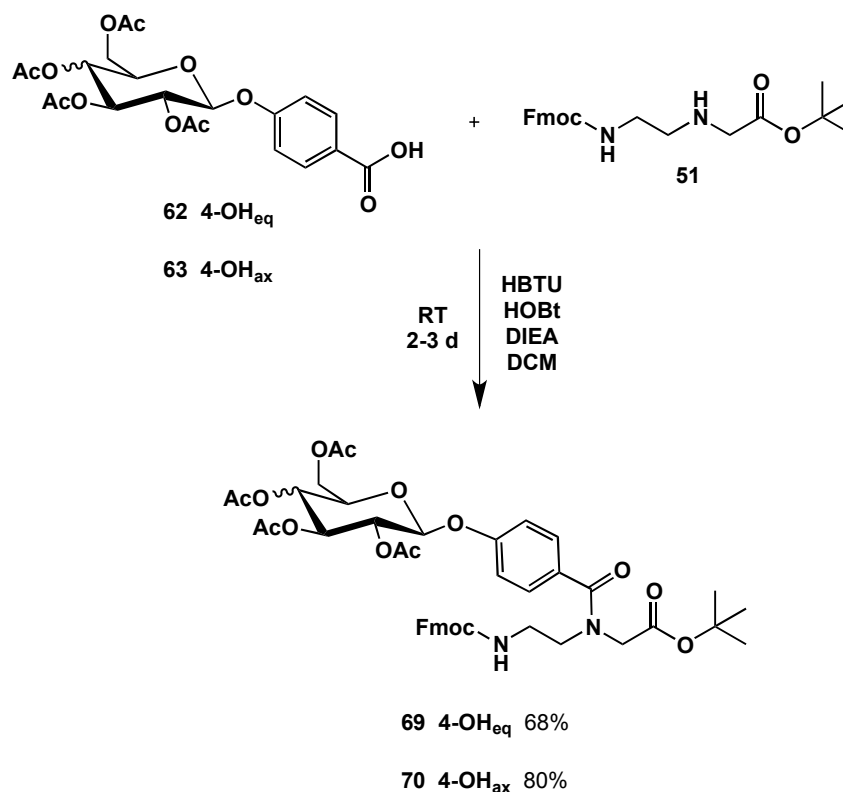
coupled PNA monomer. When these conditions were used in the benzoic acid test reaction, the desired coupled product was formed in 65% yield. Both of these literature examples only utilised the free-base form of the backbone and hence base washed the more stable hydrochloride salt of the backbone immediately before use. As the hydrochloride salt is a solid, it is easier to handle than its free-base counterpart, which is an oil. Also it is inevitable that some material will be lost in the washing and drying process. For these reasons, the coupling method used by Stafforst and Diederichsen⁴³ employing HBTU, HOBT and DIEA in DMF and reacting the hydrochloride salt of **51** was preferred for the coupling of benzoic acid to the backbone, which produced **66** in 65% yield (Scheme 3.10).



Scheme 3.10

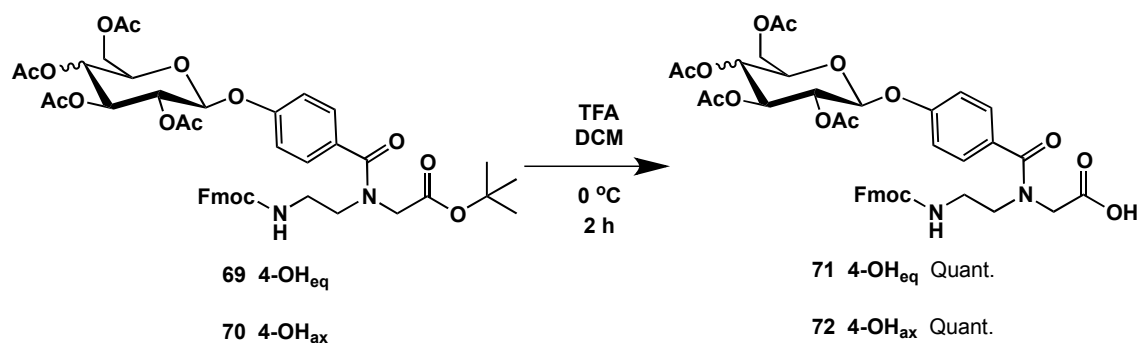
These reaction conditions were then used to couple **62** and **63** to **51** (Scheme 3.11). The coupled products **69** and **70** were produced in better yields compared to the DAST method. It was found that yield was not affected by solvent choice so DCM was used for subsequent reactions due to its ease of handling. The reaction was monitored by TLC and ceased once all of **51** had been consumed (2-3 days). The desired coupled products **69** and **70** were isolated after flash column chromatography (eluent: DCM followed by ethyl acetate) in very good yield.

CHAPTER 3 - FUNCTIONAL PNA MONOMERS



Scheme 3.11

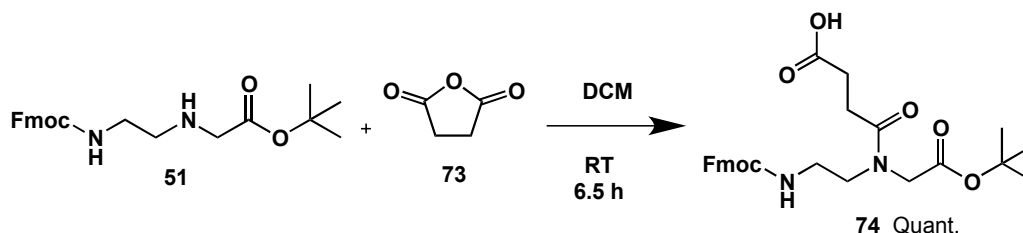
The final step required to produce our target monomers was to remove the *t*-butyl protecting group. Initially, formic acid in DCM at room temperature was trialled however reaction times of up to two weeks were required to completely cleave all of the starting material. As such long reaction times were required, a small amount of a by-product, attributed to cleavage of the peptide bond, was encountered. The use of TFA in DCM at 0 °C was more favourable (Scheme 3.12) in forming the final rigid linked glycosylated PNA monomers **71** and **72** in rapid (2 h) and quantitative yield.



Scheme 3.12

3.2.2.3. Succinic Anhydride-Linked Glycosylated Monomers

As an alternative design strategy to afford modification “Y” PNA monomers, succinic anhydride was used as an alternate flexible linker. Reaction of **51** with succinic anhydride **73** gave the substituted PNA monomer **74** in quantitative yield (Scheme 3.13). The carboxylic acid functionality of **74** will allow the coupling of glucose and galactose *via* our developed glycosylation method used for the library of sugar-conjugates in Chapter 2.



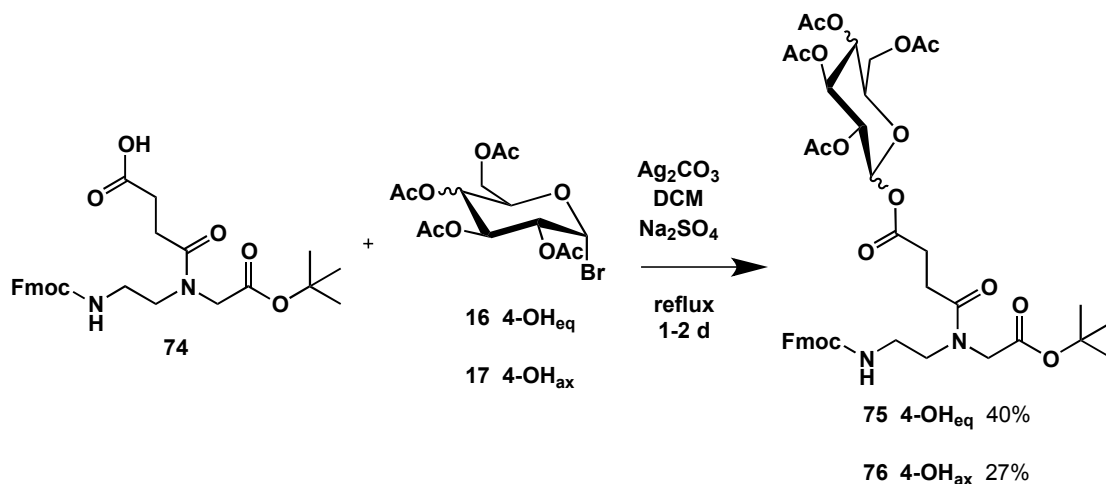
Scheme 3.13

Thin-layer chromatography (5% MeOH/DCM) was used to track the consumption of the backbone starting material, but as **51** and **74** display similar R_f values, ESI mass spectrometry was also used to track the progress of the reaction. The ^1H NMR spectrum of **74** supports product formation with the addition of two multiplets at 2.68 and 2.48 ppm, with a total integration of 4 protons, corresponding to the two adjacent methylene groups of the succinic moiety. This spectrum also displays evidence of two rotamers in approximately a 1 : 0.6 ratio with two signals representing each of the Fmoc carbamate proton, Fmoc and backbone methylene groups.

The glycosylation of **74** with glucose and galactose to afford **75** and **76** respectively were completed with Ag_2CO_3 as the promoter (Scheme 3.14) and the products purified by RP-HPLC. Compound **75** eluted at 35 minutes as measured at a wavelength of 254 nm.

The ^1H NMR spectrum attributable to compound **75** displays our assigned H-1 signal at 5.71 ppm and the signal corresponding to the C-1 carbon appears at 92.1 ppm in the ^{13}C NMR spectrum. These chemical shifts are typical of the β -glycosyl esters observed in this work, and reported elsewhere.⁴⁴ Like the starting material, there is evidence in the ^1H NMR and ^{13}C NMR spectrum of **75** that the product is a mixture of two different rotamers. There are two sets of signals for the H-1, NH,

acetate methyl and the *tert* butyl methyl protons, all in a ratio of approximately 1 : 0.85. There are also two sets of signals corresponding to a variety of carbons including C-1. The overlapping doublets corresponding to H-1 in the ^1H NMR spectrum of **75** display coupling constants of 8.0 Hz, further supporting formation of the β -anomer.



Scheme 3.14

The HPLC results of **76** were surprisingly different to that of **75**. There were two major HPLC peaks eluting at 34 and 37 minutes and ESI mass spectrometry showed both fractions contained the desired product, with signals at m/z 849.17, corresponding to the $[\text{M}+\text{Na}]^+$ ion. When the reaction time was limited to 24 h, the ratio of the isomers was 34 min : 37 min = 1 : 0.36. However when the reaction was left for longer (42 hours), the ratio was 1 : 0.08. The different reaction times gave almost the same combined product yield (27% and 26% respectively).

The ^1H NMR spectra of these fractions displayed slightly different chemical shifts for some of the sugar protons, indicating that perhaps different isomers of **76** had formed. The 34 minute isomer presents the chemical shift of H-1 as two overlapping doublets (two rotamers) at 5.70 and 5.68 ppm with coupling constants of 8.4 Hz. The signals for C-1 appears at 92.7 and 92.5 ppm in the ^{13}C NMR spectrum. This data is similar to that of **75**, the glucose derivative and consistent with formation of the β -anomer.

The 37 minute isomer of **76** presents the chemical shift of H-1 as two distinct doublets (two rotamers) at 6.39 and 6.37 ppm with coupling constants of 3.2 Hz. These lie more downfield than the H-1 signals of the 34 minutes isomer. This data is indicative of the α -anomer. Furthermore, the β -anomer of other glycosylated

derivatives prepared for this work have similarly eluted before the α -anomer, if produced.

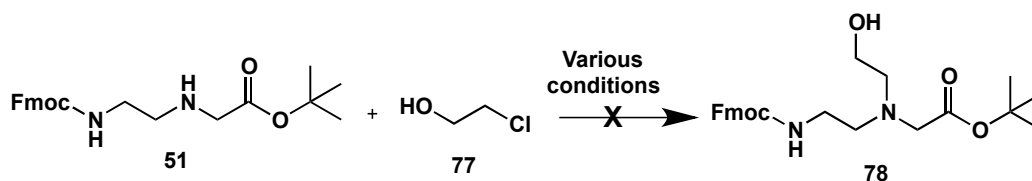
The phenomena of the galactose conjugate forming the α -anomer more readily than the glucose conjugate has been observed previously in this work with the rigid linked glycoconjugates **60** and **61**. The axial orientation of H-4 in galactose must play a role in the orientation of the attacking nucleophile necessary to form the α -anomer. The α : β ratio of **76** increases over time, under thermodynamic conditions, to favour the thermodynamically stable product, the β -anomer.

The flexibility of the succinyl linker and its ability to flip and hydrogen-bond to the backbone could explain the low yield of these glycosylation reactions (40% and 27%). Removal of the *t*-butyl protecting group of **75** and **76** was attempted using TFA however mass spectrometry and ^1H NMR analysis revealed the presence of the species in which both the *t*-butyl ester and the glycosyl ester had been cleaved. This is a problem because if **75** and **76** were to be included in PNA oligomers, they were be subjected to TFA for long periods of time in order to cleave the oligomer from the resin.

While the desired succinic anhydride-linked glycosylated monomers were successfully produced, no further work was conducted with this class of glycosylated PNA monomer as the glycosylation step was low yielding and the conditions required to remove the *t*-butyl protecting group caused the cleavage of the glycosoyl ester. These drawbacks render the succinic anhydride linker an inappropriate linker for glycosylated PNA monomers.

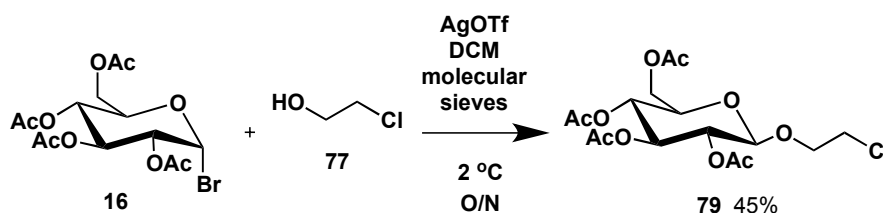
3.2.2.4. Alkyl-Linked Glycosylated Monomers

The third design strategy for the development of modification “Y” PNA monomers employed a small alkyl linker. Reaction of PNA monomer backbone **51** with 2-chloroethanol **77**, under various conditions failed to produce the desired alkyl-substituted PNA monomer **78** (Scheme 3.15).



Scheme 3.15

An alternative synthetic strategy is to attach the sugar moiety to the alkyl linker first, followed by attachment to the PNA backbone monomer. Scheme 3.16 shows the reaction of acetobromoglucose and 2-chloroethanol with silver triflate as the promoter to produce the desired glycosylated linker **79** in 45% yield after column chromatography (eluent: 5% (v/v) MeOH/DCM). Compound **79** was also successfully produced using Ag_2CO_3 as the promoter, but in lower yield (38%).



Scheme 3.16

The ^1H NMR spectrum of **79** clearly shows that glycosylation has taken place with signals corresponding to four additional protons at chemical shifts of 4.05 ppm (one proton), 3.75 ppm (one proton) and 3.63 ppm (two protons) corresponding to the two methylene groups of the 2-chloroethanol moiety. The distinct signals for individual protons of one of the methylene groups caused by the close proximity of the chiral environment of the sugar moiety, indicates that the coupling was successful. The chemical shift of the H-1 proton signal is 4.57 ppm, with a coupling constant of 7.9 Hz supports β -anomer formation, as does a chemical shift of 101.2 ppm for C-1 in the ^{13}C NMR. The ESI mass spectrum displays the expected chlorine isotope pattern with a base peak at m/z 433.2 corresponding to the $[\text{M}+\text{Na}]^+$ ion as well as a peak, one third its height, at m/z 435.2, further supporting the successful glycosylation of 2-chloroethanol.

Single crystals of **79** suitable for analysis were grown by slow evaporation of dichloromethane. The solved structure (Figure 3.15) shows the expected diaxial orientation of *H*-1 and *H*-2 and, as a consequence, the β -orientation of the chloroethyl substituent at *C*-1.

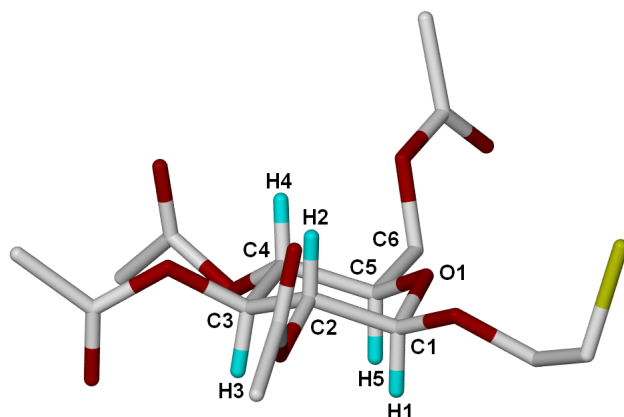
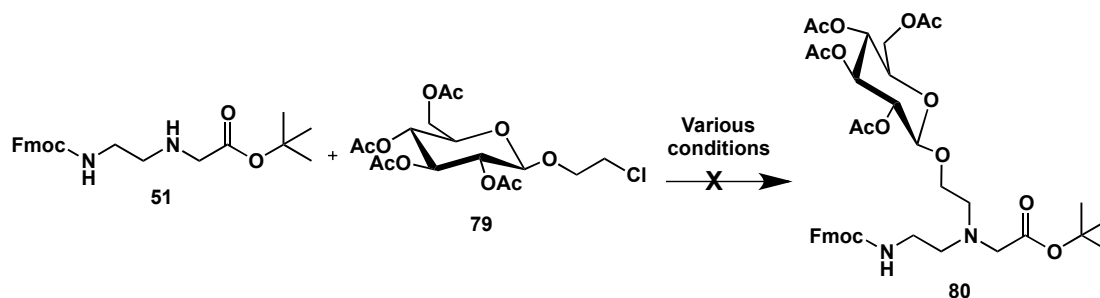


Figure 3.15: Stick representation of the X-ray structure of $C_{16}H_{23}ClO_{10}$. The absolute configuration was determined by the synthesis and was confirmed by the X-ray experiment.

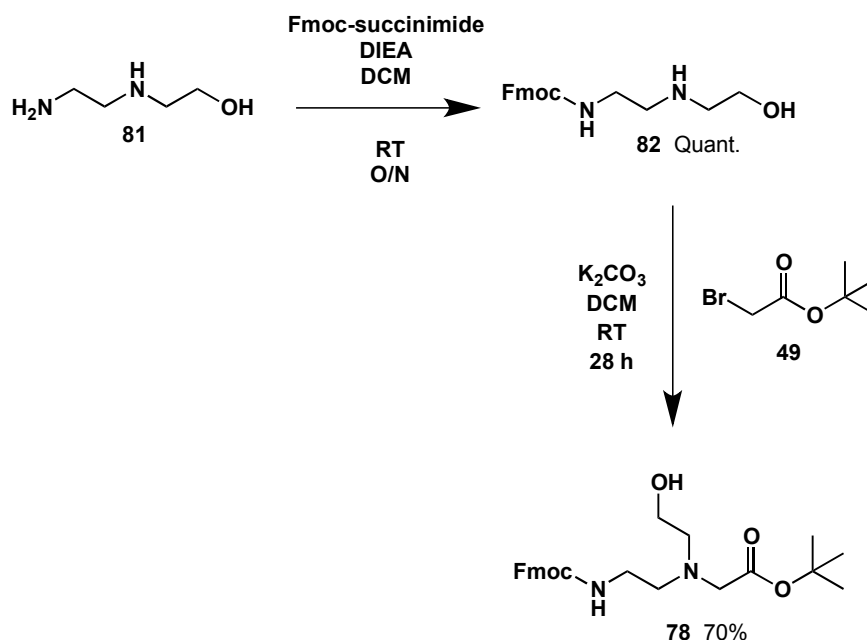
Various conditions were used to join **79** to the PNA backbone monomer **51** (Scheme 3.17), such as triethylamine in DMF and potassium iodide in refluxing DCM, however none were successful.



Scheme 3.17

With two failed reaction attempts involving the reaction of the alkyl chloride of both **77** and **79** with the secondary amine of **51**, a different synthetic approach was investigated in which the PNA monomer was constructed in a different order. Scheme 3.18 shows that by starting with 2-(2-aminoethylamino)ethanol **81**, the alkyl linker is already in place.

Fmoc protection of **81** led to the formation of the alcohol **82** as a white solid, collected by filtration in quantitative yield. The ^1H NMR spectrum supports the formation of **82** displaying characteristic signals of the Fmoc group. A peak at m/z 327.2 in the ESI mass spectrum corresponding to $[\text{M}+\text{H}]^+$ further supports the successful protection of the amine.



Scheme 3.18

Reaction of **82** with *t*-butylbromoacetate **49** in the presence of K₂CO₃, successfully produced the alkyl-substituted PNA monomer **78** as a colourless oil after column chromatography (eluent: 5% (v/v) MeOH/DCM). It was found that base selection, required to neutralise the HBr produced in the reaction, affected the yield with K₂CO₃ producing a superior yield (70%) to, for example, pyridine (43%).

The formation of **78** was supported by the ¹H NMR spectrum (Figure 3.16) that showed an additional singlet at 1.48 ppm, integrating to nine protons, which is characteristic of the *t*-butyl group. Similarly, in the ¹³C JMOD NMR spectrum, the presence of the signal at 28.4 ppm (CH₃) and 82.2 ppm (C) indicate the presence of the *t*-butyl group, while the presence of an additional CH₂ peak at 57.8 ppm also supports the formation of the product. The mass spectrum further supports product formation with a signal at *m/z* 441.2 corresponding to the [M+H]⁺ ion.

With **78** finally in hand, it was available for glycosylation to produce the desired alkyl-linked glycosylated PNA monomer. Initially, Ag₂CO₃ was used as the promoter (Scheme 3.19), and the reaction proceeded slowly with the desired single product spot appearing by TLC on the third day of the reaction. Reverse phase HPLC purification and NMR spectroscopy revealed that both the α and the β anomers had been formed for **80** and **83**.

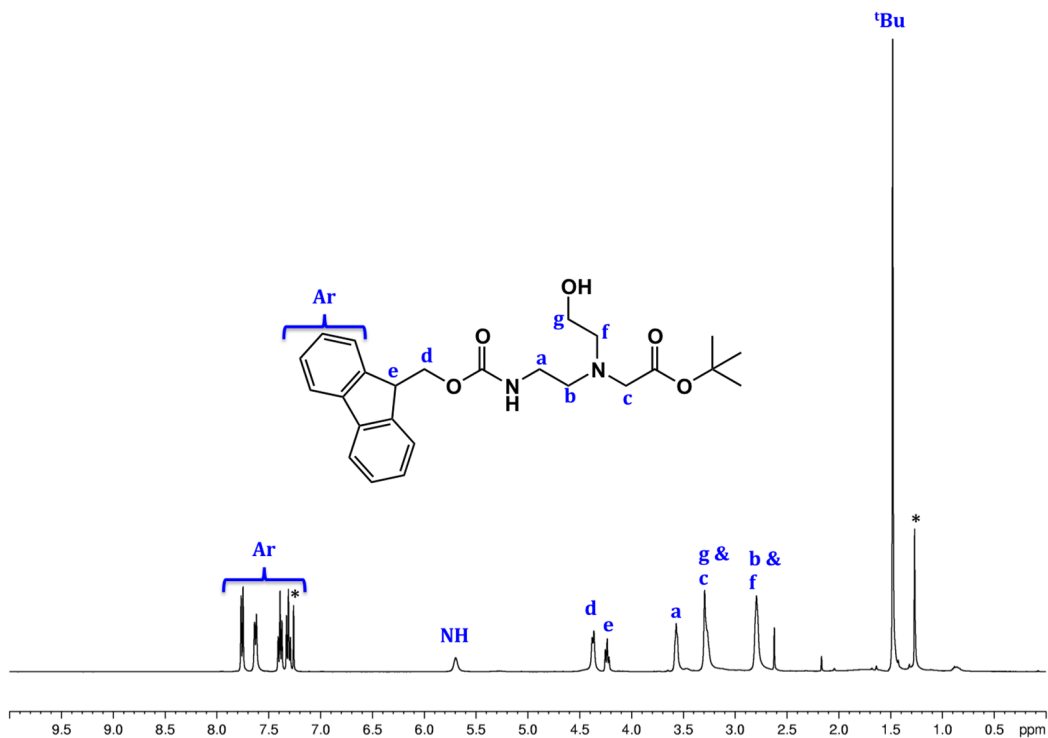
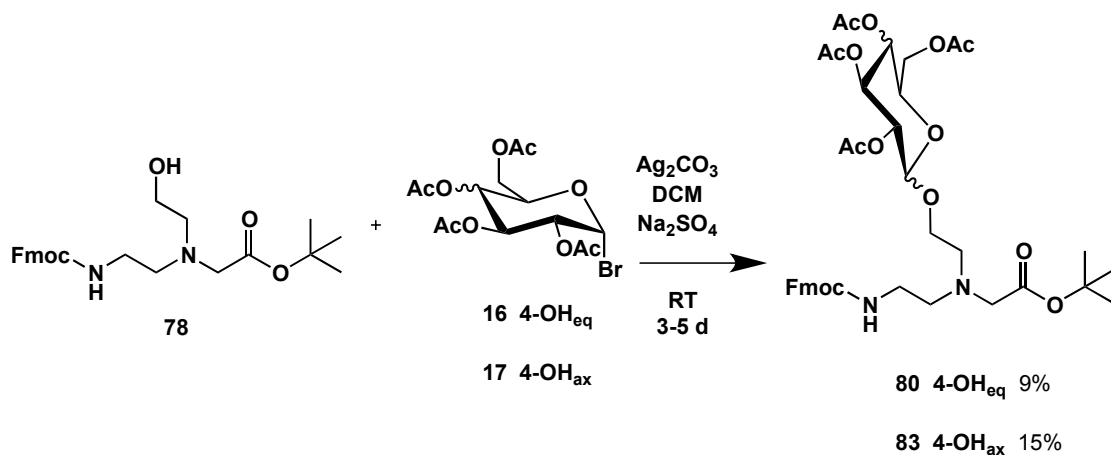


Figure 3.16: 400 MHz ^1H NMR spectrum of **78** (CDCl_3 , 300 K). * denotes residual solvent



Scheme 3.19

The ^1H NMR spectrum of the first-eluting anomer of **83** (Figure 3.17) indicates the β -anomer, with a coupling constant for H -1 being 7.6 Hz at a chemical shift of 4.48 ppm. The ^1H NMR spectrum of the second anomer (Figure 3.18) show the coupling constant for H -1 is 4.8 Hz at a chemical shift of 5.83 ppm, indicating the α -anomer.

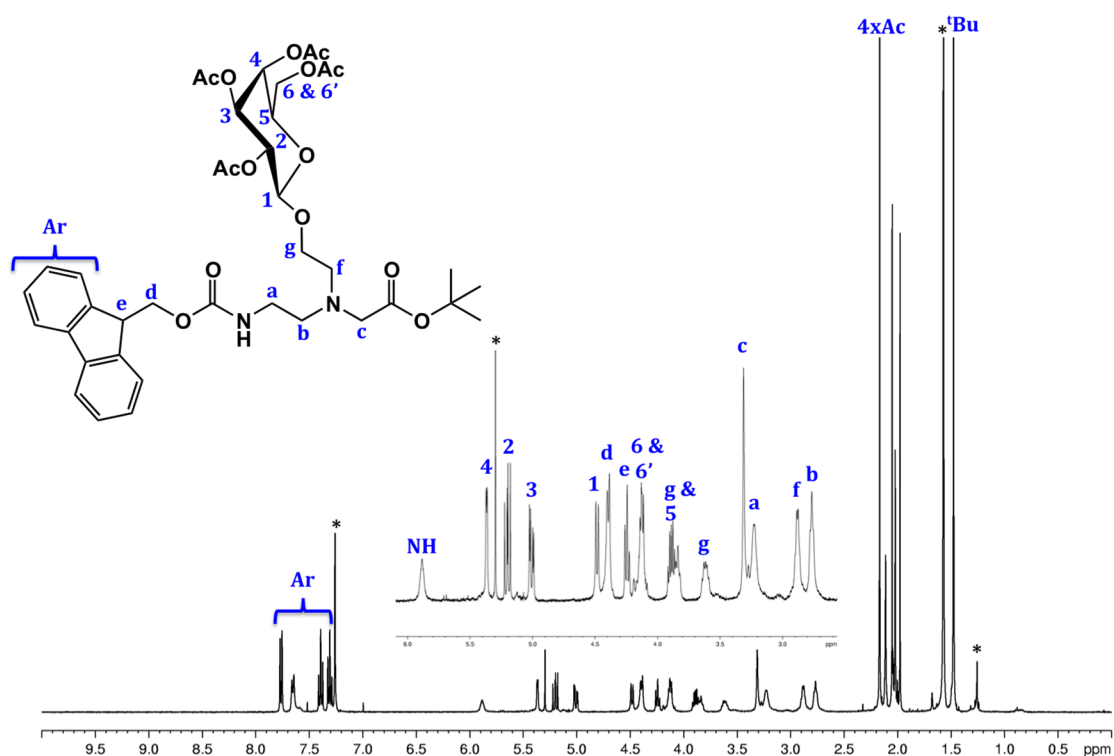


Figure 3.17: 400 MHz ^1H NMR spectrum of **83**, β -anomer (CDCl_3 , 300 K). *denotes residual solvent

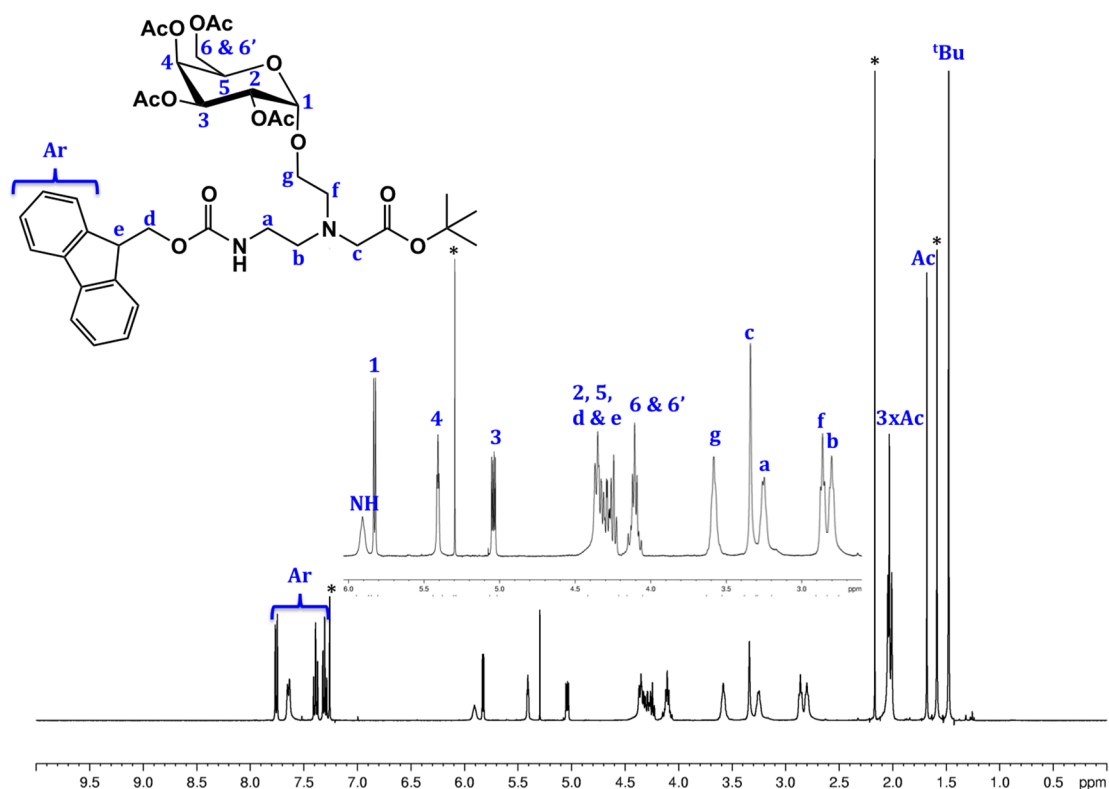
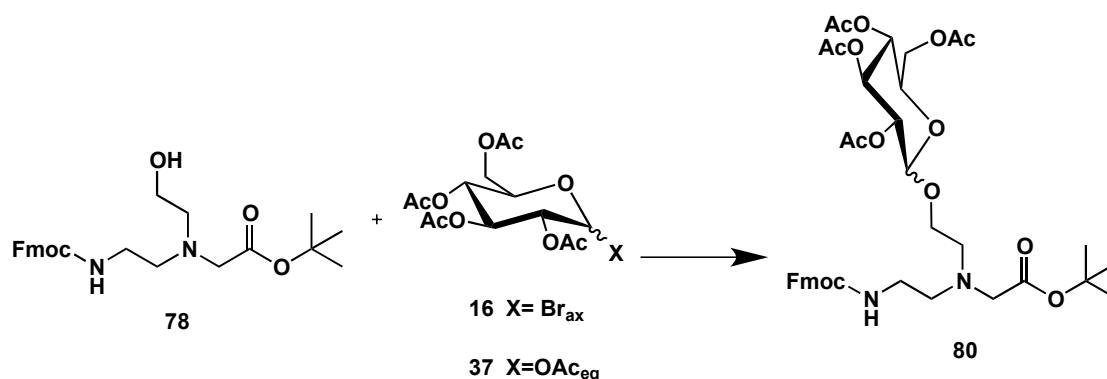


Figure 3.18: 400 MHz ^1H NMR spectrum of **83**, α -anomer (CDCl_3 , 300 K). *denotes residual solvent

As the β anomer is desired, other glycosylation conditions were explored to increase the β : α ratio of the glucose derivative. Table 3.1 lists various conditions that were explored to produce **80**.

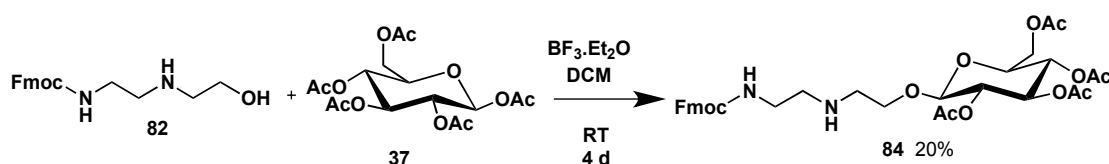
Table 3.1: Reaction conditions and associated α : β ratio for reaction



X	Promoter	Solvent	Temp (°C)	Time (days)	α : β ratio
Br _{ax}	Ag ₂ CO ₃	DCM	RT	1	2:1
Br _{ax}	Ag ₂ CO ₃	DCM	RT	3	6:1
Br _{ax}	Ag ₂ CO ₃	DCM	RT	3	5:1
Br _{ax}	Ag ₂ CO ₃	ACN	RT	4	No
Br _{ax}	Ag ₂ CO ₃	ACN	0-RT	5	1:1
Br _{ax}	Ag ₂ CO ₃	ACN	40	1	6:1
OAc _{eq}	BF ₃ .Et ₂ O	DCM	RT	3	Trace
OAc _{eq}	BF ₃ .Et ₂ O	ACN	0-RT	2	No
Br _{ax}	I ₂	ACN	RT	4	Trace
Br _{ax}	I ₂ , DDQ	ACN	RT	3	No
Br _{ax}	AgOTf	DCM	0-RT	16	Trace
OAc _{eq}	TMSOTf	ACN	0	5	No

Table 3.1 shows that in the reaction of **78** with glucose, the α -anomer was formed as the major stereoisomer. As a result, this pathway was no longer pursued.

In a final attempt to make a β -alkyl-linked glycosylated PNA monomer, a different synthetic strategy was developed involving the glycosylation of the alkyl link before the *t*-butyl ester was installed. It was anticipated that the glycosylation of the Fmoc-protected 2-(aminomethylamino)ethanol would be a more facile reaction than the glycosylation of the alkylated PNA backbone monomer. Reaction of Fmoc-protected 2-(aminomethylamino)ethanol **82** with glucose pentaacetate **37** in the presence of $\text{BF}_3 \cdot \text{Et}_2\text{O}$ produced the desired glycosylated alkyl-linked backbone segment **84**, however in low yields (Scheme 3.20). The main reason for the low yield is the limited solubility of **82** in DCM. Another solvent was sought in which the starting material was soluble and which allowed for the $\text{BF}_3 \cdot \text{Et}_2\text{O}$ promoted glycosylation reaction to take place. Compound **82** completely dissolves in acetonitrile, however no reaction was observed in this solvent, possibly because this solvent highly solvates the reactants, making them less reactive towards each other. Toluene was also used as a solvent in this reaction, however no reaction was observed at room temperature or at 50 °C. Therefore the reaction was conducted with DCM as the solvent as it allowed this reaction to proceed.



Scheme 3.20

A solution of **82** in DCM was heated and sonicated to encourage **82** to dissolve before the sugar and promoter were added. The reaction was left to stir for four days and column chromatography (eluent: 5% (v/v) MeOH/DCM followed by 10% (v/v) MeOH/DCM) was used to isolate the glycosylated product **84**. ^1H NMR (Figure 3.19) and ^{13}C NMR analysis both show that the β anomer was exclusively formed with the signal corresponding to the proton at the anomeric position displaying a coupling constant of 8.0 Hz in the ^1H NMR spectrum and the chemical shift of the anomeric carbon in the ^{13}C NMR spectrum at 101.1 ppm. The ESI mass spectrum further supported the successful formation of **84** with a signal at m/z 657.0 corresponding to the $[\text{M}+\text{H}]^+$ ion. The fixing of the anomeric stereochemistry at this early stage of the synthetic pathway makes this pathway superior to the previous one in Scheme 3.19.

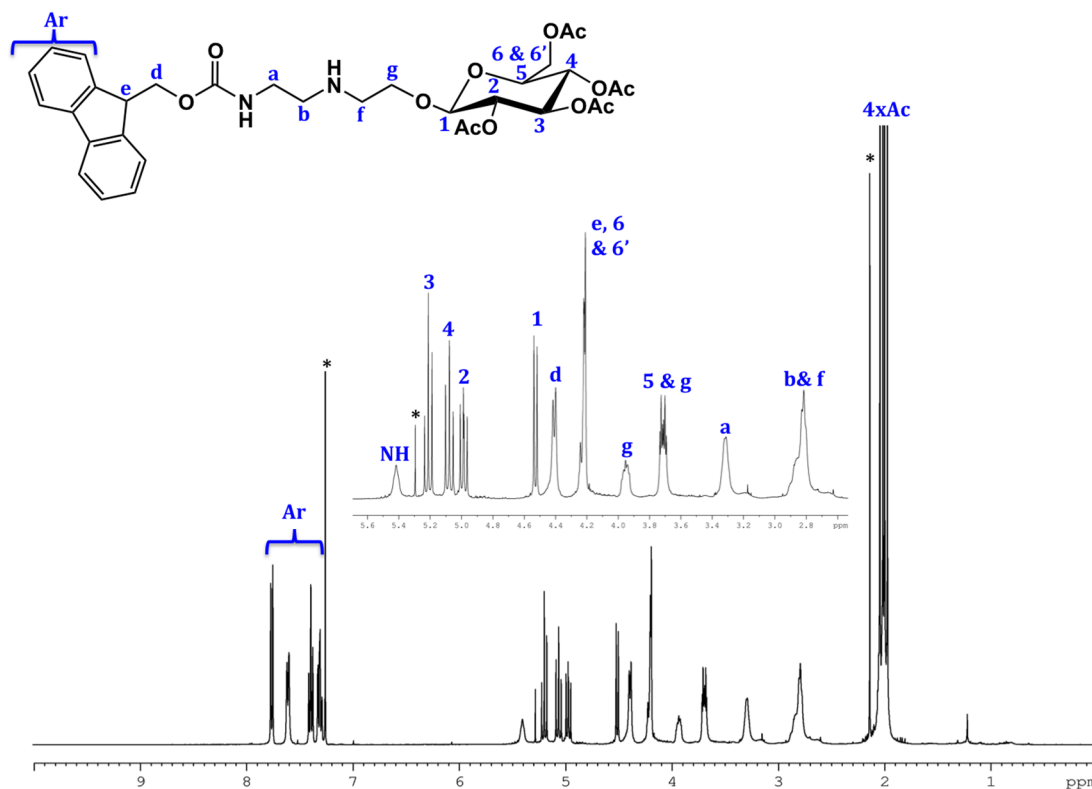
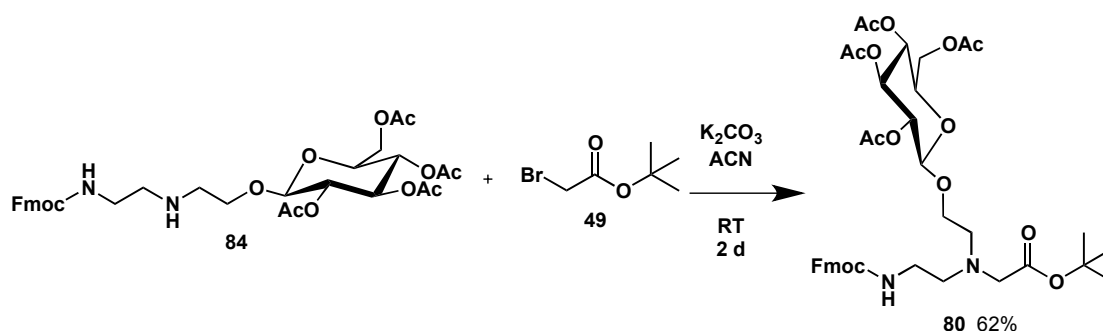


Figure 3.19: 400 MHz ^1H NMR spectrum of **84** (CDCl_3 , 300 K). * denotes residual solvent

The ^1H NMR spectrum in Figure 3.19 shows that the chiral environment accentuated by the sugar moiety, causes each of the methylene protons directly next to the glycosyl ether bond to be electronically inequivalent and hence appear at very different chemical shifts of 3.95 and 3.74 ppm.

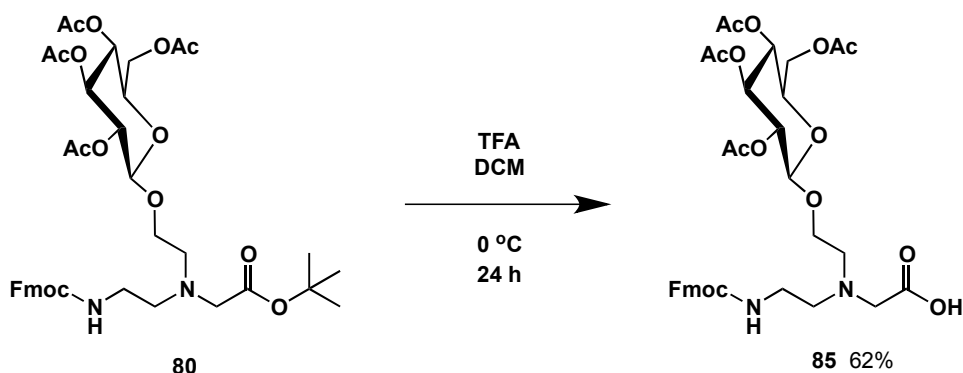
To install the second half of the PNA backbone to the glycosylated portion **84**, potassium carbonate was used as a base and dehydrating agent in acetonitrile to afford the alkylation of the secondary amine with *t*-butyl bromoacetate **49** and produce the desired alkyl-linked glycosylated PNA monomer **80** (Scheme 3.21). The reaction proceeded in good yield (62%) after two days and an excess of **49**. The reaction mixture was easily purified *via* column chromatography (eluent: DCM then ethyl acetate) to leave the desired product as a colourless oil.

The ^1H NMR spectrum of **80** displays a two-proton singlet at 3.31 ppm and a singlet (9 protons) at 1.48 ppm, attributable to the methylene group adjacent to the ester and the *t*-butyl methyl groups, respectively, supporting the successful synthesis of the complete PNA backbone monomer. The ESI mass spectrum also supported product formation with a signal at m/z 771.2, corresponding to the mass of the proton adduct of the product.



Scheme 3.21

The final step in the synthesis was to remove the *t*-butyl protecting group of **80** to leave a free C-terminus of acid **85** to allow the PNA monomer to be incorporated into a PNA sequence. This was easily achieved with TFA in DCM in an ice bath overnight (Scheme 3.22). The alkyl-link was stable under such conditions, unlike the ester link of the succinic anhydride-linked monomers. While these conditions completely removed the protecting group with no starting material evident, there was still a need for purification by column chromatography. In solution, the Fmoc protecting group degrades, producing a 9-methylene-9H-fluorene by-product. This group is easily removed with DCM on a silica column, with the desired Fmoc-protected product eluting in 10% (v/v) MeOH/DCM. The other by-product of the Fmoc degradation, the unprotected, free amine glycosylated monomer, remains on the silica.



Scheme 3.22

^{13}C NMR analysis supports the formation of **85** with the chemical shift of the anomeric carbon at 100.4 ppm, suggesting the retainment of the β -anomer, as would be expected. The signals corresponding to the *t*-butyl methyl groups in both the ^1H and ^{13}C NMR spectra are no longer present. The high resolution ESI mass

spectrum supports the cleavage of the *t*-butyl group with a peak at m/z 715.2723, corresponding to the $[M+H]^+$ ion.

3.2.3. Conclusions and Future Directions

There are many advantages of PNA as an antisense molecule such as high specificity, high mismatch sensitivity, high binding affinity and resistance to nucleases and proteases. These advantages are a result of the unnatural, uncharged, achiral backbone of PNA. The use of PNA as a therapeutic however has been limited by its poor bioavailability and inability to cross biological membranes. To overcome these problems, and to enhance the spectrum of uses of this class of antisense molecule, many variations have been made to structure of PNA.

This chapter of work explored various ways in which to include a sugar moiety in a PNA oligomer. Of the different sites available for modification on the PNA monomer, two sites for modification were explored: *N* terminal conjugation (modification X) and replacing the nucleobase of the PNA monomer (modification Y). Two strategies were explored to conjugate a sugar to the *N* terminal of a PNA oligomer. First, the chiral amino acid serine was glycosylated with glucose and galactose to produce the glycosylated building blocks **39** and **40**. The incorporation of these glycosylated building blocks is discussed in Chapter 4. Second, the glycosylation of 4-(hydroxymethyl)benzoic acid was attempted in order to form an achiral glycosylated building block that could be conjugated to the *N* terminal of a PNA oligomer *via* its free carboxylic acid. The glycosylation reaction however led to a mixture of inseparable products as both the hydroxyl and carboxylic acid groups were glycosylated. This line of work was not pursued further.

Three strategies were explored to synthesise glycosylated PNA monomers in which the nucleobases was replaced with a sugar. First, aromatic linking groups were used to produce “rigid-linked” glycosylated monomers. This strategy involved the conjugation of 4-(hydroxymethyl)benzoic acid to the PNA monomer backbone **51** to produce **52** as the first PNA monomer backbone rigid aromatic linker with a hydroxyl group available for glycosylation. Conjugation of glucose and galactose to the rigid linker of **52** produced **53** and **54** respectively. While the

desired β -anomers were formed, the yields of the glycosylation reactions were low. In an attempt to increase these yields, the carboxylic acid of 4-(hydroxymethyl)benzoic acid was initially ethyl-protected to prevent unwanted side-reactions and interferences, before the hydroxyl group was glycosylated. While the glycosylation proceeded smoothly to form the glucose conjugate **56** and galactose conjugate **57** in moderate yield, the ethyl-protecting group was unable to be removed, under various conditions, without destroying the glycosidic bond. An alternative protecting group, benzyl, was used to facilitate deprotection in the presence of the glycosidic bond. Reaction of benzyl 4-hydroxybenzoate with glucose and galactose led to the formation of **60** and **61**: the majority of each of the products were the β -anomer as deduced from the ^1H NMR spectra, however a small proportion of **60** and **61** were the α -anomer. The different anomers were separated by RP-HPLC. Removal of the benzyl protecting group from each glycosylated derivative produced **62** and **63**. Optimised peptide coupling conditions were used to couple **62** and **63** to the PNA monomer backbone **51** to produce **69** and **70**. Finally, the *t*-butyl protecting group was removed to leave the free carboxylic acid of **71** and **72**, ready for coupling in a PNA oligomer.

The second strategy that was explored to synthesise glycosylated PNA monomers involved succinic anhydride. The synthesis of the succinic acid-substituted PNA monomer backbone **74** proceeded in quantitative yield. Glycosylation of **74** with glucose and galactose produced **75** and **76** respectively in low to moderate yields. The β -anomer of **75** and **76** was produced and the α -anomer of **76** was also produced. This pathway was not pursued because it was low yielding and there were complications in removing the *C*-terminus protecting group.

The third strategy that was developed to form glycosylated PNA monomers involved the installation of an alkyl linking group. Initial attempts involving the coupling of the PNA monomer backbone **51** to an alkyl substituent to form the alkyl-substituted PNA monomer **78** failed. An alternative approach that 'built' **78** in a different order saw its success. However glycosylation of **78** with glucose and galactose to produce **80** and **83** was not overly successful. Both α and β anomers were produced for both derivatives. A further adjustment to the synthetic pathway saw the successful installation of glucose in the first step to produce **84**

exclusively as the β -anomer. The synthesis of the glycosylated alkyl-linked PNA monomer **80** was completed (62% yield) with the installation of the protected carboxylic acid as the C-terminus of the monomer. The final step saw the removal of the *t*-butyl protecting group to leave **85** ready to be incorporated into a PNA oligomer.

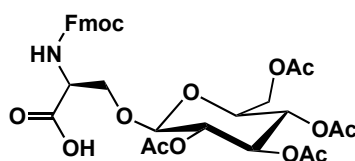
Future work in this area would include the optimisation of the synthesis of the alkyl-linked glycosylated monomer. While the final pathway discussed successfully produced the desired β -anomer exclusively, the yield of the glycosylation could be improved by further optimisation. Furthermore, the synthesis of the galactose derivative *via* the pathway described in Scheme 3.20, Scheme 3.21 and Scheme 3.22 should be completed. The incorporation of the alkyl-linked glycosylated PNA monomers into PNA oligomers should also be undertaken. This will allow for the comparison of different “Y” modifications to the PNA monomer structure, being the rigid (aromatic)-linked and the alkyl-linked glycosylated PNA monomers, as well as the comparison of different types of PNA modifications, being “X” and “Y” modifications.

3.3. Experimental

Details of general experimental methods can be found in Section 2.4.1.

3.3.1. Synthesis of Chiral Glycosylated Building Blocks

*Synthesis of 39*³⁶



Fmoc-Serine (500 mg, 1.52 mmol) and β -D-glucopyranose pentaacetate (494 mg, 1.27 mmol) were stirred in freshly distilled DCM (20 mL). The Lewis acid $\text{BF}_3 \cdot \text{Et}_2\text{O}$ (0.460 mL, 3.18 mmol) was then added *via* syringe and the solution left to stir at room temperature for 7 h. After this time the solution was washed with HCl (1M, 1 x 20 mL) and H_2O (1 x 20 mL) and dried (MgSO_4). The solvent was then removed under reduced pressure to leave a yellow oil. Purification by HPLC on a C_{18} Delta Pak column with a flow rate of 5 mL/minute. The solvent system used was 60:40 H_2O :ACN 5 minutes then a gradual change to 40:60 H_2O :ACN for 20

minutes. The desired conjugated product eluted at approximately 62 minutes as detected at 220 nm absorbance. The solvent was removed under reduced pressure to leave **39** as a flocculent white solid (180 mg, 22%).

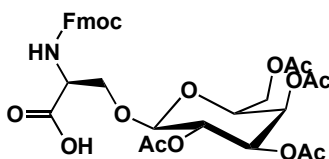
¹H NMR (400 MHz) δ : 7.76 (d, 2H, J = 9.7 Hz, Ar H); 7.60 (d, 2H, J = 7.2 Hz, Ar H); 7.40 (t, 2H, J = 7.4 Hz, Ar H); 7.32 (t, 2H, J = 7.4 Hz, Ar H); 5.70 (d, 1H, J = 7.8 Hz, NH); 5.19 (t, 1H, J = 9.4 Hz, H -3); 5.08 (t, 1H, J = 9.7 Hz, H -4); 4.96 (t, 1H, J = 8.6 Hz, H -2); 4.51 – 4.39 (m, 4H, H -1, Fmoc CH_2 & α - H); 4.29 – 4.19 (m, 4H, Fmoc CH , H -6, H -6', β - H); 3.92 (d, 1H, m, β - H); 3.67 (dt, 1H, J = 10.0, 3.6 Hz, H -5); 2.07 (s, 3H, Ac CH_3); 2.03 (s, 3H, Ac CH_3); 2.00 (s, 6H, 2 Ac CH_3).

¹³C NMR (100 MHz) δ : 171.4, 171.0, 170.6, 169.98, 169.8, 56.5, 144.0, 141.7, 128.1, 127.5, 125.4, 120.4, 101.5, 73.0, 72.3, 71.5, 70.0, 68.7, 67.5, 62.2, 47.5, 21.1, 21.0, 20.9.

MS (ESI, +ve): m/z 680.0 $[M+Na]^+$.

MP: 94-99 °C.

Synthesis of **40**³⁶



Fmoc-Serine (629 mg, 1.92 mmol) and β -D-galactopyranose pentaacetate (500 mg, 1.28 mmol) were stirred in freshly distilled DCM (20 mL). The Lewis acid $BF_3 \cdot Et_2O$ (0.730 ml, 6.40 mmol) was then added *via* syringe and the solution allowed to stir at room temperature for 7 h. After this time the solution was washed with 1M HCl (1 x 10 mL) and H_2O (1 x 10 mL) and dried ($MgSO_4$). The solvent was then removed under reduced pressure to leave a yellow oil. Purification by HPLC on a C_{18} Delta Pak column with a flow rate of 5 mL/minute. The solvent system used was 60:40 H_2O :ACN for 5 minutes then a gradual change to 40:60 H_2O :ACN for 20 minutes. The desired conjugated product eluted at approximately 61 minutes as detected at 220 nm absorbance. The solvent was removed under reduced pressure to leave **40** as a flocculent white solid (295 mg, 35%).

¹H NMR (300 MHz) δ : 7.76 (d, 2H, J = 7.6 Hz, Ar H); 7.61 (br s, 2H, Ar H); 7.39 (t, 2H, J = 7.5 Hz, Ar H); 7.32 (t, 2H, J = 7.4 Hz, Ar H); 5.67 (d, 1H, J = 7.4 Hz, NH); 5.40 (d, 1H, J = 3.2 Hz, H -4); 5.2 (t, 1H, J = 9.1 Hz, H -2); 5.00 (dd, 1H, J = 10, 3.3 Hz, H -3); 4.52 – 4.48 (m, 2H, Fmoc CH_2); 4.46 – 4.43 (m, 2H, H -1 & β - H); 4.3 (d, 1H, J = 9.2, α - H); 4.22 (t, 1H, J = 6.6 Hz, Fmoc CH); 4.16 – 4.07 (m, 2H, H -6 & H -6'); 3.92 (d, 1H, J = 9.2 Hz, β - H); 3.86 (t, 1H, J = 6.6 Hz, H -5); 2.12 (s, 3H, Ac CH_3); 2.02 (s, 3H, Ac CH_3); 2.00 (s, 3H, Ac CH_3); 1.99 (s, 3H, Ac CH_3).

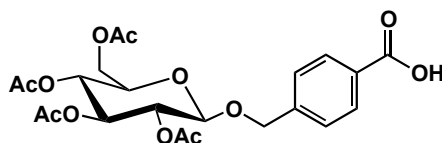
¹³C NMR (75 MHz) δ : 171.0, 170.6, 170.5, 170.2, 156.5, 149.0, 144.0, 141.7, 128.1, 127.5, 125.4, 120.4, 102.0, 77.6, 71.2, 71.0, 70.3, 69.0, 67.4, 67.3, 61.5, 47.5, 20.9, 20.9, 20.9.

MS (ESI, +ve): m/z 680.1 $[M+H]^+$, (ESI, -ve): m/z 656.2 $[M-H]^-$.

MP: 81-86 °C.

3.3.2. Synthesis of Achiral Glycosylated Building Blocks

Synthesis of 42



4-(Hydroxymethyl)benzoic acid (1.2 g, 7.7 mmol) and β -D-glucopyranose pentaacetate (3.0 g, 7.7 mmol) were stirred in freshly distilled DCM (10 mL). The Lewis acid $BF_3 \cdot Et_2O$ (6.0 mL, 48 mmol) was then added *via* syringe and the solution allowed to stir at room temperature for 24 h. After this time the solution was washed with HCl (1M, 1 x 10 mL) and H_2O (10 mL) and dried ($MgSO_4$). The solvent was then removed under reduced pressure to leave a yellow oil. Purification by HPLC on a C_{18} Delta Pak column with a flow rate of 5 mL/minute. The solvent system used was 60:40 H_2O :ACN for 5 minutes then a gradual change to 40:60 for 20 minutes. The desired conjugated product eluted at approximately 35 minutes as detected at 220 nm absorbance. The solvent was removed under reduced pressure to leave **42** as a flocculent white solid (331.3 mg, 9%).

¹H NMR (400 MHz) δ : 8.03 (d, 2H, J = 8.2 Hz, Ar H); 7.35 (d, 2H, J = 8.3 Hz, Ar H); 5.20 – 5.03 (m, 3H, H -2, H -3 & H -4); 4.93 (d, 1H, J = 13.1 Hz, $-OCH_2$); 4.66 (d, 1H, J = 13.1 Hz, $-OCH_2$); 4.57 (d, 1H, J = 7.8 Hz, H -1); 4.24 (dd, 1H, J = 12.4, 4.7 Hz, H -6);

4.13 (dd, 1H, $J = 12.3, 2.4$ Hz, $H-6'$); 3.69 (ddd, 1H, $J = 9.9, 5.4, 2.4$ Hz, $H-5$); 2.06 (s, 3H, Ac CH_3); 2.00 (s, 3H, Ac CH_3); 1.98 (s, 3H, Ac CH_3); 1.97 (s, 3H, Ac CH_3).

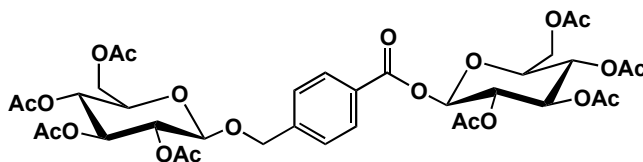
^{13}C NMR (100 MHz) δ : 170.9, 170.5, 169.7, 169.6, 169.0, 143.1, 130.4, 127.4, 100.0, 73.0, 72.2, 71.5, 70.3, 68.6, 62.2, 20.9, 20.8, 20.8, 20.8.

MS (ESI, -ve): m/z 481.0 $[M-H]^-$.

MP: 95-98 °C.

Attempted synthesis of 42

Tetraacetyl bromo- α -D-glucopyranose (67 mg, 0.16 mmol), 4-(hydroxymethyl)benzoic acid (25 mg, 0.16 mmol), silver carbonate (947 mg, 3.43 mmol) and sodium sulfate (1.87 g, 13.1 mmol) were mixed together in DCM (90 mL) at room temperature under nitrogen for 7 h. The reaction mixture was then filtered through celite and the filtrate washed with water (2 x 50 mL), dried (MgSO_4) and the solvent removed under reduced pressure to leave a clear oil. Purification was attempted by HPLC on a C_{18} Delta Pak column with a flow rate of 5 mL/minute. The solvent system used was 60:40 H_2O :ACN for 5 minutes then a gradual change to 40:60 H_2O :ACN for 20 minutes. The desired conjugated product was expected to elute at approximately 35 minutes as detected at 220 nm absorbance, however ^1H NMR analysis of the contents of this peak indicated two products were present and were not separated. A peak also eluted at approximately 62 minutes. The ^1H NMR spectrum suggested a bis sugar product was present. The solvent was removed under reduced pressure to leave **46** as a white solid product (31.5 mg, 40%).



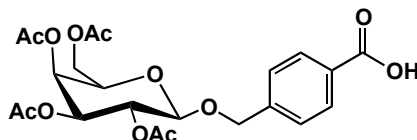
^1H NMR (200 MHz) δ : 8.01 (d, 2H, $J = 8.5$ Hz); 7.36 (d, 2H, $J = 8.5$ Hz); 5.91 (dd, 1H, $J = 5.8, 2.3$ Hz); 5.35 (d, 1H, $J = 2.9$ Hz); 5.32 (d, 1H, $J = 2.3$ Hz); 5.23 – 5.10 (m, 4H); 4.96 (d, 1H, $J = 13.2$ Hz); 4.70 – 4.55 (m, 2H); 4.37 – 4.10 (m, 4H); 3.92 (ddd, 1H, $J = 9.9, 5.4, 2.0$ Hz); 3.68 (ddd, 1H, $J = 9.9, 5.4, 2.0$ Hz); 2.10 (s, 3H); 2.07 (s, 3H); 2.04 (s, 6H); 2.04 (s, 3H), 2.02 (s, 3H); 2.00 (s, 3H); 1.99 (s, 3H).

^{13}C NMR (75 MHz) δ : 170.8, 170.8, 170.4, 170.3, 169.6, 169.6, 169.5, 169.5, 164.4, 143.5, 130.6, 128.2, 127.4, 100.0, 92.6, 73.1, 73.0, 72.9, 72.2, 71.5, 70.4, 70.2, 68.6, 68.2, 62.1, 61.7, 20.9, 20.9, 20.8.

MS (ESI, +ve): m/z 835.0 $[\text{M}+\text{Na}]^+$.

MP: 113-118 °C.

Synthesis of **43**



4-(Hydroxymethyl)benzoic acid (1.2 g, 7.7 mmol) and β -D-galactopyranose pentaacetate (3.0 g, 7.7 mmol) were stirred in freshly distilled DCM (150 mL). The Lewis acid $\text{BF}_3 \cdot \text{Et}_2\text{O}$ (6.0 ml, 48 mmol) was then added *via* syringe and the solution allowed to stir at room temperature for 24 h. After this time the solution was washed with HCl (1M, 1 x 10 mL) and H_2O (1 x 10 mL) and dried (MgSO_4). The solvent was then removed under reduced pressure to leave a yellow oil. Purification by HPLC on a C_{18} Delta Pak column with a flow rate of 5 mL/minute. The solvent system used was 60:40 H_2O :ACN for 5 minutes then a gradual change to 40:60 H_2O :ACN for 20 minutes. The desired conjugated product eluted at approximately 35 minutes as detected at 220 nm absorbance. The solvent was removed under reduced pressure to leave **43** as a flocculent white solid (264.0 mg, 7%).

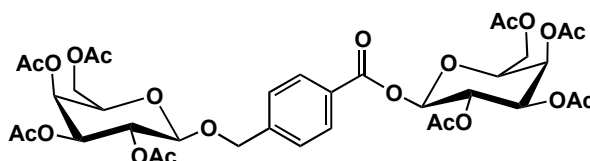
^1H NMR (300 MHz) δ : 8.03 (d, 2H, $J = 8.3$ Hz, Ar H); 7.36 (d, 2H, $J = 8.3$ Hz, Ar H); 5.37 (dd, 1H, $J = 3.4, 0.8$ Hz, $H-4$); 5.27 (dd, 1H, $J = 10.4, 7.9$ Hz, $H-2$); 4.99 (dd, 1H, $J = 10.4, 3.4$ Hz, $H-3$); 4.94 (d, 1H, $J = 13.2$ Hz, $-\text{OCH}_2$); 4.67 (d, 1H, $J = 13.1$ Hz, $-\text{OCH}_2$); 4.54 (d, 1H, $J = 7.9$ Hz, $H-1$); 4.21 – 4.03 (m, 2H, $H-6$ & $H-6'$); 3.90 (td, 1H, $J = 6.7, 0.8$ Hz, $H-5$); 2.12 (s, 3H, Ac CH_3); 2.02 (s, 3H, Ac CH_3); 2.01 (s, 3H, Ac CH_3); 1.95 (s, 3H, Ac CH_3).

^{13}C NMR (75 MHz) δ : 171.1, 170.7, 170.5, 170.4, 169.7; 143.2, 130.5, 127.4, 100.5, 71.1, 71.1, 70.3, 69.1, 67.3, 61.6, 20.9, 20.8, 20.7.

MS (ESI, +ve): m/z 505.1 $[\text{M}+\text{Na}]^+$.

Attempted synthesis of 43

Tetraacetyl bromo- α -D-galactopyranose (1.0 g, 2.4 mmol), 4-(hydroxymethyl)benzoic acid (38 mg, 0.25 mmol), silver carbonate (0.95 g, 3.4 mmol) and sodium sulfate (1.9 g, 13 mmol) were mixed together in DCM (90 mL) at room temperature under nitrogen for 7 h. The reaction mixture was then filtered through celite and the filtrate washed with water (2 x 50 mL), dried (MgSO_4) and the solvent removed under reduced pressure to leave a clear oil. Purification by HPLC on a C_{18} Delta Pak column with a flow rate of 5 mL/minute. The solvent system used was 60:40 H_2O :CAN for 5 minutes then a gradual change to 40:60 H_2O :ACN for 20 minutes. The desired conjugated product was expected to elute at approximately 35 minutes as detected at 220 nm absorbance, however ^1H NMR analysis of the contents of this peak indicated two products were present and were not separated. A peak also eluted at approximately 62 minutes. The ^1H NMR spectrum suggested a bis sugar product was present. The solvent was removed under reduced pressure to leave **47** as a white solid product (70.8 mg, 59%).



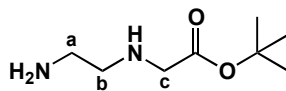
^1H NMR (200 MHz) δ : 8.04 (d, 2H, J = 8.3 Hz); 7.38 (d, 2H, J = 8.2 Hz); 5.89 (d, 1H J = 8.3 Hz); 5.54 (dd, 1H, J = 10.5, 8.3 Hz); 5.48 (d, 1H, J = 3.4 Hz); 5.40 (dd, 1H, J = 3.3, 1.0 Hz); (5.31, dd, 1H, J = 10.5, 7.8 Hz); 5.16 (dd, 1H, J = 10.5, 3.3 Hz); 5.04 – 4.94 (m, 2H); 4.69 (d, 1H, J = 13.1 Hz); 4.54 (d, 1H, J = 7.9 Hz); 4.26 – 4.10 (m, 5H); 3.91 (td, 1H, J = 6.5, 1.1 Hz); 2.20 (s, 3H); 2.17 (s, 3H); 2.07 (s, 3H); 2.06 (s, 3H); 2.05 (s, 3H); 2.02 (s, 3H); 1.99 (s, 6H).

^{13}C NMR (75 MHz) δ : 170.3, 170.2, 170.1, 169.9, 169.5, 169.4, 143.3, 130.4, 128.0, 127.2, 100.3, 92.9, 71.9, 70.9, 70.9, 70.7, 69.9, 68.8, 67.8, 67.0, 66.9, 61.3, 61.0, 20.7, 20.6, 20.5.

MS (ESI, +ve): m/z 835.0 $[\text{M}+\text{Na}]^+$.

MP: 87–91 $^{\circ}\text{C}$.

3.3.3. Synthesis of the PNA Monomer Backbone

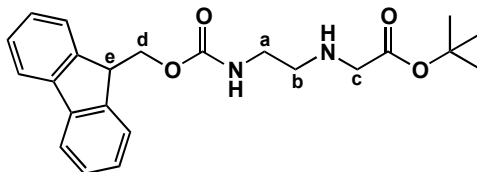
*Synthesis of 50*³⁹

Ethylenediamine (30 mL, 0.45 mol) was stirred in DCM (200 mL) at 0 °C. *t*-Butyl bromoacetate (8.2 mL, 0.050 mol) in DCM (40 mL) was added slowly over 3 h. The reaction was then allowed to stir at room temperature over night. The reaction mixture was then washed with water (3 x 100 mL) and the DCM layer dried (MgSO₄) and the solvent removed under reduced pressure to leave **50** as an opaque oil (5.4 g, 62%).

¹H NMR (400 MHz) δ : 2.79 (s, 2H, *H*-c); 2.27 (t, 2H, *J* = 5.8 Hz, *H*-a or *H*-b); 2.22 (bs, 3H, NH & NH₂); 2.16 (t, 2H, *J* = 5.8 Hz, *H*-a or *H*-b); 0.97 (s, 9H, *t*Bu CH₃).

¹³C NMR (100 MHz) δ : 171.2, 80.2, 51.1, 50.7, 40.7, 27.4.

MS (ESI, +ve): *m/z* 175.17 [M+H]⁺.

*Synthesis of 51*³⁹

Amine **50** (1.00 g, 174 mmol) was dissolved in DCM (40 mL) and diisopropylethyl amine (0.96 mL, 129 mmol) added. A solution of *N*-(9-fluorenylmethoxycarbonyloxy)succinimide (1.85 g, 337 mmol) in DCM (10 mL) was added slowly over 3 h and the reaction mixture allowed to stir for 12 h at room temperature. The mixture was then washed with HCl (1M, 4 x 35 mL) and brine (1 x 50 mL) and dried (MgSO₄). The solvent was then partially removed under reduced pressure before being stored at -20 °C for 72 h. The white solid that had precipitated was filtered, washed with cold DCM and left to dry, leaving **51** as a white solid (1.32 g, 61%).

¹H NMR (400 MHz) δ : 7.74 (d, 2H, *J* = 7.5 Hz, Ar *H*); 7.65 (d, 2H, *J* = 7.4 Hz, Ar *H*); 7.36 (t, 2H, *J* = 7.4 Hz, Ar *H*); 7.28 (td, 2H, *J* = 7.5, 1.2 Hz, Ar *H*); 6.93 (t, 1H, *J* = 5.4

Hz, amide NH); 4.31 (d, 2H, $J = 7.4$ Hz, $H-d$); 4.21 (t, 1H, $J = 7.1$ Hz, $H-e$); 3.78 (s, 2H, $H-c$); 3.73 (m, 2H, $H-a$); 3.29 (m, 2H, $H-b$); 1.45 (s, 9H, tBu).

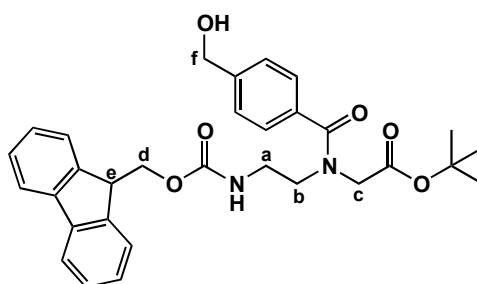
^{13}C NMR (75 MHz) δ : 171.7, 156.3, 144.3, 141.6, 128.0, 127.5, 125.8, 120.2, 85.1, 67.7, 49.2, 48.7, 47.5, 38.1, 28.3.

MS (ESI, +ve): m/z 397.3 $[\text{M}+\text{H}]^+$.

MP: 104–106 °C.

3.3.4. Synthesis of Rigid-Linked Glycosylated Monomers

Synthesis of 52



The hydrochloride salt of **51** (2.5 g, 5.8 mmol) was converted to the free base by dissolving in DCM (5 mL) and washing with sat. Na_2CO_3 (aq) (2 x 5 mL) and dried (MgSO_4) to leave a colourless oil that was combined with 4-hydroxymethylbenzoic acid (1.9 g, 13 mmol) and EDC (1.2 g, 6.1 mmol) in DMF (30 mL) under a nitrogen atmosphere at room temperature. After 45 min, a further 1.2 g (6.1 mmol) EDC was added to the reaction flask. One day later, the solvent was removed under reduced pressure to leave a thick oil. Water (30 mL) was added to this oil, which produced a white solid that was consequently removed by filtration. The oil was then purified on a gravity silica column (5% MeOH/DCM) to leave **52** as a yellow coloured oil (2.13 g, 43%).

^1H NMR* (400 MHz) δ : 7.74 (d, 2H, $J = 7.5$ Hz, Ar H); 7.60 (d, 2H, $J = 7.4$ Hz, Ar H); 7.38 (t, 2H, $J = 7.4$ Hz, Ar H); 7.28 (m, 6H, Ar H); 5.78 (bs, 1H, NH); 4.62 (m, 2H, $H-d$); 4.25 (m, 3H, $H-e$ & $H-f$); 4.08 (bs, 1H, $H-c$); 3.87 (bs, 1H, $H-c$); 3.69 (bs, 1H, $H-a$ or $H-b$); 3.46 (d, 2H, $H-a$ or $H-b$); 3.22 (bs, 1H, $H-a$ or $H-b$); 1.52 & 1.42 (s, 9H, tBu CH_3).

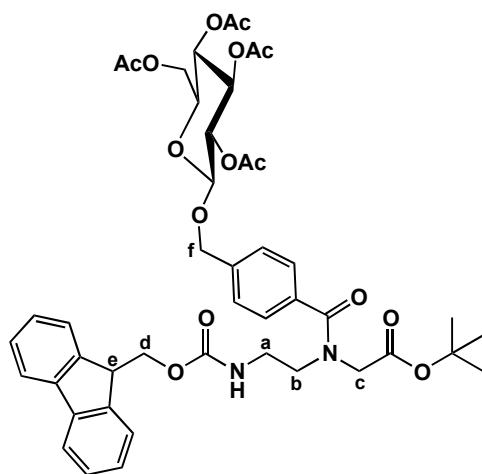
^{13}C NMR* (100 MHz) δ : 173.2, 172.6, 168.9, 156.8, 156.4, 143.9, 143.7, 141.2, 127.6, 126.7, 126.6, 126.5, 125.1, 119.9, 82.6, 82.1, 66.7, 63.9, 53.6, 48.7, 47.1, 39.1, 38.9, 28.0, 27.8.

MS (ESI, +ve): m/z 553.1 $[\text{M}+\text{Na}]^+$.

HRMS (ESI, +ve) m/z 553.23092 $[\text{M}+\text{Na}]^+$, $\text{C}_{31}\text{H}_{34}\text{N}_2\text{NaO}_6$ required m/z 553.23091.

*rotamers present.

Synthesis of **53**



Alcohol **52** (1.2 g, 2.2 mmol) was combined with tetraacetyl bromo- α -D-glucopyranose (1.4 g, 3.3 mmol), silver carbonate (13 g, 47 mmol) and sodium sulphate (26.0 g, 181 mmol) in dichloromethane (200 mL) and allowed to stir at room temperature. After 3 d, the reaction mixture was filtered through celite, washed with water (2 x 20 mL), dried and the solvent removed under reduced pressure. A flash silica column (5% methanol/dichloromethane) was used to purify the crude reaction mixture, however complete separation was not achieved. Purification was then achieved by reverse phase HPLC on a C_{18} Delta Pak column with a flow rate of 5 mL/minute. The solvent system used was 20:80 H_2O :ACN for 10 minutes, a change to 5:95 H_2O :ACN for 1 minute and held for 10 minutes, followed by a change to 0:100 H_2O :ACN over 1 minute and held for the remainder of the run. The desired product eluted at approximately 24 minutes as detected at 256 nm absorbance. The solvent was removed under reduced pressure to leave **53** as a colourless oil (155 mg, 8%).

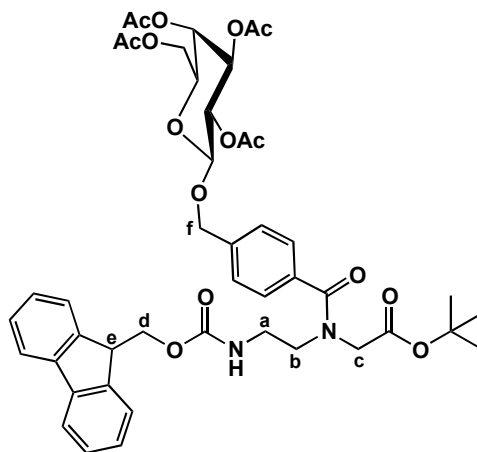
¹H NMR* (300 MHz) δ : 7.74 (d, 2H, $J = 7.4$ Hz, Ar H); 7.59 (d, 2H, $J = 7.4$ Hz, Ar H); 7.29 (m, 8H, Ar H); 5.70 (bs, 1H, NH); 5.19-4.10 (bm, 12H, H -1, H -2, H -3, H -4, H -5, H -6, H -6', H -d, H -e, H -f); 3.89 (bs, 1H, H -a, H -b or H -c); 3.70 (bs, 2H, H -a, H -b or H -c); 3.48 (m, 2H, H -a, H -b or H -c); 3.26 (bs, 1H, H -a, H -b or H -c); 2.08 (s, 3H, Ac CH_3); 2.01 (s, 3H, Ac CH_3); 1.99 (m, 6H, s, 3H, 2 x Ac CH_3); 1.52 & 1.43 (s, 9H, t Bu CH_3).

¹³C NMR* (75 MHz) δ : 170.9, 170.5, 169.7, 169.6, 144.3, 141.6, 128.5, 128.0, 127.8, 127.4, 125.5, 120.3, 100.0, 73.1, 72.3, 71.6, 70.5, 68.7, 67.2, 62.2, 47.5, 39.6, 28.4, 21.0, 20.9, 20.9.

MS (ESI, +ve): m/z 883.0 $[M+Na]^+$.

*rotamers present.

Synthesis of **54**



Alcohol **52** (1.2 g, 2.3 mmol) was combined with tetraacetyl bromo- α -D-galactopyranose (1.4 g, 3.4 mmol), silver carbonate (13 g, 49 mmol) and sodium sulfate (26.4 g, 186 mmol) in dichloromethane (150 mL) and allowed to stir at room temperature for 2 d. The reaction mixture was then filtered through celite and washed with sat. NaHCO_3 (aq) (1 x 20 mL) and H_2O (1 x 20 mL), dried (MgSO_4) and the solvent removed under reduced pressure. Purification by reverse phase HPLC on a C_{18} Delta Pak column with a flow rate of 5 mL/minute in four batches. The solvent system used was 20:80 H_2O :ACN for 10 minutes, a change to 5:95 H_2O :ACN for 1 minute and held for 10 minutes, followed by a change to 0:100 H_2O :ACN over 1 minute and held for the remainder of the run. The desired product eluted at approximately 24 minutes as detected at 256 nm absorbance.

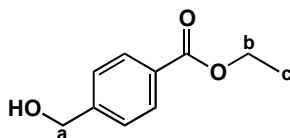
The solvent was removed under reduced pressure to leave **54** as a colourless oil (318 mg, 16%).

¹H NMR (400 MHz) δ : 7.72 (d, 2H, J = 6.8 Hz, Ar H); 7.58 (d, 2H, J = 7.2 Hz, Ar H); 7.40-7.18 (m, 8H, Ar H); 5.79 (bs, 1H, NH); 5.42-4.10 (bm, 12H, H -1, H -2, H -3, H -4, H -5, H -6, H -6', H -d, H -e, H -f); 3.86 (bs, 2H, H -a, H -b or H -c); 3.65 (bs, 1H, H -a, H -b or H -c); 3.45 (m, 2H, H -a, H -b or H -c); 3.21 (bs, 1H, H -a, H -b or H -c); 2.12-1.92 (m, 12H, 4 x Ac CH_3); 1.50 & 1.40 (s, 9H, t Bu CH_3).

¹³C NMR (100 MHz) δ : 170.6, 170.5, 170.4, 170.2, 169.9, 169.5, 156.4, 144.1, 141.4, 127.9, 127.6, 127.3, 127.0, 125.3, 120.1, 97.7, 82.8, 71.5, 71.0, 70.3, 69.0, 67.3, 67.0, 61.5, 50.6, 49.0, 47.4, 39.3, 28.2, 20.9, 20.8, 20.8, 20.7.

HRMS (ESI, +ve) m/z 883.3259 [$M+Na$]⁺, C₄₅H₅₂O₁₅Na required m/z 883.3260.

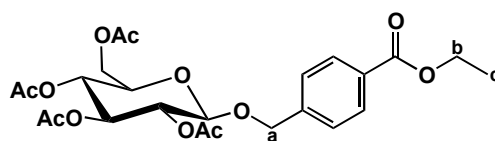
Synthesis of **55**



4-(Hydroxymethyl)benzoic acid (695 mg, 4.57 mmol), absolute ethanol (50 mL) and concentrated sulfuric acid (5 drops) were combined and heated to reflux for 22 h. The reaction mixture was then allowed to cool before being diluted with sat. NaHCO₃ (aq) (100 mL), extracted with ethyl acetate (100 mL), washed with water (2 x 100 mL), dried (MgSO₄) and the solvent was removed under reduced pressure to leave **55** as a pale yellow oil (753 mg, 92%).

¹H NMR (300 MHz): δ 7.87 (d, 2H, J = 8.3 Hz, Ar H); 7.28 (d, 2H, J = 8.1 Hz, Ar H); 4.59 (d, 2H, J = 4.9 Hz, H -a); 4.25 (q, 2H, J = 7.3 Hz, H -b); 3.99 (t, 1H, J = 5.5 Hz, OH-); 1.30 (t, 3H, J = 7.2 Hz, H -c).

¹³C NMR (100 MHz): δ 166.9, 146.3, 130.1, 129.9, 126.7, 64.9, 61.3, 14.6.

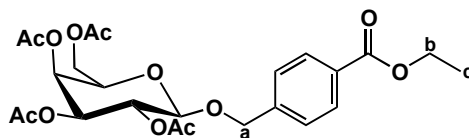
Synthesis of 56

Tetraacetyl bromo- α -D-glucopyranose (288 mg, 0.700 mmol), **55** (126 mg, 0.700 mmol), silver carbonate (4.0 g, 15 mmol) and sodium sulfate (8.0 g, 57 mmol) were stirred in DCM (10 mL) under an atmosphere of nitrogen in the dark for 5 h. The reaction mixture was then filtered through celite, the organic layer washed with sat. NaHCO_3 (aq) (1 x 20 mL) and water (1 x 20 mL), dried (MgSO_4) and the solvent removed under reduced pressure. Purification by reverse phase HPLC on a C_{18} Delta Pak column with a flow rate of 5 mL/minute. The solvent system used was 40:60 H_2O :ACN for 5 minutes then a gradual change to 20:80 H_2O :ACN for 10 minutes followed by a gradual change to 10:90 H_2O :ACN over 5 minutes and held for 10 minutes. The desired product eluted at approximately 62 minutes as detected at 256 nm absorbance. The solvent was removed under reduced pressure to leave **56** as a colourless oil (38 mg, 11% (recovered yield 14%)).

^1H NMR (300 MHz): δ 8.01 (d, 2H, $J = 8.4$ Hz, Ar H); 7.34 (d, 2H, $J = 8.5$ Hz, Ar H); 5.13 (m, 3H, H -2, H -3 & H -4); 4.93 (d, 1H, $J = 12.9$ Hz, H -a); 4.66 (d, 1H, $J = 12.9$ Hz, H -a); 4.56 (d, 1H, $J = 7.7$ Hz, H -1); 4.37 (q, 2H, $J = 7.2$ Hz, H -b); 4.26 (dd, 1H, $J = 12.3$, 4.7 Hz, H -6); 4.15 (dd, 1H, $J = 12.3$, 2.5 Hz, H -6'); 3.68 (ddd, 1H, $J = 9.6$, 4.7, 2.5 Hz, H -5); 2.08 (s, 3H, Ac CH_3); 2.02 (s, 3H, Ac CH_3); 2.01 (s, 3H, Ac CH_3); 1.99 (s, 3H, Ac CH_3); 1.38 (t, 3H, $J = 7.2$ Hz, H -c).

^{13}C NMR (75 MHz): δ 170.9, 170.5, 169.7, 169.6, 166.6, 142.1, 130.4, 130.0, 127.4, 100.0, 73.1, 72.3, 71.6, 70.4, 68.7, 62.2, 61.3, 21.0, 20.9, 20.9, 14.6.

MS (ESI, +ve) m/z 533.0 $[\text{M}+\text{Na}]^+$.

Synthesis of 57

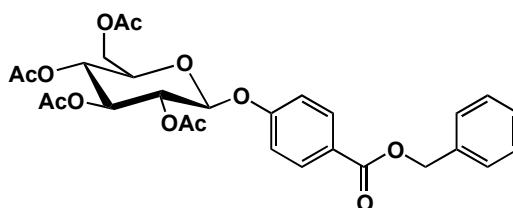
Tetraacetyl bromo- α -D-galactopyranose (2.0 g, 4.8 mmol), **55** (719 mg, 3.99 mmol), silver carbonate (10 g, 36 mmol) and sodium sulfate (30.0 g, 211 mmol) were stirred in DCM (50 mL) under an atmosphere of nitrogen in the dark for 23.5 h. The reaction mixture was then filtered through celite, the organic layer washed with sat. NaHCO_3 (aq) (1 x 20 mL) and water (1 x 20 mL), dried (MgSO_4) and the solvent removed under reduced pressure. Purification by reverse phase HPLC on a C_{18} Delta Pak column with a flow rate of 5 mL/minute. The solvent system used was 40:60 H_2O :ACN for 5 minutes then a gradual change to 10:90 H_2O :ACN for 20 minutes, held for 5 minutes followed by a change to 0:100 H_2O :ACN for 5 minutes. The desired product eluted at approximately 27 minutes as detected at 256 nm absorbance. The solvent was removed under reduced pressure to leave **57** as a colourless oil (499 mg, 25% (recovered yield 64%)).

^1H NMR (300 MHz): δ 7.94 (d, 2H, J = 8.2 Hz, Ar H); 7.28 (d, 2H, J = 8.2 Hz, Ar H); 5.33 (d, 1H, J = 3.4 Hz, H -4); 5.22 (dd, 1H, J = 10.4, 8.0 Hz, H -2); 4.95 (dd, 1H, J = 10.4, 3.4 Hz, H -3); 4.89 (d, 1H, J = 13.0 Hz, H -a); 4.62 (d, 1H, J = 13.0 Hz, H -a); 4.50 (d, 1H, J = 7.9 Hz, H -1); 4.30 (q, 2H, J = 7.1 Hz, H -b); 4.10 (m, 2H, H -6 & H -6'); 3.86 (td, 1H, J = 6.6, 0.92 Hz, H -5); 2.09 (s, 3H, Ac CH_3); 1.98 (s, 3H, Ac CH_3); 1.96 (s, 3H, Ac CH_3); 1.91 (s, 3H, Ac CH_3); 1.32 (t, 3H, J = 7.1 Hz, H -c).

^{13}C NMR (75 MHz): δ 170.5, 170.4, 170.2, 169.5, 166.4, 142.1, 130.2, 129.8, 127.3, 100.3, 71.0, 71.0, 70.2, 69.0, 67.3, 61.5, 61.1, 20.8, 20.7, 20.6, 14.4.

MS (ESI, +ve): m/z 533.0 $[\text{M}+\text{Na}]^+$.

HRMS (ESI, +ve) m/z 533.1633 $[\text{M}+\text{Na}]^+$, $\text{C}_{24}\text{H}_{30}\text{O}_{12}\text{Na}$ required m/z 533.1629.

Synthesis of 60

Benzyl-4-hydroxybenzoate (500 mg, 2.19 mmol) was dissolved with β -D-glucopyranose pentaacetate (1.28 g, 3.28 mmol) in dichloromethane (540 mL) before $\text{BF}_3 \cdot \text{Et}_2\text{O}$ (1.24 mL, 11.0 mmol) was added and the reaction was allowed to stir at room temperature for 8 h. The reaction was then quenched and washed with water (2 x 20 mL), dried (MgSO_4) and the solvent removed under reduced pressure to leave a thick pale yellow oil. Purification by reverse phase HPLC on a C_{18} Delta Pak column with a flow rate of 5 mL/minute. The solvent system used was 40:60 H_2O :ACN for 5 minutes then a gradual change to 20:80 H_2O :ACN for 5 minutes, held for 10 minutes, followed by a gradual change to 10:90 H_2O :ACN for 5 minutes, held for 10 minutes before a rapid change to 0:100 H_2O :ACN to finish the run. The desired conjugated product eluted at approximately 30 minutes as detected at 220 nm absorbance. The solvent was removed under reduced pressure to leave **60** as a white solid (574.6 mg, 47%, α : β = 0.026 : 1).

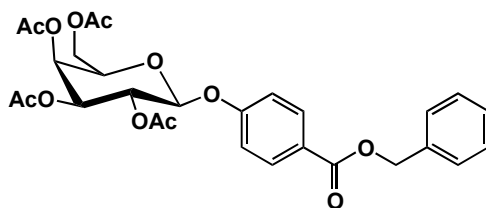
^1H NMR (400 MHz): δ 8.03 and 7.00 (ABq, 4H, J = 9.0 Hz, Ar H); 7.37 (m, 5H, Ar Bn H); 5.35 (s, 2H, Bn CH_2); 5.30 (m, 2H, H -1 & H -3); 5.17 (m, 2H, H -2 & H -4); 4.28 (dd, 1H, J = 12.4, 5.6 Hz, H -6); 4.17 (dd, 1H, J = 12.2, 2.4 Hz, H -6'); 3.89 (ddd, 1H, J = 9.9, 5.4, 2.4 Hz, H -5); 2.07 (s, 3H, Ac CH_3); 2.05 (s, 6H, 2 Ac CH_3); 2.04 (s, 3H, Ac CH_3).

^{13}C NMR (100 MHz): δ 170.8, 170.4, 169.7, 169.5, 166.0, 160.6, 136.3, 132.0, 128.9, 128.5, 128.4, 116.5, 98.5, 72.9, 72.5, 71.3, 68.5, 66.9, 62.2, 21.0, 20.9, 20.9.

MS (ESI, +ve) m/z 581.1 $[\text{M}+\text{Na}]^+$.

HRMS (ESI, +ve) m/z 581.1629 $[\text{M}+\text{Na}]^+$, $\text{C}_{28}\text{H}_{30}\text{O}_{12}\text{Na}$ required m/z 581.1629.

MP: 143-144 $^\circ\text{C}$.

Synthesis of 61

Benzyl-4-hydroxybenzoate (500 mg, 2.19 mmol) was dissolved with β -D-galactopyranose pentaacetate (1.28 g, 3.28 mmol) in dichloromethane (50 mL) before $\text{BF}_3 \cdot \text{Et}_2\text{O}$ (1.24 mL, 10.95 mmol) was added and the reaction was allowed to stir with molecular sieves under an atmosphere of nitrogen at room temperature for 1 h. The reaction was then quenched and washed with water (2 x 20 mL), dried (MgSO_4) and the solvent removed under reduced pressure to leave a thick pale yellow oil. Purification by reverse phase HPLC on a C_{18} Delta Pak column with a flow rate of 5 mL/minute. The solvent system used was 40:60 H_2O :ACN for 5 minutes then a gradual change to 20:80 H_2O :ACN for 5 minutes, held for 10 minutes, followed by a gradual change to 10:90 H_2O :ACN for 5 minutes, held for 10 minutes before a rapid change to 0:100 H_2O :ACN to finish the run. The desired conjugated product eluted at approximately 30 minutes as detected at 220 nm absorbance. The solvent was removed under reduced pressure to leave **61** as a white solid (443.7 mg, 36%, $\alpha:\beta = 0.26:1$).

 β -anomer

^1H NMR (400 MHz): δ 8.03 and 7.02 (ABq, 4H, $J = 8.8$ Hz, Ar H); 7.44 - 7.31 (m, 5H, Ar Bn H); 5.50 (dd, 1H, $J = 10.4, 8.0$ Hz, $H-2$); 5.46 (dd, 1H, $J = 3.6, 0.8$ Hz, $H-4$); 5.34 (s, 2H, Bn CH_2); 5.13 (d, 1H, $J = 8.0$ Hz, $H-1$); 5.13 (dd, 1H, $J = 10.4, 3.6$ Hz, $H-3$); 4.30 - 4.14 (m, 2H, $H-6$ & $H-6'$), 4.10 (m, 1H, $H-5$); 2.18 (s, 3H, Ac CH_3); 2.06 (s, 3H, Ac CH_3); 2.05 (s, 3H, Ac CH_3); 2.01 (s, 3H, Ac CH_3).

^{13}C NMR (100 MHz): δ 170.5, 170.4, 170.2, 170.1, 169.5, 166.0, 160.6, 136.3, 131.9, 128.8, 128.4, 128.3, 125.2, 116.4, 99.0, 71.5, 70.9, 68.7, 67.0, 66.8, 61.6, 20.9, 20.8, 20.8, 20.7.

MS (ESI, +ve) m/z 581.1 $[\text{M}+\text{Na}]^+$.

HRMS (ESI, +ve) m/z 581.1627 $[\text{M}+\text{Na}]^+$, $\text{C}_{28}\text{H}_{30}\text{O}_{12}\text{Na}$ required m/z 581.1629.

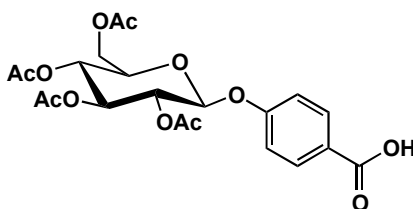
α -anomer

^1H NMR (400 MHz): δ 8.05 and 7.10 (ABq, 4H, J = 9.0 Hz, Ar H); 7.45 – 7.32 (m, 5H, Ar Bn H); 5.85 (d, 1H, J = 3.6 Hz, H -1); 5.56 (dd, 1H, J = 10.8, 3.2 Hz, H -3); 5.52 (dd, 1H, J = 3.2, 1.2 Hz, H -4); 5.35 (s, 2H, Bn CH_2); 5.30 (dd, 1H, J = 10.8, 3.6 Hz, H -2); 4.28 (t, 1H, J = 6.4 Hz, H -5); 4.11 (dd, 1H, J = 11.2, 6.0 Hz, H -6); 4.04 (dd, 1H, J = 11.2, 7.2 Hz, H -6'); 2.17 (s, 3H, Ac CH_3); 2.07 (s, 3H, Ac CH_3); 2.03 (s, 3H, Ac CH_3); 1.92 (s, 3H, Ac CH_3).

^{13}C NMR (100 MHz): δ 170.4, 170.3, 170.2, 170.1, 169.4, 165.8, 159.9, 136.2, 131.8, 128.7, 128.3, 128.2, 125.1, 116.3, 94.6, 67.8, 67.7, 67.6, 67.5, 66.6, 61.5, 20.8, 20.7, 20.7, 20.6.

MS (ESI, +ve) m/z 581.1 $[\text{M}+\text{Na}]^+$.

MP: 68–71 °C.

Synthesis of 62

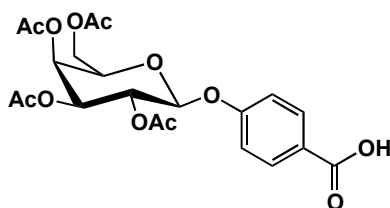
A solution of *t*-butyl ester **60** (300 mg, 0.537 mmol) in ethyl acetate (50 mL) was flushed with nitrogen gas before Pd/C (5%, 200 mg) was added and hydrogenated with a balloon of hydrogen gas at room temperature for 5 h. The solution was filtered through celite and the solvent removed under reduced pressure to give the product, **62** as a white solid (251 mg, quantitative).

^1H NMR (400 MHz): δ 8.06 and 7.04 (ABq, 4H, J = 8.6 Hz, Ar H); 5.32 (m, 2H, H -1 & H -3); 5.18 (m, 2H, H -2 & H -4); 4.29 (dd, 1H, J = 12.0, 5.6 Hz, H -6); 4.18 (dd, 1H, J = 12.4, 2.4 Hz, H -6'); 3.92 (ddd, 1H, J = 10.0, 5.6, 2.4 Hz, H -5); 2.08 (s, 3H, Ac CH_3); 2.06 (s, 3H, Ac CH_3); 2.06 (s, 3H, Ac CH_3); 2.04 (s, 3H, Ac CH_3).

^{13}C NMR (100 MHz): δ 171.0, 170.5, 170.2, 169.4, 169.3, 160.8, 132.3, 124.3, 116.3, 98.2, 72.6, 72.3, 71.1, 68.2, 62.0, 29.7, 20.6, 20.6.

MS (ESI, +ve) m/z 491.1 $[\text{M}+\text{Na}]^+$.

HRMS (ESI, +ve) m/z 491.1160 $[\text{M}+\text{Na}]^+$, $\text{C}_{21}\text{H}_{24}\text{O}_{12}\text{Na}$ required m/z 491.1160.

Synthesis of 63

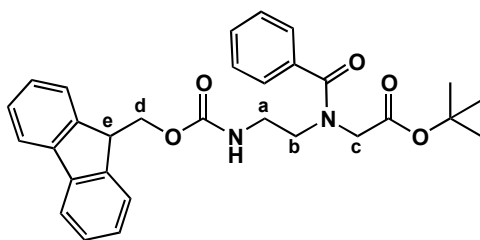
A solution of the *t*-butyl ester **61** (513 mg, 0.92 mmol) in ethyl acetate (50 mL) was flushed with nitrogen gas before Pd/C (5%, 400 mg) was added and hydrogenated with a balloon of hydrogen gas at room temperature for 5 h. The solution was filtered through celite and the solvent removed under reduced pressure to give the product, **63** as a white solid (430.7 mg, quantitative).

¹H NMR (400 MHz): δ 8.05 and 7.03 (ABq, 4H, J = 8.8 Hz, Ar H); 5.50 (dd, 1H, J = 10.4, 8.0 Hz, H -2); 5.46 (d, 1H, J = 3.2 Hz, H -4); 5.15 (d, 1H, J = 8.0 Hz, H -1); 5.13 (dd, 1H, J = 10.4, 3.6 Hz, H -3); 4.24 – 4.10 (m, 3H, H -5, H -6 & H -6'), 2.17 (s, 3H, Ac CH_3); 2.05 (s, 6H, 2 Ac CH_3); 2.01 (s, 3H, Ac CH_3).

¹³C NMR (100 MHz): δ 171.1, 170.5, 170.3, 170.2, 169.5, 161.0, 132.4, 124.4, 116.7, 98.8, 71.4, 70.8, 68.6, 67.0, 61.5, 20.8, 20.7, 20.7, 20.6.

MS (ESI, +ve) m/z 491.0 [M+Na]⁺.

HRMS (ESI, +ve) m/z 491.1157 [M+Na]⁺, C₂₁H₂₄O₁₂Na required m/z 491.1160.

Synthesis of 66Method 1⁴²

Benzoic acid (50 mg, 0.45 mmol) was dissolved in DCM (5 mL). DAST (0.08 mL, 0.59 mmol) was added and the solution was stirred for 30 min before it was poured over ice water. The organic layer was dried (MgSO₄) and the solvent removed under reduced pressure to leave a yellow coloured oil. PNA monomer backbone **51** (126 mg, 0.290 mmol) was washed with sat. NaHCO₃ (aq) (5 mL) in DCM (5 mL), then dried (MgSO₄) and the solution added to the yellow oil. The

reaction was left to stir at room temperature over night. The reaction mixture was then washed with water (2 x 20 mL), dried (MgSO_4) and the solvent removed under reduced pressure. Purification by flash silica chromatography (DCM to 1% MeOH/DCM to 5% MeOH/DCM) to leave **66** as a colourless oil (51.3 mg, 35%).

Method 2⁴³

PNA monomer backbone **51** (50 mg, 0.12 mmol), benzoic acid (18 mg, 0.15 mmol), HOBt (22 mg, 0.16 mmol), HBTU (44 mg, 0.12 mmol) and DIPEA (0.07 mL, 0.44 mmol) were combined in DMF (2 mL). The reaction was allowed to stir at room temperature for 4 d. The solvent was then removed under reduced pressure and the oily mixture was purified by column chromatography (DCM to 1% MeOH/DCM) using flash silica. The solvent was then removed under reduced pressure to leave **66** as a colourless oil (37.7 mg, 65%).

Method 3²¹

PNA monomer backbone **51** (55 mg, 0.13 mmol) was washed with sat. NaHCO_3 (aq) (5 mL) in DCM (5 mL), then dried (MgSO_4) and the solution combined with benzoic acid (19 mg, 0.15 mmol), HATU (57 mg, 0.15 mmol), HOBt (20 mg, 0.15 mmol) and DIEPA (0.04 mL, 0.25 mmol) in DMF (5 mL) and allowed to stir at room temperature over night. The solvent was then removed under reduced pressure. The remaining oil was dissolved in DCM (20 mL) and washed with H_2O (1 x 20 mL), HCl (1 x 20 mL) and sat. NaHCO_3 (aq) (20 mL). The organic layer was then dried (MgSO_4) and the solvent removed under reduced pressure. Column chromatography (DCM to 1% MeOH/DCM) on flash silica was used to purify the mixture. The desired product **66** (colourless oil) was isolated in 36% yield (23 mg).

Method 4^{17,18}

Benzoic acid (17 mg, 0.14 mmol), HBTU (52.6, 139 mmol), HOBt (29 mg, 0.21 mmol) and *N*-methyl morpholine (0.02 mL, 0.21 mmol) were combined in DCM (1 mL) and allowed to stir at room temperature for 20 m. PNA monomer backbone **51** (55 mg, 0.13 mmol) was washed with sat. NaHCO_3 (aq) (5 mL) in DCM (5 mL),

then dried (MgSO_4) and the solution combined with the benzoic acid solution. After 5 days, the solvent was removed and the remaining oily mixture was purified by flash silica column chromatography (DCM to 1% MeOH/DCM). The solvent was removed under reduced pressure to leave **66** as a colourless oil (40.7 mg, 65 %).

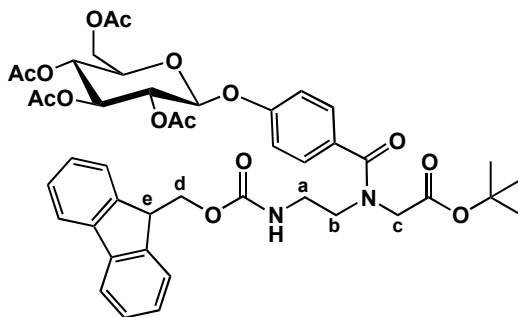
¹H NMR* (400 MHz): δ 7.76 (d, 2H, *J* = 6.8 Hz, Ar *H*); 7.62 (d, 2H, *J* = 7.2 Hz, Ar *H*); 7.39-7.27 (m, 8H, Ar *H*); 5.76 (bs, 1H, NH); 4.37 (m, 1H, *H*-e); 4.23 (m, 2H, *H*-d); 4.10 (s, 1H, *H*-c); 3.90 (s, 1H, *H*-c); 3.72 (m, 1H, *H*-a or *H*-b); 3.53 (m, 1H, *H*-a or *H*-b); 3.48 (m, 1H, *H*-a or *H*-b); 3.26 (m, 1H, *H*-a or *H*-b); 1.54 & 1.42 (s, 9H, *t*Bu CH₃).

¹³C NMR* (100 MHz): δ 173.8, 172.94, 169.7, 169.5, 156.9, 156.3, 143.9, 141.2, 135.3, 134.9, 130.5, 129.9, 128.9, 128.8, 128.6, 128.0, 127.9, 127.3, 127.2, 126.9, 126.5, 126.2, 125.5, 125.4, 120.3, 120.3, 83.2, 83.0, 67.1, 66.9, 54.1, 52.7, 51.0, 49.2, 46.8, 46.8, 38.9, 31.8, 28.2, 28.0.

MS (ESI, +ve) m/z 523.0 [M+Na]⁺.

* Rotamers present.

Synthesis of 69



Method 1

PNA monomer backbone **51** (229 mg, 0.528 mmol) was dissolved in DCM (10 mL), washed with sat. NaHCO₃ (aq) (2 x 5 mL) and then dried (MgSO₄). Acid **62** (165 mg, 0.352 mmol) was dissolved in DCM (10 mL) and DAST (0.10 mL, 0.71 mmol) was added and stirred at room temperature for 30 m. The mixture was then washed with water (5 mL), dried (MgSO₄) and the solvent then partially removed under reduced pressure. The backbone solution was then added to the sugar fluoride solution and was stirred at reflux for 3 d. The reaction mixture was then washed with water (2 x 20 mL), dried and the solvent removed under reduced pressure to leave a yellow/brown coloured oil. This was initially purified

by flash column chromatography (DCM to 0.5% MeOH/DCM to 1% MeOH/DCM to 2% MeOH/DCM) however complete separation was not achieved. Then reverse phase HPLC was used to purify in 3 batches on a C₁₈ Delta Pak column with a flow rate of 5 mL/minute and an isocratic solvent system of 20:80 H₂O:ACN. The desired product eluted at 26 minutes as detected at 256 nm absorbance. The solvent to removed under reduced pressure to leave **69** as a white solid (133.4 mg, 45%).

Method 2

Acid **62** (420 mg, 0.897 mmol) was combined in DCM (10 mL) with HBTU (330 mg, 0.870 mmol), HOBt (165 mg, 1.22 mmol), DIEA (0.55 mL, 3.3 mmol) and PNA monomer backbone **51** (377 mg, 0.870) and stirred at room temperature for 2 d. At this time, TLC analysis revealed there still to be starting material present so the same quantities again of HOBt and HBTU were added. 24 h later, the reaction mixture was washed with sat. NaHCO₃ (aq) (2 x 20 mL), HCl (1 M, 1 x 20 mL) and water (2 x 20 mL), dried (MgSO₄) and the solvent removed under reduced pressure. Purification by flash silica chromatography (DCM to ethyl acetate) isolated **69** as a colourless oil (502 mg, 68%).

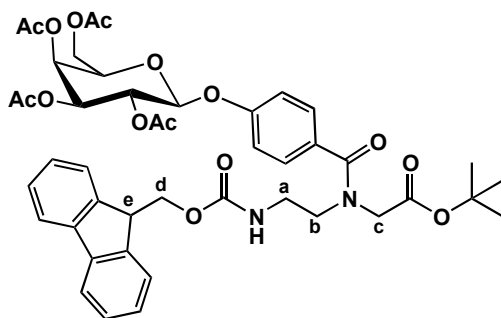
¹H NMR* (400 MHz): δ 7.79 (d, 2H, J = 9.3 Hz, Fmoc Ar H); 7.60 (d, 2H, J = 9.3 Hz, Fmoc Ar H); 7.39 (m, 2H, Fmoc Ar H); 7.32 (m, 4H, Fmoc Ar H & Ar H); 6.85 (m, 2H, Ar H); 5.76 (bs, 1H, NH); 5.38 – 3.21 (broad multiplets unresolved, 16H, H -1, H -2, H -3, H -4, H -5, H -6, H -6', H -a, H -b, H -c, H -d, H -e); 2.04 (s, 3H, Ac CH₃); 2.02 (s, 9H, Ac CH₃); 1.47 (m, 9H, t Bu CH₃).

¹³C NMR* (100 MHz): δ 171.9, 170.6, 170.3, 169.5, 169.3, 157.7, 156.9, 144.1, 141.4, 130.8, 130.5, 128.7, 127.9, 127.3, 125.3, 120.1, 116.8, 98.8, 81.7, 72.7, 72.2, 71.1, 68.2, 67.0, 61.9, 50.9, 49.1, 47.4, 39.3, 28.2, 20.8, 20.7.

MS (ESI, +ve) m/z 847.0 [M+H]⁺, m/z 869.1 [M+Na]⁺.

HRMS (ESI, +ve) m/z 869.3105 [M+Na]⁺, C₄₄H₅₀N₂NaO₁₅ required m/z 869.3103. m/z 847.3281 [M+H]⁺, C₄₄H₅₁N₂O₁₅ required m/z 847.3284.

* Rotamers present.



PNA monomer backbone **51** (351 mg, 0.810 mmol) was dissolved in DCM (10 mL), washed with sat. NaHCO₃ (aq) (2 x 5 mL) and then dried (MgSO₄). Acid **63** (253 mg, 0.540 mmol) was dissolved in DCM (10 mL), DAST (0.15 mL, 1.08 mmol) added and stirred at room temperature for 1.5 h. The mixture was then washed with water (5 mL), dried (MgSO₄) and the solvent then partially removed under reduced pressure. The backbone solution was then added to the sugar fluoride solution and was stirred at reflux for 3 d. The reaction mixture was then washed with water (2 x 20 mL), dried (MgSO₄) and the solvent removed under reduced pressure to leave a yellow/brown coloured oil. Reverse phase HPLC was used to purify in 3 batches on a C₁₈ Delta Pak column with a flow rate of 5 mL/minute and an isocratic solvent system of 20: 80 H₂O:ACN. The desired product eluted at 26 minutes as detected at 256 nm absorbance. The solvent was removed under reduced pressure to leave **70** as a white solid (178 mg, 39%).

Acid **63** (396 mg, 0.847 mmol) was combined in DCM (10 mL) with HBTU (292 mg, 0.770), HOBT (145 mg, 1.08 mmol), DIEA (0.48 mL, 2.93 mmol) and PNA monomer backbone **51** (333 mg, 0.770) and stirred at room temperature for 1 d. The reaction mixture was then washed with sat. NaHCO₃ (aq) (2 x 20 mL), HCl (1 M, 1 x 20 mL) and water (2 x 20 mL), dried (MgSO₄) and the solvent removed under reduced pressure. Purification by flash silica chromatography (DCM to ethyl acetate) to leave **70** as a colourless oil (522 mg, 80%).

160

5.79 (bs 1H, NH); 5.51 – 3.10 (broad multiplets unresolved, 16H, *H*-1, *H*-2, *H*-3, *H*-4, *H*-5, *H*-6, *H*-6', *H*-a, *H*-b, *H*-c, *H*-d, *H*-e); 2.15 (s, 3H, Ac CH₃); 1.99 (s, 9H, Ac CH₃); 1.46 (m, 9H, *t*Bu CH₃).

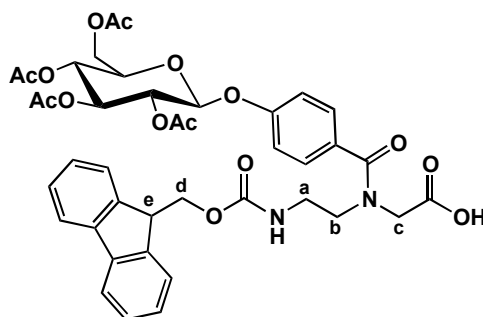
¹³C NMR* (100 MHz): δ 171.9, 170.2, 170.2, 170.0, 169.3, 157.7, 156.2, 143.9, 141.2, 130.7, 130.3, 128.6, 127.8, 127.1, 125.2, 120.0, 116.6, 99.1, 82.5, 71.0, 70.7, 68.4, 67.0, 66.8, 61.3, 50.8, 49.1, 47.2, 39.2, 28.0, 20.6, 20.6, 20.6, 20.6.

MS (ESI, +ve) m/z 847.1 $[M+H]^+$, m/z 869.0 $[M+Na]^+$.

HRMS (ESI, +ve) m/z 869.3101 $[M+Na]^+$, $C_{44}H_{50}N_2NaO_{15}$ required m/z 869.3103.
 m/z 847.3283 $[M+H]^+$, $C_{44}H_{51}N_2O_{15}$ required m/z 847.3284.

* Rotamers present.

Synthesis of 71



t-Butyl ester **69** (105 mg, 0.124 mmol) was dissolved in DCM (1 mL) in an ice bath and TFA (1 mL) was added. The reaction was allowed to stir for 4 h before the solvents were removed under reduced pressure and the reaction mixture purified by flash silica chromatography (2% MeOH/DCM to 10% MeOH/DCM). The solvent was removed under reduced pressure to leave **71** as a colourless oil (97.5 mg, quant).

¹H NMR* (400 MHz): δ 7.78 (d, 2H, *J* = 7.2 Hz Fmoc Ar *H*); 7.58 (d, 2H, *J* = 5.6 Hz, Fmoc Ar *H*); 7.40-7.25 (m, 6H, Fmoc Ar *H* & Ar *H*); 7.15-6.72 (m, 2H, Ar *H*); 5.89 (bs 1H, NH); 5.27 – 3.10 (broad multiplets unresolved, 16H, *H*-1, *H*-2, *H*-3, *H*-4, *H*-5, *H*-6, *H*-6', *H*-a, *H*-b, *H*-c, *H*-d, *H*-e); 2.09-1.91 (m, 12H, 4 x Ac CH₃).

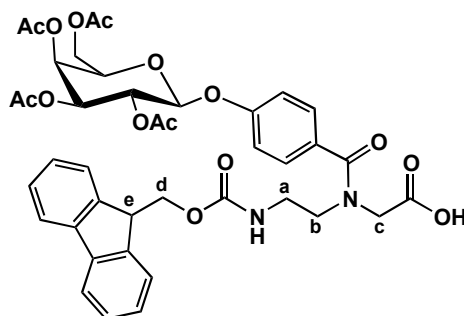
¹³C NMR* (100 MHz): δ 172.9, 170.5, 170.3, 170.2, 169.5, 157.6, 156.9, 144.0, 141.3, 129.1, 128.9, 128.0, 127.4, 127.3, 125.5, 125.2, 125.0, 120.2, 117.2, 116.7, 99.0, 71.0, 70.8, 68.5, 67.5, 67.23, 67.0, 67.0, 61.3, 51.1, 47.3, 47.1, 40.1, 39.4 20.7.

MS (ESI, +ve) m/z 790.9 $[M+H]^+$, m/z 812.8 $[M+Na]^+$.

HRMS (ESI, +ve) m/z 813.2469 $[M+Na]^+$, $C_{40}H_{42}N_2NaO_{15}$ required m/z 813.2477.
 m/z 791.2650 $[M+H]^+$, $C_{40}H_{43}N_2O_{15}$ required m/z 791.2658.

* Rotamers present.

Synthesis of **72**



t-Butyl ester **70** (522 mg, 0.617 mmol) was dissolved in DCM (2 mL) in an ice bath and TFA (2 mL) was added. The reaction was allowed to stir for 2 h before the solvents were removed under reduced pressure and the reaction mixture purified by flash silica chromatography (2% MeOH/DCM to 10% MeOH/DCM). The solvent was removed under reduced pressure to leave **72** as a colourless oil (480 mg, quant).

¹H NMR* (400 MHz): δ 7.72 (m, 2H, Fmoc Ar *H*); 7.56 (m, 2H, Fmoc Ar *H*); 7.45–7.25 (m, 6H, Fmoc Ar *H* & Ar *H*); 7.05–6.70 (m, 2H, Ar *H*); 5.99 (bs 1H, NH); 5.80–3.10 (broad multiplets unresolved, 16H, *H*-1, *H*-2, *H*-3, *H*-4, *H*-5, *H*-6, *H*-6', *H*-a, *H*-b, *H*-c, *H*-d, *H*-e); 2.15–1.85 (m, 12H, 4 x Ac CH₃).

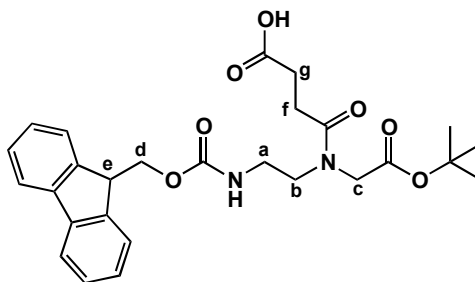
¹³C NMR* (100 MHz): δ 172.9, 170.7, 170.3, 169.5, 169.4, 157.3, 143.9, 143.6, 141.4, 130.3, 129.0, 128.8, 128.0, 127.3, 125.4, 125.1, 125.0, 120.2, 117.0, 116.8, 98.6, 72.7, 72.0, 71.0, 68.3, 68.2, 67.6, 67.2, 61.9, 61.7, 51.0, 47.2, 47.0, 40.0, 39.3, 20.7.

MS (ESI, +ve) m/z 791.0 $[M+H]^+$, m/z 812.8 $[M+Na]^+$.

HRMS (ESI, +ve) m/z 813.2478 $[M+Na]^+$, $C_{40}H_{42}N_2NaO_{15}$ required m/z 813.2477.
 m/z 791.2647 $[M+H]^+$, $C_{40}H_{43}N_2O_{15}$ required m/z 791.2658.

*Rotamers present.

3.3.5. Synthesis of Succinic Anhydride-Linked Glycosylated Monomers

Synthesis of 74

PNA monomer backbone **51** (52 mg, 0.13 mmol) and succinic anhydride (13 mg, 0.13 mmol) were combined in DCM (5 mL) and stirred at room temperature for 2 h. More succinic anhydride (8 mg) was added and the reaction mixture allowed to stir at room temperature for a further 4.5 h. The reaction mixture was then washed with water (2 x 20 mL), dried (MgSO_4) and the solvent removed under reduced pressure to leave **74** as a colourless oil (65 mg, quant.).

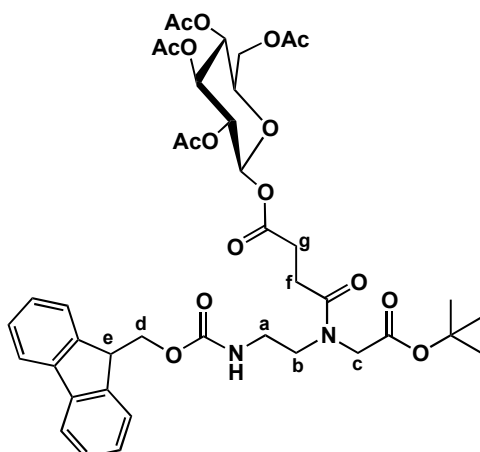
^1H NMR* (400 MHz): δ 7.74 (d, 2H, J = 7.2 Hz, Fmoc Ar H); 7.58 (d, 2H, J = 7.6 Hz, Fmoc Ar H); 7.38 (t, 2H, J = 7.6 Hz, Fmoc Ar H); 7.30 (t, 2H, J = 7.4 Hz, Fmoc Ar H); 5.98 & 5.60 (bs, 1H, NH); 4.37 & 4.33 (d, 2H, J = 7.2 Hz Fmoc CH_2); 4.20 (m, 1H, Fmoc CH); 3.97 & 3.91 (s, 2H, H -c); 3.52 (m, 2H, H -a or H -b); 3.36 (m, 2H, H -a or H -b); 2.65-2.41 (m, 4H, H -f & H -g); 1.47 (s, 9H, $t\text{Bu}$ CH_3).

^{13}C NMR* (100 MHz): δ 176.3, 173.3, 172.5, 156.7, 143.9, 141.3, 127.7, 127.1, 125.1, 120.0, 82.4, 66.8, 50.2, 49.6, 47.4, 39.6, 29.5, 28.3, 27.9.

MS (ESI, +ve) m/z 497.25 $[\text{M}+\text{H}]^+$, m/z 519.16 $[\text{M}+\text{Na}]^+$.

HRMS (ESI, +ve) m/z 519.2100 $[\text{M}+\text{Na}]^+$, $\text{C}_{27}\text{H}_{32}\text{N}_2\text{NaO}_7$ required m/z 519.2102. m/z 497.2284 $[\text{M}+\text{H}]^+$, $\text{C}_{27}\text{H}_{33}\text{N}_2\text{O}_7$ required m/z 497.2282.

* Rotamers present.

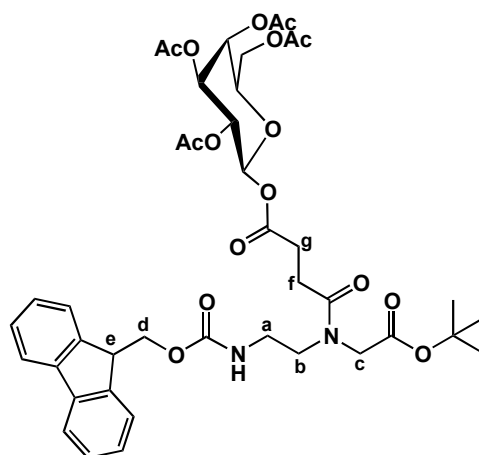
Synthesis of 75

Tetraacetyl bromo- α -D-glucopyranose (693 mg, 1.69 mmol), acid **74** (558 mg, 1.12 mmol), silver carbonate (6.55 g, 23.7 mmol) and sodium sulfate (12.9 g, 90.9 mmol) were stirred in DCM (40 mL) at reflux, under an atmosphere of nitrogen in the dark for 44 h. The reaction mixture was then filtered through celite, the organic layer washed with sat. NaHCO_3 (aq) (1 x 20 mL) and water (1 x 20 mL), dried (MgSO_4) and the solvent removed under reduced pressure. Purification by reverse phase HPLC on a C_{18} Delta Pak column with a flow rate of 5 mL/minute. The solvent system used was 40:60 H_2O :ACN for 5 minutes then a gradual change to 20:80 H_2O :ACN for 10 minutes followed by a gradual change to 10:90 H_2O :ACN over 5 minutes and held for 10 minutes. The desired product eluted at approximately 35 minutes as detected at 256 nm absorbance. The solvent was removed under reduced pressure to leave **75** as a colourless oil (347 mg, 40%).

^1H NMR (400 MHz): δ 7.76 (d, 2H, $J = 7.6$ Hz, Fmoc Ar H); 7.60 (d, 2H, $J = 7.6$ Hz, Fmoc Ar H); 7.40 (t, 2H, $J = 7.2$ Hz, Fmoc Ar H); 7.31 (t, 2H, $J = 7.2$ Hz, Fmoc Ar H); 5.95 & 5.48 (m, 1H, NH); 5.71 & 5.70 (d, 1H, $J = 8.0$ Hz H -1); 5.24 – 5.05 (m, 3H, H -2, H -3 & H -4); 4.36 (m, 2H, Fmoc CH_2); 4.21 (m, 2H, Fmoc CH & H -6); 4.09 – 3.84 (m, 3H, H -c & H -6'); 3.74 (m, 1H, H -5); 3.51 (m, 2H, H -a or H -b); 3.37 (m, 2H, H -a or H -b); 2.79 – 2.43 (m, 4H, H -f & H -g); 2.06 & 2.03 (s, 3H, Ac CH_3); 2.04 (s, 3H, Ac CH_3); 2.02 (s, 3H, Ac CH_3); 2.00 (s, 3H, Ac CH_3); 1.49 & 1.47 (s, 9H, $t\text{Bu}$ CH_3).

^{13}C NMR (100 MHz): δ 171.7, 171.3, 171.2, 170.9, 170.4, 169.9, 169.7, 157.0, 144.4, 141.7, 128.1, 127.4, 125.4, 120.4, 92.1, 73.1, 70.5, 68.2, 67.3, 61.8, 50.1, 49.6, 47.6, 39.8, 29.5, 28.4, 27.7, 21.0, 21.0, 21.0.

MS (ESI, +ve) m/z 827.09 $[\text{M}+\text{H}]^+$, 849.05 $[\text{M}+\text{Na}]^+$, 865.17 $[\text{M}+\text{K}]^+$.

Synthesis of 76

Tetraacetyl bromo- α -D-galactopyranose (131 mg, 0.318 mmol), **74** (132 mg, 0.265 mmol), silver carbonate (1.55 g, 5.62 mmol) and sodium sulfate (3.06 g, 21.5 mmol) were stirred in DCM (20 mL) at reflux, under an atmosphere of nitrogen in the dark for 24 h. The reaction mixture was then filtered through celite, the organic layer washed with sat. NaHCO_3 (aq) (1 x 20 mL) and water (1 x 20 mL), dried (MgSO_4) and the solvent removed under reduced pressure. Purification by reverse phase HPLC on a C_{18} Delta Pak column with a flow rate of 5 mL/minute. The solvent system used was 40:60 H_2O :ACN for 5 minutes then a gradual change to 20:80 H_2O :ACN for 10 minutes followed by a gradual change to 10:90 H_2O :ACN over 5 minutes and held for 10 minutes. The desired product eluted at approximately 34 and 37 minutes as detected at 256 nm absorbance. The solvent was removed under reduced pressure to leave **76** as a colourless oil (combined 57.6 mg, 27%).

 β -anomer

^1H NMR* (400 MHz): δ 7.76 (d, 2H, $J = 7.6$ Hz, Fmoc Ar H); 7.60 (d, 2H, $J = 7.6$ Hz, Fmoc Ar H); 7.40 (t, 2H, $J = 7.6$ Hz, Fmoc Ar H); 7.31 (t, 2H, $J = 7.4$ Hz, Fmoc Ar H); 6.00 & 5.48 (m, 1H, NH); 5.68 (dd, 1H, $J = 8.4, 2.0$ Hz, $H-1$); 5.39 (d, 1H, $J = 2.8$ Hz, $H-4$); 5.32 (t, 1H, $J = 9.4$ Hz, $H-2$); 5.04 (m, 1H, $H-3$); 4.38 (m, 2H, Fmoc CH_2); 4.22 (m, 1H, Fmoc CH); 4.09 (m, 2H, $H-6$ & $H-6'$); 3.93 (m, 3H, $H-5$ & $H-c$); 3.55 (m, 2H, $H-a$ or $H-b$); 3.37 (m, 2H, $H-a$ or $H-b$); 2.75 – 2.41 (m, 4H, $H-f$ & $H-g$); 2.14 & 2.12 (s, 3H, Ac CH_3); 2.06 & 2.06 (s, 3H, Ac CH_3); 2.01 & 2.00 (s, 3H, Ac CH_3); 1.98 (s, 3H, Ac CH_3); 1.49 & 1.47 (s, 9H, $t\text{Bu}$ CH_3).

¹³C NMR* (100 MHz): δ 171.8, 171.3, 171.3, 170.6, 170.4, 170.3, 170.1, 157.0, 144.2, 141.7, 128.1, 127.4, 125.4, 120.3, 92.7, 92.5, 83.5, 72.0, 71.1, 68.0, 67.3, 67.1, 61.3, 50.2, 49.6, 47.6, 39.8, 29.5, 28.4, 27.8, 21.0, 20.9, 20.9, 20.8.

MS (ESI, +ve) m/z 827.09 [M+H]⁺, 849.17 [M+Na]⁺, 865.17 [M+K]⁺.

α -anomer

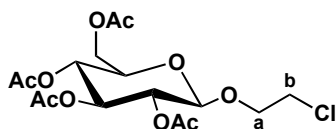
¹H NMR* (400 MHz): δ 7.76 (m, 2H, Fmoc Ar *H*); 7.60 (m, 2H, Fmoc Ar *H*); 7.40 (m, 2H, Fmoc Ar *H*); 7.31 (t, 2H, $J = 7.6$ Hz, Fmoc Ar *H*); 6.39 & 6.37 (d, 1H, $J = 3.2$ Hz, *H*-1); 5.92 (m, 1H, NH); 5.51 (m, 1H, *H*-4); 5.34 (m, 2H, *H*-2 & *H*-3); 4.36 (m, 3H, Fmoc CH₂ & *H*-5); 4.22 (m, 1H, Fmoc CH); 4.14 - 4.03 (m, 2H, *H*-6 & *H*-6'); 4.00 (s, 1H, *H*-c); 3.91 (s, 1H, *H*-c); 3.54 (m, 2H, *H*-a or *H*-b); 3.38 (m, 2H, *H*-a or *H*-b); 2.70 (m, 4H, *H*-f & *H*-g); 2.14 (s, 3H, Ac CH₃); 2.03 (s, 3H, Ac CH₃); 2.01 (s, 3H, Ac CH₃); 2.00 (s, 3H, Ac CH₃); 1.49 & 1.47 (s, 9H, *t*Bu CH₃).

MS (ESI, +ve) m/z 849.17 [M+Na]⁺, 865.17 [M+K]⁺.

*Rotamers present.

3.3.6. Synthesis of Alkyl-Linked Glycosylated Monomers

Synthesis of 79



Tetraacetyl bromo- α -D-glucopyranose (50 mg, 0.12 mmol) and 2-chloroethanol (0.25 mL, 3.1 mmol) were dissolved in DCM (15 mL) over 4Å molecular sieves and stirred at room temperature under an atmosphere of nitrogen for 1 h. The reaction flask was then put in an ice bath (~ 2 °C) and silver triflate (68 mg, 0.27 mmol) was added and left to stir for 12 h. The reaction mixture was then filtered (celite) and the organic layer washed with sat. NaHCO₃ (aq) (1 x 20 mL) and water (1 x 20 mL), dried (MgSO₄) and the solvent removed under reduced pressure. Purification by flash chromatography (5% methanol/DCM; $R_f = 0.55$). The solvent was removed under reduced pressure to leave **79** as a white solid (22.4 mg, 45%).

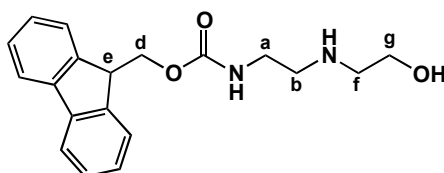
¹H NMR (300 MHz): δ 5.22 (t, 1H, *J* = 9.5 Hz, *H*-3); 5.08 (t, 1H, *J* = 9.6 Hz, *H*-4); 5.01 (dd, 1H, *J* = 9.6, 7.9 Hz, *H*-2); 4.57 (d, 1H, *J* = 7.9 Hz, *H*-1); 4.25 (dd, 1H, *J* = 12.3, 4.8 Hz, *H*-6); 4.14 (dd, 1H, *J* = 12.4, 2.3 Hz, *H*-6'); 4.05 (m, 1H, *H*-a); 3.75 (m, 2H, *H*-5 & *H*-a); 3.63 (m, 2H, *H*-b); 2.08 (s, 3H, Ac CH₃); 2.05 (s, 3H, Ac CH₃); 2.02 (s, 3H, Ac CH₃); 2.00 (s, 3H, Ac CH₃).

¹³C NMR (75 MHz): δ 170.7, 170.3, 169.5, 169.5, 101.2, 72.8, 72.1, 71.2, 70.0, 68.5, 62.0, 42.5, 20.8, 20.7, 20.7, 20.7.

MS (ESI, +ve) m/z 433.2 [M+Na]⁺ (³⁵Cl), 435.2 [M+Na]⁺ (³⁷Cl).

X-ray crystallography: For data, see Appendix.

Synthesis of 82



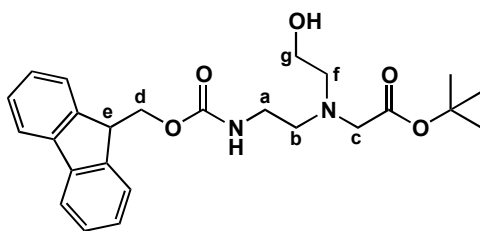
2-(2-aminoethylamino)-ethanol (0.90 mL, 8.9 mmol) and DIEA (1.6 mL, 8.9 mmol) were stirred in DCM (25 mL) at room temperature. Fmoc succinimide (3.0 g, 8.9 mmol) was dissolved in DCM (25 mL) and slowly added to the reaction mixture *via* a dropping funnel. After stirring for 15 h, the reaction mixture was filtered and the white solid product collected and washed with cold DCM and left to dry, leaving **82** as a white solid (2.90 g, quant.).

¹H NMR (400 MHz): δ 7.76 (d, 2H, *J* = 7.6 Hz, Fmoc Ar *H*); 7.59 (dd, 2H, *J* = 7.6, 0.8 Hz, Fmoc Ar *H*); 7.39 (t, 2H, *J* = 7.6 Hz, Fmoc Ar *H*); 7.31 (td, 2H, *J* = 7.6, 1.2 Hz, Fmoc Ar *H*); 5.27(bs, 1H, NH); 4.43 (d, 2H, *J* = 6.4 Hz, *H*-d); 4.21 (t, 1H, *J* = 6.4 Hz, *H*-e); 3.63 (t, 2H, *J* = 5.2 Hz, *H*-g); 3.28 (d, 2H, *J* = 5.2 Hz, *H*-a); 2.75 (m, 4H, *H*-b & *H*-f); 2.01 (bs, 2H, NH & OH).

¹³C NMR (100 MHz): δ 157.0, 144.3, 141.7, 128.0, 127.3, 125.3, 120.3, 66.9, 61.4, 51.2, 49.1, 47.7, 41.2.

MS (ESI, +ve) m/z 327.2 [M+H]⁺.

MP: 111-113 °C

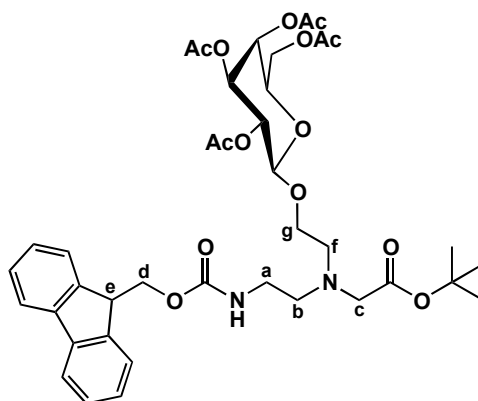
Synthesis of 78

Amine **82** (200 mg, 0.613 mmol) and potassium carbonate (845 mg, 0.61 mmol) were stirred in DCM (10 mL) in an icebath. *t*-Butyl bromoacetate (0.14 mL, 0.92 mmol) dissolved in DCM (3 mL) was slowly added to the reaction mixture. The solution was allowed to stir at room temperature for 28 h, after which time it was washed with HCl (1M, 10 mL) and then brine (10 mL). The DCM layer was dried (MgSO₄) and removed under reduced pressure to leave a mixture of the product, by-product and excess *t*-butyl bromoacetate. Purification by column chromatography (DCM to 5% MeOH/DCM). The solvent was removed under reduced pressure from the appropriate fraction to leave **78** as a colourless oil (188 mg, 70%).

¹H NMR (400 MHz): δ 7.75 (d, 2H, J = 7.6 Hz, Fmoc Ar H); 7.62 (d, 2H, J = 7.6 Hz, Fmoc Ar H); 7.39 (t, 2H, J = 7.4 Hz, Fmoc Ar H); 7.31 (td, 2H, J = 7.4, 1.2 Hz, Fmoc Ar H); 5.69 (bs, 1H, NH); 4.37 (d, 2H, J = 7.2 Hz, H -d); 4.23 (t, 1H, J = 7.2 Hz, H -e); 3.57 (t, 2H, J = 5.2 Hz, H -g); 3.30 (m, 4H, H -a & H -c); 2.80 (m, 4H, H -b & H -f); 1.48 (s, 9H, *t*Bu CH₃); 1.46 (s, 1H, OH).

¹³C NMR (100 MHz): δ 172.3, 157.0, 144.4, 141.6, 128.0, 127.4, 125.5, 120.2, 82.2, 67.1, 60.0, 57.8, 56.9, 55.4, 47.6, 39.8, 28.4.

MS (ESI, +ve) m/z 441.2 [M+H]⁺.

Synthesis of 83

Alcohol **78** (55 mg, 0.12 mmol) was combined with tetraacetyl bromo- α -D-galactopyranose (76 mg, 0.19 mmol); silver carbonate (725 mg, 2.63 mmol) and sodium sulfate (1.43 g, 10.0 mmol) in dichloromethane (20 mL) with molecular sieves under an atmosphere of nitrogen at room temperature in the dark. One day later a further 100 mg of acetobromogalactose was added to the reaction. A further four days after that, the reaction mixture was filtered through celite, washed with water (20 mL), dried (MgSO_4) and the solvent removed under reduced pressure. Purification by reverse phase HPLC on a C₁₈ Delta Pak column with a flow rate of 5 mL/minute. The solvent system used was 20:80 H₂O:ACN for 10 minutes then a gradual change to 15:85 H₂O:ACN for 10 minutes. The conjugated products eluted at 34 and 37 minutes as detected at 220 nm absorbance. The solvent was removed under reduced pressure to leave **83** as a colourless clear oil (total product 14 mg, 15%).

 β -anomer

¹H NMR (400 MHz): δ 7.76 (d, 2H, $J = 7.6$ Hz, Fmoc Ar H); 7.65 (d, 2H, $J = 7.2$ Hz, Fmoc Ar H); 7.39 (t, 2H, $J = 7.6$ Hz, Fmoc Ar H); 7.31 (t, 2H, $J = 7.2$ Hz, Fmoc Ar H); 5.88 (bs, 1H, NH); 5.37 (d, 1H, $J = 2.8$ Hz, H -4); 5.20 (dd, 1H, $J = 10.4, 8.0$ Hz, H -2); 5.00 (dd, 1H, $J = 10.4, 3.6$ Hz, H -3); 4.48 (d, 1H, $J = 7.6$ Hz, H -1); 4.39 (d, 2H, $J = 6.8$ Hz, H -d); 4.24 (t, 1H, $J = 7.2$ Hz, H -e); 4.13 (m, 2H, H -6 & H -6'); 3.89 (m, 2H, H -g & H -5); 3.62 (m, 1H, H -g); 3.31 (s, 2H, H -c); 3.23 (bs, 2H, H -a); 2.88 (m, 2H, H -f); 2.77 (bs, 2H, H -b); 2.12 (s, 3H, Ac CH_3); 2.05 (s, 3H, Ac CH_3); 2.02 (s, 3H, Ac CH_3); 1.98 (s, 3H, Ac CH_3); 1.48 (s, 9H, $t\text{Bu}$ CH_3).

¹³C NMR (100 MHz): δ 170.4, 169.8, 144.5, 141.7, 128.0, 127.4, 125.6, 120.3, 101.4, 81.7, 71.3, 71.1, 69.2, 68.6, 67.4, 66.9, 61.6, 57.0, 54.4, 53.7, 47.7, 39.6, 28.5, 21.1, 21.0, 21.0, 20.9.

MS (ESI, +ve) *m/z* 771.1 [M+H]⁺.

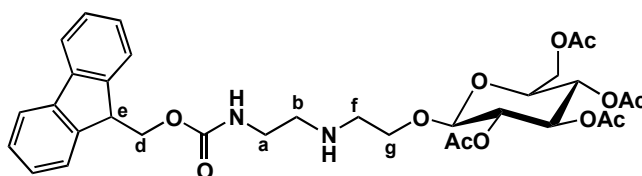
α-anomer

¹H NMR (400 MHz): δ 7.76 (d, 2H, *J* = 7.6 Hz, Fmoc Ar *H*); 7.64 (d, 2H, *J* = 7.2 Hz, Fmoc Ar *H*); 7.39 (t, 2H, *J* = 7.4 Hz, Fmoc Ar *H*); 7.31 (td, 2H, *J* = 7.4, 1.2 Hz, Fmoc Ar *H*); 5.91 (bs, 1H, NH); 5.83 (d, 1H, *J* = 4.8 Hz, *H*-1); 5.41 (t, 1H, *J* = 2.8 Hz, *H*-4); 5.04 (q, 1H, *J* = 3.2 Hz, *H*-3); 4.37 – 4.24 (m, 5H, *H*-2, *H*-5, *H*-d & *H*-e); 4.12 (m, 2H, *H*-6 & *H*-6'); 3.58 (bs, 2H, *H*-g); 3.34 (s, 2H, *H*-c); 3.25 (m, 2H, *H*-a); 2.86 (m, 2H, *H*-f); 2.80 (m, 2H, *H*-b); 2.05 (s, 3H, Ac CH₃); 2.03 (s, 3H, Ac CH₃); 2.01 (s, 3H, Ac CH₃); 1.68 (s, 3H, Ac CH₃), 1.48 (s, 9H, *t*Bu CH₃).

¹³C NMR (100 MHz): δ 170.8, 170.4, 170.1, 157.0, 144.5, 141.6, 128.0, 127.4, 125.6, 120.3, 97.9, 81.6, 74.3, 71.8, 69.5, 67.1, 66.3, 61.7, 61.7, 56.9, 54.3, 53.5, 47.7, 39.5, 28.5, 24.4, 21.0, 21.0, 20.8.

MS (ESI, +ve) *m/z* 771.1 [M+H]⁺.

Synthesis of 84



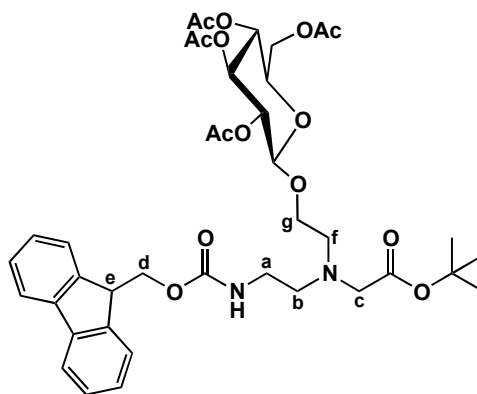
Amine **82** (200 mg, 0.613 mmol) was added to dry DCM (50 mL). The solution was then heated and sonicated to encourage the solid material to dissolve. β-D-glucopyranose pentaacetate (359 mg, 0.920 mmol) and BF₃·Et₂O (0.209 mL, 1.84 mmol) were then added and the reaction was allowed to stir at room temperature under a nitrogen atmosphere for 4 d. The reaction was quenched and washed with water (3 x 20 mL), dried (MgSO₄) and the solvent removed under reduced pressure. Purification by flash silica chromatography (DCM to 5% MeOH/DCM to 10% MeOH/DCM to acetone). The solvent was removed from the appropriate fractions under reduced pressure to leave **84** as a colourless oil (79 mg, 20%). Note: Product must be refrigerated to avoid decomposition.

¹H NMR (400 MHz): δ 7.75 (d, 2H, J = 7.6 Hz, Fmoc Ar H); 7.61 (d, 2H, J = 7.2 Hz, Fmoc Ar H); 7.39 (t, 2H, J = 7.6 Hz, Fmoc Ar H); 7.30 (t, 2H, J = 7.4 Hz, Fmoc Ar H); 5.59 (bs, 1H, NH); 5.20 (t, 1H, J = 9.5 Hz, H -3); 5.06 (t, 1H, J = 9.7 Hz, H -4); 4.96 (dd, 1H, J = 9.5, 8.02 Hz, H -2); 4.52 (d, 1H, J = 8.0 Hz, H -1); 4.39 (d, 2H, J = 6.6 Hz, H -d); 4.21 (m, 3H, H -e, H -6 & H -6'); 3.95 (m, 1H, H -g); 3.74 (m, 2H, H -5 & H -g); 3.30 (m, 2H, H -a); 2.85 (m, 4H, H -b & H -f); 2.05 (s, 3H, Ac CH_3); 2.03 (s, 3H, Ac CH_3); 2.01 (s, 3H, Ac CH_3); 1.98 (s, 3H, Ac CH_3).

¹³C NMR (100 MHz): δ 170.9, 170.3, 169.7, 169.5, 156.9, 144.1, 141.5, 127.8, 127.2, 125.2, 120.1, 101.1, 72.8, 72.2, 71.5, 69.2, 68.4, 66.8, 61.9, 48.9, 48.7, 47.4, 40.5, 20.9, 20.9, 20.7.

MS (ESI, +ve) m/z 657.0 $[M+H]^+$.

Synthesis of **80**



Method 1

Glycosylated amine **84** (79 mg, 0.12 mmol) was combined with potassium carbonate (33 mg, 0.24 mmol) and *t*-butyl bromoacetate (34 μ L, 0.24 mmol) in ACN (5 mL). The reaction was allowed to stir at room temperature under a nitrogen atmosphere for two d. The product was then extracted into DCM (10 mL), washed with water (2 x 10 mL), dried ($MgSO_4$) and the solvent removed under reduced pressure. Purification by silica column chromatography (DCM to ethyl acetate) and the solvent was removed from the appropriate fractions to leave **80** as a colourless oil (57 mg, 62%).

¹H NMR (400 MHz): δ 7.76 (d, 2H, J = 7.2 Hz, Fmoc Ar H); 7.65 (d, 2H, J = 7.6 Hz, Fmoc Ar H); 7.39 (t, 2H, J = 7.4 Hz, Fmoc Ar H); 7.31 (t, 2H, J = 7.4 Hz, Fmoc Ar H); 5.90 (bs, 1H, NH); 5.20 (t, 1H, J = 9.2 Hz, H -3); 5.07 (dd, 1H, J = 10.0, 9.2 Hz, H -4);

4.90 (dd, 1H, $J = 9.6, 8.0$ Hz, $H-2$); 4.53 (d, 1H $J = 8.0$ Hz, $H-1$); 4.39 (m, 2H, $H-d$); 4.24 (m, 2H, $H-e$ & $H-6$); 4.11 (m, 1H, $H-6'$); 3.86 (m, 1H, $H-g$); 3.64 (m, 2H, $H-g$ & $H-5$); 3.31 (s, 2H, $H-c$); 3.21 (m, 2H, $H-a$); 2.87 (m, 2H, $H-f$); 2.76 (t, 2H, $J = 5.2$ Hz, $H-b$); 2.06 (s, 3H, Ac CH_3); 2.03 (s, 3H, Ac CH_3); 2.00 (s, 3H, Ac CH_3); 1.98 (s, 3H, Ac CH_3); 1.48 (s, 9H, tBu CH_3).

MS (ESI, +ve) m/z 771.2 $[M+H]^+$.

Method 2

Alcohol **78** (35 mg, 0.08 mmol) was combined with tetraacetyl bromo- α -D-glucopyranose (130.5 mg, 0.32 mmol), silver carbonate (438 mg, 1.59 mmol) and sodium sulfate (865 mg, 6.09 mmol) in DCM (5 mL) with molecular sieves under an atmosphere of nitrogen at room temperature in the dark. After three days, the reaction mixture was filtered through celite, washed with water (1 x 20 mL), dried ($MgSO_4$) and the solvent removed under reduced pressure. Purification by reverse phase HPLC on a C_{18} Delta Pak column with a flow rate of 5 mL/minute. The solvent system used was 20:80 H_2O :ACN for 10 minutes then a gradual change to 15:85 H_2O :ACN for 10 minutes. The conjugated products eluted at 35 and 36 minutes as detected at 220 nm absorbance. The solvent was removed under reduced pressure to leave **80** as a colourless clear oil. (3.4 mg, 9%).

β -anomer

See characterisation data above

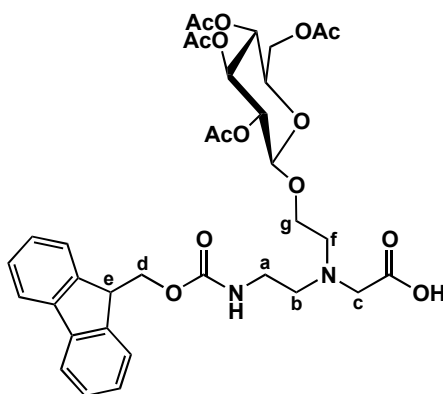
α -anomer

1H NMR (400 MHz): δ 7.75 (d, 2H, $J = 7.6$ Hz, Fmoc Ar H); 7.65 (d, 2H, $J = 7.6$ Hz, Fmoc Ar H); 7.39 (t, 2H, $J = 7.6$ Hz, Fmoc Ar H); 7.31 (td, 2H, $J = 7.6, 1.2$ Hz, Fmoc Ar H); 5.89 (bs, 1H, NH); 5.74 (d, 1H, $J = 5.2$ Hz, $H-1$); 5.18 (t, 1H, $J = 2.8$ Hz, $H-3$) 4.88 (dd, 1H, $J = 9.6, 2.8$ Hz, $H-4$); 4.36 (m, 3H, $H-2$ & $H-d$); 4.25 (t, 1H, $J = 7.2$ Hz, $H-e$); 4.18 (m, 2H, $H-6$ & $H-6'$); 3.93 (m, 1H, $H-5$); 3.55 (m, 2H, $H-g$); 3.32 (s, 2H, $H-c$); 3.24 (m, 2H, $H-a$); 2.84 (m, 2H, $H-f$); 2.79 (m, 2H, $H-b$); 2.07 (s, 3H, Ac CH_3); 2.06 (s, 3H, Ac CH_3); 2.04 (s, 3H, Ac CH_3); 1.73 (s, 3H, Ac CH_3); 1.47 (s, 9H, tBu CH_3).

^{13}C NMR (100 MHz): δ 171.5, 171.0, 170.0, 170.0, 157.0, 144.5, 141.6, 128.0, 127.4, 125.6, 120.3, 97.4, 81.6, 73.7, 70.6, 68.5, 67.5, 67.1, 63.4, 62.6, 57.0, 54.5, 54.153.8, 47.7, 39.6, 28.5, 21.4, 21.1, 21.1, 21.0.

MS (ESI, +ve) m/z 771.2 $[\text{M}+\text{H}]^+$.

Synthesis of **85**



t-Butyl ester **80** (57 mg, 0.07 mmol) was dissolved in DCM (1 mL) in an ice bath and TFA (1 mL) was added. The reaction was allowed to stir for 24 h before the solvents were removed under reduced pressure and the reaction mixture purified by flash silica chromatography (5% MeOH/DCM to 10% MeOH/DCM) to leave **85** as a colourless oil (32.7 mg, 62%).

^1H NMR (400 MHz): δ 7.75 (d, 2H, J = 7.6 Hz, Fmoc Ar H); 7.60 (d, 2H, J = 7.2 Hz, Fmoc Ar H); 7.38 (t, 2H, J = 7.4 Hz, Fmoc Ar H); 7.30 (t, J = 7.4 Hz, Fmoc Ar H); 5.17 (t, 1H, J = 9.6 Hz, H -3); 5.06 (t, 1H, J = 9.6 Hz, H -4); 4.95 (dd, 1H, J = 9.6, 8.0 Hz, H -2); 4.42 (m, 3H, H -1 & H -d); 4.21 (t, 1H, J = 6.4 Hz, H -e); 4.11 (m, 2H, H -6 & H -6'); 3.85 (m, 1H, H -g); 3.63 (m, 1H, H -g); 3.56 (m, 1H, H -5); 3.42 (s, 2H, H -c); 3.35 (bs, 2H, H -a); 2.99 (bs, 2H, H -f); 2.91 (bs, 2H, H -b); 2.03 (s, 3H, Ac CH_3); 2.03 (s, 3H, Ac CH_3); 2.01 (s, 3H, Ac CH_3); 1.97 (s, 3H, Ac CH_3).

^{13}C NMR (100 MHz): δ 171.6, 170.8, 170.3, 170.0, 169.5, 157.2, 144.1, 141.4, 127.9, 127.3, 125.3, 120.1, 100.4, 72.7, 72.1, 71.3, 68.4, 66.7, 66.3, 61.7, 57.7, 55.3, 54.2, 47.4, 38.5, 20.8, 20.7, 20.7.

MS (ESI, +ve) m/z 715.0 $[\text{M}+\text{H}]^+$.

HRMS (ESI, +ve) m/z 715.2723 $[\text{M}+\text{H}]^+$, $\text{C}_{35}\text{H}_{43}\text{N}_2\text{O}_{14}$ required 715.2709.

3.4. References

1. Nielsen, P. E., Egholm, M., Berg, R. H. and Buchardt, O., *Science*, **1991**, 254, 1497-1500.
2. Hanvey, J. C., Pepper, N. J., Bisi, J. E., Thomson, S. A., Cadilla, R., Josey, J. A., Ricca, D. J., Hassman, C. F., Bonham, M. A., Au, K. G., Carter, S. G., Bruckestein, D. A., Boyd, A. L., Nobel, S. A. and Babiss, L. E., *Science*, **1992**, 258, 1481-1485.
3. Demidov, V., Potaman, V., Frank-Kamenetski, M., Egholm, M., Buchard, O., Sonnichsen, S. and Nielsen, P., *Biochem. Pharmacol.*, **1994**, 48, 1310-1313.
4. Nielsen, P. E., Egholm, M. and Buchardt, O., *Bioconjugate Chem.*, **1994**, 5, 3-7.
5. Nielsen, P. E., *Chem. Biodiversity*, **2010**, 7, 786-804.
6. Pensato, S., Saviano, M. and Romanelli, A., *Expert Opin. Biol. Ther.*, **2007**, 7, 1219-1232.
7. Howarth, N. M., *Lett. Org. Chem.*, **2006**, 3, 495-503.
8. Basu, S. and Wickstrom, E., *Bioconjugate Chem.*, **1997**, 8, 481-488.
9. Ljungstrom, T., Knudsen, H. and Nielsen, P. E., *Bioconjugate Chem.*, **1999**, 10, 965-972.
10. Hudson, R. H. E., Viirre, R. D., Liu, Y. H., Wojciechowski, F. and Dambeniek, A. K., *Pure Appl. Chem.*, **2004**, 76, 1591-1598.
11. Manicardi, A., Accetta, A., Tedeschi, T., Sforza, S., Marchelli, R. and Corrandini, R., *Artif. DNA PNA XNA*, **2012**, 3, 56-62.
12. Jordan, S., Schwemler, C., Kosch, W., Kretschmer, A., Schwenner, E., Stropp, U. and Mielke, B., *Bioorg. Med. Chem. Lett.*, **1997**, 7, 681-686.
13. Englund, E. A. and Appella, D. H., *Org. Lett.*, **2005**, 7, 3465-3467.
14. Rossi, S., Calabretta, A., Tedeschi, T., Sforza, S., Arcioni, S., Baldoni, L., Corradini, R. and Marchelli, R., *Artif. DNA PNA XNA*, **2012**, 3, 63-72.
15. Joshi, T., Gasser, G., Martin, L. L. and Spiccia, L., *R. Soc. Chem. Adv.*, **2012**, 2, 4703-4712.
16. Shibata, N., Das, B. K., Honjo, H. and Takeuchi, Y., *J. Chem. Soc., Perkin Trans. 1*, **2001**, 1, 1605-1611.
17. Gasser, G., Belousoff, M., Bond, A. and Spiccia, L., *J. Org. Chem.*, **2006**, 71, 7565 - 7573.
18. Gasser, G., Husken, N., Koster, S. D. and Metzler-Nolte, N., *Chem. Commun.*, **2008**, 3675-3677.

19. Gasser, G., Brosch, O., Ewers, A., Weyhermuller, T. and Metzler-Nolte, N., *Dalton Trans.*, **2009**, 4310-4317.
20. Joshi, T., Barbante, G. J., Francis, P. S., Hogan, C. F., Bond, A. M., Gasser, G. and Spiccia, L., *Inorg. Chem.*, **2012**, 51, 3302-3315.
21. Challa, H. and Woski, S., *Tetrahedron Lett.*, **1999**, 40, 419-422.
22. Wakelin, L. P. G., *Med. Res. Rev.*, **1986**, 6, 275-340.
23. MacKinnon, K. F., Qualley, D. F. and Woski, S. A., *Tetrahedron Lett.*, **2007**, 48, 8074-8077.
24. Wojciechowski, F. and Hudson, R. H. E., *Curr. Top. Med. Chem.*, **2001**, 7, 667-679.
25. Ray, A. and Norden, B., *FASEB J.*, **2000**, 14, 1041-1060.
26. Wittung, P., Kajanus, J., Edwards, K., Nielsen, P. E., Norden, B. and Malmstrom, B. G., *FEBS Lett.*, **1995**, 365, 27-29.
27. Nielsen, P. E., *Q. Rev. Biophys.*, **2005**, 38, 345-350.
28. Gildea, B. D., Casey, S., MacNeill, J., Perry-O'Keefe, H., Sorensen, D. and Coull, J. M., *Tetrahedron Lett.*, **1998**, 39, 7255-7258.
29. Koppelhus, U. and Nielsen, P. E., *Adv. Drug Delivery Rev.*, **2003**, 55, 267-280.
30. Koppelhus, U., Awasthi, S. K., Zachar, V., Holst, H. U., Ebbesen, P. and Nielsen, P. E., *Antisense Nucleic Acid Drug Dev.*, **2002**, 12, 51-63.
31. Cheah, I. K., PhD Thesis *Antisense peptide nucleic acids as therapeutic agents for the treatment of neurodegeneration*, Monash University, **2006**.
32. Uhlmann, E., Will, D. W., Breipohl, G., Langner, D. and Rytte, A., *Angew. Chem., Int. Ed. Engl.*, **1996**, 35, 2632-2635.
33. Hamzavi, R., Dolle, F., Tavitian, B., Dahl, O. and Nielsen, P. E., *Bioconjugate Chem.*, **2003**, 14, 941-954.
34. Hamzavi, R., Meyer, C. and Metzler-Nolte, N., *Org. Biomol. Chem.*, **2005**, 4, 3648-3651.
35. Elofsson, M., Walse, B. and Kihlberg, J., *Tetrahedron Lett.*, **1991**, 32, 7613-7616.
36. Salvador, L. A., Elofsson, M. and Kihlberg, J., *Tetrahedron*, **1995**, 51, 5643-5656.
37. Daniell, K., Stewart, M., Madsen, E., Le, M., Handl, H., Brooks, N., Kiakos, K., Hartley, J. A. and Lee, M., *Bioorg. Med. Chem. Lett.*, **2005**, 15, 177-180.

38. Sagan, S., Milcent, T., Ponsinet, R., Convert, O., Tasseau, O., Chassaing, G., Lavielle, S. and Lequin, O., *Eur. J. Biochem.*, **2003**, *270*, 939-949.
39. Thomson, S. A., Josey, J. A., Cadilla, R., Gaul, M. D., Hassman, C. F., Luzzio, M. J., Pipe, A. J., Reed, K. L., Ricca, D. J., Wiethe, R. W., and Noble, S. A., *Tetrahedron*, **1995**, *51*, 6179-6194.
40. Dean, D. A., *Adv. Drug Delivery Rev.*, **2000**, *44*, 81-95.
41. Dragulescu-Andrasi, A., Rapireddy, S., Frezza, B. M., Gayathri, C., Gil, R. R. and Ly, D. H., *J. Am. Chem. Soc.*, **2006**, *128*, 10258-10267.
42. Kaduk, C., Wenschuh, H., Beyermann, M., Forner, K., Carpino, L. and Bienert, M., *Lett. Pept. Sci.*, **1995**, *2*, 285 - 288.
43. Stafforst, T. and Diederichsen, U., *Eur. J. Org. Chem.*, **2007**, 681-688.
44. Kappes, T. and Waldmann, H., *Carbohydr. Res.*, **1998**, *305*, 341-349.

CHAPTER 4

CONJUGATED PEPTIDE NUCLEIC ACIDS AND THEIR PHYSICAL MEASUREMENTS

Chapter 4. Conjugated Peptide Nucleic Acids and their Physical Measurements

4.1. Introduction

This chapter consists of three smaller sections, connected by a common theme of peptide nucleic acids (PNAs). The first section details the synthesis, purification and characterisation of the library of PNA molecules synthesised in this project. Glycosylated building blocks **38**, **39** (modified amino acids), **71** and **72** (rigid-linked glycosylated monomers) were attached to the ends of PNA sequences on the solid phase. A total of 34 different PNA sequences were synthesised, including 32 different glycosylated PNA conjugates.

The behaviour of the glycosylated PNA oligomers on a supported lipid bilayer was investigated using a Quartz Crystal Microbalance (QCM). In a form of biomimicry, a synthetic lipid bilayer was constructed on a gold-coated sensor so that the cell penetrating abilities of the glycosylated PNA oligomers could be compared with those of unconjugated PNA oligomers.

The stability of the glycosylated oligomers with complementary DNA oligomers is vital for their therapeutic success. The heat released upon binding is indicative of the binding strength of two molecules: a highly exothermic response will result from a favourable interaction. Two techniques have been used in the present project to measure the thermodynamic properties of a selection of conjugated PNA sequences in the presence of their complementary DNA sequence: PNA/DNA thermal melt using a UV-visible spectrophotometer, and isothermal titration calorimetry (ITC). The aim of these thermodynamic analyses is to compare PNA sequences with and without conjugated sugar molecules, and investigate whether or not the conjugation of glycosylated building blocks decreases the binding ability of the SOD1 PNA sequence to its complementary DNA sequence.

4.2. Peptide Nucleic Acid Preparation

4.2.1. Peptide Nucleic Acid Synthesis

PNA synthesis is carried out using the Expedite 8909 Nucleic Acid Synthesis System. The resin on which the PNA sequence was built was a poly(ethylene glycol)/polystyrene (PEG-PS) resin, with a 9-fluorenylmethoxycarbonyl (Fmoc) protected amine. The standard monomers used in the synthesis contain an achiral *N*-(2-aminoethyl)glycine backbone with an Fmoc-protected amine and a free carboxylic acid. The backbone is bound to one of four bases: A, C, G or T as shown in Figure 4.1. Those bases with exocyclic amines (A, C and G) were protected with benzhydryloxycarbonyl (Bhoc), which is an acid labile group, complementary to the base sensitive Fmoc group.¹

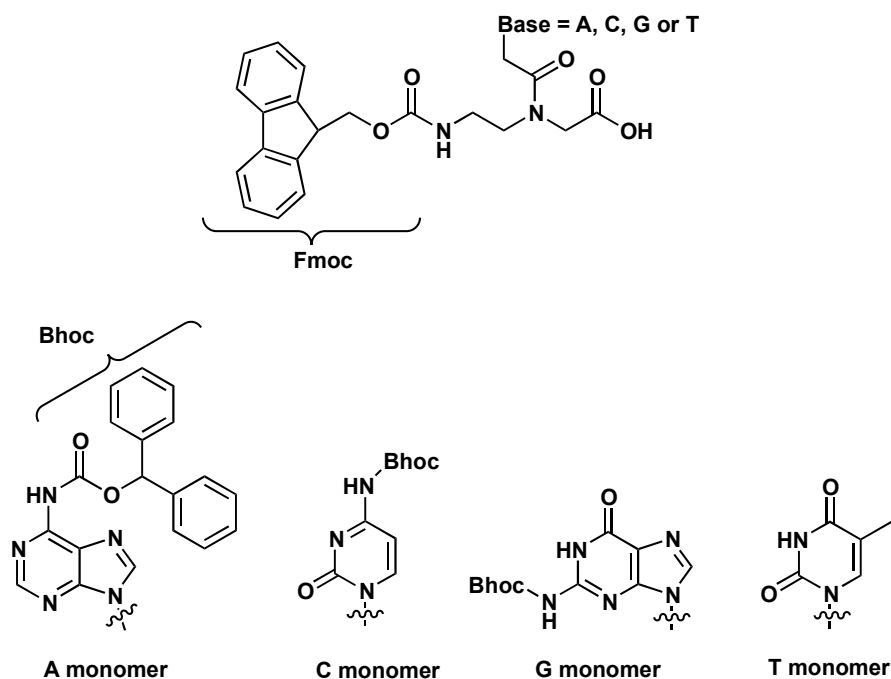


Figure 4.1: Nucleobases on the PNA backbone form the PNA monomers.

The same automated protocol was used for PNA synthesis, regardless of sequence identity (Figure 4.2). The first step of the synthetic cycle involves the removal of the Fmoc protecting group using 20% *v/v* piperidine in DMF. Next, the monomer to be added to the sequence is activated using HATU mixed with lutidine and DIEA in DMF, and is coupled to the free amine on the resin. HATU activates the carboxylic acid of the next monomer in the sequence so it is more electrophilic for attack by the free amine of the growing sequence. Lutidine and DIEA are bulky

bases and so cannot act as nucleophiles towards the carbonyl groups of the new monomers.

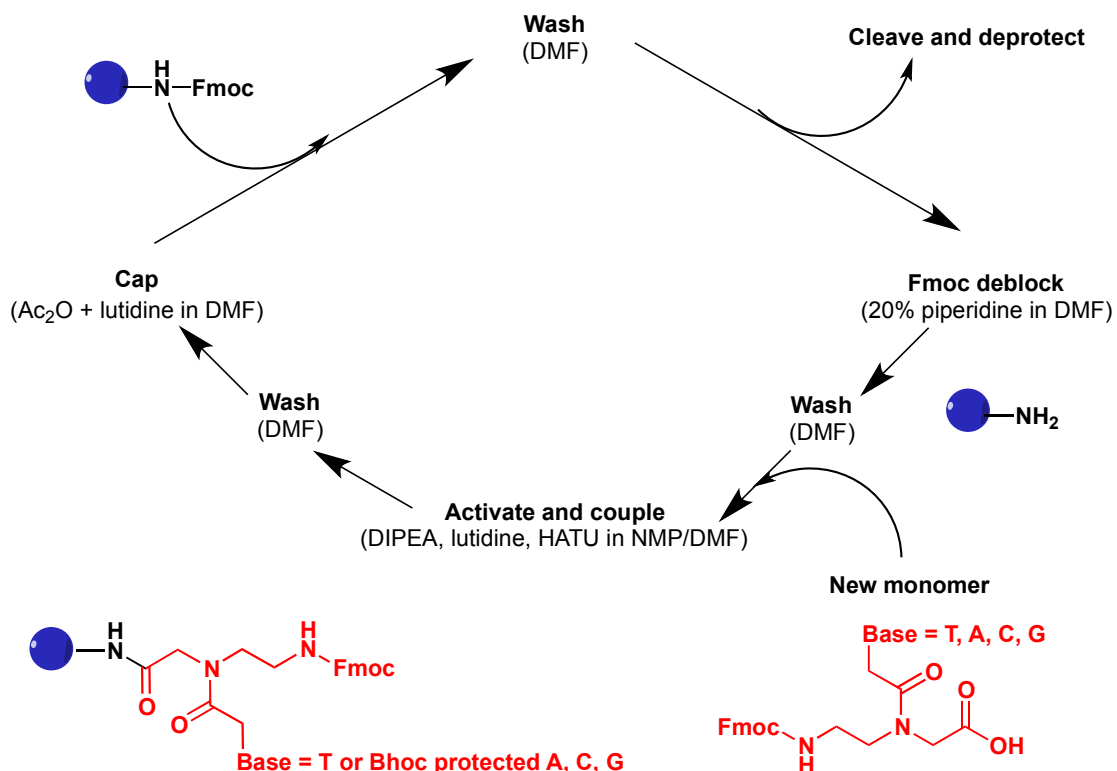


Figure 4.2: PNA synthetic cycle.

Capping involves the acetylation of any uncoupled oligomers on the resin using acetic anhydride (lutidine, DMF). As a result of this step, any unreacted free amines generated through the cycle will be acetylated ensuring that the next monomer cannot be coupled to them under the reaction conditions. Consequently, this step reduces the formation of sequences containing deletions and so this step also aids in the purification process. A DMF wash separates each step to remove any reagents or uncoupled monomers from the resin which may complicate the next step in the cycle. Once the desired sequence of monomers has been coupled, a final deblock is performed twice, to remove the Fmoc protecting group of the last monomer, thus affording a free amine.

To demonstrate the flexibility and ease by which the glycosylated building blocks BBGluOH, BBGalOH, SerGluOH, SerGalOH, BBGluAc, BBGalAc, SerGluAc and SerGalAc were incorporated into PNA sequences, each was dissolved in NMP (0.2 M) and inserted into the PNA synthesiser, in the same manner as standard PNA monomers. The desired sequence was programmed in the synthesiser. A typical

program sees that a PNA sequence is synthesised in the *C'* to the *N'* direction and, to ensure the greatest number of amine sites on the resin are in use, the first coupling event is repeated (double coupled). In light of this, the glycosylated building block was, in most cases, programmed to be coupled last at the *N'* terminus, to maximise its use.

Once synthesis of the desired sequence was complete, the resin was removed from the synthesiser so that post-synthesis modifications could be performed. When required, a mixture of triethylamine, methanol and water (5:3:2)² was used to cleave the acetate protecting groups from the sugar moieties. The resin-bound PNA sequence was left in this solution overnight before the solution was decanted off and the resin rinsed with methanol.

To cleave the PNA from the resin, a 4:1 TFA:*m*-cresol mix was used. This solution also cleaved the Bhoc protecting group from the nucleobases. *m*-Cresol acts as a radical scavenger to remove the highly reactive carbonium cations from Bhoc that would otherwise attach onto a free amine of another or the same base. The resin was left to sit in a TFA - *m*-cresol solution for one hour before the solution (now containing the PNA product) was removed from the resin and the process repeated with fresh cleavage solution. Cold diethyl ether was added to the combined cleavage solutions to precipitate the PNA product typically as a white solid. Centrifugation was used to compact the white solid into a pellet from which the diethyl ether could be evaporated. Figure 4.3 shows the general steps involved in this final phase of PNA preparation.

CHAPTER 4 - CONJUGATED PEPTIDE NUCLEIC ACIDS

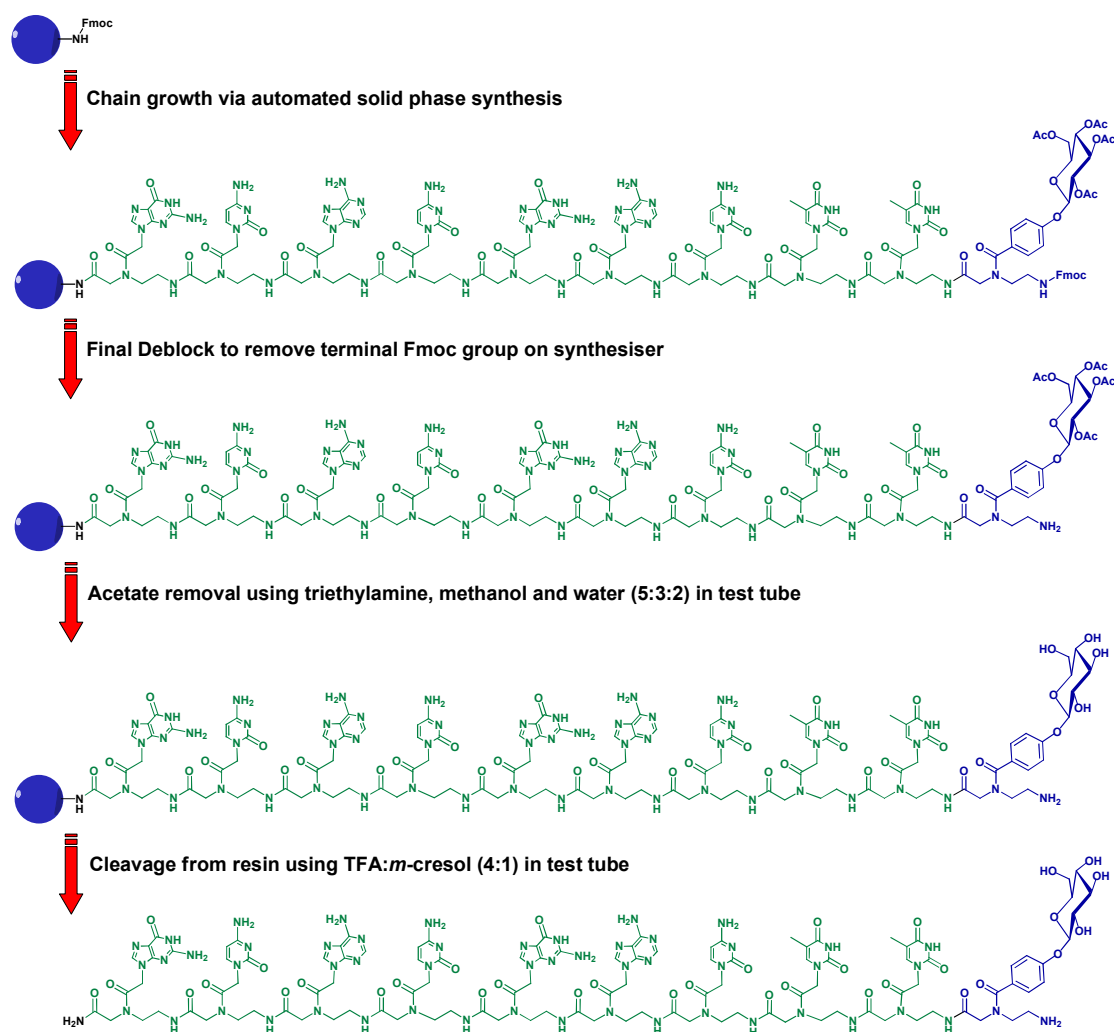


Figure 4.3: Steps of PNA preparation.

The rationale behind the creation of the PNA-sugar conjugate library in this project was two-fold. Firstly, from a synthetic point of view, we wanted to demonstrate that amino acid conjugates could be incorporated into PNA chemistry and that the sugar-substituted PNA backbone monomers would not be sterically hindered, or be sterically hindering, in PNA synthesis. For use in therapeutics and diagnostics, PNA sequence integrity is essential therefore the SOD1 and GluR3 sequences could not be interrupted. In light of this design restriction, the glycosylated building blocks were only added to the sequences at the terminal positions. The PNA sequence grows from the *C'* end to the *N'* end in the synthesiser. In order to maximise the number of positions on the resin from which a sequence can grow, the first monomer of the sequence is 'double coupled'. In order to use minimal amounts of the precious glycosylated building blocks, these monomers were usually added to the *N'* terminus of the sequence. However, some

conjugated sequences were synthesised with the glycosylated building block starting the chain as the first monomer at the C' terminus in order to demonstrate the synthetic flexibility of these building blocks. Their flexibility was also demonstrated by the synthesis of sequences that contain sequential glycosylated building blocks.

The second consideration behind the rationale of the PNA conjugate library was the potential to investigate the effect of numerous variations in sequence design on the binding ability of the conjugated PNA sequences.

Table 4.1 lists the components of the synthesised PNA sequences. This table is to be read in conjunction with Table 4.2, which lists each PNA sequence that has been synthesised for this project. In Table 4.2, each sequence has been given a name based on the number, type, and location of glycosylated building blocks incorporated in the sequence, as well as the sequence itself. Table 4.1 explains the terminology used. This naming system will be used for the remainder of this chapter and has been used in preference to a standard compound numbering system, so that the PNA sequence of interest, and its particular variables, can be easily identified by its name only. This system is considered important for the present chapter because this chapter is concerned with the comparison of different variables within the PNA sequence.

Table 4.1: PNA sequence component index

Sequence Name Component	Number in Sequence	Meaning	Sequence Name Component	Number in Sequence	Meaning
SOD1	-	PNA sequence N' – TTCAGCACG – C'	GluR3	-	PNA sequence N' – TCCGTGAGAAATG – C'
SerGluAc	1		SerGalAc	2	
SerGluOH	3		SerGalOH	4	
BBGluAc	5		BBGalAc	6	
BBGluOH	7		BBGalOH	8	
S	S	Spacer 	2	-	The preceding component is coupled twice

Table 4.2: Summary of synthesised PNA sequences

Compound	Sequence (<i>N'</i> – <i>C'</i>)	Calculated Molecular Weight (Da)	Observed Molecular Weight (Da) [^]	HPLC Solvent System*	Elution Time (min)
SOD1	TTC AGC ACG	2435.0	2435.0	1, 8 ^a	12
GluR3	TCC GTG AGA ATG	3307.3	3307.8	1, 8 ^a	11
SOD SerGluAc	1S TTC AGC ACG	2997.2	2998.3	1	37
SOD SerGalAc	2S TTC AGC ACG	2997.2	2997.1	1	36
SOD SerGluOH	3S TTC AGC ACG	2829.1	2829.3	2	27
SOD SerGalOH	4S TTC AGC ACG	2829.1	2829.3	2	27
SOD SerGlu2Ac	11S TTC AGC ACG	3414.3	3415.0	1	37
SOD SerGal2Ac	22S TTC AGC ACG	3414.3	3414.7	1	37
SOD SerGlu2OH	33S TTC AGC ACG	3078.2	3078.4	7	37
SOD SerGal2OH	44S TTC AGC ACG	3078.2	3078.2	7	37
SOD BBGluAc	5 TTC AGC ACG	2985.2	2985.3	7, 8 ^b	14
SOD BBGalAc	6 TTC AGC ACG	2985.2	2985.7	7	57
SOD BBGluOH	7 TTC AGC ACG	2817.1	2817.0	7	36
SOD BBGalOH	8 TTC AGC ACG	2817.1	2817.2	7	36
SOD BBGlu2Ac	55 TTC AGC ACG	3535.3	3536.1	7, 8 ^b	15
SOD BBGal2Ac	66 TTC AGC ACG	3535.3	3535.8	7, 8 ^b	15

CHAPTER 4 - CONJUGATED PEPTIDE NUCLEIC ACIDS

SOD BBGlu2OH	77 TTC AGC ACG	3199.3	3199.6	7	37
SOD BBGal2OH	88 TTC AGC ACG	3199.3	3199.8	7	36
GluR3 SerGluAc	1S TCC GTG AGA ATG	3869.5	3869.2	1	37
GluR3 SerGalAc	2S TCC GTG AGA ATG	3869.5	3870.9	1	37
GluR3 SerGluOH	3S TCC GTG AGA ATG	3701.5	3702.5	6	33
GluR3 SerGalOH	4S TCC GTG AGA ATG	3701.5	3701.1	6	34
GluR3 SerGlu2Ac	11S TCC GTG AGA ATG	4286.6	4287.3	1	37
GluR3 SerGal2Ac	22S TCC GTG AGA ATG	4286.6	4287.6	1	36
GluR3 SerGlu2OH	33S TCC GTG AGA ATG	3950.6	3951.2	7	37
GluR3 SerGal2OH	44S TCC GTG AGA ATG	3950.6	3951.2	7	37
SerGal-S-SOD-S-SerGal	4S TTC AGC ACG S4	3223.3	3223.6	7	39
BBGal-SOD-BBGal	8 TTC AGC ACG 8	3199.3	3200.6	7	37
BBGal-S-SOD-S-BBGal	8S TTC AGC ACG S8	3489.4	3490.1	7	40
SOD-S-BBGal	8S TTC AGC ACG	2962.2	2962.3	7	38
SOD-S-BBGlu	7S TTC AGC ACG	2962.2	2962.7	7	38
BBGlu-SOD-BBGlu	7 TTC AGC ACG 7	3199.3	3200.0	7	38
BBGlu-S-SOD	TTC AGC ACG S7	2962.2	2962.6	7	40
BBGluAc-SOD-BBGluAc	5 TTC AGC ACG 5	3535.3	3536.3	7	56

^a This represents crude purification by conditions 1 followed by repurification using conditions 8.

^b This represents crude purification by conditions 7 followed by repurification using condition 8.

[^] Calculated from multiply charged peaks in ESI mass spectrum.

***HPLC solvent systems**

A = H₂O with 0.1% TFA, B = ACN with 0.1% TFA, rate = 2 mL min⁻¹

- 1.** Time 0–5 min 1% B, time 25 min 10% B, time 30 min 100% B.
- 2.** Time 0-10 min 5% B, time 40 min 60% B, time 45 min 5% B.
- 3.** Time 0-5 min 1% B, time 25-35 min 10% B, time 45 min 100% B.
- 4.** Time 0-10 min 5% B, time 30-40 min 35% B, time 45-50 min 100% B, time 51 min 5% B.
- 5.** Time 0-10 min 5% B, time 40-45 min 30% B, time 50-55 min 100% B, time 56 min 5% B.
- 6.** Time 0-10 min 5% B, time 40 min 30% B, time 45-50 min 100% B, time 51 min 5% B.
- 7.** Time 0-10 min 5% B, time 40-45 min 20% B, time 50-55 min 100% B, time 56 min 5% B.
- 8.** Time 0-1 min 20% B, time 10 min 90% B.

4.2.2. Peptide Nucleic Acid Purification

Once ESI mass spectrometry confirmed the presence of the desired product in the crude pellet, preparative reverse phase HPLC was used to purify all PNA sequences. Factors such as number of sugars attached (0, 1 or 2), and whether or not the sugars were acetate protected, influenced the elution time of the sequences. The identity of the sequence (SOD1 or GluR3) did not significantly affect the elution time. The impurities included incomplete capped sequences, uncoupled capped monomers and acetate protected glycosylated sequences when the deprotected glycosylated sequence was desired. Table 4.2 shows each PNA sequence synthesised, the conditions used to purify it, and its elution time.

Generally, conjugates with unprotected sugars eluted much earlier than those with acetylated sugars, as would be expected on a reverse-phase column. For many of the deprotected sugar sequences, peaks were observed in the HPLC run that corresponded to the protected sugar product, indicating that complete acetate cleavage was not always achieved. Optimisation of the acetate cleavage step will be needed in the future.

4.2.3. Peptide Nucleic Acid Characterisation

Characterisation of the purified PNA sequences was achieved by ESI mass spectrometry. A small sample of the HPLC fraction of interest was diluted with methanol before use. Typically, PNA sequences display characteristic multiply charged peaks in ESI mass spectra. The most common signals correlate to the $[M+3H]^3+$, $[M+4H]^4+$ and $[M+5H]^5+$ ions, and occasionally the $[M+2H]^2+$ and $[M+6H]^6+$ ions are observed. For example, in the case of SOD BBGal2OH, a molecular mass of 3199.8 is calculated with observed peaks at m/z 1067.6 $[M+3H]^3+$, 800.9 $[M+4H]^4+$ and 641.0 $[M+5H]^5+$.

ESI mass spectral analysis of HPLC fractions not containing the desired PNA products gave an insight into the PNA synthesis procedure, and possibly the acetate cleavage procedure. For example, in the cases of SOD BBGalOH and SOD BBGluAc, the ESI mass spectra of the 40 minute HPLC fractions revealed the presence of a species in which the sugar moiety (including the *para*-substituted benzene ring) had been cleaved from the backbone. These spectra show peaks at m/z 507.8 $[M+5H]^5+$, 634.7 $[M+4H]^4+$ and 845.7 $[M+3H]^3+$, which correlate to a

molecular mass of 2534.8, or a mass loss of 283 in the case of SOD BBGalOH, and a mass loss of 453 in the case of SOD BBGluAc. As these mass losses are a result of the cleavage of the amide bond from the backbone, it is likely that this deletion occurred during the overnight cleavage of the sugar acetate groups in triethylamine, methanol and water.

In each case, the desired HPLC fraction was freeze-dried overnight to leave a flocculent white solid. The PNA sequences were stored in individual sealed glass vials at -20 °C until they were required for the various techniques discussed in the following sections.

4.3. Quartz Crystal Microbalance: Analysis of PNA – Membrane Interaction

4.3.1. Overview

The Quartz Crystal Microbalance (QCM) is a convenient, highly sensitive analytical technique that is used to accurately detect nanogram/cm² (in solution) and picogram/cm² (in vacuum) changes in mass. The technique is based around a piezoelectric quartz crystal, in the form of a thin gold-coated, 1 cm diameter, silicon oxide sensor.³ When an oscillating voltage is applied to the sensor, an acoustic wave spreads in the direction perpendicular to the surface of the sensor.³ The frequency of this wave is dampened due to the mass deposited on the sensor's surface.³ There is a number of review articles that describe this instrument and technique in great detail.³⁻⁶

A selection of traditional applications of the QCM include:

- gas phase detection of moisture and hydrocarbons using a coating on the sensor's surface to be selective for specific volatiles;⁷
- immunosensors in which the quartz sensors are pre-coated with an antigen so that the antibody activity of an antibody solution can be determined by the thickness of the antibody layer formed on the crystal.⁸ Examples of analytes that have been detected include HIV antibodies, pesticides, bacteria, viruses, human IgM and α -fetoprotein;³
- electrochemical applications including metal deposition monitoring, examination of redox processes and mass transfer, electron transfer, rate of film growth and determination of the mass of an electrodeposited film;⁹ and

- DNA biosensors in which the crystal surface was initially modified with a polymer, a nucleic acid was covalently attached to the polymer (and the quartz surface) and hybridisation of a target sequence from a test solution was detected as a mass increase (frequency decrease).¹⁰ Peptide nucleic acids attached to the QCM surface have been used,¹¹⁻¹⁴ which in most cases, compared to their DNA counterparts, create more sensitive and selective biosensors.

The progression of the QCM technique for applications in the liquid phase led to its use in examining the viscoelastic properties of materials deposited on its surface. The quartz crystal microbalance with dissipation monitoring (QCM-D) is able to give both quantitative masses and structural information in liquid. The temporal change in frequency reflects the mass change on the surface of the crystal, while the change in dissipation indicates the nature (rigid or viscoelastic) of the sensor surface. If the sensor surface is viscoelastic or viscous, its internal friction will dissipate more energy¹⁵ and produce an increased dissipation factor.

To exploit this use, supported lipid bilayers (SLB) can be attached to the quartz sensor's surface to provide an environment in which pseudo-physiological interactions can be monitored.¹⁶ An advantage of QCM over other surface-sensitive techniques is that it inherently monitors mass and structural changes as a result of a particular biomolecule/molecule in real-time, with no need for additional labelling.¹⁶

A SLB can be anchored to the sensor's surface by first appropriately modifying the surface, which is achieved by the formation of a self-assembled monolayer. Using a gold coated sensor (silver and oxide surfaces have also been used in various surface-sensitive techniques¹⁶), a sulfur-containing molecule is often used to modify the surface due to its strong and unrivalled affinity for gold. Examples of sulfur-containing molecules include thiolipids, alkylthiols, and terminal derivitised alkylthiols with carboxylate, ammonium or hydroxyl groups. The nature of the sulfur-containing compound will determine the properties of the self-assembled surface: alkyl chains are hydrophobic, hydroxyls are hydrophilic and carboxylate and ammonium groups create a charged, hydrophilic surface, as a function of the pH of the surrounding solution.¹⁶

Martin and co-workers have used the QCM with attached SLB to examine various peptide-membrane interactions.¹⁷⁻²⁴ Further to this, and more relevant, is the pioneering work for the analysis of PNA-metal conjugate derivatives and their interactions with SLB using QCM-D.²⁵ The present project aims to use the QCM technique in a similar way: to investigate and compare the interactions of glycosylated PNA sequences with a supported lipid bilayer.

Our intention is to use a supported lipid bilayer (SLB) on a gold-coated quartz crystal microbalance to mimic a plasma cell membrane, or perhaps a BBB, in order to determine if a conjugated sugar molecule (both acetylated and deacetylated) influences the interaction of the PNA sequence with the lipid bilayer. The aim of PNA glycosylation was to increase PNA transport to the CNS by means of carrier-mediated transport utilising the GLUT-1 transporter. As an isolated GLUT-1 transporter protein was not acquired for this project, the use of QCM can be seen as a preliminary assessment of the effect a conjugated sugar has on the interaction of a PNA sequence with a lipid bilayer. Owing to its simple experimental set-up and relatively quick experimental run time, QCM is a very efficient technique from which much *in vitro* data can be obtained.

One point of interest is whether or not a conjugated sugar alters the behaviour of the PNA sequence to interact with the lipid bilayer, or remain on its surface. Information regarding the depth, or extent of interaction can be inferred by the difference in change of frequency and dissipation of the various harmonics of the resonating quartz crystal, or the overtone effects.²¹ Figure 4.4 shows the depth of interaction of each of the harmonics in the SLB. The penetration depth of each harmonic is inversely proportional to its frequency.^{15,23}

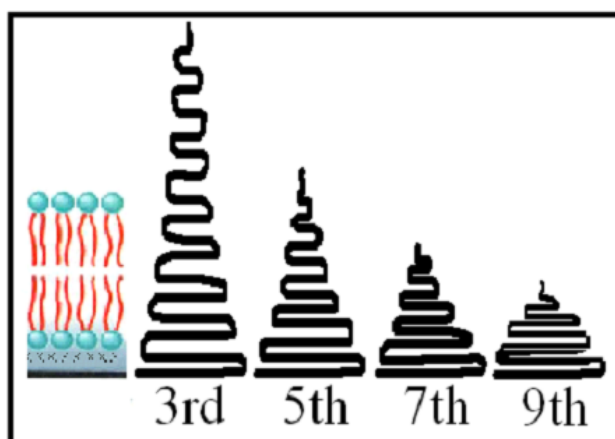


Figure 4.4: Schematic representation of the depth of penetration of the 3rd, 5th, 7th and 9th harmonics of the fundamental frequency compared to the height of a SLB. Comparison of the changes in frequency and dissipation in the different harmonics provides 3D information of mass change over the entire sensor surface.

The information contained across these different harmonics is very important when investigating the interaction of biomolecules with a SLB. As the 3rd harmonic probes at the surface of the lipid bilayer, the 5th and 7th harmonics probe within the lipid bilayer and the 9th harmonic probes near the sensor surface and therefore near the underside of the lipid bilayer, the extent of an interaction with the lipid bilayer can be inferred. For example, if all harmonics were affected equally, it is reasonable to infer that the test compound had transversed the lipid bilayer. If on the other hand, for example, only the 3rd harmonic displayed a change in frequency (and dissipation), it could reasonably be inferred that the test compound had only interacted with the surface of the lipid bilayer.

4.3.2. Procedure

4.3.2.1. Lipid Preparation

The lipid composition for the present QCM experiments was 80% v/v 1,2-dimyristoyl-sn-glycero-3-phosphocholine (PC) and 20% v/v cholesterol. These proportions are designed to mimic a biological cell membrane. Each lipid preparation was made up into 5 mM chloroform solutions so that 1 mL cholesterol solution and 250 μ L PC solution could be added to each test tube in the batch. The chloroform was evaporated under a stream of nitrogen while the test tube was slowly rotated to promote an even lipid film formed on the surface of the test tube.

This is an important factor in the success of the formation of a lipid bilayer on the quartz sensor. The tubes were then placed *in vacuo* to ensure that all the solvent was removed, then stored in the freezer until required.

4.3.2.2. Quartz Crystal Microbalance Preparation

The AT-cut quartz chips used as the sensor crystals, were polished, gold-coated and only ever handled with round-tipped tweezers at the edge of the quartz and not the gold surface to avoid scratching the gold surface. These sensors had a fundamental oscillating frequency of *ca.* 5 MHz. The quartz sensors were cleaned in a hydrogen peroxide/ammonia/water solution for 20 minutes at approximately 70 °C. This was to ensure the removal of everything from the surface of the sensor. The sensors were then rinsed with H₂O, followed by isopropanol (in preparation for the next solution) and then surface modified by submersion in a 1 mM 3-mercaptopropionic acid (MPA) solution in isopropanol for approximately 30 minutes. As can be seen from Figure 4.5, MPA has a terminal thiol group and hence can participate in a gold-sulfur interaction, forming a self-assembled monolayer on the sensor's surface (see yellow and red components of Figure 4.5 below).

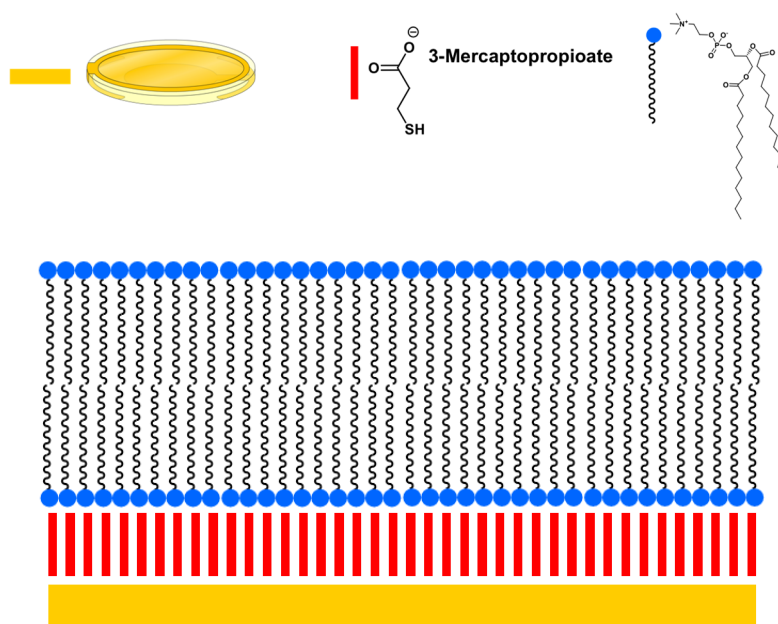


Figure 4.5: Schematic representation of a surface modified quartz sensor used for each QCM experiment.

After this time, excess MPA solution was rinsed from the sensors with isopropanol, and the sensors thoroughly dried under a stream of N₂. The sensors

were then loaded into the QCM-D chambers with their edges not touching the edges of the chambers as contact of the sensor with the edges of the chamber would interfere with the oscillation of the sensor. The system used in the present experiments was an E4 system with flow cells (Q-Sense, Vastra Frolunda, Sweden). Once the instrument was switched on, the temperature was set to 22 °C and H₂O pumped through the cells at maximum speed to flush the system, followed by absolute ethanol, at maximum speed to flush the system of air bubbles, followed by H₂O again to remove the ethanol from the system. The pump was then switched off and the sensors turned on using the QSoft 401 software. The oscillating frequency range for each harmonic of each sensor was checked to ensure each sensor has been placed correctly in the cell. Once everything was established as operational, recording of the experiment in real time commenced.

Figure 4.6 shows a typical time dependence of Δf and ΔD , obtained during the QCM experiment. As the QCM contains four cells, a time dependence plot is produced for each cell and so one experiment will produce four sets of data. The experiment begins with the pumps turned off to establish a frequency and dissipation baseline, however, a small amount of drift can sometimes be observed from the expected origin as a result of the temperature dependence of the viscosity of the water introduced to the system. PBS buffer was introduced at a rate of 300 $\mu\text{L}/\text{minute}$. A bulk shift in the frequency and dissipation values is expected with the change in solvent due to viscosity effects. Once a stable baseline was established, the flow was ceased while the lipid was prepared. One lipid test tube was removed from the freezer, the lipid resuspended in 1 mL PBS buffer and heated to 37 °C in an incubator for at least 30 minutes. The suspension was then subjected to sonication and agitation (vortex) to dislodge the lipid composition from the walls of the test tube to create a cloudy suspension. This step is important for the formation of a lipid bilayer on the sensor surface.

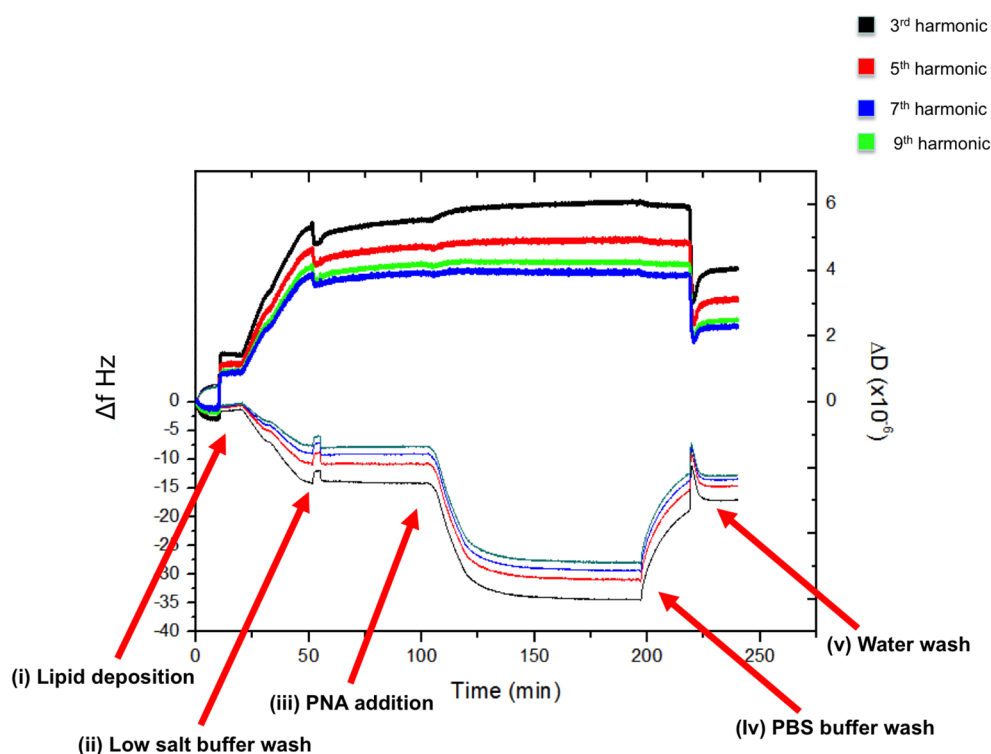


Figure 4.6: Typical real-time QCM run. Thin lines show change in frequency and thick lines show change in dissipation. One QCM experiment employs 4 chambers. The data (above) would be produced by each cell.

The lipid solution was diluted in PBS buffer (0.5 mL lipid in 4.5 mL buffer) and thoroughly mixed to encourage liposomes of even composition before it was introduced to the QCM at 100 $\mu\text{L}/\text{minute}$ (“lipid deposition” in Figure 4.6). The slower flow rate was used to increase the contact time between the positively charged “head” of the PC molecules and the negatively charged MPA of the SAM on the sensors’ surface so that the desired lipid bilayer could form (see Figure 4.5). Lipid flow was continued until the change in frequency from before lipid deposition is at least a minimum value of 15 Hz. The lipid deposition process was repeated if the sensors’ surface was not adequately coated.

The aim is for the liposomes to burst after they reach the quartz sensor and so create a lipid bilayer. If they don’t burst spontaneously, a change in the osmotic pressure of the surrounding solution with a low salt buffer can be used.²⁰ The low salt buffer is introduced to the system at 300 $\mu\text{L}/\text{minute}$ and usually only for 1-2 minutes. The bursting of the liposomes results in the release of the water trapped in the liposomes hence a decrease in mass is observed, and corresponding increase in frequency. If the exposure to the low salt buffer is too extensive, there is a risk

of stripping the quartz sensor completely of lipid. Following this, the PBS buffer is returned to high salt concentration and is used to establish a flat baseline in preparation for the addition of the PNA sequences into the QCM.

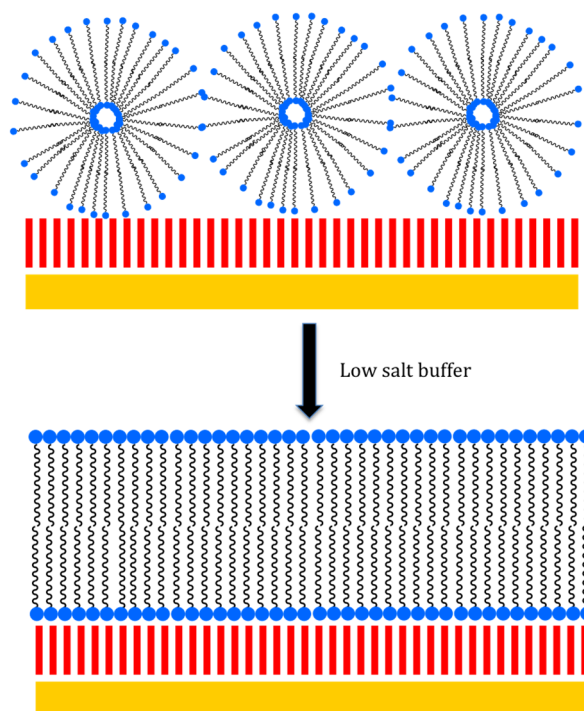


Figure 4.7: Liposomes that initially form on modified quartz sensor are burst with low salt buffer. Trapped water is released and lipids form a bilayer.

As there are 4 chambers in the QCM instrument, 4 different PNA sequences can be examined in each run. Each PNA sample was carefully weighed on a microgram-sensitive balance, transferred to a screw-capped plastic vial and dissolved in a precise amount of PBS buffer to make up a 100 μM stock solution. From this stock solution, 1 ml of either 20 μM or 40 μM solutions were prepared for each experiment. To ensure complete dissolution of the PNA in PBS buffer, both the stock solution and the 1 mL experimental solution were sonicated until a clear solution was observed. The stock solutions were stored in the freezer in between experiments and thawed at room temperature prior to use.

Once a stable frequency baseline had been established with PBS, the flow rate was diminished to 50 μL per minute to ensure maximum contact time of the PNA with the lipid bilayer on the surface of the sensor. Twenty minutes was allowed for each of the 1 mL PNA solutions to be simultaneously pumped through the QCM system. To make certain that no air bubbles entered the system, the pump was

switched off just prior to the PNA solution vials emptying. The system was then left undisturbed for 1 hour, while real-time data was recorded, to allow any further, longer-term interactions of the PNA compounds with the synthetic lipid bilayer to be observed.

To conclude the experiment, the pump was switched back on, flow rate set to 300 μL per minute and PBS flushed through the system. After approximately 10 minutes, water was flushed through the system for a further 10 minutes before data recording was ceased, the pump and QCM instrument switched off and the sensors removed from the chambers.

4.3.2.3. Experimental Design to Investigate Effects of PNA Glycosylation

Only synthesised PNA conjugates were analysed using the QCM. Various conjugated SOD1 sequences were selected for analysis so that the following questions could be investigated:

- Does the presence of a sugar change the interaction?
- Does the type of sugar change the interaction?
- Does the type of linker change the interaction?
- Does more than one sugar change the interaction?
- Do protecting groups on the sugar change the interaction?

The sequences selected to answer these questions were unconjugated SOD1, SOD SerGluOH, SOD SerGalOH, SOD BBGluOH, SOD BBGalOH, SOD (BBGlu)₂ OH, SOD SerGalAc and SOD BBGalAc. Their selection was based on both the features the molecules possessed, e.g. acetate protected sugar or two conjugated sugars, as well as the amount of compound available. Each PNA compound was tested, in triplicate, at each of two concentrations (20 μM and 40 μM).

Table 4.3 shows how the comparison of certain PNA molecules can be used to answer the questions above. This highlights the efficiency of the QCM technique to investigate the effect that different modifications can have on the interactions of compounds with a lipid bilayer.

Table 4.3: Information matrix for QCM experiments

	SOD1	SOD SerGluOH	SOD SerGalOH	SOD BBGluOH	SOD BBGalOH	SOD BBGlu2OH	SOD SerGalAC	SOD BBGalAC
SOD1		Sugar	Sugar	Sugar	Sugar	2 sugars	Protected sugar	Protected sugar
SOD SerGluOH	Sugar		Type of sugar	Type of linker				
SOD SerGalOH	Sugar	Type of sugar			Type of linker		Protected sugar	
SOD BBGluOH	Sugar	Type of linker			Type of sugar	2 sugars		
SOD BBGalOH	Sugar		Type of linker	Type of sugar				Protected sugar
SOD BBGlu2OH	2 sugars			2 sugars				
SOD SerGalAc	Protected sugar		Protected sugar					Type of linker
SOD BBGalAc	Protected sugar				Protected sugar		Type of linker	

4.3.3. Results and Discussion

The main stages of a typical experiment can be seen in Figure 4.6. During the QCM experiments, the relative changes of frequency and energy dissipation of the sensor were recorded simultaneously for the 1st, 3rd, 5th, 7th and 9th harmonics. The information recorded for the 1st harmonic, i.e. fundamental frequency of the crystal, is deliberately not shown as it contains too much noise to be useful.

It is possible to convert these raw data to a plot that exemplifies the change in frequency and dissipation. This plot is called an *f vs d plot* and shows the relationship between negative change in frequency ($-\Delta f$) and change in dissipation (ΔD).²⁶ The data for these plots are taken from the time the PNA enters the QCM system. As shown in Figure 4.8, this plot is a way of analysing the observed change in frequency and dissipation data to interpret the data in terms of the structure of the synthetic lipid bilayer. For example, an increase in negative frequency means more mass has been deposited on the sensor's surface and conversely, a decrease in negative frequency suggests a mass loss from the sensor's surface. An increase in energy dissipation can be aligned with an increase in the viscoelastic nature of the sensor's surface and conversely, a decrease in the measured energy dissipation suggests a shift towards a more ridged sensor surface. In this context, viscoelasticity relates to the disruption of the lipid bilayer.

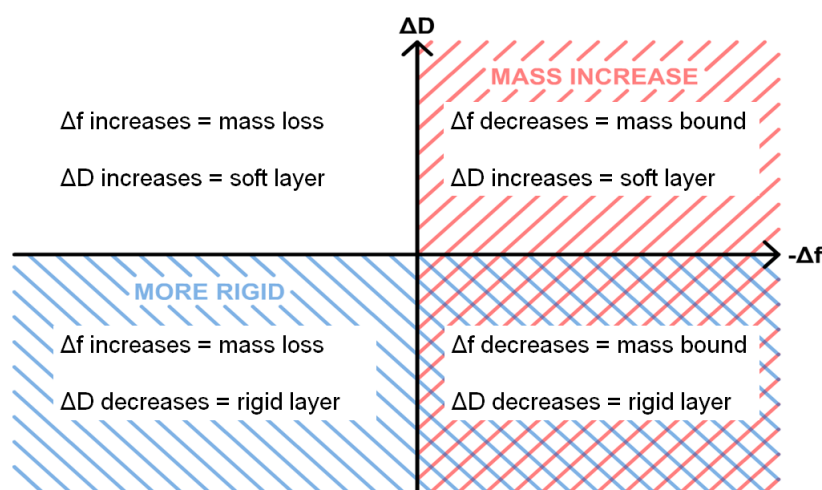


Figure 4.8: Four quadrants of an *f vs d plot* illustrating structural explanations of observed changes in frequency and dissipation.

The *f vs d plots* of all of our tested PNA compounds consistently showed data in the upper right quadrant. We can conclude from this that the influence the PNA

compounds have on the surface of quartz sensor is to increase mass and (slightly) increase the viscoelastic nature of the sensor's surface. We can extrapolate these results to suggest that generally, the tested PNA compounds do interact with the synthetic lipid bilayer. The degree and type of interaction, and whether the presence of various conjugated sugars effects these interactions will be discussed in detail in the next sections.

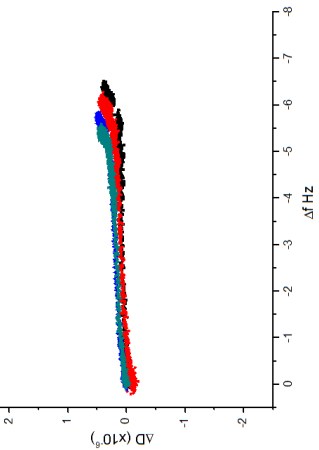
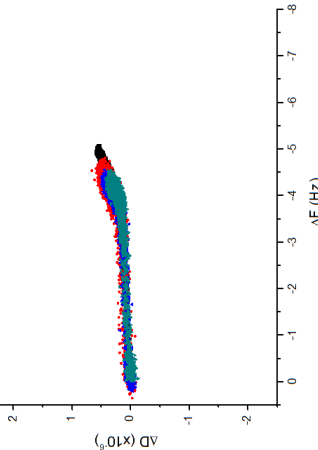
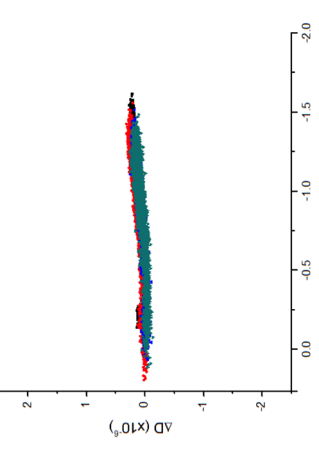
The results indicate that while different concentrations of the same PNA compound causes a difference in the change of frequency observed, generally the change in frequency is not proportional to the change in concentration. Therefore, the discussion in the following sections will not include comparisons of the different concentrations.

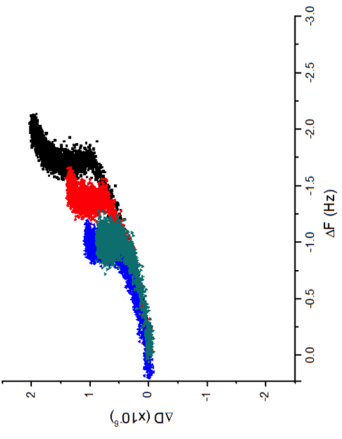
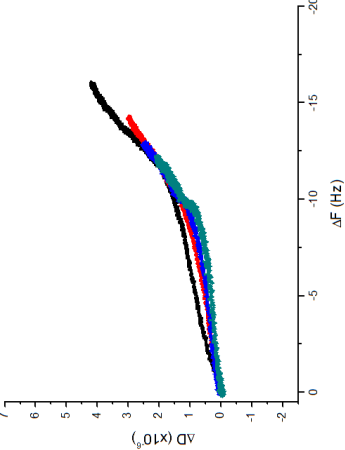
Lipid variability can greatly influence the observed changes in frequency and dissipation. More often than not, the lipid surface is not a perfect bilayer and embedded vesicles and patches of multilayers can result. Hence it is important to note that these experiments are averages across the sensor surface. During the lipid deposition phase of a QCM experiment, care is taken to ensure a bilayer forms and that liposomes are removed (dissipation of 6 or greater and spread harmonics are indicators that structures other than a bilayer are present). However the lipid is a viscoelastic material and the frequency and dissipation indicators do not always provide an accurate reflection of its structure. Furthermore, factors such as the quality and extent of lipid deposition and surface integrity of the quartz sensors can influence the data produced by a QCM run.

Table 4.4 summarises the general trend observed over multiple experiments ($n>3$) for each PNA sequence. Some experiments produced outliers in terms of frequency and dissipation changes. Other than lipid variability and other various influencing factors discussed above, the reasons for the outliers are unknown. The outliers are not discussed in Table 4.4.

Table 4.4: Summary QCM experimental results

	Dissipation	Harmonics	Frequency	Interaction	Example <i>f</i> vs <i>d</i> plot
SOD1	Minimal to no change	Affected equally, except in some cases, the 3 rd harmonic shows greater change in frequency	3-5 Hz negative change	Transmembrane insertion	
SOD SerGluOH	Increases gradually to ~0.5-1	Affected equally, except in some cases the 3 rd harmonic shows greater change in frequency	1-4 Hz negative change	Transmembrane insertion with possibly some PNA on surface, increasing viscoelastic nature of surface	
SOD SerGalOH	Increases gradually to ~0.5	Affected equally, except in some cases 3 rd harmonic shows slightly lower dissipation	2-8 Hz negative change	Transmembrane insertion with possibly some PNA on surface	

SOD BBGluOH	Increases only at maximum frequency to ~0.5	Affected equally	2-7 Hz negative change	Transmembrane insertion	
SOD BBGalOH	Increases only at maximum frequency to ~0.5	Affected equally	2-10 Hz negative change	Transmembrane insertion	
SOD BBGlu2OH	Increases gradually to ~0.5-1	Affected equally	1.5-25 Hz negative change	Transmembrane insertion	

SOD SerGalAc	Increases to ~1-2	Affected equally except 3 rd harmonic shows greater dissipation and frequency	2.5-4.5 Hz negative change	Transmembrane insertion with a small increase in viscoelasticity of surface	
SOD BBGalAc	Increases to ~1-4	Affected equally except 3 rd harmonic shows greater dissipation and frequency	5-15 Hz negative change	Transmembrane insertion with an increase in viscoelasticity of surface	

4.3.3.1. *Does the Presence of a Glycosylated Building Block Influence the Interaction with Membrane?*

A comparison of the typical f vs D plots of each of the glycosylated sequences studied with that of the SOD1 sequence will provide insight into the influence on attached glycosylated building blocks. It appears that the glycosylated PNA sequences generally cause a small increase in dissipation compared to the unglycosylated SOD1 sequence, which has little or no change in dissipation as it binds. This suggests that the presence of a glycosylated building block does not affect the membrane binding of glycosylated oligomers. The change in frequency observed for the unglycosylated SOD1 sequence is similar to that of the glycosylated PNA sequences however it is generally towards the lower end of the range of frequency changes observed for the glycosylated PNA sequences. This suggests that the presence of a glycosylated building block slightly enhances the interaction of the PNA sequence with the lipid, possibly through hydrogen-bonding interactions of the sugar moieties and the lipid molecules.

4.3.3.2. *Does the Type of Sugar Influence the Interaction?*

The two types of sugars used in the glycosylated building blocks were glucose and galactose. According to Table 4.3, the comparison of SOD SerGluOH with SOD SerGalOH and the comparison of SOD BBGluOH with SOD BBGalOH can be used to examine the influence of the type of sugar. Table 4.4 shows that the typical interactions of SOD BBGluOH and SOD BBGalOH with the SLB are almost identical, indicating that the type of sugar does not influence the membrane interaction. This is not surprising because the structures of glucose and galactose only differ by the orientation of one hydroxyl group (OH-4 is equatorial in glucose but axial in galactose) and it is reasonable to assume that such a small structural difference would not influence the interaction of a 9-mer PNA sequence. However, this gave confidence in the QCM method used to distinguish between membrane interactions for this family of PNA sequences.

While the typical interactions of SOD SerGluOH and SOD SerGalOH presented in Table 4.4 are not identical, the differences are within experimental variability and as such are still consistent with the conclusion that the type of sugar does not influence the interaction of the PNA sequence with the synthetic lipid membrane.

4.3.3.3. Does the Type of Linker Influence the Interaction?

The two types of linkers used in the synthesis of the various glycosylated building blocks were L-serine and a 4-hydroxymethylbenzoic acid derivative attached to the secondary amine of the PNA backbone. The serine linker is chiral and smaller than the achiral benzoic acid backbone linker. The comparison of SOD SerGluOH with SOD BBGluOH, the comparison of SOD SerGalOH with SOD BBGalOH and the comparison of SOD SerGalAc with SOD BBGalAc can be used to examine what influence, if any, the type of linker has on the interaction of the PNA with the lipid.

Table 4.4 shows that the typical interactions of SOD SerGluOH and SOD BBGluOH and SOD SerGalOH and SOD BBGalOH are similar. In both sets of cases, a slight increase in dissipation was observed and the ranges of frequency change were almost identical. Generally the harmonics were equally affected however the 3rd harmonic in some cases of SOD SerGluOH shows a slightly greater change in frequency while in some cases of SOD SerGalOH, the 3rd harmonic showed slightly lower dissipation. However as these differences are very minor and did not occur in every experiment, they were attributed to random lipid variability. However it is interesting that these differences were both observed for the serine-linked glycosylated building blocks. Perhaps the smaller size of this linker resulted in the sugar moiety being closer to the PNA sequence than its benzoic acid backbone counterpart. This structural implication of the smaller serine linker may cause changes with the PNA interaction with the surface of the SLB and hence affect the 3rd harmonic to a small extent, more than the other harmonics.

The other set of results that can be compared to examine the influence of the linker is SOD SerGalAc and SOD BBGalAc. The typical results for these PNA conjugates are nearly identical, with the main difference being the change in frequency range for SOD BBGalAc is much larger than that of SOD SerGalAc. It should be noted however that not all frequency changes observed for the various SOD BBGalAc experiments were large and many were in the range of those observed for SOD SerGalAc. Therefore based on this comparison, it appears that the type of linker does not influence the interaction.

Based on three sets of data comparisons, it is reasonable to conclude that the type of linker does not significantly influence the interaction of the PNA sequence

with the lipid and in any event, the interactions observed were consistent with transmembrane insertion.

4.3.3.4. Does More than One Sugar Influence the Interaction?

A comparison of SOD BBGluOH with SOD BBGlu2OH will allow an examination of the influence that more than one sugar has on the interaction of the glycosylated PNA sequence with the lipid. The typical interactions described in Table 4.4 for these glycosylated PNA sequences share many similarities. In both cases, all harmonics are equally affected, indicating that the presence of a second sugar moiety does not prevent transmembrane insertion or promote surface aggregation. While the dissipation increases in both cases, a larger increase was observed in some experiments of the SOD BBGlu2OH sequence. While this could be caused by random lipid variability, it may indicate that the presence of the second sugar could cause more disruption to the integrity of the lipid bilayer than a single sugar moiety.

The significant difference between these PNAs was the increased change in frequency observed for SOD BBGlu2OH compared with the single sugar derivative. However, while some cases of SOD BBGlu2OH resulted in larger frequency changes (up to 25 Hz negative change) than SOD BBGluOH, the majority of cases for these two conjugates displayed similar frequency changes (1.5-7 Hz negative change). This indicates that generally, the presence of a second sugar does not influence the extent of PNA interaction with the lipid, although, a slight indication of more binding could be concluded.

4.3.3.5. Does the Presence of Protecting Groups on the Sugar Influence the Interaction?

The synthesis of all glycosylated building blocks involved acetate protected sugar moieties. The protecting groups were removed from selected glycosylated PNA sequences once synthesis was complete but before the sequences were cleaved from the resin. It is expected that *in vivo*, acetate protecting groups would be cleaved by endogenous enzymes before the PNA reached the BBB, as a pro-drug. Nevertheless, according to Table 4.3 the comparison of SOD SerGalAc with SOD SerGalOH and the comparison of SOD BBGalAc with SOD BBGalOH can be used

to examine the influence the sugar protecting groups have on the interaction of the PNA with the lipid.

The most striking difference of the example *f vs D plots* in Table 4.4 for both comparison sets is that the change in dissipation for both SOD SerGalAc and SOD BBGalAc is significantly more than that of their unprotected counterparts. This indicates that the presence of acetate protecting groups alters the integrity of the synthetic lipid bilayer. This could be due to increased solvation associated with the acetate protecting groups within the bilayer.

The ranges of frequency change associated with both SOD SerGalAc and SOD BBGalAc are very similar to the ranges observed for SOD SerGalOH and SOD BBGalOH, with no discernible pattern suggesting that differences are due to random lipid variability.

The harmonics for the acetate protected conjugates were equally affected with the 3rd harmonic displaying higher frequency and dissipation in both cases. The increased frequency and dissipation of the 3rd harmonic was not as pronounced for SOD SerGalOH and SOD BBGalOH. These observations indicate that acetate protecting groups on the sugar moiety cause disruption or otherwise alter the surface of the lipid bilayer in a way that the unprotected sugar moieties do not.

4.3.3.6. Overall Conclusions

The overall conclusion that can be drawn from the QCM experiments conducted and summarised in Table 4.4 is that all PNA sequences interact with the SLB in a transmembrane fashion, which has previously been observed for PNA conjugates.²⁵ The evidence supporting this conclusion is that in all cases, the harmonics are equally affected and there is a negative change in frequency. This therefore means that the attachment of one or two glycosylated building blocks does not significantly interfere with the interaction of the PNA sequence with the lipid. It has been acknowledged that a major challenge in the use of QCM in mass analysis is that it cannot distinguish between specific signals, or real mass changes, and non-specific signals.¹⁶ However any variability observed is likely due to the inhomogeneity of the lipid surface layer as mentioned earlier. The results summarised in Table 4.4 indicate that attached glycosylated building blocks do not negatively interfere with the interaction of the SOD1 PNA sequence with the

synthetic lipid bilayer. There are, however, some structural features of the glycosylated building blocks that influence the type and extent of interaction. Factors such as the presence of a sugar at all, the presence of two sugars and acetate protecting groups on the sugar moieties have been shown to influence the interaction of the conjugated PNA sequence with the synthetic lipid bilayer.

4.4. Thermodynamic Investigation of PNA Conjugates

4.4.1. PNA/DNA Binding

The complementarity of nucleic acids is the fundamental feature that allows the various endogenous forms to perform their specific roles. The elegance of processes such as transcription and translation is due to simple base pairing rules – adenine binds to thymine and cytosine binds to guanine – that should allow for the seamless transfer of genetic information from DNA in the nucleus through to protein products in the cytosol. At the atomic level, it is hydrogen bonds (two between adenine and thymine; three between cytosine and guanine) that are responsible for physically binding two nucleic acid strands. Watson and Crick discovered the orientation that the bases must be in to enable base pairing to occur and hence that complementarity is key.²⁷

There are many examples of the role of complementarity during transcription and translation. RNA polymerase reads the antisense strand of the double stranded DNA in the nucleus to transcribe the sequence to mRNA. The mRNA sequence is complementary to the antisense strand and so is called the sense strand. Accordingly, any sequence that binds to mRNA is deemed antisense. mRNA is able to leave the nucleus. In the cytosol it is translated into its corresponding polypeptide chain by the complementary action of tRNA reading the mRNA sequence and supplying the appropriate amino acid.

When used as a diagnostic, or a therapeutic, PNA acts by binding to complementary nucleic acids such as DNA or RNA. It is the superior binding ability of PNA over DNA, due to the neutral backbone of PNA, which makes it the preferred nucleic acid for diagnostic purposes.²⁸

In the context of the present project, it is important that conjugated PNA sequences are able to bind complementary nucleic acids, without a decrease in binding strength. It is expected that the glycosylated building blocks, as they have

been added to the PNA sequences at the terminals only, should not negatively interfere with the binding ability of the PNA sequence.

4.4.2. Thermodynamic Analysis to Determine Binding Ability

4.4.2.1. Thermal Melt: UV-vis (Theory)

A PNA/DNA duplex has different absorption properties than dissociated single DNA and PNA strands. In duplex form, the UV-active nucleobases are stacked in an ordered manner and consequently, their UV absorbance of nucleic acid is lower relative to their dissociated, single strand form. However as the temperature increases and associations between complementary strands decrease, the UV absorbance approaches that of the sum of the individual nucleotides of the strand and hence *increases*. This concept is known as *hyperchromicity*. Accordingly, the amount of *hypochromicity*, or the extent to which the absorbance of an associated duplex is *less* than that of the constituent nucleotides, is a measure of the base pairing and stacking of the duplex.

Complementary DNA and PNA strands will form a duplex at room temperature and be completely dissociated at approximately 85 °C. Therefore, a temperature controlled cell in a UV-vis spectrophotometer can be used to measure the thermal melt curve of a PNA strand and its complementary DNA strand (Figure 4.9). The more stable, or favourable, an association is between two strands, the higher the temperature required to dissociate the strands. The melting temperature (T_m) is defined as the temperature at which 50% of the nucleic acid is associated with its complementary strand in a duplex. Therefore the more favourable the association of a particular PNA strand, the higher the T_m will be for that PNA strand. The resulting melting curve, which plots absorbance against temperature, can be further analysed to give thermodynamic information about the association such as enthalpy (ΔH), entropy (ΔS) and Gibbs free energy (ΔG). A detailed guide to calculations involved in such analyses has been published.²⁹

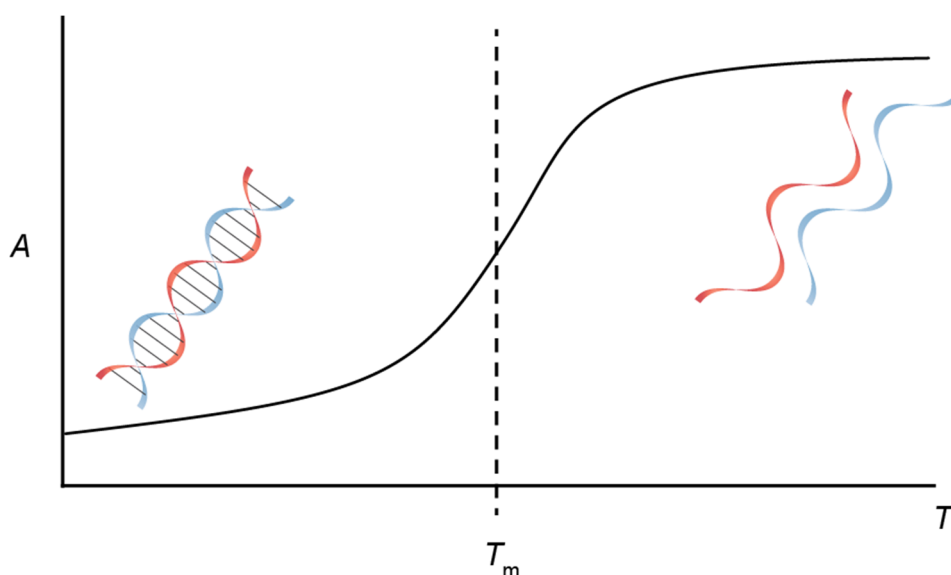


Figure 4.9: A typical UV-melting curve. At low temperatures, complementary nucleic acid strands are hybridised and exhibit low UV-absorbance. At high temperatures, the strands dissociate, corresponding to high UV-absorbance. The melting temperature, T_m is the temperature at which 50% of the strands have dissociated, or the mid-point of the sigmoidal curve.³⁰

The melting curves of a selection of PNA sugar conjugates have been measured and the T_m for each has been calculated. The effect of the conjugated sugar can be inferred by comparing the T_m of the PNA sugar conjugates with that of the unconjugated PNA sequence.

4.4.2.2. *Isothermal Titration Calorimetry (Theory and Uses)*

The nature of molecular interactions is at the core of modern biological and pharmaceutical research.³¹ Isothermal titration calorimetry (ITC) is able to provide information about molecular interactions such as how tightly molecules bind to each other, the nature of their interactions and how quickly the interactions take place.³¹ It is therefore able to give thermodynamic parameters of interactions as well as kinetics information of the associations, however ITC is more often used for the former.³¹ It is a very versatile technique that can examine the interactions of a broad range of molecule classes including protein interactions with other proteins, small molecules, metal ions, lipids, nucleic acids and carbohydrates, nucleic acid interactions with other nucleic acids and small molecules.^{31,32}

ITC works by measuring the heat released, or absorbed, when two molecules bind or interact. This heat energy is the enthalpy of the interaction (ΔH) and

indicates the strength of the interaction. The basis of the energy measurement is a comparison of the temperature of the sample cell with the temperature of a reference cell (Figure 4.10). The amount of energy required to maintain a constant temperature between the two cells is used to calculate the energy released or absorbed by the interaction.

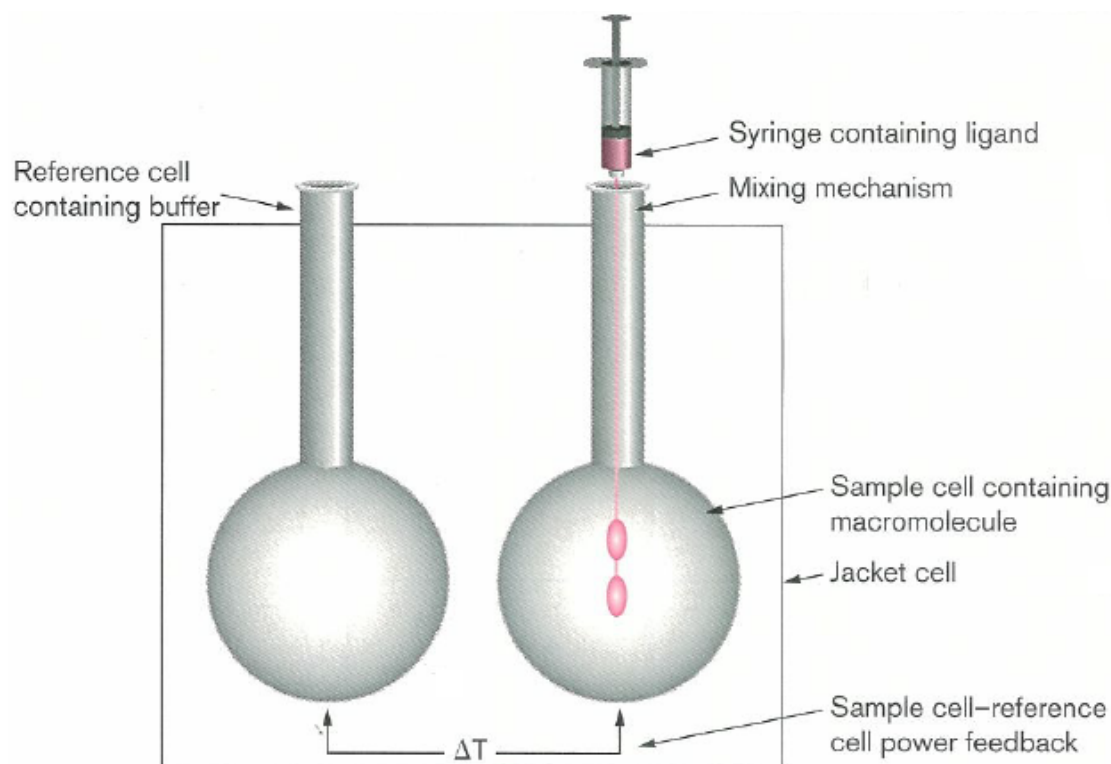


Figure 4.10: Sample and Reference cells of an ITC. The change in temperature in Sample cell caused by heat produced or absorbed by interaction is compared to temperature of Reference cell.³³

One component (e.g. PNA) of the interaction starts in the sample cell in relatively low concentration, while the other component (e.g. DNA) of the interaction is loaded into a burette, in relatively high concentration, and is titrated into the sample cell over a period of time. Consequently, binding curves, binding constants and the reaction stoichiometry can be established and thermodynamic information obtained.

The distinguishing feature of ITC is that it *directly* measures these parameters, rather than, for example, requiring the conversion of UV-absorbance measurements into thermodynamic data, chemical modification of sample

compounds to attach a probe or physical attachment of sample compounds to a surface.^{32,34}

4.4.2.3. *Our Aim*

The aim of these initial thermodynamic investigations is to compare glycosylated and unglycosylated PNA sequences in terms of their binding ability. In other words, this section aims to investigate whether or not the addition of glycosylated building blocks to a PNA sequence affects its binding ability.

As with the QCM analyses, only a selection of SOD1 sequences was investigated for this section. The two techniques, UV-thermal melt and ITC were used to obtain the same thermodynamic information of the binding of the selected PNA conjugates with their complementary DNA sequences. The thermodynamic parameters calculated for the unconjugated PNA sequence were compared with those of the selected sugar conjugated PNA sequences. The trend observed for these comparisons using the UV-thermal melt technique was confirmed by that observed using the ITC.

The SOD1 PNA sequence used in this project was previously designed³⁵ to act as the complementary sequence to a section of mRNA corresponding to part of the SOD1 gene. The PNA sequence was designed to act in an antiparallel fashion: the *N'* terminal of one sequence to bind the *C'* terminal of the other sequence. The current binding studies examine the binding interaction of the conjugated SOD1 PNA sequences with the complementary single stranded DNA sequence. Figure 4.11 shows a schematic representation of the expected PNA/DNA duplex.

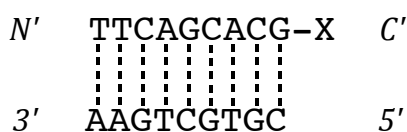


Figure 4.11: SOD1 PNA sequence in *N'* to *C'* direction (top) binding in antiparallel fashion to a model complementary single DNA strand in 3' to 5' direction (bottom). “-X” represents one or more glycosylated building blocks, with or without a spacer.

4.4.3. UV-vis Thermal Melt Method

4.4.3.1. Procedure

The duplex solution prepared in the ITC experiment (PNA and DNA in phosphate buffer, details discussed in further detail in 4.4.4.1) was used directly in the UV-vis thermal melt experiments.³⁶ To begin the thermal melt procedure, a pre-treatment of the duplex solution was performed. This involved heating the duplex solution to 80 °C to ensure the strands were completely dissociated before returning the temperature slowly to room temperature. The duplex solution was placed in sample cell 1, and buffer in the reference cell, starting with the temperature at 20 °C. The temperature was then manually increased by 10 °C every 5 minutes until it reached 80 °C. The duplex sample and reference buffer were kept at this maximum temperature for 4 minutes before they were removed from the cell holder and the air bubbles that had formed in each of the solutions removed (by lightly taping the cells on the bench). This step is important because air bubbles have the potential to interfere with subsequent UV absorbance measurements. The cells were then returned to the cell holder and the temperature decreased by 10 °C every 5 minutes until it reached 20 °C. At this temperature, the nucleic acids are assumed to be in duplex form. The sample and reference cells were left to sit in the cell holders for 25 minutes before the thermal melt measurements were commenced.

The software used for the thermal melt was *Thermal*,³⁷ which allowed for the entire process, from graduated temperature increase and decrease of the sample, UV-absorbance measurements at specified time points and calculation of thermodynamic parameters to be programmed and therefore automated. The wavelength at which the absorbance was measured was 260 nm because nucleic acids display an absorption peak at this wavelength. The temperature was set to increase from 20 °C to 80 °C at a rate of 0.5 °C/minute, held for 3 minutes, then decrease back to 20 °C at a rate of 5 °C/minute. Data (UV- absorbance) was measured every 0.2 °C. *Thermal* used internal algorithms to calculate T_m for each PNA-DNA duplex. These were compared with those manually calculated from the thermal melting curves derived from the absorbance measurements recorded by *Thermal*.

A thermal melting curve was recorded for a selection of the synthesised PNA conjugates, as well as for the unglycosylated SOD1 sequence. The conjugates selected were SOD SerGluOH, SOD SerGalOH, SOD SerGlu2OH, SOD BBGluOH, SOD BBGalOH and SOD BBGlu2OH. With this selection, the effect of the type of sugar, the type of linker as well as the number of sugars on the thermodynamic properties of the PNA sequence could be examined.

4.4.3.2. Results and Discussion

From the raw UV-absorbance data (sigmoidal curve, Figure 4.12), the thermal melting temperature (T_m) of each PNA conjugate was determined according to a known method.²⁹

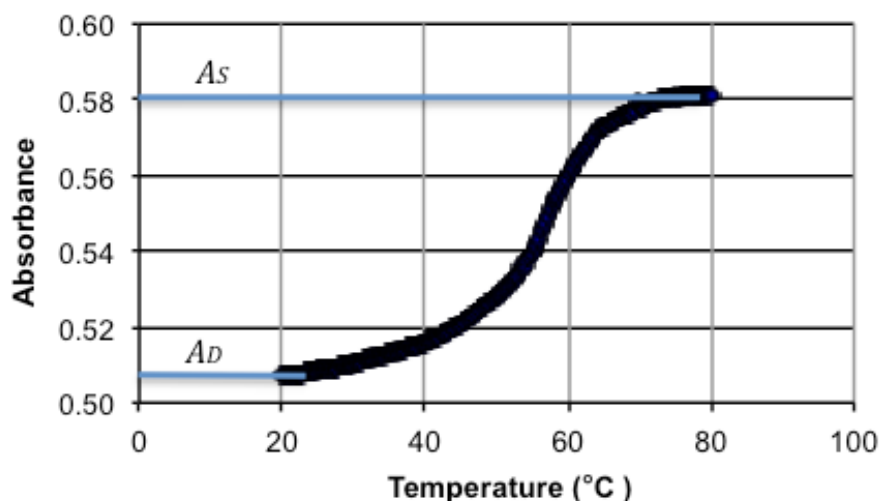


Figure 4.12: Representative sigmoidal curve of raw absorbance data showing A_s and A_D .

The T_m of a nucleic acid interaction is defined as the temperature at which 50% of the strand is melted, or dissociated, and not in a duplex. The fraction of strands in duplex form (α) is calculated by Equation 1

$$\alpha = \frac{(A_s - A)}{(A_s - A) + (A - A_D)} \quad \text{Equation 1}$$

where A is an absorbance, A_s is the absorbance of single strands (upper baseline of sigmoidal curve, see Figure 4.12) and A_D is the absorbance of the duplex (lower baseline of the sigmoidal curve, see Figure 4.12). A plot of α vs temperature could then be constructed, and was used to determine the T_m of the respective PNA conjugate by reading the temperature that corresponded to $\alpha = 0.5$ against the curve plotted, as demonstrated in Figure 4.13.

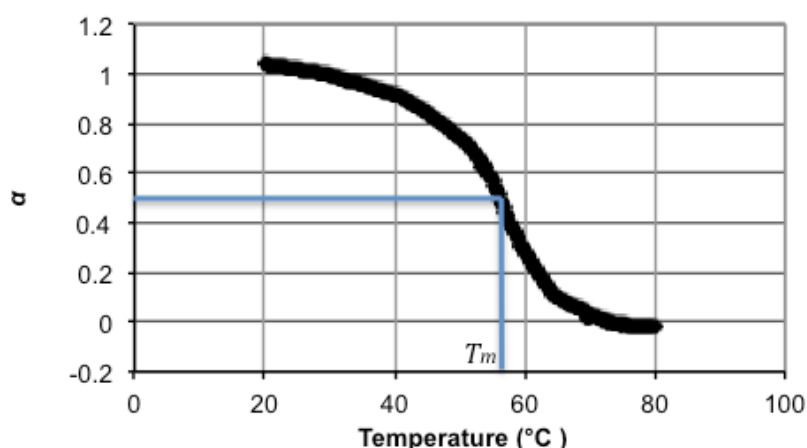


Figure 4.13: Representative alpha curve from which T_m can be read.

Table 4.5 shows the T_m for the selected PNA conjugates. Experiments were conducted in triplicate and the average temperatures are shown with the calculated standard error.

Table 4.5: Average melting temperatures for selected PNA/DNA complexes in 10 mM sodium phosphate buffer, pH 7; and the relative difference in melting temperature of conjugated PNA compared to unconjugated SOD1

PNA	T_m (°C)	ΔT_m (°C) ^a
SOD1	54.7 ± 1.0	
SOD SerGlu	56.5 ± 1.0	+1.8
SOD SerGal	56.7 ± 0.18	+2.0
SOD SerGlu2OH	56.6 ± 0.53	+1.9
SOD BBGluOH	57.6 ± 0.87	+2.9
SOD BBGalOH	49.3 ± 0.47	-5.4
SOD BBGlu2OH	56.3 ± 0.68	+1.6

^aComparison of T_m of SOD1 PNA conjugate with T_m of SOD1

The results in Table 4.5 show that the addition of a glycosylated building block (or two) does not significantly decrease the binding ability, or the thermal stability of the SOD1 PNA/complementary DNA duplex. In fact, generally, the melting temperature of the conjugated PNA sequences was slightly higher (greater than the error) than that of the unconjugated SOD1 sequence. In these cases, it is possible that a cooperative effect is being observed between the conjugated sugar and the complementary DNA strand. The conjugated sugar could be having a stabilising effect on the duplex, however the differences in melting temperature of

the conjugated PNA sequences and that of the unconjugated SOD1 sequence are too small to determine this conclusively. The melting temperatures of SOD SerGlu, SOD SerGal, SOD SerGlu2OH, SOD BBGluOH and SOD BBGlu2OH suggest that the addition of the relative glycosylated building block(s) does not prevent the SOD1 PNA sequence binding to its complementary DNA sequence.

The one PNA conjugate that consistently displayed a lower melting temperature was SOD1BBGalOH. The reason for the lower T_m of this particular PNA conjugate, compared to that of the unconjugated SOD1 sequence and relative to that of the other forms of glycosylated PNA conjugates, is not known. The most structurally similar PNA conjugate to SOD BBGalOH is SOD BBGluOH, in which the hydroxyl group at the C-4 position of the sugar is axial in SOD BBGalOH but equatorial in SOD BBGluOH. It seems unlikely that the difference of the orientation of one hydroxyl group could result in an average of 8.3 °C difference in T_m between these otherwise identical conjugated PNA sequences, despite triplicate treatment.

The other conjugated PNA sequence that contains an axial C-4 hydroxyl group is SOD1SerGal. While the glycosylated building block of this conjugated PNA sequence is significantly smaller (9 atoms) compared to the backbone (BB) building block (26 atoms), a comparatively similar T_m was consistently displayed between SOD1SerGal and SOD1SerGlu, further suggesting that the different sugar is not solely responsible for the lower T_m of SOD BBGalOH.

Apart from structural features of the glycosylated building block, other possible factors that could be responsible for the unexpected lower T_m of SOD BBGalOH are sample and experimental quality. However, the BBGalOH building block as well as the SOD BBGalOH PNA sequence underwent rigorous purification with analytical HPLC confirming the purity of the SOD BBGalOH final product. All final conjugated PNA sequences were lyophilised overnight and the triplicate absorbance measurements were performed on three different batches of the same product, therefore, the reason for the consistently lower T_m of SOD BBGalOH relative to that of SOD1 is unknown.

It should be noted that despite the T_m of SOD BBGalOH being found to be lower than that of SOD1, it is still considered a “decent” T_m suggesting the PNA is binding to the complementary DNA strand and hence the conjugated glycosylated building block is not significantly preventing the duplex forming. There have been reports,

for example, of as much as a 12 °C decrease in T_m of a PNA/DNA duplex as a result of fluorescein conjugation to the PNA strand,³⁸ 15-20 °C decrease in T_m as a result of mismatched sequences,³⁹ 7.6 °C decrease in T_m as a result of glutamic acid conjugation to the PNA sequence⁴⁰ and 23 °C decrease in T_m as a result of insertion of alkyne- or ferrocene-containing monomers in the middle of a PNA sequence,⁴¹ suggesting that an average decrease of only 5.4 °C in T_m for SOD BBGalOH relative to that of SOD1, is not significant in our overall goals.

Furthermore, similar work in the area of glycosylated PNA monomers found that insertion of a glycosylated thymine monomer in the middle of a PNA sequence caused only a slight (3 °C and 4 °C respectively) decrease in T_m .^{2,42} While this result was considered a positive outcome in the context of the cited studies (as is a decrease of only 5.4 °C in T_m for SOD BBGalOH in the present project), it highlights the excellent results achieved in the present project: the general trend of a slight *increase* of T_m , as evidenced by the T_m of SOD SerGlu, SOD SerGalOH, SOD SerGlu2OH, SOD BBGluOH and SOD BBGlu2OH. Compared to the outcome achieved by insertion of a glycosylated thymine monomer in the middle of a PNA sequence,^{2,42} the general trend observed in the present project illustrates the advantage of conjugating glycosylated building blocks (one or two) at the terminal position in a PNA sequence.

The thermodynamic parameters ΔS , ΔH and ΔG were also calculated from the absorbance data of the thermal melting curves of the selected PNA sequences following known methods.^{29,43} Specifically, the equilibrium constant K was calculated by Equation 2:²⁹

$$K = \frac{\alpha}{(C_T/n)^{n-1}(1-\alpha)^n} \quad \text{Equation 2}$$

where C_T is the total strand concentration and n is the number of strands that associate to form the complex, which in the case of a duplex, is 2. Total strand concentration can be calculated according to Equation 3:

$$C_T = \frac{A}{\varepsilon L} \quad \text{Equation 3}$$

where A is the absorbance of the strands in single, or dissociated form, L is the path length (1 dm) and ε is the average extinction coefficient of the PNA strand and

the DNA strand.^{36,44} These were calculated based on the sum of the extinction coefficients for each monomer, as listed in Table 4.6.

Table 4.6: Extinction coefficients of DNA and PNA nucleoside bases^{41,45}

	$\epsilon_{DNA} (M^{-1}cm^{-1})$	$\epsilon_{PNA} (M^{-1}cm^{-1})$
A	15,300	13,700
C	7,600	6,600
G	12,220	11,700
T	8,700	8,600

A van't Hoff plot ($\ln K$ vs $1/T$, where T is calculated in Kelvin) was then constructed, usually for $0.59 < \alpha < 0.85$, as K values are most precise in this region.⁴³ The entropy (ΔS°) and enthalpy (ΔH°) were estimated from the van't Hoff plot according to Equation 4 and Equation 5^{43,46} respectively (where $R = 8.314 \text{ Jmol}^{-1}\text{K}^{-1}$) and the averages are shown in Table 4.7 with the calculated standard error. Correlation coefficients were generally $R = 0.99$. The standard change in Gibbs free energy (ΔG°) was then calculated according to Equation 6^{29,46} at 298 K and the averages and calculated standard error are also shown in Table 4.7.

$$\Delta S^\circ = \text{intercept}(\ln K \text{ vs } 1/T) \times R \quad \text{Equation 4}$$

$$\Delta H^\circ = \text{slope}(\ln K \text{ vs } 1/T) \times R \quad \text{Equation 5}$$

$$\Delta G^\circ = \Delta H^\circ - T\Delta S \quad \text{Equation 6}$$

Table 4.7 shows that when error is taken into account, there is no significant difference in thermodynamic parameters of the different conjugated PNA sequences compared with that of the unconjugated SOD1 sequence. The change in Gibbs free energy (ΔG°) was found to be negative in all cases, indicating that binding is favourable.

Table 4.7: Thermodynamic data (van't Hoff Analysis) for selected PNA/DNA complexes calculated from thermal melt data

PNA	ΔS° (Jmol ⁻¹ K ⁻¹)	ΔH° (kJmol ⁻¹)	ΔG° (kJmol ⁻¹) ^a
SOD1	-671 ± 47	-219 ± 15	-19.0 ± 1.6
SOD SerGlu	-539 ± 58	-176 ± 19	-15.6 ± 2.1
SOD SerGal	-519 ± 42	-170 ± 14	-15.3 ± 1.2
SOD SerGlu2OH	-714 ± 33	-233 ± 11	-21.3 ± 1.1
SOD BBGluOH	-572 ± 85	-189 ± 28	-18.4 ± 2.9
SOD BBGalOH	-666 ± 102	-213 ± 33	-14.1 ± 2.1
SOD BBGlu2OH	-405 ± 56	-133 ± 19	-12.4 ± 1.8

^aCalculated at 298 K

According to Equation 6, Gibb's free energy is negative when enthalpy is more negative than entropy. Enthalpy (ΔH°) is a measure of the heat released upon binding and hence strength of binding (more negative means more heat released upon binding, which is favourable). Entropy (ΔS°) on the other hand, is the measure of disorder of a system and is connected with solvation (more negative means less disorder upon binding, which is not favourable). Therefore enthalpy and entropy must be read together as they are competing factors in the overall likelihood of a reaction (in this case, duplex formation) being favourable. Table 4.7 consistently shows that the favourable release of heat upon binding of the PNA to DNA, outweighs the unfavourable reduction in disorder upon binding.

This therefore supports the finding that binding of a glycosylated PNA sequence with its complementary DNA sequence is still favourable and hence, one or two glycosylated building blocks attached to the terminus of the SOD1 PNA sequence do not interfere with duplex formation.

4.4.4. Isothermal Titration Calorimetry (ITC) Method

4.4.4.1. Procedure

The concentrations of the PNA and the DNA solutions to be used in the ITC experiments were determined accurately before use. The complementary DNA sequence was purchased from Sigma-Aldrich, buffer added to form a ~0.3 mM stock solution, then further diluted to a final concentration of ~0.05 mM.

For each selected PNA conjugate, the concentration of a stock solution which determined by the average absorbance measurement at 260 nm and assuming an extinction coefficient of the PNA strand of $87,800 \text{ M}^{-1} \text{ cm}^{-1}$. As a concentration of approximately $4 \text{ }\mu\text{M}$ was required for the ITC experiments, an appropriate dilution of the stock solution was made, and the new concentration determined accurately, as above. Prior to each set of absorbance readings, the solution was sonicated for 20 minutes to ensure complete dissolution of the PNA in the buffer, the solution was then heated to 80°C for 5 minutes (bases unstacked) in the UV spectrophotometer, and immediately prior to measuring, the air bubbles that had formed in the solution were removed.

The ITC instrument contains a reference cell and a sample cell (1 mL volume). The PNA solution was added to the sample cell and distilled water was added to the reference cell. While the ITC experiments could have been performed with the PNA or DNA solution in the sample cell and either solution in the syringe, the PNA solution was always placed in the sample cell and the DNA always in the syringe. This was because the solution in the syringe was required to be at a much higher concentration than that in the sample cell and the DNA had a higher solubility than the PNA.

A mimic syringe was also inserted into the reference cell to mimic the environment of the sample cell. Care was taken to ensure no air bubbles were present in either cell. The syringe ($100 \text{ }\mu\text{L}$, paddle stirrer tip) was filled with the DNA solution and inserted into the burette (burette in 'up' position). The tip of the syringe was wiped with a lint-free tissue to absorb the first drop of solution. This created an air bubble at the tip of the syringe that acts as a barrier between the DNA solution and the PNA solution to prevent mixing before the first injection. The burette was loaded into the instrument (paddle stirrer syringe in sample cell) and the stirrer turned on at a rate of 250 RPM and the instrument was allowed to equilibrate before the experiment was commenced.

A typical experiment involved $4 \text{ }\mu\text{L}$ injections of the DNA solution into the PNA solution every 5 minutes. At the conclusion of each experiment the solution containing the newly formed PNA/DNA duplex was removed from the sample cell and transferred to a sealed vial and used directly in the UV-vis thermal melt experiments discussed in 4.4.3.

4.4.4.2. Results and Discussion

The raw data obtained from each ITC experiment was viewed and manipulated in *NanoAnalyze*.⁴⁷ Figure 4.14 shows the raw ITC data as the heat energy released over time. This corresponds to each injection of DNA solution into PNA solution at 300 second time intervals. As each injection corresponds to an increase in heat energy, it can be concluded that the interaction of the PNA with DNA is favourable. The first peak is very small as the first injection volume was less than the usual 4 μL due to the air bubble at the tip of the syringe. As the ratio of PNA and DNA in the sample cell reach 1:1, the heat released upon subsequent injections becomes less and less as there is no PNA available for binding with DNA.

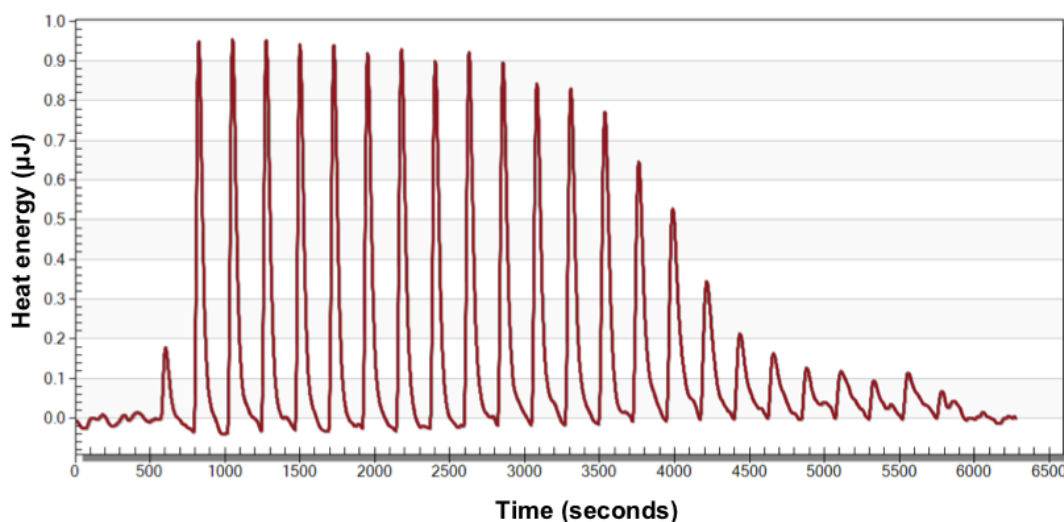


Figure 4.14: Typical raw titration data from an ITC experiment. 4 μL injections of 0.05411 mM DNA solution made at 5 minute intervals into 3.22 μM PNA solution, both in 10 mM sodium phosphate buffer, pH 7 at 25 $^{\circ}\text{C}$.

The raw heat data for SOD1 and SOD SerGluOH appeared, as would be expected, like that of Figure 4.14. The raw heat data for the other PNA sequences that were tested did not appear like this. Due to time restraints, these unexpected results were not investigated further. As mentioned previously, each sample of PNA/DNA duplex was taken directly from the ITC sample cell to the UV-vis spectrophotometer and their melting temperature recorded. The results obtained from the thermal melt experiments were all consistent and within expected ranges. Therefore, the unexpected results obtained from the ITC experiments were unlikely to be caused by unusual binding behaviour of the molecules, but rather a malfunction of the instrument (e.g. the syringe did not inject 4 μL each at

each time interval). In light of this, the ITC results of SOD1 and SOD SerGluOH will be the focus of this section.

NanoAnalyze integrated the raw heat data obtained from the ITC instrument (Figure 4.15) with additional parameters such as sample cell concentration, syringe concentration, injection volume, temperature and baseline constant to subtract (due to heat of dilution⁴⁸).

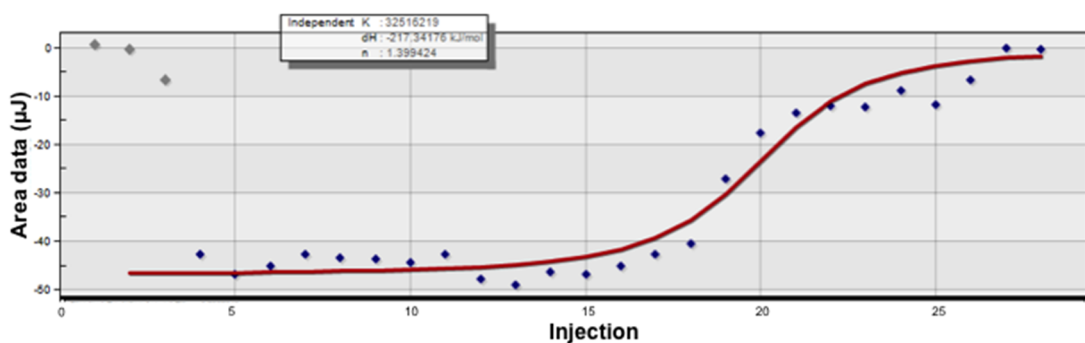


Figure 4.15: Typical integrated heat of reaction plot against injection number (blue diamonds) with sigmoidal line of best fit (red line), as determined by *NanoAnalyze*.

An “independent” model was used by *NanoAnalyze* to fit a sigmoidal line of best fit to the data points. Particular data points were manually deselected from inclusion, particularly from the initial injections, as they were not considered appropriate. Reaction parameters such as ΔH° , K , the equilibrium constant and n , the number of binding sites (expected to be 1 for all complex-forming reactions), were calculated by *NanoAnalyze*. Table 4.8 shows ΔH° and K for the selected PNA/DNA complexes. Experiments were conducted in triplicate and the average enthalpies are shown with the calculated standard error.

Table 4.8: Average enthalpy and binding constants for selected PNA/DNA complexes calculated from ITC data using *NanoAnalyze*

PNA	ΔH° (kJmol ⁻¹)	K (x10 ⁷ M ⁻¹)
SOD1	-247 ± 11	2.6 ± 0.57
SOD SerGluOH	-291 ± 3	4.5 ± 0.38

The enthalpy values determined from the ITC data, like those determined from the thermal melt data (Table 4.7), suggest that the addition of a glycosylated building block to the end of the SOD1 PNA sequence does not interfere with duplex

formation. While the enthalpy values obtained from the ITC data are different from those obtained from the thermal melt data, the values are similar. In other words, the enthalpy values derived from the ITC experiments indicate that binding of a glycosylated PNA sequence with its complementary DNA sequence releases heat and is therefore a favourable process.

Differences in enthalpy values obtained from ITC data and thermal melt data have been observed previously^{44,48} for PNA/DNA duplexes. Chakrabarti and Schwarz³⁶ similarly found that enthalpy values determined from ITC and DSC measurements were not consistent for all PNA/DNA and DNA/DNA duplexes that were analysed. It has been widely acknowledged that these differences are as a result of the temperatures at which the different experiments are conducted. ITC data is recorded at ambient temperature while the thermal melt data is recorded at temperatures up to 80 °C and the state of the PNA and DNA sequences are different at these different temperatures.^{36,44} Specifically, single strands are thermodynamically different at the duplex melting temperature and at ambient temperature: at ambient temperature, single-stranded structure or order exists that needs to be broken before hybridisation with an external strand can occur.^{36,38,44,48,49} Therefore the heat of reaction measured in an ITC experiment may include contributions from, for example, the denaturation/renaturation of the single strands,⁴⁸ destacking of bases in the single strands or dissociation of self-associated strands³⁸ or other intramolecular interaction that prepares the strands for duplex formation enthalpically.⁴⁹ Conversely, the data obtained from thermal melt experiments of the single strand is measured at the duplex melting temperature. Therefore when thermodynamic parameters are determined by extrapolating this data to ambient temperature, the potential single-stranded order should be accounted for.⁴⁴ However as the purpose of the present study was to compare the binding of the SOD1 PNA sequence and that of various glycosylated SOD1 PNA sequences, the general trend of the data presented in Table 4.7, Table 4.8 and Table 4.9 (below) is of importance, and not the absolute values.

The *K* values, or binding constants, listed in Table 4.8 suggest that duplex formation is a favourable reaction for both the SOD1 and SOD SerGluOH PNA sequences with their complementary DNA sequences: a large binding constant equates to a high binding affinity. The binding constant of a reaction is a

parameter that the ITC instrument is able to measure directly, but cannot be calculated from the UV thermal melt data. The overall stability of the duplex is reflected in the binding constant associated with its formation, and this is made up of competing changes in enthalpy and entropy upon duplex formation.⁵⁰ Table 4.9 lists the change in entropy (ΔS°) and change in Gibb's free energy (ΔG°) based on the ITC data (ΔH° and K values obtained from *NanoAnalyze*), and calculated according to Equation 7 and Equation 8 respectively.⁴⁴

$$\Delta S^\circ = (\Delta H^\circ - \Delta G^\circ)/T \quad \text{Equation 7}$$

$$\Delta G^\circ = -RT\ln(K) \quad \text{Equation 8}$$

Table 4.9: Thermodynamic data for selected PNA/DNA complexes calculated from ITC *NanoAnalyze* data at 298 °K

PNA	ΔS° (Jmol ⁻¹ K ⁻¹)	ΔG° (kJmol ⁻¹)
SOD1	-650 ± 48	-42.2 ± 0.47
SOD SerGluOH	-832 ± 11	-43.7 ± 0.20

Once again, while the absolute values for ΔG° are different when calculated from the thermal melt data (Table 4.7) compared to when calculated from the ITC data (Table 4.9), the ΔG° values presented in Table 4.9 are negative, indicating once again that binding is favourable for the SOD1 PNA sequence as well as the glycosylated sequence. These values further support the finding that the attachment of a glycosylated building block to the end of a PNA sequence does not interfere with duplex formation.

It appears that the more favourable change in enthalpy (Table 4.8) calculated for the SOD SerGluOH sequence, compared with the SOD1 sequence was compensated for by a less favourable change in entropy, resulting in very similar K and ΔG° values and hence overall stability.

4.5. Conclusions and Future Directions

A library of glycosylated PNA sequences was synthesised on the solid phase, purified by preparative reverse phase HPLC and characterised by ESI mass spectrometry. The completed conjugated sequences contained one or two glycosylated building blocks BBGluOH, BBGalOH, SerGluOH, SerGalOH, BBGluAc,

BBGalAc, SerGluAc or SerGalAc at either the *N'* and *C'* terminal. The successful synthesis of the library of glycosylated PNA sequences, as presented in Table 4.2, confirms that both forms of glycosylated building blocks (glycosylated serine and glycosylated backbone monomer) can be incorporated into PNA automated solid phase synthesis. Carbohydrate acetate protecting groups were successfully removed on the solid phase. Each of the glycosylated building blocks can be multiply attached, either with or without a spacer molecule, potentially leading to multi-carbohydrate sequences.

A selection of SOD1 glycosylated PNA sequences was analysed on a QCM to determine the effect of the various glycosylated building blocks on the ability of the PNA sequence to interact with a SLB. It was generally found that all PNA sequences displayed transmembrane insertion (decrease in frequency observed for all harmonics) with minimal change to membrane integrity (minimal dissipation change). It therefore appears that the type of glycosylated building block (including the type of linker, type of sugar, acetate protected or not) and number of glycosylated building blocks, do not affect the interaction of the PNA sequence with the synthetic lipid bilayer.

The T_m calculated for each selected glycosylated PNA/DNA duplex from the UV thermal melt data indicates that the duplex formed is slightly more thermally stable than that of the unconjugated SOD1 sequence in most cases. The ΔG° values calculated from the thermal melt data indicated in all cases that duplex formation was favourable and hence the presence of glycosylated building blocks in the PNA sequence does not interfere with duplex formation.

ITC experiments were also conducted to provide supporting thermodynamic data to that obtained in the UV-vis thermal melt experiments. This technique directly measured the binding constant and change in enthalpy associated with duplex formation. The binding constants and negative ΔH° values obtained from the ITC experiments support the findings of the UV-vis thermal melt experiments that the attachment of a glycosylated building block does not interfere with duplex formation. Further work to be done in this analysis includes repeating the ITC experiments for SOD SerGalOH, SOD SerGlu2OH, SOD BBGluOH, SOD BBGalOH and SOD BBGlu2OH to investigate the unusual raw heat titration data obtained.

While these preliminary results indicate that the various glycosylated building blocks on the terminals of the SOD1 PNA sequence do not interfere with DNA binding or membrane interaction, and hence the therapeutic PNA sequence is not inhibited from acting as an antisense agent, the ability of the attached sugar moieties to enhance BBB penetration is still unknown. During the course of this project, investigations were made into testing the BBB penetration abilities of the various glycosylated PNA sequences in sheep. The proposed experimental design involved injecting the sample PNA into the neck of a sheep and then extracting blood samples through the top of the head at regular time intervals. The sheep are not harmed during this process. The blood samples would then be analysed by mass spectrometry and/or HPLC to determine if the PNA sample was present in the blood and hence had crossed the BBB. The amount of each PNA sample detected in the blood would be compared to determine the efficiency of each type of glycosylated building block in BBB penetration.

Unfortunately this experimental design required at least 5 mg of each PNA sample. The scope of this project did not allow for those quantities of PNA samples in addition to the quantities required for the QCM and thermodynamic studies. However despite this testing method not being viable for the present project, it is a relatively simple and straightforward method to determine the efficiency of the attached glycosylated building block in enhancing the transport of the PNA sequence through the BBB.

Therefore future work that is required for this project includes the *in vivo* determination of the ability of attached glycosylated building blocks to enhance the ability of the therapeutic PNA sequence to cross the BBB.

4.6. References

1. Porcheddu, A. and Giacomelli, G., *Curr. Med. Chem.*, **2005**, 12, 2561-2599.
2. Hamzavi, R., Meyer, C. and Metzler-Nolte, N., *Org. Biomol. Chem.*, **2005**, 4, 3648-3651.
3. O'Sullivan, C. K. and Guilbault, G. G., *Biosens. Bioelectron.*, **1999**, 14, 663-670.
4. Buttry, D. A. and Ward, M. D., *Chem. Rev.*, **1992**, 92, 1355-1379.
5. Marx, K. A., *Biomacromolecules*, **2003**, 4, 1099-1120.

6. Speight, R. and Cooper, M. A., *J. Mol. Recognit.*, **2012**, 25, 451-473.
7. King, W. H. J., *Anal. Chem.*, **1964**, 36, 1735-1741.
8. Shons, A., Dorman, F. and Najarian, J., *J. Biomed. Mater. Res.*, **1972**, 6, 565-570.
9. Deakin, M. R. and Buttry, D. A., *Anal. Chem.*, **1989**, 61, 1147-1154.
10. Fawcett, N. C., Evans, J. A., Chien, L. and Flowers, N., *Anal. Lett.*, **1988**, 21, 1099-1114.
11. Wang, J., Nielsen, P. E., Jiang, M., Cai, X., Fernandes, J. R., Grant, D. H., Ozsoz, M., Beglieter, A. and Mowat, M., *Anal. Chem.*, **1997**, 69, 5200-5202.
12. Hook, F., Ray, A., Norden, B. and Kasemo, B., *Langmuir*, **2001**, 17, 8305-8312.
13. Wang, J., *Biosens. Bioelectron.*, **1998**, 13, 757-762.
14. Wang, J., *Curr. Iss. Mol. Biol.*, **1999**, 1, 117-122.
15. Rodahl, M. and Kasemo, B., *Sens. Actuators, A*, **1996**, 54, 448-456.
16. Heyse, S., Schmid, E., Lakey, J. H. and Vogel, H., *Biochim. Biophys. Acta*, **1998**, 85507, 319-338.
17. Praporski, S., Ng, S. M., Nguyen, A. D., Corbin, C. J., Mechler, A., Zheng, J., Conley, A. J. and Martin, L. L., *J. Biol. Chem.*, **2009**, 284, 33224-33232.
18. Sherman, P. J., Jackway, R. J., Gehman, J. D., Praporski, S., McCubbin, G. A., Mechler, A., Martin, L. L., Separovic, F. and Bowie, J. H., *Biochemistry*, **2009**, 48, 11892-11901.
19. McCubbin, G. A., Praporski, S., Piantavigna, S., Knappe, D., Hoffmann, R., Bowie, J. H., Separovic, F. and Martin, L. L., *Eur. Biophys. J.*, **2011**, 40, 437-446.
20. Piantavigna, S., McCubbin, G. A., Boehnke, S., Graham, B., Spiccia, L. and Martin, L. L., *Biochim. Biophys. Acta*, **2011**, 1808, 1811-1817.
21. Mechler, A., Praporski, S., Atmuri, K., Boland, M., Separovic, F. and Martin, L. L., *Biophys. J.*, **2007**, 93, 3907-3916.
22. Piantavigna, S., Czihal, P., Mechler, A., Richter, M., Hoffmann, R. and Martin, L. L., *Int. J. Pept. Res. Ther.*, **2009**, 15, 139-146.
23. Piantavigna, S., McCubbin, G. A., Boehnke, S., Graham, B., Spiccia, L. and Martin, L. L., *BBA Biomembranes*, **2011**, 1808, 1811-1817.
24. Knappe, D., Piantavigna, S., Hansen, A., Mechler, A., Binas, A., Nolte, O., Martin, L. L. and Hoffmann, R., *J. Med. Chem.*, **2010**, 53, 5240-5247.

CHAPTER 4 - CONJUGATED PEPTIDE NUCLEIC ACIDS

25. Joshi, T., Gasser, G., Martin, L. L. and Spiccia, L., *R. Soc. Chem. Adv.*, **2012**, 2, 4703-4712.
26. Rodahl, M., Hook, F., Fredriksson, C., Keller, C. A., Krozer, A., Brzezinski, P., Voinova, M. and Kasemo, B., *Faraday Discuss.*, **1997**, 107, 229-246.
27. Watson, J. D. and Crick, F. H. C., *Nature*, **1953**, 171, 737-738.
28. Shakeel, S., Karim, S. and Ali, A., *J. Chem. Technol. Biotechnol.*, **2006**, 81, 892-899.
29. Marky, L. A. and Breslauer, K. J., *Biopolymers*, **1987**, 26, 1601-1620.
30. *ATDBio Nucleic Acids Book*, DNA duplex stability, **2013**, <http://www.atdbio.com/nucleic-acids-book>.
31. Falconer, R. J. and Collins, B. M., *J. Mol. Recognit.*, **2011**, 24, 1-16.
32. Doyle, M., *Curr. Opin. Biotech.*, **1997**, 8, 31-35.
33. Ladbury, J. E. and Chowdhry, B. Z., *Chem. Biol.*, **1996**, 3, 791-801.
34. Ward, W. H. J. and Holdgate, G. A., *Prog. Med. Chem.*, **2001**, 38, 309-376.
35. Cheah, I. K., PhD Thesis *Antisense peptide nucleic acids as therapeutic agents for the treatment of neurodegeneration*, Monash University, **2006**.
36. Chakrabarti, M. C. and Schwarz, F. P., *Nucleic Acid Res.*, **1999**, 27, 4801-4806.
37. *Thermal*, **2011**, Agilent Technologies, Cary WinUV, Version 4.20 (468).
38. Ratilainen, T., Holmen, A., Tuite, E., Haaima, G., Christensen, L., Neilsen, P. E. and Norden, B., *Biochemistry*, **1998**, 37, 12331-12342.
39. Ratilainen, T., Holmen, A., Tuite, E., Neilsen, P. E. and Norden, B., *Biochemistry*, **2000**, 39, 7781-7791.
40. Silvester, N. C., Bushell, G. R., Searles, D. J. and Brown, C. L., *Org. Biomol. Chem.*, **2007**, 5, 917-923.
41. Sosniak, A. M., Gasser, G. and Metzler-Nolte, N., *Org. Biomol. Chem.*, **2009**, 7, 4992-5000.
42. Hamzavi, R., Dolle, F., Tavitian, B., Dahl, O. and Nielsen, P. E., *Bioconjugate Chem.*, **2003**, 14, 941-954.
43. Puglisi, J. D. and Tinoco, I., *Meth. Enzymol.*, **1989**, 180, 304-325.
44. Schwarz, F. P., Robinson, S. and Butler, J. M., *Nucleic Acids Res.*, **1999**, 27, 4792-4800.

CHAPTER 4 - CONJUGATED PEPTIDE NUCLEIC ACIDS

45. Dawson, R. M. C., Elliott, D. C., Elliott, W. H. and Jones, K. M. *Data for biochemical research*; Oxford University Press: New York, 1986, 103-114.
46. Silvester, N. C., Doctor of Philosophy Thesis, Griffith University, **2008**.
47. *NanoAnalyze Data Analysis*, **2010**, TA Instruments, Version 2.1.13.
48. Ratilainen, T. and Norden, B., *Methods Mol. Biol.*, **2002**, 208: *Peptide Nucleic Acids: Methods and Protocols*, 59-88.
49. Vesnaver, G. and Breslauer, K. J., *Proc. Natl. Acad. Sci. USA*, **1991**, 88, 3569-3573.
50. Lagriffoule, P., Wittung, P., Eriksson, M., Jensen, K. K., Norden, B., Buchardt, O. and Nielsen, P. E., *Chem. Eur. J.*, **1997**, 3, 912-919.

APPENDIX

Appendix

Table A1. Crystal data and structure refinement for **1a**

Identification code	ck2p1
Empirical formula	C ₂₁ H ₂₄ O ₁₁
Formula weight	452.4
Temperature	123(2) K
Wavelength	0.71073 Å
Crystal system, space group	Triclinic, P 1
Unit cell dimensions	a = 5.6245(5) Å alpha = 81.106(3) deg. b = 8.9511(7) Å beta = 86.542(3) deg. c = 11.2955(9) Å gamma = 87.757(3) deg.
Volume	560.56(8) Å ³
Z, Calculated density	1, 1.340 Mg/m ³
Absorption coefficient	0.110 mm ⁻¹
F(000)	238
Crystal size	0.20 x 0.20 x 0.20 mm
Theta range for data collection	2.30 to 26.00 deg.
Limiting indices	-6 ≤ h ≤ 6, -11 ≤ k ≤ 10, -13 ≤ l ≤ 13
Reflections collected / unique	5978 / 2115 [R(int) = 0.0197]
Completeness to theta = 26.00	96.70%
Absorption correction	Semi-empirical from equivalents
Max. and min. transmission	1.00 and 0.91
Refinement method	Full-matrix least-squares on F ²
Data / restraints / parameters	2115 / 3 / 293
Goodness-of-fit on F ²	1.053
Final R indices [I > 2σ(I)]	R1 = 0.0270, wR2 = 0.0699
R indices (all data)	R1 = 0.0271, wR2 = 0.0700
Largest diff. peak and hole	0.264 and -0.166 e.Å ⁻³

Table A2. Crystal data and structure refinement for **79**.

Identification code	ck267
Empirical formula	C ₁₆ H ₂₃ Cl O ₁₀
Formula weight	410.79
Temperature	123(2) K
Wavelength	0.71073 Å
Crystal system, space group	Monoclinic, P 2 ₁
Unit cell dimensions	a = 9.3686(5) Å alpha = 90 deg. b = 9.6296(4) Å beta = 96.331(3) deg. c = 10.9849(6) Å gamma = 90 deg.
Volume	984.97(9) Å ³
Z, Calculated density	2, 1.385 Mg/m ³
Absorption coefficient	0.244 mm ⁻¹
F(000)	432
Crystal size	0.20 x 0.18 x 0.10 mm
Theta range for data collection	2.71 to 27.50 deg.
Limiting indices	-11<=h<=12, -12<=k<=12, -14<=l<=14
Reflections collected / unique	7349 / 3797 [R(int) = 0.0340]
Completeness to theta = 25.00	99.60%
Absorption correction	Semi-empirical from equivalents
Max. and min. transmission	1.00 and 0.89
Refinement method	Full-matrix least-squares on F ²
Data / restraints / parameters	3797 / 1 / 248
Goodness-of-fit on F ²	1.041
Final R indices [I>2sigma(I)]	R1 = 0.0463, wR2 = 0.1000
R indices (all data)	R1 = 0.0547, wR2 = 0.1084
Absolute structure parameter	0.01(9)
Largest diff. peak and hole	0.256 and -0.368 e.Å ⁻³